Downloaded from orbit.dtu.dk on: Apr 26, 2024

DTU Library

NO_X formation and reduction in fluidized bed combustion of biomass

Ulusoy, Burak

Publication date:
2019

Document Version
Publisher's PDF, also known as Version of record

Link back to DTU Orbit

Citation (APA):
Ulusoy, B. (2019). *NO_X formation and reduction in fluidized bed combustion of biomass*. Technical University of Denmark.

General rights
Copyright and moral rights for the publications made accessible in the public portal are retained by the authors and/or other copyright owners and it is a condition of accessing publications that users recognise and abide by the legal requirements associated with these rights.

- Users may download and print one copy of any publication from the public portal for the purpose of private study or research.
- You may not further distribute the material or use it for any profit-making activity or commercial gain
- You may freely distribute the URL identifying the publication in the public portal

If you believe that this document breaches copyright please contact us providing details, and we will remove access to the work immediately and investigate your claim.

DTU Technical University of Denmark

NO_X formation and reduction in fluidized bed combustion of biomass

Burak Ulusoy

PhD thesis

August 2019

Supervisors Kim Dam-Johansen (DTU Chemical Engineering)

Hao Wu (DTU Chemical Engineering)

Weigang Lin (DTU Chemical Engineering)

Wei Wang (CAS, Institute of Process Engineering)

DTU Chemical Engineering
Department of Chemical and Biochemical Engineering

SDC The university partnership Denmark – China

Preface and Acknowledgments

This dissertation is the result of three years of research, from 2016 to 2019, conducted in the Combustion and Harmful Emission Control (CHEC) research center, at the Department of Chemical & Biochemical Engineering, Technical University of Denmark (DTU), in collaboration with the Institute of Process Engineering, Chinese Academy of Sciences (CAS). The research is performed within the framework of the Sino-Danish Centre (SDC) for Education and Research. The PhD project was supervised by Professor Kim Dam-Johansen, Associate Professor Hao Wu, Associate Professor Weigang Lin, and Professor Wei Wang.

I would like to extend my sincerest gratitude and appreciation to my supervisors for their support and guidance during this PhD study. I have learned a great deal from the experiences and knowledge of all of you, and for that, I am forever grateful. I am especially grateful to Hao Wu and Weigang Lin for their always-available guidance and encouragement. You have truly been amazing supervisors, allowing me to propose ideas of my own and to try many different things. I am grateful to Kim Dam-Johansen for his fruitful discussions, and continued support and encouragement. Furthermore, I am thankful to my supervisor in China, Wei Wang, for his professional help and guidance throughout my stay in China. I am also thankful to Peter Glarborg and Oskar Karlström for their support within the (now hopefully slightly less) mysterious world of NO_X chemistry. In addition, a special thanks goes to Knud Villy Christensen from SDU, from whom I have learned a lot.

I would like to thank the talented CHEC employees, Anders, Nikolaj, Søren P., Malene, and Lillian, as well as the brilliant technicians from the workshop, Jens and Søren, for their invaluable support with the use, construction, commissioning, and troubleshooting of the experimental setups.

I would like to thank all of the students and researchers I have met and had the pleasure to interact with during the three years at DTU. I would especially like to thank my dear friends Yash, Hadi, Giovanni, Guoliang (Dagi), Bozo, Xueting, Ari, and Guofeng, who made each day more enjoyable and memorable than the other. Time flies when in (your) good company.

Above all, I would like to thank my parents, Yusuf and Halime, and my brothers, Bünyamin and Berat, for their continued support, love, and understanding throughout the entirety of my life. In my moments of hardship, you have been the pillars that I could always lean on. I will never be able to repay nor express in words, what you mean to me. Without you, I would not have made it this far in life, thank you so dearly.

August 2019

Burak Ulusoy

Summary

Biomass has received growing interest in heat and power production due to it being a renewable and CO_2 neutral alternative to coal. A promising technology for the utilization of biomass is fluidized bed combustion, offering fuel flexibility and high combustion efficiency. However, the nitrogen content in different biomass varies considerably and can reach up to several weight percent, possibly higher than coal. This may lead to increased emissions of nitrogen oxides, i.e. NO_X (NO and NO_2) and N_2O, which have a detrimental impact on the environment, as NO_X lead to the formation of acid rain and photochemical smog, while N_2O is a greenhouse gas and ozone depleter. In combination with the tightening regulations on NO_X emissions from solid fuel combustion, the understanding of the mechanism of NO_X and N_2O emissions from fluidized bed biomass combustion and the development of effective countermeasures are of essential importance.

The formation and reduction of NO_X and N_2O in fluidized bed combustion of biomass has been investigated in this PhD project. Continuous combustion experiments were performed in a lab scale fluidized bed reactor to elucidate the influence of co-combustion, fuel properties (nitrogen and ash forming element content), and operating conditions (air staging, temperature, and gas phase composition) on NO_X emissions. Based on the results, an additive-based technique for the simultaneous reduction of NO_X emissions and bed agglomeration was proposed and examined. In addition, the formation and reduction of NO and N_2O during biomass/waste char combustion were studied in a lab scale fixed bed reactor at conditions resembling that of fluidized bed combustion.

Fluidized bed mono- and co-combustion of biomass were conducted at air staged and un-staged conditions, from which effluent and local gas composition data were obtained. The investigated fuels included pine wood, beech wood, straw, sunflower husk, sewage sludge, and sunflower seed. The results reveal that from fluidized bed mono-combustion of biomass under un-staged conditions, the fuel bound nitrogen (fuel-N) to NO conversion decreased with an increase in the fuel-N content. This may be related to the larger release of nitrogen species such as NH_3 with the volatiles thereby facilitating thermal $DeNO_X$ reactions. At un-staged conditions, a synergy effect was observed during straw-sewage sludge and straw-sunflower seed co-combustion, while straw-sunflower husk co-combustion was additive. The interaction during straw-sewage sludge co-combustion was elucidated, showing that at a low ash content in the bed (2-25 g), the NH_3 released from sewage sludge facilitated thermal $DeNO_X$ reactions leading to a low NO emission. As more ash accumulated in the bed, the oxidation of NH_3 catalyzed by sewage sludge ash increased the NO emission. The catalytic effect of sewage sludge ash on NO forming reactions during straw combustion increased with a lower ash preparation temperature and a better mixing of the ash with straw. In straw-sunflower seed combustion, the effluent NO concentration was approximated well by the weighted average of the individual fuels, while the NH_3 and NO concentrations above the bed were significantly higher than the weighted values. Air staging proved to be an efficient method for minimizing NO emission from

mono- and co-combustion. In addition, the influence of sewage sludge ash on NO forming oxidation reactions was less pronounced at air staged conditions.

The influence of fuel properties and operating conditions on NO_X emissions was investigated during fluidized bed combustion. Batch fluidized bed combustion experiments of pine wood, beech wood, straw, sunflower husk, sewage sludge, and sunflower seed revealed that similar to continuous combustion, the fuel-N to NO conversion decreased with an increase in fuel-N content. The volatile-NO was generally the main contributor to the total NO, while in the case of beech wood, up to 55% of the NO was released during char combustion. Continuous fluidized bed combustion of pine wood, straw, washed straw, and potassium (KCl, K_2CO_3, and KOH) doped pine wood and washed straw were conducted. Washing of straw resulted in a higher fuel-N to NO conversion and lower CO emission. All three K-compounds increased CO emission when doped to washed straw. KCl and KOH further decreased the fuel-N to NO conversion, while K_2CO_3 had a negligible influence. For pine wood, KCl doping increased CO emission without affecting fuel-N to NO conversion, while the other K-compounds did not change the measurements. The increased CO and decreased NO emissions by KCl addition were more pronounced at air staged (primary to total air ratio (λ_1/λ) of 0.04) compared to un-staged ($\lambda_1/\lambda = 1$) conditions. This may be attributed to the radical recombination property of KCl. In addition, the influence of air staging was investigated during continuous straw and sunflower husk combustion, indicating a minimum in NO emission and fuel-N to NO conversion for λ_1/λ values between 0.5 and 0.75. Moreover, the fuel-N to NO conversion increased slightly with increasing temperature for straw combustion, while the fuel-N to NO conversion for KCl-doped washed straw combustion increased and levelled off with temperature. This was related to the inverse trend in the effluent CO concentration. Furthermore, the fuel-N to NO conversion and CO emission were unaffected by replacing the bed partially with kaolin and CaO, or completely with CaO at $\lambda_1/\lambda = 1$, or by changing the primary gas from N_2 to CO_2 at $\lambda_1/\lambda = 0$ and 0.04 during straw combustion

The use of additives for the simultaneous reduction of NO_X emissions and bed agglomeration during fluidized bed combustion of straw was investigated. Other parameters, such as fuel type, additive particle size and introduction method, and air staging, were additionally examined. During straw combustion, kaolin, CaO, and $MgCO_3$ prevented defluidization without changing the fuel-N to NO conversion, while urea decreased the fuel-N to NO conversion without affecting the defluidization tendency. To reduce NO_X, the NH-functionality was a necessity. NH_4MgPO_4 and $AlNH_4(SO_4)_2$ prevented defluidization while reducing the fuel-N to NO conversion by 40% in straw and 30% in sunflower husk combustion. Local gas composition measurements revealed that the NH-based additives released NH_3 above the fuel inlet and/or the bubbling bed. Some additives (urea, $(NH_4)_2SO_4$, NH_4MgPO_4, and $AlNH_4(SO_4)_2$) favored the reduction of NO by thermal $DeNO_X$, while additives that contained Fe ($(NH_4)_2Fe(SO_4)_2$, $NH_4Fe(SO_4)_2$, and $(NH_4)_3[Fe(C_2O_4)_3]$) or facilitated bed agglomeration, i.e. induced poor mixing, ($(NH_4)_2HPO_4$) increased NO emission near the bed and led to negligible differences in the effluent NO measurements relative to raw straw combustion. When premixing additive and fuel, the larger particles of $(NH_4)_2SO_4$ dropped to the bed, increasing the NH_3 release above the fluidized bed and prolonging the time for defluidization. In comparison, no significant differences in the fuel-N to NO conversion and defluidization tendency were observed when batch adding pellets compared to premixing, possibly related to differences in release

mechanism and location. In addition, air staging ($\lambda_1/\lambda = 0.5$) resulted in a 40% reduction of the fuel-N to NO conversion during straw combustion, while the use of NH_4MgPO_4 and $AlNH_4(SO_4)_2$ under air staged conditions slightly increased the fuel-N to NO conversion. This was related to the increased oxidation of NH_3 in the secondary air jet. The accumulation of sunflower husk ash increased NO and decreased NH_3 concentrations above the bed. In addition, the temporal variations were dampened at higher ash content in the bed. This was attributed to the incipient defluidization leading to poorer mixing and the catalytic effect of ash on the nitrogen chemistry.

The formation of NO and N_2O during raw and demineralized biomass (pine wood, straw, waste wood, bran, sunflower seed, and dried distillers grains with solubles) char combustion was investigated in a fixed bed reactor. The results reveal that the conversion of char-N to NO decreased with an increase in char-N content. As this trend did not correlate with the NO reduction reactivity of the chars, a contributing factor may be the higher yield of N_2O from high-N chars. The presence of ash forming elements largely dominated the NO reduction reactivity, showing a reasonable correlation between the NO reduction reactivity and the (K+Ca)/C molar ratio for the chars with a low P content. Chars with high char-P did not follow the correlation, possibly due to the formation of less catalytically active species such as KPO_3. The NO reduction reactivity of the raw and demineralized chars did not correlate with the initial porosity, surface area, char-N content, or nitrogen and oxygen functionality or content. The surface of the chars were enriched with (-CN) and/or (-CO) species during NO treatment. The accumulated (-CN) species may exhibit a different reactivity towards NO reduction compared to inherent (-CN) sites.

The conversion of char-N during sewage sludge, refuse derived fuel (RDF), and straw char combustion, and the reactivity of these chars towards NO were investigated in a fixed bed reactor. The reactivity of the sewage sludge and RDF chars were an order of magnitude and six-fold higher than that of straw, respectively. This was attributed to the larger Ca and Fe content in the waste based chars. The initial reactivity of the employed chars correlated well with the (K+Fe+Ca)/C molar ratio. As fractional order or random pore model expressions did not yield any obvious advantages, a simple concentration-averaged, first order reaction expression was used to describe the char-NO reaction. The simplified expression was used in a one-dimensional, transient, heterogeneous reactor model, which predicted reasonably well the conversion of char-N to NO during combustion. The reactivities of the waste chars exceeded those of selected coal and biomass char found in literature.

This work provides an improved understanding of the conversion of nitrogen during fluidized combustion of biomass. The observed trends may be extrapolated to practical fluidized bed combustion systems for improvement of design and operation to minimize NO_X emissions.

Dansk resumé

Som et potentielt CO_2-neutralt brændsel er biomasse interessant til varme- og energiproduktion. Fluid bed forbrænding er grundet brændselsfleksibilitet samt høj forbrændingseffektivitet en lovende teknologi til anvendelse af biomasse. Imidlertid er nitrogenindholdet i forskellige biomasser variabelt og kan nå op til flere vægtprocent. Dette kan føre til væsentlig emission af nitrogenoxider, NO_X (NO og NO_2) og N_2O, som har skadelige virkninger på miljøet. NO_X fører til dannelsen af syreregn og fotokemisk smog, mens N_2O nedbryder ozonlaget og er en drivhusgas. I forbindelse med stramningen af lovgivningen for NO_X emission fra fast brændselsfyrede krafttværker er forståelsen af mekanismen for NO_X og N_2O emission fra fluid bed biomasseforbrænding samt udviklingen af effektive modforanstaltninger af væsentlig betydning.

I dette ph.d. projekt blev dannelse og reduktion af NO_X og N_2O under fluid bed forbrænding af biomasse undersøgt. Kontinuerlige forbrændingseksperimenter blev udført i en laboratorieskala fluid bed reaktor for at belyse påvirkningen af samfyring, brændselsegenskaber (nitrogen og mineralindhold) og driftsbetingelser (trinvis forbrænding, temperatur og gasfasesammensætning) på NO_X emission. Med udgangspunkt i de opnåede resultater blev en additiv-baseret teknik til samtidig reduktion af NO_X emission og bed agglomerering udviklet samt undersøgt. Derudover blev dannelse og reduktion af NO_X og N_2O under forbrænding af biomasse/affaldskoks i en laboratorieskala fixed bed reaktor undersøgt ved forhold tilsvarende fluid bed forbrænding.

Fluid bed enkelt- og samfyring af biomasse blev udført med og uden brug af trinvis lufttilsætning. Gassammensætningen blev målt igennem reaktoren og ved udgang. De undersøgte brændsler inkluderede fyrretræ, bøgetræ, hvedehalm, solsikkefrøskal, spildevandsslam og solsikkefrø. Resultaterne afslører, at omdannelsen af brændstofbundet nitrogen (brændsel-N) til NO faldt med en stigning i N-indholdet ved forbrænding i et enkelt trin. Dette kan være relateret til den større frigivelse af reducerende nitrogenforbindelser såsom NH_3 til gasfasen, hvormed termiske $DeNO_X$ reaktioner blev fremmet. En synergieffekt blev observeret under halm-spildevandsslam og halm-solsikkefrø samfyring under enkelt trins forbrænding, mens halm-solsikkefrøskal samfyring var additiv. Mekanismen af interaktionen under samfyring af halm og spildevandsslam blev belyst, hvilket viste, at ved et lavt indhold af aske i reaktoren (2-25 g) blev NH_3, frigivet fra spildevandsslam, i større grad brugt til at reducere NO. Efterhånden som asken fra spildevandsslam ophobede sig i reaktoren, steg NO emissionen på grund af katalytisk oxidation af NH_3 til NO. Under halmforbrænding steg den katalytiske effekt af spildevandsslamaske på NO dannende reaktioner med en lavere fremstillingstemperatur af asken og en bedre blanding af asken med halm. Under halm-solsikkefrø samfyring var udløbskoncentrationen af NO godt beskrevet fra det vægtede gennemsnit af de rene brændsler, mens NH_3 og NO koncentrationerne over beden var signifikant højere end de vægtede værdier. Trinvis lufttilsætning viste sig at være en effektiv metode til at minimere NO emission fra enkelt- og samfyring af biomasse. Derudover havde aske fra spildevandsslam kun lille effekt på NO_X dannelse ved trinvis lufttilsætning.

Påvirkningen af brændselsegenskaber og driftsbetingelser på NO_X emission blev undersøgt ved fluid bed forbrænding. Batch-forbrændingseksperimenter af fyrretræ, bøgetræ, hvedehalm, solsikkefrøskal, spildevandsslam og solsikkefrø afslørede, at omdannelsen af brændsel-N til NO faldt med stigende N-indhold tilsvarende observationerne fra kontinuerlig forbrænding. NO dannet ved flygtig gas forbrænding var generelt den største bidrager til den samlede NO emission. Dog blev op til 55% af NO dannet ved koksforbrænding for bøgetræ. Kontinuerlig fluid bed forbrænding af fyrretræ, halm, vasket halm samt kaliumberiget (KCl, K_2CO_3, and KOH) fyrretræ og vasket halm blev udført. Brændsel-N til NO omdannelsen var højere og CO emissionen lavere for vasket halm. Dosering af alle tre K-forbindelser til vasket halm øgede CO emissionen. KCl og KOH reducerede yderligere brændsel-N til NO, mens K_2CO_3 havde en ubetydelig indflydelse. Dosering af KCl til fyrretræ øgede CO emissionen uden at påvirke brændsel-N til NO, mens de andre K-forbindelser havde en ubetydelig effekt på de målte data. Den øgede CO og reducerede NO emission ved tilsætning af KCl var mere udtalt under trinvis lufttilsætning (forholdet mellem primærluft og total luft (λ_1/λ) lig 0,04) sammenlignet med forbrænding i et enkelt trin ($\lambda_1/\lambda = 1$). Grunden til dette blev tilskrevet KCl's evne til at nedbringe radikalkoncentrationen. Herudover blev påvirkningen af trinvis forbrænding undersøgt under kontinuerlig forbrænding af halm og solsikkefrøskal. Resultaterne viste et minimum i NO emissionen og brændsel-N til NO omdannelsen for λ_1/λ værdier mellem 0,5 og 0,75. Desuden steg brændsel-N til NO med stigende temperatur for halmforbrænding, mens brændsel-N til NO under KCl beriget vasket halmforbrænding steg og udjævnes med temperaturen. Tilsvarende blev den omvendte tendens i CO observeret. Brændsel-N til NO omdannelsen og CO emissionen var ikke påvirket af ændringer i bedsammensætningen (kvartssand, CaO og kaolin) ved $\lambda_1/\lambda = 1$ og primærgassammensætningen (N_2 og CO_2) ved $\lambda_1/\lambda = 0$ og 0,04 under halmforbrænding.

Anvendelsen af additiver til samtidig reduktion af NO_X emission og bed agglomerering blev undersøgt under fluid bed forbrænding af halm. Andre parametre, såsom brændselstype, additiv partikelstørrelse samt infødningsmetode og trinvis luftintroduktion, blev også studeret. Kaolin, CaO og $MgCO_3$ forhindrede defluidisering uden at ændre brændsel-N til NO omdannelsen under halmforbrænding, mens urea reducerede brændsel-N til NO uden at ændre defluidiseringstendensen. En NH-funktionalitet i additivet var nødvendig for at reducere NO_X emissionen. NH_4MgPO_4 og $AlNH_4(SO_4)_2$ forhindrede defluidisering, mens brændsel-N til NO blev reduceret med 40% i halm- og 30% i solsikkefrøskalforbrænding. Den lokale gassammensætning afslørede, at NH-holdige additiver frigav NH_3 over brændselsindløbet og/eller fluid beden. Nogle additiver (urea, $(NH_4)_2SO_4$, NH_4MgPO_4 og $AlNH_4(SO_4)_2$) favoriserede reduktionen af NO ved termisk $DeNO_X$, mens additiver, der indeholdt Fe ($(NH_4)_2Fe(SO_4)_2$, $NH_4Fe(SO_4)_2$, og $(NH_4)_3[Fe(C_2O_4)_3]$) eller fremskyndte defluidiseringen, dvs. inducerede dårlig opblanding ($(NH_4)_2HPO_4$), førte til øget NO emission over fluid beden og dermed en ubetydelig ændring i NO udløbskoncentrationen relativt til rent halmfyring. Ved forbrænding af halm og $(NH_4)_2SO_4$ faldt større partikler af $(NH_4)_2SO_4$ til beden, hvilket øgede koncentrationen af NH_3 over fluid beden og forlængede tiden før defluidisering. Til sammenligning var det ubetydeligt for brændsel-N til NO og defludiseringstendensen om additivet blev introduceret separat i pilleform eller forblandet med halm, hvilket muligvis er relateret til forskelle i frigørelsesmekanisme og -lokation. Derudover resulterede trinvis lufttilsætning ($\lambda_1/\lambda = 0.5$) i en 40% reduktion af brændsel-N til NO omdannelsen fra halmforbrænding, mens anvendelsen af additiver

under trinvis lufttilsætning øgede brændsel-N til NO omdannelsen en smule. Dette var forårsaget af den øgede oxidation af NH_3 i den sekundære luftstrøm. Akkumuleringen af solsikkefrøskalaske øgede NO og mindskede NH_3 koncentrationen over beden. Derudover blev de tidsafhængige koncentrationsvariationer dæmpet ved et højere askeindhold i beden. Dette blev tilskrevet den katalytiske effekt af asken på nitrogenkemien og den begyndende defluidisering af beden, som ledte til dårlig opblanding.

Dannelsen af NO og N_2O under forbrænding af koks fra rå og demineraliseret biomasse (fyrretræ, hvedehalm, affaldstræ, klid, solsikkefrø og bærme) blev undersøgt i en fixed bed reaktor. Det blev observeret, at omdannelsen af koks-N til NO faldt med en stigning i koks-N indhold. Da koks-N til NO ikke udviste nogen sammenhæng til NO reduktionsreaktiviteten af det undersøgte koks, blev det højere udbytte af N_2O for koks med højt N-indhold tilskrevet en medvirkende effekt. Indholdet af mineraler dominerede NO reduktionsreaktiviteten, hvilket korrelerede lineært med (K+Ca)/C molforholdet for koks med et lavt P indhold. Koks med et højt P indhold fulgte ikke korrelation muligvis på grund af dannelsen af mindre katalytiske aktive forbindelser såsom KPO_3. NO reduktionsreaktiviteten af de rå og demineraliserede koks korrelerede ikke med det indledende overfladeareal, porøsitet, koks-N indhold eller overfladefunktionalitet samt –indhold af nitrogen og oxygen. Under NO behandling blev overfladen af de undersøgte koks beriget med (-CN) og/eller (-CO) arter. Reaktiviteten af de akkumulerede (-CN) forbindelser mod NO reduktion kunne være anderledes sammenlignet med de allerede eksisterende (-CN) arter.

Omdannelsen af nitrogen under forbrænding af koks fra spildevandsslam, affaldsafledt brændsel (RDF) og halm, samt reaktionen mellem NO og disse koks blev undersøgt i en fixed bed reaktor. Reaktiviteten af spildevandsslam- og RDF-koks var henholdsvis en størrelsesorden og seks gange højere end halmkoks. Grunden til dette blev tilskrevet det større indhold af Ca og Fe i de affaldsbaserede koks. Den indledende reaktivitet af de anvendte koks korrelerede godt med (K+Fe+Ca)/C molforholdet. Reaktionen mellem koks og NO blev beskrevet ved et simpelt, koncentrationsvægtet første ordens udtryk. Dette blev brugt i en en-dimensionel, tidsafhængig, heterogen reaktor model, hvilket forudsagde omdannelsen af koks-N til NO under koksforbrænding med en rimelig præcision. NO reduktionsreaktiviteten af spildevandsslam- og RDF-koks oversteg reaktiviteterne af udvalgte kul- og biomasse koks fundet i litteraturen.

Dette studie har resulteret i en udvidet forståelse af omdannelsen af nitrogen under fluid bed forbrænding af biomasse. De observerede tendenser kan muligvis ekstrapoleres til praktiske forbrændingssystemer for at optimere design og operation til minimering af NO_X emission.

Contents

List of Figures

List of Tables

Abbreviations and Symbols

Abbreviations

BAT	Best Available Techniques
BET	Brunauer-Emmett-Teller
BJH	Barrett-Joyner-Halenda
Char-NO	NO formed from char combustion
DDGS	Dried distillers grains with solubles
Dfl./No dfl.	Defluidization/No defluidization
DKP	2,5-diketopiperazine
DM	Demineralized
Eq	Equation
FTIR	Fourier Transformed Infrared
ICP-OES	Inductively coupled plasma emission spectroscopy
ID	Internal Diameter
IZD	5-substituted-2,4-imidazolidinediones
MLE	Maximum Likelihood Estimation
N-5 or N5	Pyrrolic nitogen
N-6 or N6	Pyrridinic nitrogen
NO_X	NO and NO_2
N-Q or NQ	Quartenary oxygen
N-X or NX	Oxidic nitrogen
OW	Organic washed
phase-N	Nitrogen bound to phase, phase = volatile, fuel, biomass, char, tar, soot, and light gas
R	Reaction
RDF	Refuse Derived Fuel
SCR	Selective Catalytic Reduction
SEM-EDX	Scanning electron microscopy and energy dispersive x-ray
SNCR	Selective Noncatalytic Reduction
Volatile-NO	NO formed from volatile combustion
TGA	Thermogravimetric Analysis
WW	Water washed
XPS	X-ray Photoelectron Spectroscopy
XRD	X-ray Diffraction

Subscripts

0	Initial condition
b	Bulk, refers to that formed from combustion
C	Combustion
g/gas	Gas
in	inlet
int	Interstitial
mix	Mixture
out	Outlet
S	Straw
sf	Secondary fuel

Symbols

(-X)	-	Element(s) X bound to the char surface
A		Pre-exponential factor
A_J	-	Trace element effect – chain branching
A_J'	-	Trace element effect – chain terminating
A_C	-	Pre-exponential factor for the Arrhenius
B_J	-	Trace element effect – propagating, sensitizing
C	mol/m^3	Concentration
C_p	kJ mol^{-1} K^{-1}	Specific heat capacity
D_{ax}	m^2/s	Axial dispersion coefficient
$d_{p,mean}$	nm	Mean pore diameter
E_a	kJ/mol	Activation energy
f	-	Fraction
fa	-	Factor – catalytic or dilution
h	kJ m^{-2} s^{-1} K^{-1}	Gas-solid heat transfer coefficient
h_{react}	m	Reactor height
I_A	ppmv·s	Integrated area from a plot of concentration versus time
J	-	Trace species
k	m^3 mol^{-1} s^{-1}	Rate constant
k_{NO}	m^3 s^{-1} kgC^{-1}	Reduction rate constant from the char-NO reaction
k_{NOmax}	m^3 s^{-1} kgC^{-1}	Maximum in $k_{NO}(t)$, similar to transient k_{NO}
k_{eff}	kJ m^{-1} s^{-1} K^{-1}	Effective thermal conductivity
m	kg	Amount in weight
M	kg/mol	Molar mass
n	mol	Molar amount
r	mol m^{-3}_{gas} s^{-1}	Reaction rate
r’	mol kgC^{-1} s^{-1}	Reaction rate based on mass of carbon
R_g	m^3 Pa K^{-1} mol^{-1}	Gas constant
R_{NO}	-	Fractional conversion of NO
S	m^2/m^3	Volumetric solid surface area
SA	m^2/g	Specific surface area
t	s	Time
T	ºC or K	Temperature
u	m/s	Velocity
V_g	Nm^3/s	Volumetric gas flow – often given at normal conditions
V_P	cm^3/g	Pore volume
w	kg/kg	Weight fraction
W	kg C	Instanteneous carbon mass
x	m	Spatial coordinate
X	-	Instantaneous conversion during reduction experiments
y	mol/mol	Molar ratio

Greek letters

ΔH_R	kJ/mol	Reaction enthalpy
ε	m^3_{void}/m^3_{bed}	Bed void fraction
η	-	Conversion during combustion
λ	-	Total excess air ratio
λ_1	-	Primary gas excess air ratio
τ	s	Residence time

1 Introduction

Biomass as a renewable fuel does not contribute to a net increase in the CO_2 emission, which is one of the main reasons why it is highly desired to increase the share of biomass in heat and power production. However, the emission of nitrogen oxides, i.e. NO_X (NO and NO_2) and N_2O, is one of the major environmental concerns for biomass-fired heat and power plants, which may become especially troublesome for high-nitrogen biomass fuels. NO and NO_2 have been shown to contribute to the formation of acid rain and photochemical smog, while N_2O is a greenhouse gas and additionally leads to ozone depletion [1,2]. Moreover, exposure to NO_2 has been shown to have a harmful effect on human health [3]. As a result of the adverse effects of nitrogen oxides, rigorous and stringent environmental laws and regulations have been implemented for controlling their emissions [4]. The legislation in the European Union is to be further tightened in stationary combustion of coal and biomass, based on the reference documents for Best Available Techniques (BAT) [5,6]. For existing 100-300 MW_{th} combustion plants, the daily average NO_X emissions are to be limited from 250 mg/Nm^3 to 50-150 mg/Nm^3 for waste combustion and from 250 mg/Nm^3 to 100-220 mg/Nm^3 for biomass combustion [6–8].

Fluidized bed combustion offers a promising technology for biomass combustion with high fuel flexibility and energy efficiency [9]. The temperature in fluidized bed combustion is typically around 800-900ºC, lower than other combustion technologies such as pulverized fuel combustion [9,10]. The lower temperatures and presence of fuel-bound nitrogen (fuel-N) implies that the emitted NO_X is formed primarily from fuel-N, i.e. fuel NO_X, and the contribution of the thermal and prompt NO_X mechanisms is negligible [10–15]. While the fuel NO_X chemistry in combustion has been widely studied [16,17], several areas still contain unknowns and uncertainties.

The influence of ash forming elements on NO_X emissions are predominantly conducted under well-controlled conditions; consequently, data from practical systems, such as fluidized bed combustion of biomass are scarce. Moreover, contradictory results have been observed on the presence of a synergy effect on NO_X emissions during co-combustion. Studies on co-combustion mainly focus on the co-combustion of coal and biomass, and little work has been done on NO_X emissions in co-combustion of different biomass in fluidized beds. In most combustion studies, the information of NO_X emissions is obtained by measuring the outlet flue gas composition. Thus, the effect of local conditions on the N-chemistry is lacking. Hence, it is desirable to obtain an improved understanding of the NO_X chemistry during mono and co-combustion by local gas composition measurements. Based on the results, possible countermeasures may be proposed. The countermeasures for NO_X emissions generally target this area specifically, thereby opening up possibilities for novel techniques

such as the use of multifunctional additives to reduce NO_X emissions and bed agglomeration simultaneously.

While the gaseous nitrogen chemistry is fairly well established [17,18], the conversion of char-N to NO and N_2O is less understood, especially in the case of high-nitrogen biomass. Consequently, fundamental knowledge of NO and N_2O formation and reduction during biomass char combustion is lacking.

1.1 Project objectives

This PhD project aims at improving the current understanding of NO_X emissions from fluidized bed combustion of biomass. Specifically, this work focuses on

- the interaction effect on NO_X emissions during fluidized bed co-combustion of biomass.
- the influence of ash forming elements and operating conditions on NO_X and N_2O emissions in fluidized bed combustion of biomass.
- the effect of multifunctional additives on NO_X emissions and bed agglomeration in fluidized bed combustion of biomass.
- the formation and reduction of NO_X and N_2O during biomass and waste char combustion.

1.2 Structure of this thesis

Including the introduction, this thesis is divided into eight chapters.

Chapter 2: Background

This chapter provides an overview of the nitrogen conversion during combustion, including the fate of nitrogen during biomass pyrolysis, and the mechanisms of NO_X and N_2O formation and reduction during solid fuel combustion. NO_X and N_2O emissions from fluidized bed combustion of biomass were reviewed, summarizing the effects of fuel properties and operating conditions. In addition, techniques for control of NO_X emissions are introduced.

Chapter 3: NO_X emissions from fluidized bed mono- and co-combustion of biomass

This chapter presents experimental results from laboratory scale fluidized bed mono- and co-combustion of biomass. The investigated fuels include various types of biomass with a wide range of nitrogen contents, pine wood, beech wood, straw, sunflower husk, sewage sludge, and sunflower seed. The presence of a synergy effect between the fuels during co-combustion was investigated, along with the influence of air staging on the NO_X and N_2O emissions. The obtained results were described based on a more thorough investigation of the formation and reduction of NO_X and N_2O within the reactor.

Chapter 4: Influence of fuel properties and operating conditions on NO_X emissions

This chapter summarizes the experimental results on the influence of fuel properties and operating conditions on NO_X emissions during fluidized bed combustion. Batch fluidized bed combustion experiments were conducted to separate NO_X from volatile and char combustion. In addition, the influence of ash forming elements were investigated by continuous fluidized bed combustion of washed and potassium doped biomass. The studied fuels included pine wood, raw and washed straw, and potassium (KCl, KOH, K_2CO_3) doped pine wood and washed straw. Moreover, the influence of air-staging, temperature, gas phase composition, and type of bed material on the NO_X emissions from raw fuel combustion was investigated.

Chapter 5: Additives against NO_X emissions and bed agglomeration

This chapter summarizes the experimental results on the influence of solid additives on NO_X emissions and bed agglomeration. The employed additives were divided in three categories based on their hypothesized effect, namely de-agglomeration (kaolin, coal fly ash, CaO, $MgCO_3$, clay), NO_X reduction (urea), and multifunctional (NH_4MgPO_4, $(NH_4)_2HPO_4$, $(NH_4)_2SO_4$, $(NH_4)_2Fe(SO_4)_2$, $NH_4Fe(SO_4)_2$, $AlNH_4(SO_4)_2$, $(NH_4)_3[Fe(C_2O_4)_3]$). The performance of the additives were investigated during air un-staged straw combustion. The most effective additives against bed agglomeration and NO_X emissions were additionally investigated during air staged straw and un-staged sunflower husk combustion.

Chapter 6: Formation of NO and N_2O during raw and demineralized biomass char combustion

This chapter describes the conversion of char nitrogen during biomass char combustion in a fixed bed reactor. The fuels included pine wood, straw, waste wood, bran, sunflower seed, and DDGS. Demineralization was performed to investigate the influence of ash forming elements. The formation of nitrogen combustion products and the reduction of NO over char were investigated.

Chapter 7: Reactivity of sewage sludge, RDF, and straw chars towards NO

This chapter presents the experimental result on the reduction of NO over biomass and waste chars. Demineralization was employed to describe the influence of ash forming elements on the NO reduction reactivity, which was correlated to the char chemical and physical properties. The obtained NO reduction reactivity was used in a simplified, one-dimensional, transient packed bed reactor model to predict the conversion of char nitrogen to NO. Lastly, a discussion of the reaction rate expression and a comparison of the obtained results with those in literature were made.

Chapter 8: Concluding remarks and future work

In this chapter, a summary of the main conclusions from this PhD and suggestions for future work are presented.

2 Background

This chapter provides an overview of the nitrogen conversion in fluidized bed combustion of biomass. The partitioning of nitrogen during biomass pyrolysis, and the formation and reduction mechanisms of NO_X and N_2O in combustion are reviewed, along with the influence of fuel properties and operating conditions on NO_X and N_2O emissions in fluidized bed combustion. Moreover, several techniques for NO_X reduction are described.

2.1 Biomass fuels

Biomass is a complex heterogeneous material composed of organic and inorganic matter. The organic combustible fraction is mainly composed of cellulose, hemicellulose, and lignin, whereas the inorganics can be present as mineral species (e.g., phosphates, silicates, chlorides) or organically bound ions (e.g., Ca-Mg-K-Na oxalates) [19]. Biomass wastes may additionally contain other polymeric constituents such as plastics, textiles, etc. [20,21]. In most biomass, the nitrogen and sulfur are predominantly bound in proteins and amino acids [22–28]. In addition, some nitrogen exist in DNA, RNA, alkaloids, porphyrin, and chlorophyll [22]. In general, protein nitrogen accounts for 50-100% of the total nitrogen in biomass [29,30]. The elemental composition of biomass is variable and depends on external factors such as climate, growth, and harvest conditions. Biomass fuels can commonly be classified into several categories listed below, separated by their biological diversity, source, and origin [19]. The typical composition and variability of selected biomass fuels from each category is summarized in Table 2.1.

- Wood and woody biomass, e.g., bark, wood chips, sawdust
- Herbaceous and agricultural biomass, e.g., bamboo, straw, sunflower seed
- Aquatic biomass, e.g., algae, seaweed
- Biomass wastes
    - Animal and human biomass wastes, e.g., chicken litter, manures
    - Industrial wastes, e.g., refuse derived fuel, waste wood, sewage sludge

Table 2.1: Properties and composition of different biomass. The data were compiled from multiple sources [29,31–38].

	Wood		Cereal straw		Dried algae		Dried sewage sludge	
	Mean	**Variation**	**Mean**	**Variation**	**Mean**	**Variation**	**Mean**	**Variation**
Moisture [wt% w.b.]	45	20-60	14	8-23	6.32	5.3-7.1	10.9	3.6-19
LHV [MJ/kg d.b.]	19.3	18.3-20.3	17.8	17.2-18.1	14.26	5.5-19.5	11.9	10-13
Volatiles [wt% d.b.]	81	70-85	78	75-81	67.8	42-75	51.2	45-57
Ash [wt% d.b.]	1.0	0.3-6	4.5	2-7	27.16	16-66	39.3	19-51
Chemical composition, wt% d.b.								
C	50	49-52	47.5	47-48	36.44	15-48	29.3	24-33
H	5.8	5.2-6.1	5.9	5.4-6.4	5.3	3.1-6.5	4.2	3.8-4.6
N	0.3	0.1-0.8	0.7	0.3-1.5	4.9	1.24-11.0	4	3.5-4.4
O	43.3	40-46	43.0	41.0-45.0	42-48	35-55	22.1	12-38
S	0.05	<0.1	0.15	0.1-0.2	0.8	0.17-1.44	1.1	0.9-1.3
Cl	0.02	<0.1	0.4	0.1-1.1	0.9	0.4-2.0	0.07	<0.2
Si	0.1	<0.1	0.8	0.1-1.5	1.9	0.35-6.4	6.4	4.5-8.5
Al	0.015	<0.1	0.005	<0.03	1.8	0.01-2.5	2.4	1.8-3.4
Fe	0.015	<0.1	0.01	<0.03	0.6	0.06-2.7	4.7	1.0-8.5
Ca	0.2	0.1-0.9	0.4	0.2-0.5	1.6	0.26-3.3	3.7	1.8-6.3
Mg	0.04	<0.1	0.07	0.04-0.13	0.9	0.6-1.19	0.5	0.3-0.8
P	0.02	<0.1	0.08	0.03-0.2	0.5	0.2-0.8	3.4	2.2-4.0
Na	0.015	<0.1	0.05	<0.03	0.6	0.2-1.5	0.4	0.2-0.8
K	0.1	0.05-0.4	1.0	0.2-1.9	1.2	0.8-2.1	0.6	0.4-0.9

As shown in Table 2.1, the nitrogen content in different biomass can vary significantly, from 0.1wt% in woody fuels to several wt% in agricultural, aquatic, and waste biomass. In Figure 2.1, the range of nitrogen on the basis of the lower heating value is given for selected biomass fuels and coal. The nitrogen content in the wood is lower than while the straw is comparable to that of coal. However, some agricultural, aquatic, and waste biomass can exhibit nitrogen contents much higher than that of coal. In combination with the tightening emission regulations, the emissions of NO_X and N_2O from biomass combustion could be significant, thereby highlighting the importance of understanding and improving NO_X and N_2O emission control.

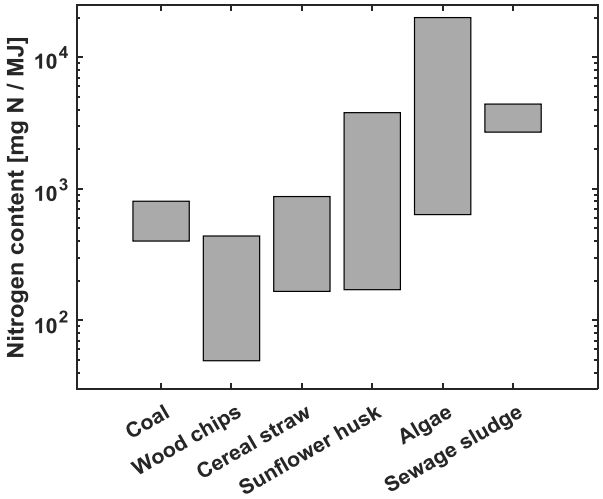

Figure 2.1: Fuel nitrogen content (mg N/kg fuel) over lower heating value (MJ/kg fuel). The data for wood chips, cereal straw, algae, and sewage sludge were calculated from Table 2.1, while coal and sunflower husk data were extracted from [34] and [39], respectively.

2.2 Thermal conversion behavior of biomass-N

When exposed to high temperatures, the nitrogen in biomass (biomass-N) is partitioned between the volatile (volatile-N) and char (char-N), simplistically demonstrated in Figure 2.2. The volatile-N consists mainly of light gas-N (NH_3, HCN, and HNCO) and tar-N. Tar-N and char-N can further decompose, forming light nitrogen species and aliphatic side chains, while the solid matrix undergoes ring condensation. In the presence of oxygen, the nitrogen in the light gases, soot, and char participate in a series of oxidation and reduction reactions, thereby forming nitrogen products such as NO, NO_2, N_2O, and N_2 [16]. The following sections focus on the conversion of biomass-N to NO_X precursors during pyrolysis along with the functionality of the precursors in the volatile and char phases.

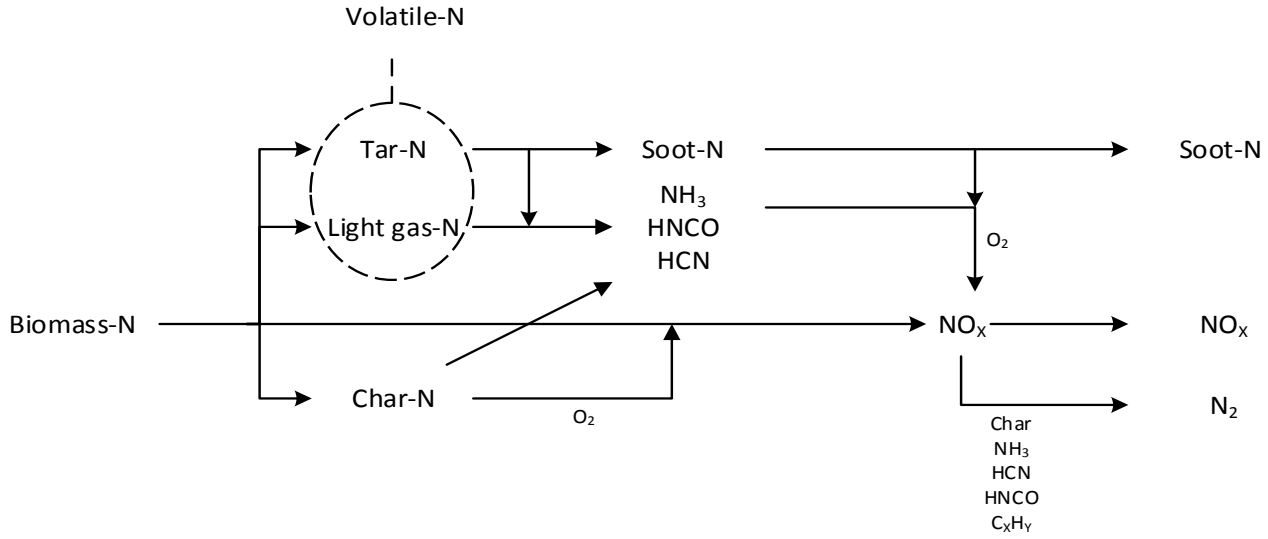

Figure 2.2: Simplified diagram showing the thermal conversion of biomass nitrogen. Inspired by [40].

Figure 2.3a shows the fraction of fuel nitrogen retained in the char after devolatilization of biomass using a variety of techniques [26,41–45]. In general, the release of volatile-N from biomass initiated at 200-300°C. At low temperatures, nitrogen was preferentially retained in the char, while at higher temperatures, nitrogen was released due to the increased rate of bond breakage. At 600°C, as much as 60-90% of fuel nitrogen was released as volatile-N. In selected cases, an increase in the char-N retention was observed at temperatures above 800°C. This was especially prominent for low-nitrogen chars and attributed to the uptake of purge N_2 and volatile-N by char in a high temperature and inert atmosphere. The char-N from N_2-recapture exhibited a higher propensity for forming NO during combustion [42]. The capture of N_2 by char has further been supported by density functional theory calculations, showing a possible pathway for this process [46]. However, additional studies are necessary to elucidate the relevance, possibility, and mechanism behind N_2 uptake by char. In addition to fuel type and temperature, nitrogen was preferentially retained in the char from solid fuel pyrolysis at short particle residence time [47–50] and low heating rate [42,51,52]. While a short residence time would reduce the extent of reaction, several explanations have been suggested for the influence of heating rate. A low heating rate may favor the formation pathway for char-N formation over volatile-N [42,53] or increase the importance of nitrogen recapture by char within the particle [16]. A low heating rate would result in longer gas residence time in the particle, thereby enhancing char-N formation by recombination of the volatile-N to the solid phase. This would additionally explain the increasing char-N retention at higher pressures and for larger particles [51,54,55]. Of the ash forming elements, Ca increased the nitrogen retention in char by inhibiting protein decomposition, while Na enhanced protein decomposition [56]. While K may promote char formation [57], the char-N retention decreased by the addition of KOH to coal [58] and straw [59].

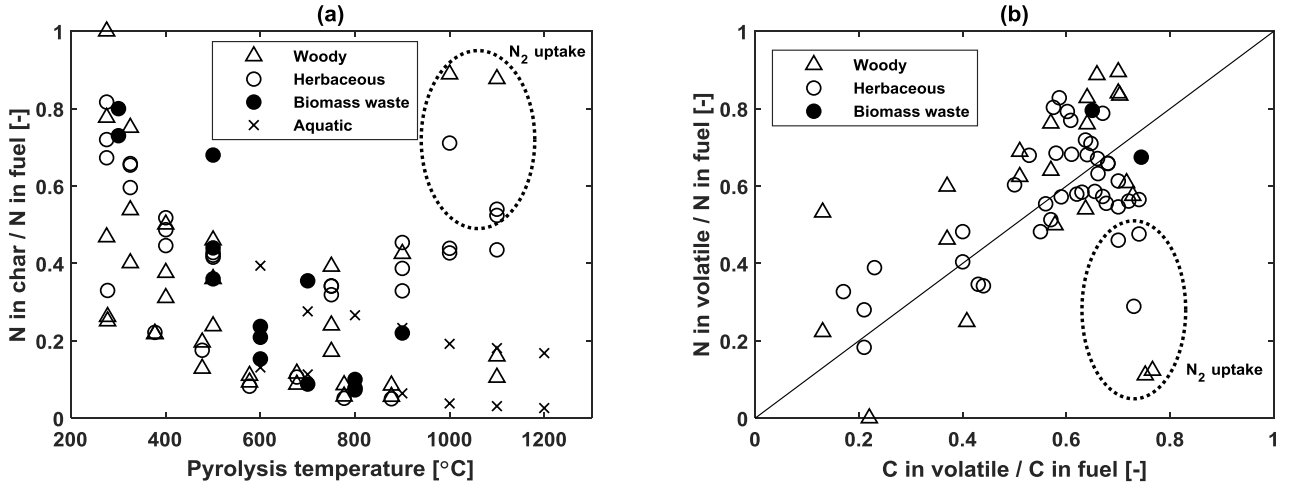

Figure 2.3: Retention of nitrogen in char of different biomass fuels at varying pyrolysis temperatures (a). Data compiled from [26,41–45]. Conditions: heating rate: 0.2-10^3 K/s, particle size: <150 µm-4 mm, residence time: 4-300 min. Fraction of volatile nitrogen against fraction of volatile carbon for different biomass fuels (b). Data compiled from [42,60–62]. Conditions: heating rate: 0.3-100 K/s, particle size: 200 µm-3 mm, residence time: 10-25 min.

As observed from Figure 2.3b, the release of nitrogen from biomass, i.e. fraction of volatile-N, is fairly well correlated with the release of carbon, as both elements participate in char stabilization. In addition, the presence [63,64] and absence [55] of a correlation between the fraction of volatile-N

and the total volatile matter of the fuels have been reported. These discrepancies may arise due to the differences in O and H content of fuels, since these elements predominantly release as volatiles [55].

2.2.1 Light gas-N from model compound pyrolysis

The release and speciation of nitrogen in the light gaseous phase during biomass pyrolysis is conceivably related to the functionalities of nitrogen in the fuel. Consequently, proteins and amino acids have been employed in model compound pyrolysis studies to gain insight into the pyrolysis behavior of biomass. During protein and amino acid decomposition a large number of reactions may occur simultaneously. Some of the most important reactions are presented in the simplified scheme in Figure 2.4 [29,30,65,66]. The primary pathways for amino acid/protein decomposition are decarboxylation and dehydration. The product of decarboxylation is an amine, while dehydration forms cyclic amides, the most common being 2,5-diketopiperazine (DKP). In comparison to decarboxylation and dehydration, the contribution from deamination was small [29]. Consequently, it has been suggested that NH_3, HCN, and HNCO are not primary but instead secondary products of amino acid/protein pyrolysis [29,67]. Numerous pathways exist for the secondary decomposition of DKP, which may form nitriles, imines, pyrolline, hydantoins, and α-lactam [29]. The final product from DKP decomposition is HCN, but also some NH_3 and HNCO may be formed. The cracking of amines and amides presumably forms NH_3. In addition, cross-linking reactions provide important pathways for the stabilization of the residue from protein pyrolysis and thereby favor char formation. One of the products of cross-linking reactions is 5-substituted-2,4-imidazolidinediones (IZD), which may further decompose to HCN and HNCO. Char formation was favored for polar amino acid side chains compared to nonpolar side chains, due to enhanced cross-linking reactions in the former [22,30].

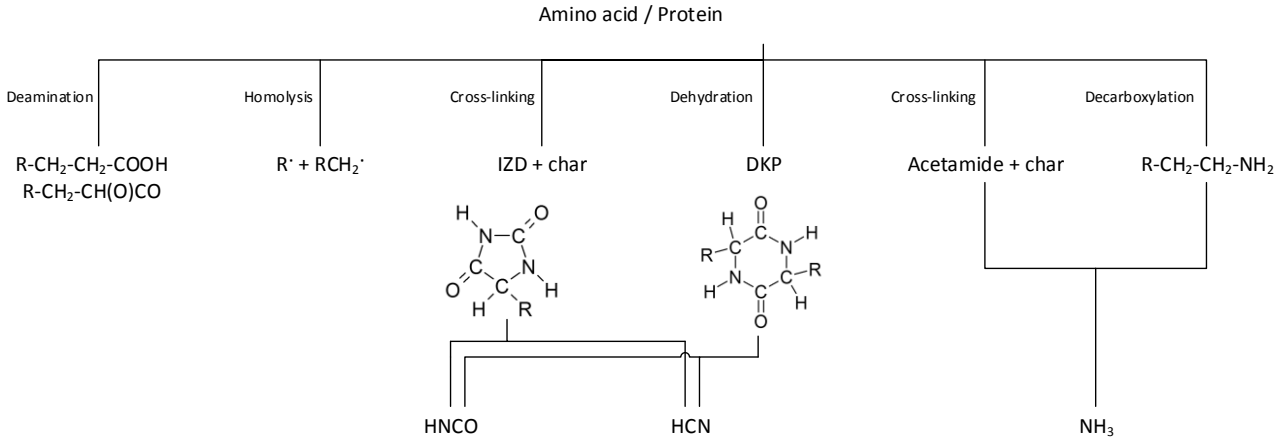

Figure 2.4: Simplified diagram of some amino acid/protein decomposition pathways during pyrolysis. Figure was inspired by [29,30,65,66].

Several studies have investigated the nitrogen product distribution from model compound pyrolysis. Different compounds favor distinct decomposition pathways and thereby differ in the nitrogen product distribution from pyrolysis. Some amino acids and proteins predominantly decomposed to NH_3, while in other cases HCN was the major product [22,23,68,69]. The NH_3/HCN and HNCO/HCN

ratios decreased with increasing temperature, due to the facilitation of thermal cracking reactions leading to HCN [23]. The presence of cellulose, hemicellulose, and lignin changed the preferred decomposition pathway and thereby affected the NH_3/HCN ratio from model compounds pyrolysis [70,71]. In the case of proline and glutamic acid, the presence of hemicellulose inhibited, while lignin promoted the conversion of nitrogen to NH_3 [71]. In addition, mineral matter may influence the decomposition pathway of different model compounds differently [72]. Ca increased the HCN yield at the expense of NH_3 during DKP and leucine pyrolysis, while it promoted both NH_3 and HCN in phenylalanine and aspartic acid pyrolysis [72,73]. The presence of K favored NH_3 during aspartic acid pyrolysis and HCN during leucine pyrolysis [72]. Fe [74] and red mud [75] decreased the yield of NH_3 by catalyzing the thermal decomposition to N_2. Moreover, zeolite catalysts increased the formation of NH_3 by altering the preferred reaction pathway during pyrolysis [76,77]. The presence of O_2 during pyrolysis promoted thermal decomposition reactions, thereby increasing the formation of NO, HNCO, and to some extent HCN. CO_2 decreased the yields of HNCO and HCN, presumed to be due to the suppression of DKP formation [29,78]. In fluidized bed pyrolysis of various model compounds, the presence of a OH functionality was noted to increase the formation of NH_3, most likely by the hydrogenation of HCN by R2.1, favored at low oxygen concentrations [79,80].

$$HCN \overset{+OH}{-} HNCO \overset{+H}{\rightarrow} NH_2 \overset{+H,H_2O}{-} NH_3 \qquad \text{R2.1}$$

2.2.2 Light gas-N from biomass devolatilization

The light gas-N species from biomass pyrolysis generally consists of HCN, NH_3, HNCO, and N_2 [68,75,81]. Besides these, trace amounts of NO_X have been reported, due to the high content of oxygen in biomass [40,55,82]. The NH_3/HCN ratio from high heating rate pyrolysis of different biomass is summarized in Figure 2.5 [23,24,88–90,43,63,82–87]. It has been widely accepted that the NH_3/HCN ratio from biomass pyrolysis is higher than that of coal [18]. However, in several studies HCN was the dominant nitrogen species in the gas phase. Hence, it is difficult to predict the speciation of nitrogen in the gas phase without experimentation. The ratio of NH_3/HCN generally decreased with temperature, which was attributed to the relative increase in the rate of thermal cracking reactions forming HCN [91] and the thermal decomposition of NH_3 to N_2 and H_2 [92]. Moreover, lower heating rates and larger particle sizes favored NH_3 over HCN, in consequence of the enhanced hydrogenation of HCN on the char surface as it diffuses out of the particle (R2.1) [16,85,91,93]. Additionally, the NH_3/HCN ratio was suggested to depend on the fuel-O/fuel-N [84,94] and fuel-H/fuel-N ratio [95]. In contrast to the elemental ratios, it was suggested that the functionality of nitrogen is determining for NH_3/HCN ratio [23]. At batch conditions resembling that of grate combustion, the NH_3/HCN ratio correlated reasonably well with the fuel-N content [32]. In comparison to NH_3 and HCN, HNCO was a minor product of biomass pyrolysis, which became increasingly important at lower temperatures [22,23,68] and possibly at lower H_2O concentration [85]. In terms of gas atmosphere, O_2 increased HCN and HNCO, and decreased NH_3 formation, in consequence of the facilitation of thermal cracking of heterocyclic structures by O_2. The presence of CO_2 suppressed HNCO formation while decreasing the HCN and increasing the NH_3 yield. This was explained by an increase in H radicals and the consumption of HCN-producing (-CN) sites during gasification of H-rich char [78]. H_2O

increased NH_3 while decreasing HCN yield, explained by the promotion of hydrogenation of volatile-N and char-N compounds [96–98]. In addition, the presence of acetone decreased NH_3 yield, as acetone reacts with NH_3 to produce binary clusters or amine [56]. Ash forming elements can additionally affect the speciation of nitrogen during solid fuel pyrolysis either by gas-solid and/or solid phase reactions [16], the effect of which seems to be temperature dependent. At temperatures between 500-600ºC, sewage sludge ash increased the retention of nitrogen in the char compared to demineralized sewage sludge, while at 600-800ºC, more volatile nitrogen was released in which HCN was suppressed and NH_3 promoted [99]. Ca and K increased NH_3 and N_2 formation at the expense of char-N, tar-N, and HCN [58,100–102]. Fe promoted N_2 formation at the expense of nitrogen in the light gases, char, and tar [103–105]. Si and Al additionally suppressed the conversion of fuel-N to HCN, HNCO, and NH_3, possibly due to a higher yield of N_2 [104]. Moreover, in high heating rate co-pyrolysis, a synergy effect of the nitrogen speciation and release was reported [106]. At lower heating rate, the synergy effect was only prominent in few cases containing a large content of ash forming elements [107].

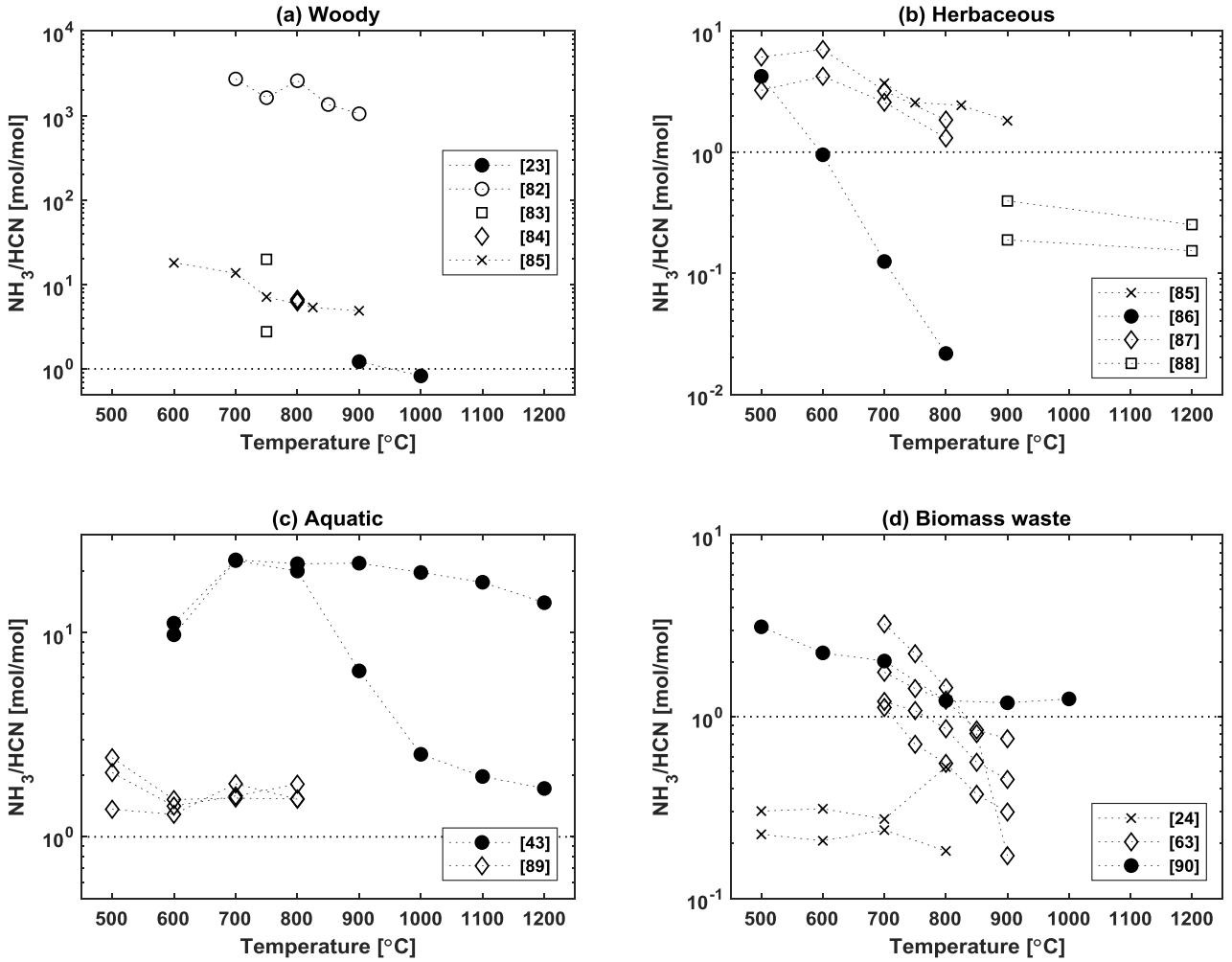

Figure 2.5: The NH_3/HCN ratio from pyrolysis woody (a), herbaceous (b), aquatic (c), and biomass waste (d) at varying temperatures using methods ensuring a high heating rate. The data were compiled from [23,24,88–90,43,63,82–87]. Conditions: heating rate: high heating rates, i.e., sample pushed into hot reactor or heated foil reactor, particle size: <300 µm-4 mm, residence time: 10 s-30 min.

2.2.3 Biomass char-N

During pyrolysis, cross-linking reactions stabilize the residual solid thereby forming char. The nitrogen functionalities present in both biomass and coal char are similar [26,56,62,108–113]. In general, the N-functionalities in char are amine/amide, pyrridinic (N-6), pyrrolic (N-5), quartenary (N-Q), and oxidic (N-X) nitrogen, exemplified in Figure 2.6 [114]. The relative abundance of N-6 and N-Q in chars increased with the severity of heat treatment, i.e., temperature and holding time, due to the thermal stabilities of these compounds [109,114,115]. During combustion by O_2 or gasification by CO_2, the functionality distribution changed such that N-Q decreased due to bond cleavage, while N-6 and N-5 functionalities increased [114]. Demineralization of coal chars post-pyrolysis showed little influence on the nitrogen distribution in the chars [110], while a slight change in the functionality was observed when demineralizing straw prior to charring [62].

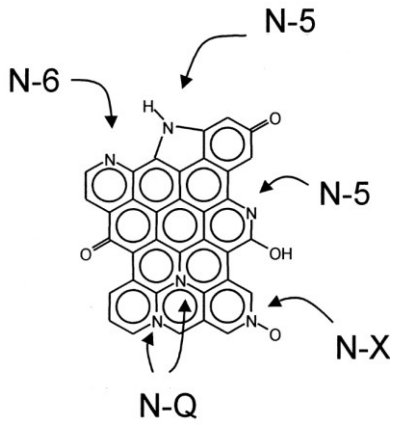

Figure 2.6: Illustration showing the nitrogen functionalities in char [114].

2.2.4 Biomass Tar-N and soot-N

The term tar-nitrogen encompasses a large number of aliphatic and aromatic compounds containing nitrogen. The nitrogen in biomass tar generally exhibit similar functionalities as the char, i.e. amine, nitrile, and heterocyclic bound nitrogen [69,90]. The functionalities of biomass tar-N seem to be similar to that of coal tar with differences in the relative distribution of these compounds [116,117]. During the secondary stage of pyrolysis, the tar decomposes thereby releasing a majority of its nitrogen in the form of soot-N, NH_3, and HCN, depending on the preferred decomposition pathway [16]. As a result of thermal cracking, soot particles generally consist of smaller chemical compounds, e.g. various polyaromatic hydrocarbons, alkanes, furans, benzofurans, nitrils and more, some of which are demonstrated in Figure 2.7 along with possible tar-N constituents [118]. Once formed, the soot-N can participate in NO_X reduction, be oxidized to NO_X, or escape the reactor with the flue gas [16]. Depending on the pyrolysis technique, the amount of tar-N could be considerable, e.g. in pyrolysis employing high heating rate and short gas residence time at temperatures around 400-600ºC [119,120]. At temperatures above 500-600 ºC and long gas residence times, the thermal cracking reactions of tar are promoted, thereby increasing soot-N and light gas-N [30]. Hence, the yield of tar-N may exhibit a maximum as a function of temperature [93,121,122]. In addition, the yield of tar was lower for larger particles, due to the intraparticle conversion of tar [16]. At higher heating rates

depending on the Biot number, the propensity for dehydration and other cross-linking reactions, leading to char formation and stabilization, was diminished, thereby increasing the yield of tar [123–125]. However, the influence of the heating rate is not always consistent [24].

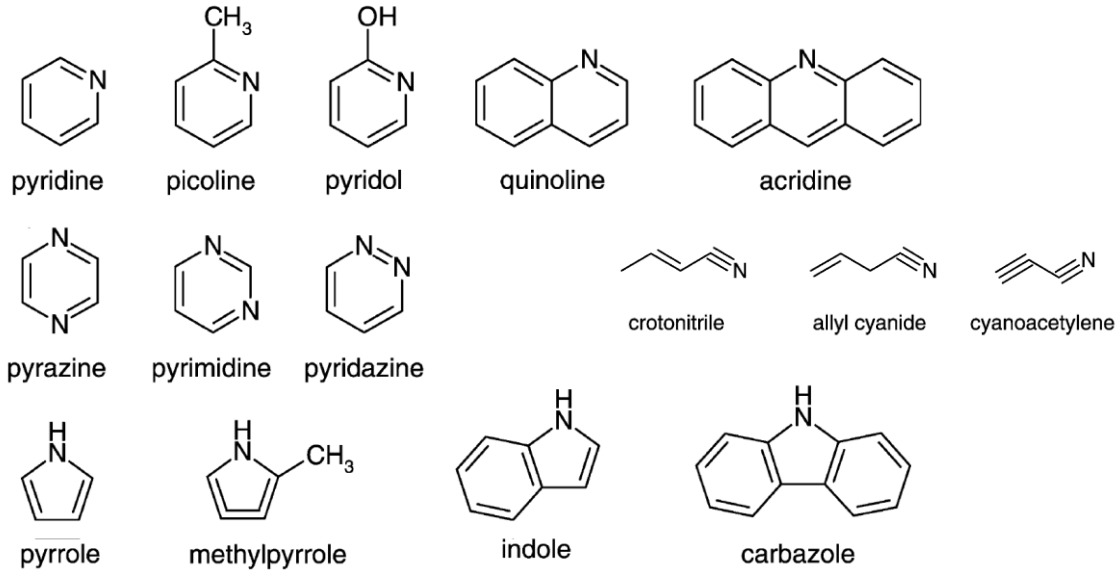

Figure 2.7: Selected nitrogen containing aromatic and aliphatic compounds, possibly formed during combustion [16].

2.3 NO_X formation and reduction during combustion

The final NO_X and N_2O emissions from combustion are determined by the competing NO_X and N_2O formation and reduction reactions. Three pathways exist for the formation of NO_X in combustion processes, termed thermal, prompt, and fuel NO_X. The major steps in the production of NO_X from each of these mechanisms are demonstrated in the simplified reaction path diagram shown in Figure 2.8. The thermal NO or Zeldovich mechanism involves the attack of an oxygen atom on the triple bond of N_2. Thermal NO requires high temperatures (>1300ºC) and is important in high temperature gas or pulverized fuel combustion [17]. Prompt NO is initiated by the attack of CH_i radicals on N_2, thereby forming intermediates that can further be oxidized to NO. In solid fuel combustion, this mechanism could be of importance for high-volatile fuels with low nitrogen content [16,126–128]. The third mechanism involves the formation of NO from fuel-N by volatile and char oxidation. Exposed to high temperatures, the nitrogen in the fuel is converted into intermediates (NH_i, NCO, and CN), which by oxidation form NO, N_2O, or N_2. Due to the lower temperatures and presence/abundance of fuel-N in fluidized bed combustion of solid fuels, the general consensus is that thermal and prompt NO_X can be neglected; hence, the major contributor to NO is from fuel-N [10–15]. The following review focuses on the formation of NO and N_2O from fuel-N and their simultaneous reduction by gas phase or gas-solid reactions. The gas phase reactivity is described by radical chemistry, the importance of which in fluidized bed combustion has previously been described [94,129].

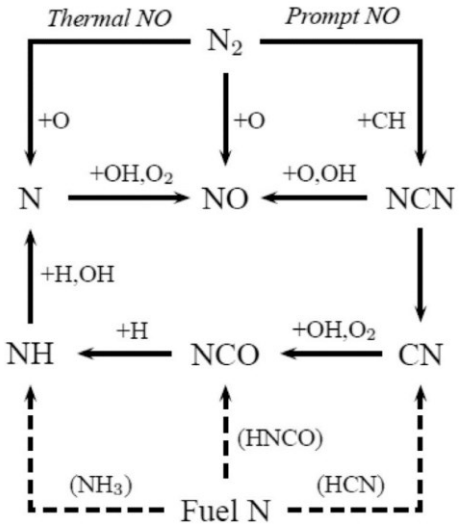

Figure 2.8: Simplified scheme showing the formation of NO by the thermal, prompt and fuel NO_X mechanisms [17].

2.3.1 Light gas-N oxidation

2.3.1.1 NH_3 oxidation

The major products of NH_3 oxidation are NO and N_2 with a lesser amount of N_2O [130,131], demonstrated by the reaction pathway diagram in Figure 2.9. NH_3 initially undergoes H abstraction by the O/H radical pool producing NH_2, which may undergo further H abstraction forming NH and N. The pathway for hydrogen abstraction becomes of increasing importance at higher temperatures. The NH_i radicals can subsequently react with O, OH, or O_2 forming NO, or with NO leading to the formation of N_2 and possibly N_2O. The competition between these reactions determines the selectivity for forming NO or N_2 from NH_3 oxidation [17]. The oxidation of CH_4 doped with NH_3 showed that the stoichiometry had a strong impact on the NO formation. At fuel-rich conditions, NH_3 oxidation was initiated at 850 ºC, but the reaction rate was slow, and preferentially formed N_2. At fuel-lean conditions, NH_3 was depleted around 775 ºC with an increasing amount of NO being formed as temperature increased. The presence of CH_4 provided additional pathways during NH_3 oxidation [132]. Moreover, the presence of NO desensitized the initiation of NH_3 oxidation which commenced at around 775 ºC [17].

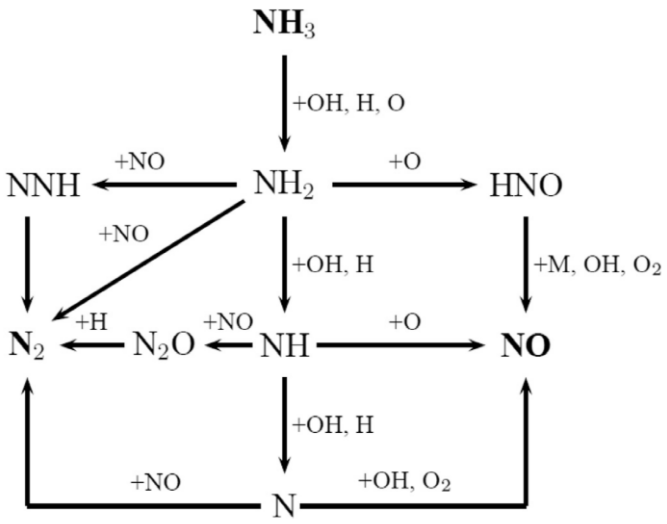

Figure 2.9: Diagram of the reaction pathways during NH_3 oxidation [17].

2.3.1.2 HCN oxidation

The main nitrogen products of HCN oxidation are NO, N_2O, and N_2 [130,131]. Figure 2.10 illustrates the reaction pathway diagram of HCN at fuel-lean conditions. The reaction of HCN with the O/H radical pool forms NCO either directly or through CN. The subsequent reactions of NCO determines the selectivity of the nitrogen products. In the absence of CO and abundance of O_2 and H_2O, OH becomes the dominant chain carrier by the branching sequences demonstrated in R2.2-R2.3. Consequently, HCN is initially converted to CN followed by the production NCO. At lower temperatures, NCO reacts with H_2O to form HNCO, while at higher temperatures the production of NCO from HNCO and the oxidation of NCO to NO becomes of increasing importance. In the presence of combustibles such as CO, the sequence R2.4 to R2.2 becomes a source of radicals, thereby

shifting the HCN oxidation chemistry to lower temperatures, while suppressing HNCO formation. As CO reacts rapidly with OH, the importance of reactions involving the OH radical decreases. The increasing O-radical concentration increases the relative importance of the reactions of this with HCN and NCO thus forming a large quantity of NO from NCO. At high temperature, fuel-rich conditions, HCN is quickly equilibrated with HNC and partially equilibrated with CN. Once produced the HNC accounts for the majority of HCN consumption by reacting with OH, forming HNCO, which is then rapidly fed to the amine pool, finally forming NH_3 (R2.5-R2.8). Under fuel-lean conditions, the importance of HNC is smaller [17,133].

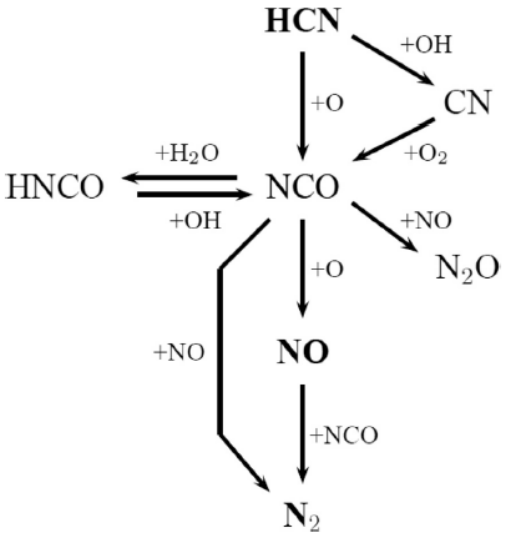

Figure 2.10: Reaction path diagram showing the oxidation pathways of HCN under fuel-lean conditions [17].

$$H + O_2 \rightarrow O + OH \quad \text{R2.2}$$

$$O + H_2O \rightarrow OH + OH \quad \text{R2.3}$$

$$CO + OH \rightarrow CO_2 + H \quad \text{R2.4}$$

$$HCN + M \text{ or } H \rightleftarrows HNC + M \text{ or } H \quad \text{R2.5}$$

$$HNC + OH \rightarrow HNCO + H \quad \text{R2.6}$$

$$HNCO + H \rightleftarrows NH_2 + CO \quad \text{R2.7}$$

$$NH_2 + H_2 \rightleftarrows NH_3 + H \quad \text{R2.8}$$

2.3.1.3 HNCO oxidation

The products of HNCO oxidation are NO, N_2O, and N_2. In the absence of CO, the oxidation of HNCO is slow at temperatures below 1030ºC. In the presence of CO, the replenishment of the radical pool by chain branching, enhances the rate of HNCO oxidation, the mechanism of which is shown in Figure 2.11. HNCO is primarily consumed by OH forming NCO, which then participates in a similar oxidation scheme as HCN. In addition, HNCO can react with H, O, H_2O or O_2 thus adding into the amine pool [17].

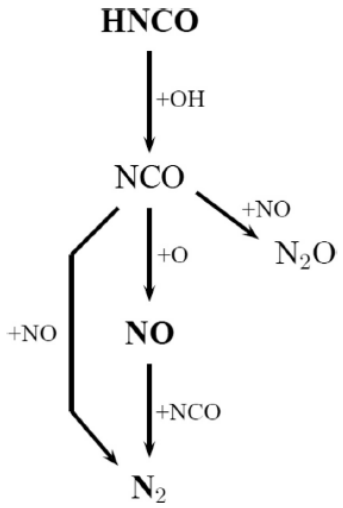

Figure 2.11: Reaction pathway diagram showing the oxidation of HNCO in fuel-lean conditions [17].

2.3.2 Char-N oxidation

A wide range of nitrogen products have been reported from biomass char combustion, including NO, N_2O, N_2, HCN, NH_3, and HNCO [16]. Of these, NO and N_2 were the major products from char-N oxidation [16,134], while N_2O increased in importance for high-nitrogen chars [62,135] and at lower temperatures [16]. The emissions of NO and N_2O from char-N combustion are determined by the simultaneous formation and reduction reactions. Both homogeneous and heterogeneous mechanisms have been reported for the formation of NO and N_2O during char combustion. The relative importance of these pathways has yet to be elucidated [136]. The heterogeneous formation of NO and N_2O by reaction of organically bound nitrogen with O_2 is demonstrated by R2.9-R2.12.

$$O_2 + (\text{-C}) + (\text{-CN}) \rightarrow (\text{-CO}) + (\text{-CNO}) \quad \text{R2.9}$$

$$(\text{-CNO}) \rightarrow NO + (\text{-C}) \quad \text{R2.10}$$

$$(\text{-CN}) + (\text{-CNO}) \rightarrow N_2O + 2\,(\text{-C}) \quad \text{R2.11}$$

$$NO + (\text{-CNO}) \rightarrow N_2O + (\text{-C}) \quad \text{R2.12}$$

Here, (-CX) denotes a carbon surface complex of either nitrogen or oxygen, while (-C) is a free carbon active site. In the homogeneous mechanism, HCN or HNCO is released during char oxidation, the reactions of which were described in Section 2.3.1.2 and 2.3.1.3, respectively. The fractional conversion of char-N to NO increased with increasing temperature up to 800-1000 ºC, above which the char-N to NO conversion decreased [16]. This trend was attributed to the relative effect of temperature on NO formation (char + O_2) and reduction (char + NO). At lower temperature, the formation and selectivity of NO was higher, while at higher temperatures and for larger particles the reduction of NO (R2.23-R2.30) was favored due to diffusion limitations of the reaction between char and O_2 [16,137]. At temperatures relevant for fluidized bed combustion (800-900 ºC), an increase in O_2 decreased the char-N to NO conversion [138], while a negligible effect was observed at higher temperatures [16]. This has additionally been attributed to the increasing importance of diffusion

[138] or changes in preferred pathways [16] at higher temperatures. However, the importance of O_2 at fluidized bed combustion temperatures is not always prominent [139–141]. In comparison, the conversion of char-N to N_2O decreased with an increase in O_2 and temperature [16,140]. At 1200ºC, the conversion of coal char-N to NO was between 70-80% at fuel-lean conditions and 30-40% at fuel-rich conditions [131,142]. During combustion of small, highly devolatilized char particles at single particle conditions, the coal char-N to NO conversion was between 75-100%, while that of biomass was between 25-75%, implying a significant reduction of NO during biomass char combustion [143].

2.3.3 Tar-N and soot-N oxidation

Homogeneous and heterogeneous secondary tar reactions such as cracking, partial oxidation, and polymerization determine the fate of tar-N [144]. Studies on tar-N and soot-N collected from biomass pyrolysis are scarce. Consequently, the conversion of tar-N and soot-N is evaluated from the oxidation of model compounds of pyridinic, pyrollic, and amino functionalities, from which the main combustion products were NO, N_2O, and N_2 [16,79,145,146]. In some studies, the influence of the nitrogen functionality on the NO and N_2O formation was negligible [145], while in others a clear influence was observed. Aromatic nitrogen such as nitrobenzene and to some extent aniline exhibited a higher conversion to NO compared to that of amine and heterocyclic nitrogen [146].

2.3.4 NO reactions

2.3.4.1 Homogeneous reactions

NO formed during combustion can be reduced in the gas phase by amine or cyanide compounds. The selective non-catalytic reduction (SNCR) of NO using NH_3 as reducing agent is commonly termed Thermal DeNO$_X$. NH_2, formed from H abstraction of NH_3, may react with NO either directly or through the NNH intermediate to yield N_2 and possibly N_2O, demonstrated by R2.13-R2.18. The contribution of other NH_i radicals to the NH_3 oxidation reactions increases with increasing temperature. Figure 2.12 demonstrates the NO, NH_3, N_2O, and NO_2 concentrations against temperature at variable concentrations of CO, H_2O, and NH_3 using the detailed chemical kinetic model of Glarborg et al. [17]. The capability of the model to capture qualitative and quantitative trends in experimental data has been shown in the referred paper. Hence, purely modeling results are presented here to illustrate the gas phase chemistry interactions. At lower temperatures, no considerable reaction takes place due to the low residence time and reaction rate. At moderate temperatures, the reduction of NO dominates, while the oxidation of NH_3 becomes of increasing importance at higher temperatures. The presence of H_2O slightly shifts the reaction to higher temperatures due to its high collider efficiency ($H + O_2 + M \rightarrow HO_2 + M$) [17]. In a separate study, H_2O increased the NO removal efficiency during SNCR without shifting the optimum temperature range [147]. A higher concentration of NH_3 widens the window of NO reduction as the availability of NH_i increases, while CO narrows and shifts it to lower temperatures due to its influence on the radical pool by R2.2-R2.4. A similar shift in the NO reduction window to lower temperatures was observed for $C_XH_YO_Z$ additives (CH_4, C_2H_6, C_2H_4, C_2H_2, CH_3OH, and C_2H_5OH) [148]. Moreover, alkali (Na and K) additives above 50 ppmv increased the NO removal efficiency during SNCR, and

additionally exhibited a synergetic effect on NO reduction when mixed with coal fly ash collected from a circulating fluidized bed boiler [147].

$$NH_2 + NO \rightleftarrows NNH + OH \quad \text{R2.13}$$

$$NNH \rightleftarrows N_2 + H \quad \text{R2.14}$$

$$NH_2 + NO \rightleftarrows N_2 + H_2O \quad \text{R2.15}$$

$$NH_2 + NO_2 \rightleftarrows N_2O + H_2 \quad \text{R2.16}$$

$$NH + NO \rightleftarrows N_2O + H \quad \text{R2.17}$$

$$NNH + O \rightleftarrows N_2O + H \quad \text{R2.18}$$

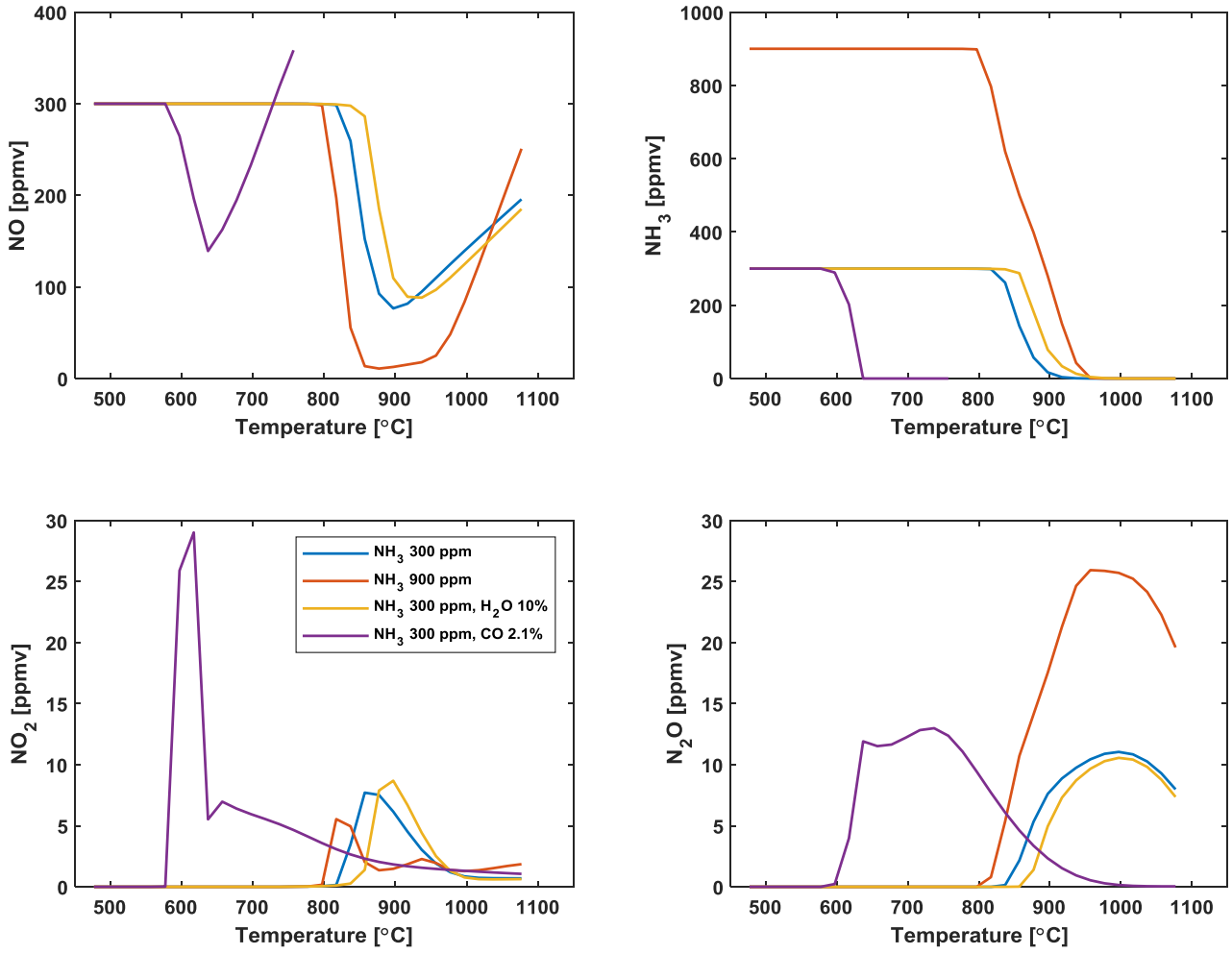

Figure 2.12: Flow reactor modeling predictions for the reduction of NO by NH_3: effect of CO, H_2O, and NH_3. The varied initial concentrations are specified in the legend. Persistent initial concentrations: 4.0% O_2, 300 ppm NO, balance N_2. Pressure is 1.1 atm. Residence time (s) = 188.56(s/K) / T(K). Reactor surface/volume ratio was 4.4 cm^{-1}.

In addition to NH_3, the introduction of cyanuric acid (RapReNO$_X$ [149]) or urea (NO$_X$out [150]) results in SNCR of NO by HNCO in a certain temperature range. The key reactions for NO removal by HNCO are that between NCO and NO, demonstrated in R2.19-R2.20. In the presence of H_2O, the window for NO removal shifts towards lower temperatures, due to the change from O to OH as the

main chain carrier. CO additionally shifts the reduction window to lower temperatures [17,93]. Similar to NO removal by NH_3, the presence of Na_2CO_3 promoted the NO reduction by urea especially at low O_2 concentration and temperature [151].

$$NCO + NO \rightleftarrows N_2O + CO \quad \text{R2.19}$$

$$NCO + NO \rightleftarrows N_2 + CO_2 \quad \text{R2.20}$$

In hydrocarbon radical (C_XH_Y) rich regions, NO may react to form cyanides and possibly NH_3. The subsequent conversion of these species to N_2 and NO may lead to a net reduction in NO. Using the detailed model of Glarborg et al. [17], the concentration of NO and total reactive nitrogen species (NO, NO_2, N_2O, NH_3, HCN, HNCO) against the ratio of the actual O_2 concentration over the stoichiometric O_2 concentration ($O_2/O_{2,stoichiometric}$) is shown in Figure 2.13. A significant reduction in the NO and total reactive nitrogen concentrations are observed at fluidized bed combustion temperatures under fuel-rich conditions. The reduction of NO by CH_4 was promoted by K and Na additives at low excess air ratios, while it did not promote and to some extent inhibited NO reduction at high excess air ratios [152].

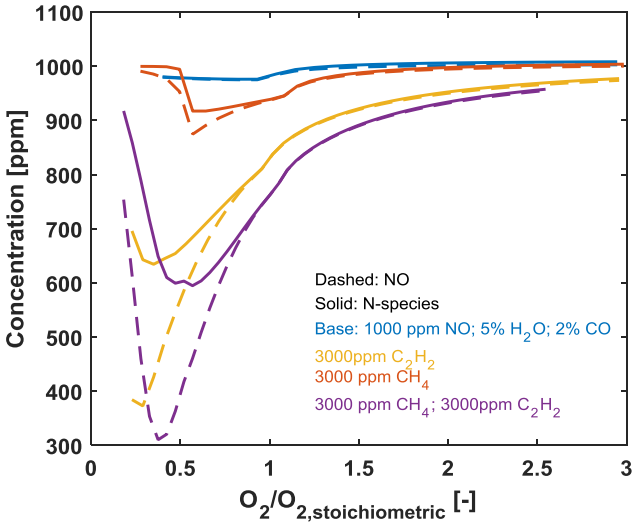

Figure 2.13: Flow reactor modeling predictions for the reduction of NO during reburning. Dashed lines show the NO concentration, while the solid refers to the sum of NO, NO_2, N_2O, NH_3, HCN, and HNCO. The varied initial concentrations of C_XH_Y-species are specified in the legend. Persistent initial concentrations: 1000 ppm NO, 5% H_2O, 2% CO, varying O_2, balance N_2. Pressure is 1.1 atm. Reactor temperature = 850ºC. Residence time = 250 ms. Reactor surface/volume ratio was 4.4 cm^{-1}.

Moreover, NO may be oxidized to NO_2 by HO_2 radicals in the combustion zone or by O_2 in the post-combustion zone, shown by R2.21 [93] and R2.22 [153], respectively. In atmospheric fluidized bed combustion with temperatures around 800-900ºC, R2.21 is limited by a low equilibrium concentration [131].

$$NO + HO_2 \rightleftarrows NO_2 + OH \quad \text{R2.21}$$

$$2\,NO + O_2 \rightarrow 2\,NO_2 \quad \text{R2.22}$$

2.3.4.2 NO reduction by char

The reduction mechanism for NO in an O_2/N_2 system during char combustion is summarized in R2.23-R2.30 [61,98,154–156]. In the initial step (R2.23), NO undergoes dissociative adsorption on an active carbon free site, followed by reduction via R2.24 and R2.25. The active site is regenerated by the desorption of CO or CO_2 (R2.29-R2.30). The presence of CO has been shown to reduce NO by the non-elementary R2.26 catalyzed by char or possibly other ash forming elements such as CaO or coal ash [131,157]. In addition, the presence of ash forming elements (M) such as Na [158], K [159,160], Mg [161], Ca, and Fe [162] have been shown to promote the NO reduction reactivity of char, presumably by R2.27-R2.28. The surface area, and pore availability and size have also been shown to influence the NO reduction reactivity [163,164].

$$NO + 2\,(\text{-C}) \rightarrow (\text{-CO}) + (\text{-CN}) \quad \text{R2.23}$$

$$2\,(\text{-CN}) \rightarrow N_2 + 2\,(\text{-C}) \quad \text{R2.24}$$

$$(\text{-CN}) + NO \rightarrow N_2 + (\text{-CO}) \quad \text{R2.25}$$

$$2\,NO + 2\,CO \rightarrow N_2 + 2\,CO_2 \quad \text{(over char)} \quad \text{R2.26}$$

$$(\text{-}M_XO_Y) + (\text{-C}) + NO \rightarrow (\text{-}M_XO_{Y+1}) + (\text{-CN}) \quad \text{R2.27}$$

$$(\text{-}M_XO_{Y+1}) + (\text{-C}) \rightarrow (\text{-}M_XO_Y) + (\text{-CO}) \quad \text{R2.28}$$

$$(\text{-CO}) \rightarrow CO + (\text{-C}) \quad \text{R2.29}$$

$$(\text{-CO}) + CO \rightarrow CO_2 + (\text{-C}) \quad \text{R2.30}$$

2.3.5 N_2O reduction

In the temperature conditions of fluidized bed combustion (800-900 ºC), the main gaseous reduction pathway for N_2O reduction to N_2 is by reaction with OH (R2.31) [131]. In addition, thermal decomposition of N_2O at higher temperatures form N_2 according to R2.32-R2.34 [165]. The decomposition can occur with and without the presence of a catalyst, e.g., zeolites or CaO [9]. Moreover, N_2O can be reduced over char with and without the presence of CO, demonstrated by R2.35-R2.36 [135,136].

$$N_2O + OH \rightarrow N_2 + HO_2 \quad \text{R2.31}$$

$$N_2O + M \rightarrow N_2 + O + M \quad \text{R2.32}$$

$$N_2O + O \rightarrow N_2 + O_2 \quad \text{R2.33}$$

$$N_2O + O \rightarrow 2\,NO \quad \text{R2.34}$$

$$N_2O + (\text{-C}) \rightarrow N_2 + (\text{-CO}) \quad \text{R2.35}$$

$$N_2O + CO \rightarrow N_2 + CO_2 \quad \text{(over char)} \quad \text{R2.36}$$

2.4 Fluidized bed combustion of biomass

Fluidized bed reactors are widely used in gasification and combustion applications for power and heat production. The advantages of fluidized bed reactors are fuel flexibility, high combustion efficiency, good heat transfer, and low temperature [9,10]. The two most common types of fluidized bed boilers are bubbling and circulating fluidized bed combustors, illustrated in Figure 2.14 [10]. In both systems, a bed of particles (most often silica sand) is fluidized by primary combustion air, introduced through an air distributor at the bottom of the reactor. The main difference between circulating and bubbling boilers is the gas velocity. In bubbling fluidized bed combustion, the velocity is kept relatively low to minimize elutriation of fuel and bed particles. In circulating boilers, the gas velocity is much higher, necessitating the use of solid recirculation. In both combustors, secondary and tertiary air or fuel introduction can be used for emission control. Depending on the fuel reactivity, size, and crushability, over- and under-bed fuel feeding systems may be employed. The temperature in the bed is generally kept between 800 and 900°C [9]. While Section 2.3 described the fundamental aspects of NO_X formation and reduction in combustion, the following sections mainly summarize results on NO_X emissions from bubbling fluidized bed combustion of biomass.

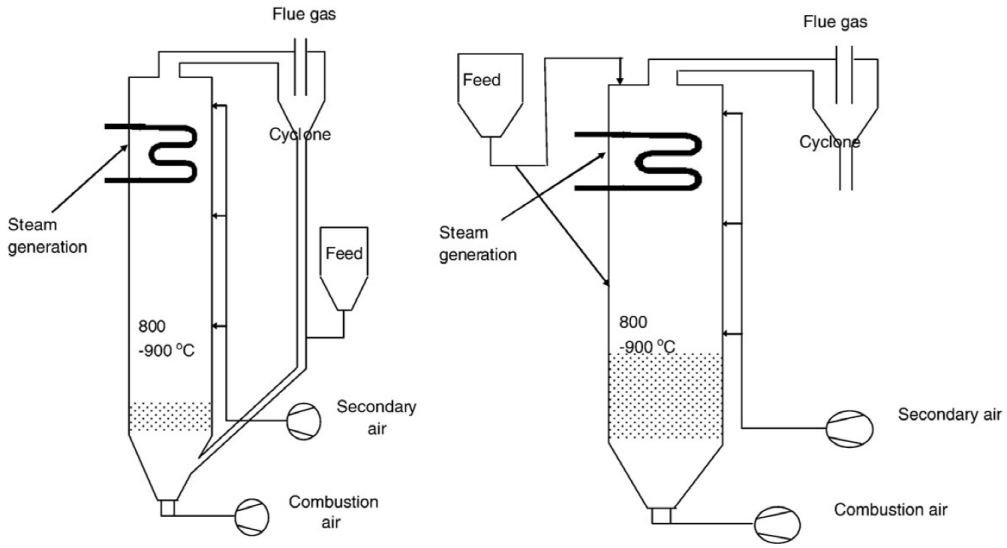

Figure 2.14: Schematic showing the working principle of circulating (left) and bubbling (right) fluidized bed combustors [10].

2.4.1 Effect of fuel properties on NO_X

Several parameters have been recommended to predict the NO and N_2O emissions from fluid bed combustion, e.g. CH/N [166], fixed carbon/volatile matter content [167], and O/N ratio [84,168]. Multivariate data analysis methods have also been used to describe the conversion of fuel-N to NO_X in gas turbines [169]. However, no universally accepted parameter or correlation were identified, most likely due to the influence of other parameters during combustion, as the NO_X emissions are a complex function of mixing, temperature, fluid dynamics, and chemistry [170].

2.4.1.1 Nitrogen and volatile content

In comparison to stoichiometry and nitrogen content, the speciation of the gas phase has been shown to be of lesser importance for the NO emission at high temperatures, while the distribution of nitrogen between NH_3, HCN, and char-N may determine the NO emission at lower temperatures, i.e., in fluidized bed combustors [146,171]. However, from model compound combustion studies under fuel-lean conditions, the conversion of nitrogen to NO showed no correlation to the functionality and instead decreased with increasing fuel-N content and decreasing O_2 concentration [79,145]. Konttinen et al. [172] attempted to characterize the conversion of fuel-N to NO under air un-staged, fluidized bed combustion conditions. Their results along with that of other studies are summarized in Figure 2.15 [84,95,172–175]. They noted that the conversion of fuel-N to NO decreased with an increase in fuel-N content, explained by the facilitation of thermal $DeNO_x$ reactions in the presence of a higher gas phase nitrogen concentration (NH_i radicals) [95,172,174,176]. Moreover, the conversion of volatile-N and char-N to NO decreased with an increase in volatile-N and char-N content, respectively. The former was attributed to the facilitation of thermal $DeNO_X$ reactions, while the influence of char-N was presumed to be caused by the larger reduction of NO over char due to high local concentrations of NO [155,172]. A similar influence of the fuel-N content on the conversion of fuel-N to NO was observed under staged conditions [175]. In addition to volatile-N, the conversion of fuel-N to NO and N_2O generally decreased with an increase in fuel volatile content in lab scale fluidized bed combustion [13,177,178].

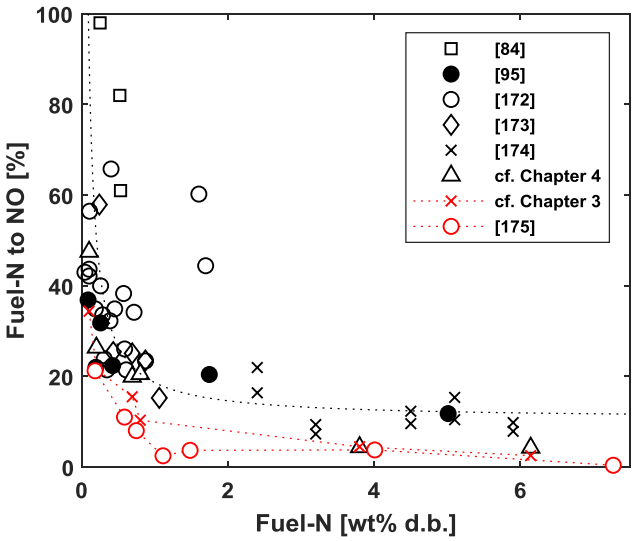

Figure 2.15: Fuel-N to NO conversion as a function of the fuel-N content. The results are from fixed bed combustion [173], single particle combustion in a single particle reactor [174] and un-staged fluidized bed [95,172], dilute suspension combustion in an entrained flow reactor [84], batch combustion of a particle size distribution of biomass in a fluidized bed reactor (cf. Chapter 4), continuous air staged fluid bed biomass combustion [175], and continuous air un-staged fluid bed biomass combustion (cf. Chapter 3). Conditions: Temperature: 800-850ºC, stoichiometry: fuel lean.

2.4.1.2 Fuel particle size and moisture content

NO_X emissions generally decreased with an increase in coal particle size, explained by differences in particle heating rate and peak temperature, which affect the devolatilization rate. In addition, larger particles provide higher propensity for reduction within the particle during combustion [179,180]. In

fluidized bed combustion, too small particle sizes may result in the elutriation of char particles, and thereby potentially an increase in NO_X emissions depending on the relative influence of the char-NO reaction [181]. The NO_X emissions from vortexing fluidized bed combustion increased with increasing particle size. This was attributed to the inverse trend in CO, caused by the limited residence time of the smaller particles [182].

The inherent moisture content of the fuel influences the devolatilization time, and could thereby affect the NO_X emissions by local concentration and temperature differences within the combustor [183]. In addition, H_2O could affect the radical pool and thereby combustion chemistry further described in Section 2.4.2.3. NO_X emissions decreased with increasing inherent moisture content in bubbling [36,184] and swirling fluidized bed combustion [185]. This decrease was attributed to the facilitation of NO_X reducing reactions, i.e. by CO or NH_3, and a decrease in temperature in the presence of high H_2O concentrations.

2.4.1.3 Influence of ash forming elements

Ash forming elements in the biomass may either directly or indirectly influence the NO emission during combustion. The parameters affected by the inorganics are volatile-N product distribution and amount (Section 2.2.2), reactivity of the char towards NO reduction (Section 2.3.4.2), and interaction between ash forming elements and gaseous species. The latter describes the catalytic effect of ash, e.g. the enhancement of NH_3 oxidation by sewage sludge ash [167], and the interaction between ash forming elements and the radical pool, e.g. surface radical recombination [129]. While it was previously stated that Fe enhanced the formation of N_2 in the absence of O_2, it has been reported to enhance the formation of NO and to lesser extent N_2O from NH_3 and HCN in the presence of O_2 [167,186]. In addition, the NO_X emissions increased and N_2O decreased in the presence of Ca [187–189]. These observations were caused by the increased NO_X selectivity over N_2O and N_2 from heterogeneous oxidation [63,93], while the decrease in N_2O may also be related to the decreased release of HCN during pyrolysis (cf. Section 2.2.2). Employing a bed consisting of alumina sand increased the conversion of fuel-N to NO, caused by a decreased concentration of CO and C_XH_Y species [190].

In the gas phase, trace species from combustion such as alkali metals and halogens may affect the concentration of pollutants through mechanisms A_J (chain-branching, i.e. promoting), A_J' (terminating, i.e. inhibiting), and B_J (propagating, sensitizing; if radical goes from less to more reactive, then promoting).

A_J:

$$J + XY \rightarrow JX + Y \quad \text{R2.37}$$
$$JX\ (+M) \rightarrow J + X(+M) \quad \text{R2.38}$$

A_J':

$$J + X(+M) \rightarrow JX(+M) \quad \text{R2.39}$$
$$JX + Y \rightarrow J + XY \quad \text{R2.40}$$

B_J:

$$J + RO_2 \rightarrow JO + RO \quad \text{R2.41}$$
$$JO + R \rightarrow J + RO \quad \text{R2.42}$$

Here, J is trace species, and X and Y may be H, O, or OH. In A_J, two radicals X and Y are formed each cycle, while the trace species are regenerated thereby acting as a catalyst. A_J' is the reverse sequence of A_J. In sequence B_J, the lesser reactive peroxide radical (RO_2) is converted to a more reactive radical (RO) [171]. Alkali metals generally inhibit fuel oxidation by recombination of OH and H radicals through A_J', most prominent at reducing conditions [171,191]. At higher concentrations of K a saturation effect was observed [192]. At low radical levels, alkali metals may promote fuel oxidation through the A cycle [171]. The influence of alkali metals on the NO_X chemistry is most likely indirect rather than a direct interaction between alkali and N-species [171]. The presence of halogens F, Cl, Br, and I generally inhibit fuel oxidation by recombination of most likely OH [171,193–195]. The effect of halides on the radical pool in decreasing order is I, Br, Cl, and F [196]. In entrained flow reactor combustion at fluidized bed combustion temperatures and circulating fluidized bed combustion, the introduction of HCl and $CaBr_2 \cdot ½\ H_2O$ increased CO and decreased NO_X concentrations in the flue gas, while not affecting the N_2O emission [197,198]. Similar to alkali metals, the influence of halogens on the NO_X chemistry is most likely indirect by recombination of OH, H, and O [171,198,199].

2.4.2 Effect of operating conditions on NO_X

2.4.2.1 Bed particle size and height, and gas velocity

NO_X emissions increased [200] or were unchanged [201,202] by an increase in bed particle size. Through modelling of pressurized fluidized bed coal combustion [181,203], the NO_X emissions were shown to increase with particle size followed by a plateau. For coarser particles, the flow of gas through the dense phase could increase, providing more oxidizing conditions and consequently lower concentrations of CO and char. In addition, the major gaseous constituents and temperature were unchanged [184,204,205] or increased [206] with increasing bed height. The increase was attributed local temperature and concentration gradients and higher surface area for surface catalytic reactions. Moreover, keeping a constant overall excess air, the emission of NO_X slightly increased [207] or decreased [208] with an increase in fluidization velocity during coal combustion. The increase may be attributed to the more intense mixing in the bed as it was in the fast fluidization regime [209], while the decrease was most likely related to the higher concentration of CO, due to a decrease in gas residence time. The differences in operating conditions such as bed particle size and height may be related to differences in fuel feeding method. In under-bed-fired bubbling fluidized bed combustion, the fuel is fed directly to the bed, thereby increasing the importance of bed chemistry. In overfired systems, the fuel is fed above the bubbling bed, thereby leading to the possibility of low turn-over of fuel particles, and consequently low importance of bed chemistry. In over-bed-fired systems, the bed particle size and height were deemed unimportant [184,201,202,204,205].

2.4.2.2 Temperature and overall excess air

The general consensus in literature is that the conversion of fuel-N to NO increases and that to N_2O decreases with an increase in temperature [182,185,210,211]. The increase in NO was attributed to the lower concentrations of CO and char at higher temperatures [210], and differences in activation energy of the ongoing reactions [93]. The latter explanation and the enhanced thermal decomposition

of N_2O at higher temperatures explains the decreasing tendency of this with temperature [210]. The influence of temperature on the NO emission is not always prominent, as in some cases NO was unaffected by changes in temperature [212]. In addition, the emissions of NO and N_2O generally increase when increasing the overall excess air during combustion [9,173,175,182,213]. This is again related to the CO and char contents in the reactor and the enhanced rate of oxidation of nitrogenous intermediates, e.g. NH_i, NCO, and (-CN).

2.4.2.3 Gas phase composition

Flow reactor experiments revealed that a high CO_2 concentration enhanced NO formation from NH_3 at fuel-rich conditions, whereas it inhibited NO formation at stoichiometric and fuel-lean conditions. The influence of CO_2 on the gaseous nitrogen chemistry was indirect and attributed to the enhanced CO concentration and alterations in the amount and partitioning of O/H radicals [132,214,215]. In addition, during CO_2 gasification of char, nitrogen was primarily released as N_2 and to lesser extent NO [216]. Moreover, SO_2 was shown to participate in radical recombination reactions, thereby increasing CO and N_2O, and decreasing NO from fluidized bed combustion of coal [217]. Furthermore, the fuel-N to NO conversion decreased with the addition of water vapor or alcohols to model compound [145] and antibiotic mycelial residue [218] combustion. However, at higher concentrations of O_2 in combustion of distilled spirit lees in a lab scale fluidized bed combustor, H_2O increased the conversion of fuel-N to NO [219]. The reducing property at low O_2 concentration was attributed to the dilution of O_2, thereby creating a comparably more reducing atmosphere with higher concentrations of H_2, CO, and H (R.2.43, R2.44, and R2.4). At higher O_2 concentration, the H_2O would decompose to OH by the radical branching R2.3, thereby increasing the oxidation capability of the combustion atmosphere, which would lower CO and char concentrations. In addition, the CO and NO levels were inherently related in fluidized bed combustion, showing a decrease in NO with an increase in CO [220] and char loading [221], the latter of which was in the case of circulating fluidized bed combustion.

$$H_2O \rightarrow H + OH \qquad \text{R2.43}$$

$$OH + H_2 \rightarrow H + H_2O \qquad \text{R2.44}$$

2.5 Methods for NO_X minimization in fluidized bed combustion

Primary and secondary measures are commonly applied to control NO_X emissions in fluidized bed combustion. The primary measures are based on combustion modifications, i.e. take place within the combustion zone, while secondary measures are applied to the post-combustion effluent.

2.5.1 Primary measures

Primary measures employed for NO_X emission control in fluidized bed combustion are air staging [213,222], temperature adjustment [9,223], SNCR [224], lowering excess air [9], reburning (fuel staging) [225,226], flue gas recirculation [227], and fuel blending [63]. Hybrid systems such as SNCR and air staging [224], and reburning and SNCR (advanced reburning) [228,229] have additionally been used for NO_X reduction from combustion. The working principles of air staging, reburning, SNCR, and selective high temperature reduction (SHTR) are illustrated in Figure 2.16, along with typical NO_X removal efficiency ranges in boilers based on [230–233]. In air and fuel staging, the combustion is divided into several zones in which the excess air ratio (λ) is manipulated in such a way as to minimize NO_X emissions. In air staging, part of the combustion air is supplied to the bed, which is kept at sub-stoichiometric conditions. The remaining air is introduced upstream to achieve high combustion efficiencies. In fuel staging, the primary fuel is fed to the reactor and combusted under fuel-lean conditions. Upstream a secondary fuel is introduced to create a fuel-rich region in which the formed NO_X is reduced. Further upstream, air is introduced to remove combustibles. The NO_X reduction efficiency in staged combustion depends on the residence time, temperature, and excess air ratio in the reduction zone [234–236]. The concept of SNCR was described in Section 2.3.4.1. The introduction of NH_3 to the combustion system may reduce NO depending on the temperature and stoichiometry. In the SHTR process, SNCR occurs in the sub-stoichiometric zone of air-staged combustion. In fluidized bed combustion, staged combustion may lead to a decreased N_2O emission [237,238], while in pulverized fuel combustion little change was observed, possibly due to the importance of N_2O decomposition at higher temperatures [35]. In addition, NO_X reduction by NH_3 resulted in increased [237,239] or unaffected N_2O emission [237]. The increased N_2O emission was predominant at high NH_3/NO ratios or temperatures. Moreover, using cyanuric acid or urea for NO reduction increased N_2O emissions [240].

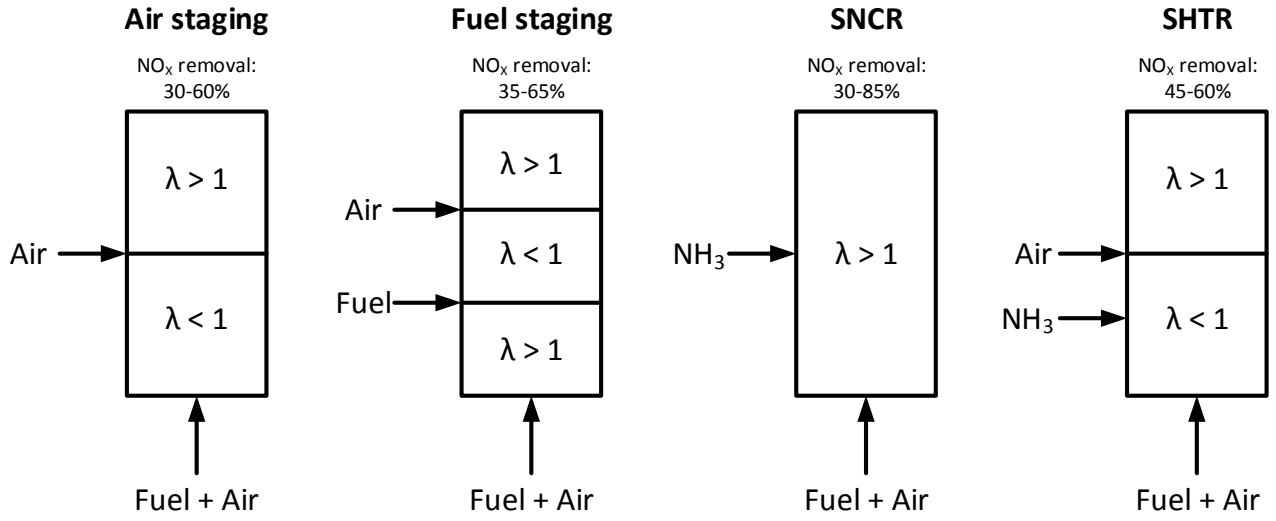

Figure 2.16: Simplified illustration showing the working principle of some primary NO_X reduction measures. The excess air ratio (λ) refers to the available air compared to that of stoichiometric combustion. SNCR: selective non-catalytic reduction, SHTR: selective high temperature reduction (combination of air staging and SNCR). The typical NO_X removal ranges were extracted from [230–233]. This figure was inspired by [232].

2.5.2 Secondary measures

Depending on the location of NH_3 injection, SNCR may additionally be classified as a secondary technique to treat the flue gas from combustion. The reduction of NO by NH_3 can be enhanced in the presence of heterogeneous catalysts in a process termed selective catalytic reduction (SCR). In the presence of O_2 and at a temperature of 250-400ºC, the presence of catalysts such as vanadium and titanium oxides promote the NO reduction, leading to NO removal efficiencies of up to 80-90% [230]. The most important reactions for the removal of NO_X from the post-combustion flue gas are summarized in R2.45-R2.46. Main factors affecting SCR performance are temperature, NH_3/NO_X ratio, O_2 concentration, and catalyst loading and type [233]. Similar to SNCR, N_2O may be a byproduct (R2.47) of the NO removal, the selectivity of which depends on the SCR system [241,242].

$$4\ NO + 4\ NH_3 + O_2 \rightarrow 4\ N_2 + 6\ H_2O \qquad \text{R2.45}$$

$$6\ NO_2 + 8\ NH_3 \rightarrow 7\ N_2 + 12\ H_2O \qquad \text{R2.46}$$

$$4\ NO + 4\ NH_3 + 3\ O_2 \rightarrow 4\ N_2O + 6\ H_2O \qquad \text{R2.47}$$

2.6 Summary of literature study

Biomass is a CO_2 neutral feedstock with nitrogen contents varying from 0.01wt% to several wt%. Consequently, high NO_X and N_2O emissions from biomass combustion may be possible. Upon heating, the nitrogen in biomass is partitioned between the volatile and char. Decreasing temperature, particle residence time, and heating rate, and increasing particle size and pressure favored the retention of nitrogen in the char. Ca increased char-N retention, while Na and K promoted the formation of volatile-N. The functionality of nitrogen in the light gas during biomass pyrolysis was predominantly HCN, NH_3, HNCO, and N_2. The NH_3/HCN ratio decreased with increasing temperature and heating rate, and decreasing particle size. The gas atmosphere and mineral content additionally affected the speciation of the light gases. While a qualitative understanding of the nitrogen release from biomass has been established, a quantitative description of the observed trends is not possible. Therefore, the amount and functionality of nitrogen released from biomass pyrolysis cannot be known prior to experimentation.

The oxidation of fuel-N is the major contributor to NO_X and N_2O emissions from fluidized bed combustion. Numerous reactions occur within the combustor, which can be simplified to competing NO_X and N_2O formation and reduction reactions. The net emissions of these compounds are consequently determined by the relative rates of these. The gaseous nitrogen chemistry is fairly well established and can be described reasonably well with existing models. In comparison, the conversion of char-N to NO and N_2O is less understood, especially in the case of high-nitrogen biomass. Fundamental studies are necessary to understand the underlying mechanisms of NO and N_2O formation and reduction during char oxidation.

The influence of several process parameters on the conversion of fuel-N to NO and N_2O in fluidized bed combustion of biomass are qualitatively summarized in Table 2.2. In addition to these, other operating conditions such as bed particle diameter and height, and fluidization velocity, and fuel properties such as particle size, moisture and mineral content, and presence of trace elements may affect NO_X and N_2O emissions. While higher fuel-N may lead to lower conversion of fuel-N to NO and N_2O, the total emissions may increase with an increase in fuel-N. For several of the process parameters, contradicting results have been obtained, which may be related to differences in experimental setup. In addition, conclusions are often drawn based on the outlet gas concentrations, which may hide interactions during combustion due to differences in local conditions. Therefore, local gas composition data would be of interest for the study of the NO_X chemistry. Moreover, the influence of ash forming elements on NO_X emissions is commonly studied under well-controlled conditions, and data from fluidized bed systems are lacking.

Several primary and secondary countermeasures exist to solely minimize NO_X emissions. Studies on multifunctional countermeasures tackling both NO_X emissions and other operational issues such as bed agglomeration are lacking.

Table 2.2: Influence of several process parameters on fuel-N to NO and N_2O conversion in bubbling fluidized bed combustion.

Increasing parameter	Fuel-N to N_2O	Fuel-N to NO
Temperature	↓	↑, -
Fuel-N content		↓
Fuel volatile content	↓	↓
Excess air	↑	↑
Air staging	↓	↓
Fuel staging (reburning)	↓	↓
SNCR – NH_3	↑, -	↓
SNCR – urea	↑	↓
SCR	↑, -	↓

3 NO_X emissions from fluidized bed mono- and co-combustion of biomass

Abstract: NO_X emissions from mono- and co-combustion of biomass at air staged and un-staged conditions were investigated in a continuous lab-scale bubbling fluidized bed reactor by effluent and local gas composition measurements. The biomass fuels were pine wood, beech wood, straw, sunflower husk, sewage sludge, and sunflower seed. The results show that the conversion of fuel-N to NO decreased with an increase in fuel-N content, predominantly related to the higher concentration of nitrogen intermediates, such as NH_3, which facilitated NO reduction by thermal $DeNO_X$. Co-combustion of straw and sewage sludge revealed a synergy effect, showing that the NO emission was higher than the weighted values. The main cause of this was the presence of sewage sludge ash, which could catalyze the formation of NO from NH_3 and HCN. The catalytic effect of the ash increased with lower ash preparation temperature and better mixing of the ash with straw. During straw-sewage sludge co-combustion, the NH_3 released from sewage sludge initially reduced the formed NO, while at a higher content of ash in the bed, the NO emission was significantly higher. Local concentration measurements during straw-sunflower seed co-combustion indicated an interaction in the nitrogen chemistry of the two fuels, which was otherwise unnoticeable in the effluent concentration of NO. Air staging was an efficient way of reducing NO_X emissions and the influence of sewage sludge ash.

3.1 Introduction

Many studies have investigated NO_X emissions from co-combustion of coal and biomass in bubbling [63,167,243–245] or circulating [209,246–249] fluidized bed combustors, pulverized fuel burners [35,170,250,251], and fixed bed reactors [37,173,252,253]. In bubbling fluidized bed combustors, NO_X emissions decreased with an increase in the fuel volatile content [63,244], concentration of NH_i radicals [63,243], and char NO reduction reactivity [244]. Moreover, the presence of ash forming elements such as Fe and Ca may increase or decrease NO_X emissions depending on their relative impact on NO_X formation and reduction reactions [167,244]. However, several co-combustion studies showed the absence of interaction between fuel particles of different origin at well-controlled conditions, indicating that NO_X emissions from co-combustion are additive and therefore described by the propensity of the individual fuels for forming NO_X [245,251]. The observed interaction was consequently attributed to changes in fluid mechanics and temperature [63,251]. The lack of consensus on the existence of an interaction effect during co-combustion along with the scarcity of fluidized bed biomass co-combustion studies in the literature provide the motivation for this work.

This study investigates the emissions of NO_X during mono- and co-combustion of biomass in a lab scale bubbling fluidized bed reactor. Continuous combustion experiments were performed at air

staged and un-staged conditions. Effluent and local gas concentration data were measured, thereby providing a deeper understanding of the nitrogen conversion during biomass co-combustion. Special emphasis was placed on the co-combustion using sewage sludge, due to its distinct interaction with other fuels.

3.2 Experimental section

3.2.1 Materials

The chemical composition of the investigated biomass, pine wood, beech wood, wheat straw, sunflower husk, sewage sludge, and sunflower seed, are shown in Table 3.1. The nitrogen contents varied from 0.1-6.1 wt%, thereby covering a wide range of nitrogen contents in biomass. Wheat straw, sunflower husk, and sunflower seed pellets were grinded and sieved to a size range of 0.6-4 mm, while sewage sludge (0.5-2 mm), pine wood (1-3 mm), and beech wood (0.6-1 mm) were used as received. These particle size ranges allowed for continuous sample admission, while minimizing fuel elutriation. Mixtures of fuels were prepared in a mechanical mixer for several hours prior to combustion. Silica sand was used as bed material in the fluidized bed (D_{50} 273 μm, Geldart B).

Table 3.1: Fuel chemical composition.

	Unit	Pine wood	Beech wood	Wheat straw	Sunfl. husk	Sew. slu.	Sunfl. seed
Moisture	% w.b.	7.1	8.4	12.5	9.1	10.8	8.7
VM	% d.b.	85.6	77.1	76.5	75.8	49.3	-
Ash		0.43	2.7	4.6	3.2	50.2	14
C		49.5	51.2	48.7	51.7	29	40.5
H		6.1	5.7	5.8	5.7	3.8	5.7
N		<0.1	0.20	0.69	0.80	3.8	6.1
S		0.006	0.0027	0.08	0.14	0.96	0.23
Cl		0.02	0.017	0.18	0.04	0.05	-
O		43.8	40.2	40.0	38.4	12.2	33.5
Al	mg/kg d.b.	90	310	230	55	18000	3095
Ca		950	4600	3600	3700	37000	3095
Fe		53	1600	180	94	85000	7328
K		507	4600	8000	9600	6300	18416
Mg		94	830	630	2100	4300	6724
Na		15	280	280	21	2400	410
P		35	230	750	660	34000	12810
Si		299	1700	11000	290	75000	640
Ti		-	34	17	<5	2200	49

3.2.2 Sewage sludge ash and char preparation

Sewage sludge ash was prepared at three different temperatures (550, 850, 1000ºC) in a muffle furnace with continuous air supply (around 200 mL/min). The holding times at 550 ºC, 850 ºC, and 1000ºC were 5 h, 4 h, and 1 h, respectively, to ensure complete combustion. The absence of combustibles were confirmed by CHNS analysis of the prepared ash.

Sewage sludge char was prepared in a horizontal oven at 850ºC with a N_2 flow of 2.5 NL/min. An alumina crucible containing approximately 10-20 g of sewage sludge was pushed into the preheated oven and kept there for 10 min. After 10 min, the crucible was withdrawn to a water cooled section. The chemical composition and BET surface area of the sewage sludge char are summarized in Table 3.2.

Table 3.2: Chemical composition and BET surface area of sewage sludge char. The char yield refers to the ash and fixed carbon content.

	wt% d.b.							m^2/g
	C	**H**	**N**	**S**	**O**	**Ash**	**Char yield**	**BET surface area**
Sew. slu. char	14.51	0.46	1.48	0.16	0.51	82.9	54.6	53.1

3.2.3 Lab scale fluidized bed reactor

Continuous combustion experiments were performed in a stainless steel fluidized bed reactor illustrated in Figure 3.1. The setup consists of three sections, preheater (ID 100 mm), main reaction chamber (ID 61 mm), and upper freeboard (ID 100 mm). The fluidizing gas was heated in the preheating section and fed to the main chamber through an air distributor. Biomass was continuously introduced to the main chamber above the dense bed (300 mm above the air distributor) using a screw feeder (K-Tron K-ML-KT20). To maintain stable fuel feeding and to prevent fuel pipe blockage, secondary gas was fed together with fuel. The composition of the secondary gas varied and in the case air was used, the fuel feeding pipe was considered as the secondary air injection point. The outlet gas was led through a cyclone and two filters to remove elutriated particles. One part of the exhaust gas was led to the gas analyzers (NGA2000, Fischer-Rosemount) to determine the flue gas concentrations of CO_2, CO, O_2, NO, and SO_2, while the other part was sent to the ventilation. In selected cases, the total NO_x (NO and NO_2) was quantized (Eco Physics CLD 700 EL). As NO_2 accounted for less than 5% of the total NO_X in the flue gas (Appendix A.1), it was not further considered in this study.

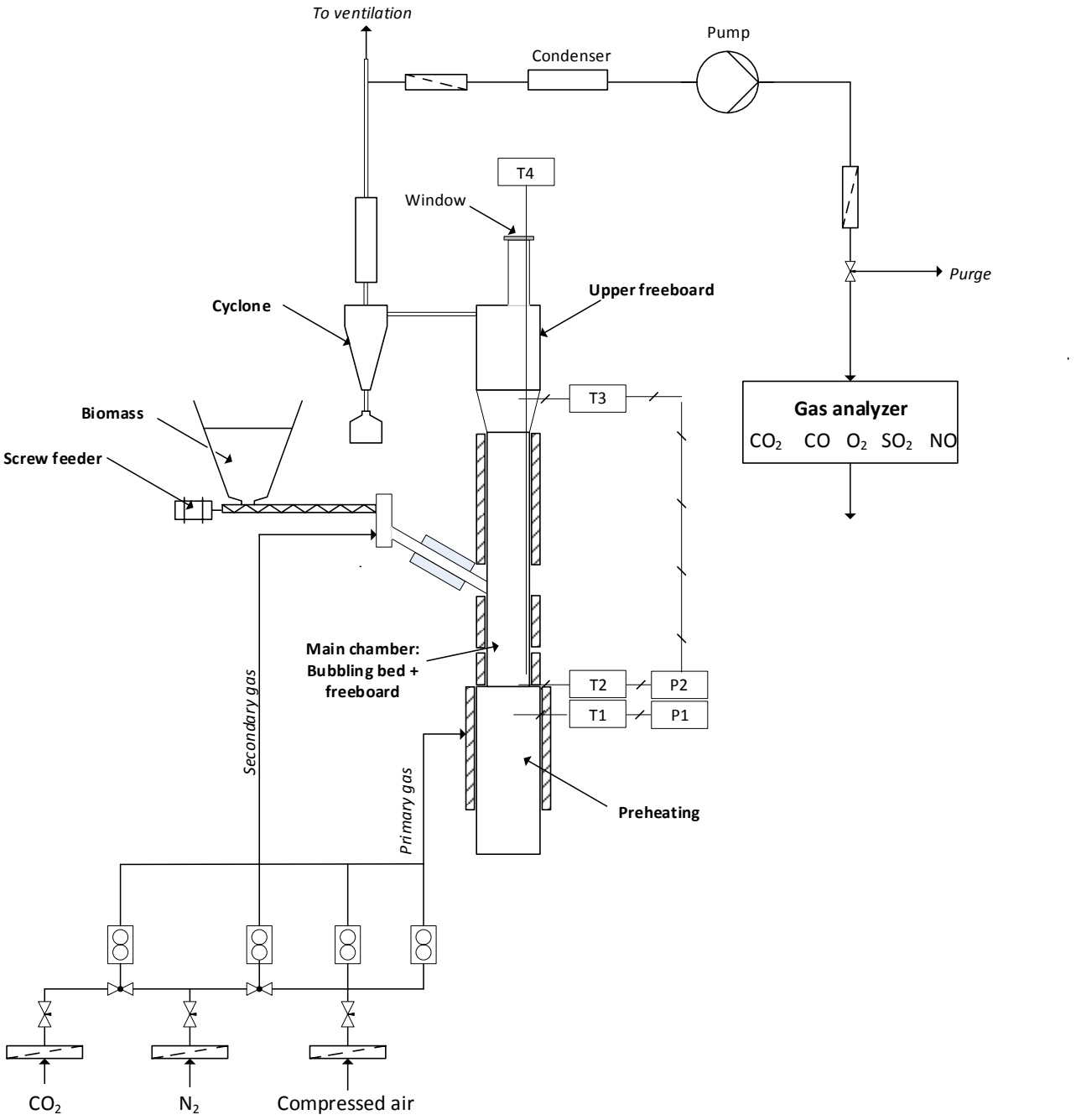

Figure 3.1: Schematic of the bubbling fluidized bed reactor.

3.2.4 Experimental procedure

Approximately 0.5 kg of sand was used in each run, which corresponds to a static bed height of 10 cm. The bed temperature was kept at 850°C in all experiments by varying the degree of external heating while ensuring a constant outlet O_2 concentration ($Q_{reactor} = Q_{heating\ element} + Q_{combustion}$). The set points for the external heating depended on the biomass properties and the extent of combustion taking place in the bed. Upon reaching the set point temperature, fuel feeding was initiated. The fuel feeding rate was varied between 1.6 and 2.6 g/min, depending on the fuel to keep a constant excess

air ratio (λ). The total amount of air supplied to the system was 11.5 NL/min, corresponding to λ = 1.4. At air un-staged conditions, all the air was introduced as primary gas (λ_1/λ = 1), while 15.5 NL/min of N_2 was fed through the fuel feeding pipe to facilitate the biomass feeding. In air staged experiments, half of the primary air was replaced with N_2 and the corresponding amount of air was supplied through the feeding pipe as secondary air (λ_1/λ = 0.5). Hence the total flow of gas in the system was kept constant, leading to an operation velocity of 4 times minimum fluidization velocity (u_g/u_{mf} = 4) [254].

Figure 3.2 demonstrates the flue gas composition (a), and bed temperature and pressure drop (b) during air un-staged combustion of straw. Notably, the flue gas composition data were corrected for the dilution by secondary gas, i.e. N_2. Following an initial phase, a steady state was reached in the flue gas composition, and bed temperature and pressure. The combustion experiments were continued at steady state for 1-3 h. For sunflower husk and straw combustion, the experiments were performed until the point of defluidization, demonstrated by a sudden increase (cake formation) or decrease (channeling) in the bed pressure drop.

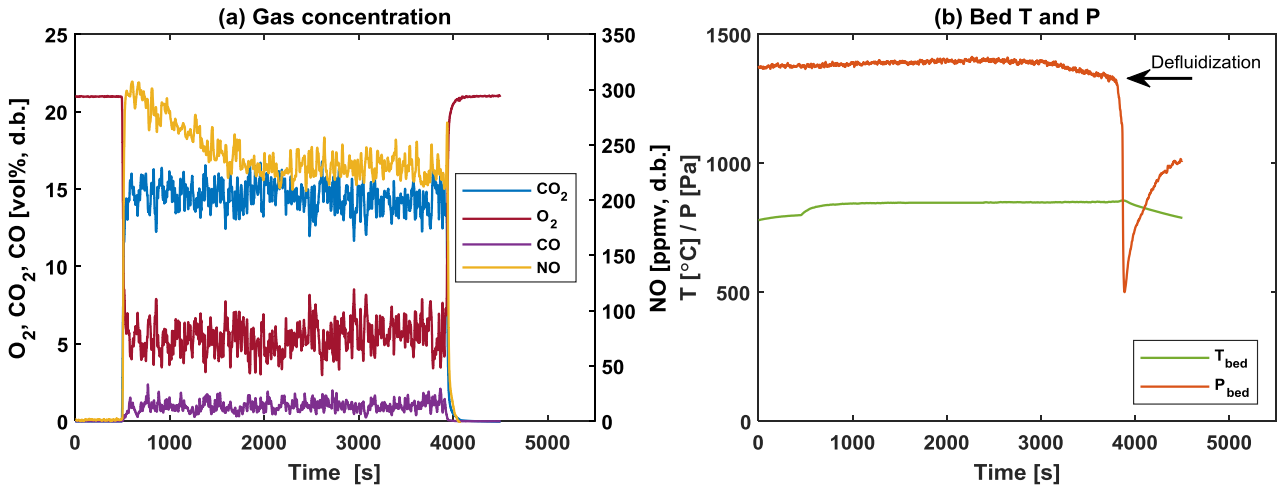

Figure 3.2: Flue gas concentration (a), and bed pressure drop and temperature (b) during combustion of straw. Conditions: T_{bed} = 850ºC; λ = 1.4; λ_1/λ = 1.

3.2.5 Local gas composition and temperature measurements

The axial temperature profile in the reactor was measured by insertion of a movable thermocouple (T4 in Figure 3.1) from the top. The gas composition within the reactor was measured using a water cooled stainless steel probe inserted vertically from the top of the reactor. The design and working principle of the probe is shown in Appendix A.2, along with the commissioning of this and procedure for local concentration measurements. The sample gas was sent to a Fourier Transform Infrared spectrometer (FTIR) (Multigas 2030 FTIR, MKS instruments) from which the concentration of a variety of species, e.g. NH_3, CO, HNCO, NO, NO_2, CH_4 etc., were determined. As no calibration for HCN was available, this was not measured. The repeatability of the local concentration measurements from straw combustion at air staged and un-staged conditions was reasonable as demonstrated in Appendix A.3. In some cases, the maximum range of the calibration in the FTIR was exceeded.

Hence, caution must be taken since additional error may appear from the extrapolation of the calibration curves. The ranges of the most relevant measured species are summarized in Table 3.3.

Table 3.3: Maximum range of FTIR calibration of selected compounds.

	NO	**N_2O**	**NH_3**	**HNCO**	**CO**	**CH_4**
Maximum range	3000 ppmv	300 ppmv	3000 ppmv	300 ppmv	1 %	3000 ppmv

3.2.6 Estimation of bed height

While the fluidized bed height fluctuates with time, an absolute value was estimated to provide an overview of the local gas and temperature measurements. The bed height was estimated from the bed pressure measurement in the experiments employing the probe. When the probe reached the top of the bed, the bed pressure would increase as demonstrated in Figure 3.3. The bed height was thus estimated to be 125 mm above the air distributor.

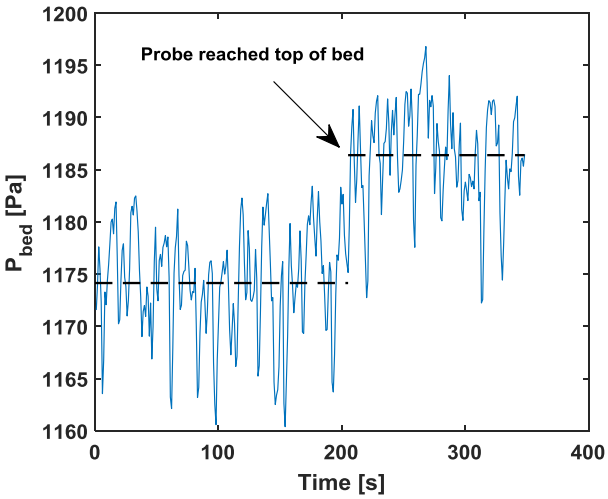

Figure 3.3: Bed pressure versus time during fluidized bed sunflower husk combustion. The point at which the bed pressure increases corresponds to a height 125 mm above the air distributor. Conditions: T_{bed} = 850ºC; λ = 1.4; λ_1/λ = 1.

3.2.7 Effluent data treatment

The conversion of fuel-N to NO was calculated from the ratio between the total amount of NO emitted and the total amount of N fed to the reactor, both expressed in mole. The relevant equations are demonstrated in Eq. 3.1-3.4. In the calculations, only the steady state combustion region, determined by the O_2 and CO_2 outlet concentrations, was included.

$$I_{A,NO} = \int_{t_1}^{t_2} NO(t)\, dt \qquad \text{Eq. 3.1}$$

$$n_{NO} = I_{A,NO} \cdot 10^{-6} \cdot V_g \cdot \frac{P}{R_g \cdot T} \; [=] \; \text{molfrac NO} \cdot s \cdot \frac{Nm^3}{s} \cdot \frac{mol}{Nm^3} \; [=] \; \text{mol NO} \qquad \text{Eq. 3.2}$$

$$n_{N,fuel} = m_{fuel} \cdot w_N / M_N \; [=] \; \text{mol N} \qquad \text{Eq. 3.3}$$

$$\text{fuel-N to NO} = \frac{n_{NO}}{n_{N,fuel}} \qquad \text{Eq. 3.4}$$

Here, $I_{A,NO}$ (ppmv·s) is the integrated area from t_1 to t_2 of the steady state section of the NO concentration plot, n_{NO} (mol) is the amount of NO formed from combustion, V_g (Nm^3/s) is the gas volumetric flow rate, $n_{N,fuel}$ (mol) is the amount of fuel nitrogen fed from t_1 to t_2, m_{fuel} (kg fuel) is the mass of fuel fed from t_1 to t_2, w_N (kg N/kg fuel) is the nitrogen weight fraction in the fuel, and M_N (kg/mol) is the molar weight of nitrogen.

3.3 Results and discussion

3.3.1 Un-staged mono-combustion of biomass

Figure 3.4a-d summarize the experimental results obtained from fluidized bed combustion of biomass. The NO effluent concentration during steady stage combustion was constant for most biomass with the only exception being sewage sludge. In sewage sludge combustion, relatively large fluctuations and an increase in the NO signal were observed. The fluctuations may be caused by the presence of smaller fuel particles, system inherent fluctuations, and oscillations in the feeding rate. The increase in NO concentration was most likely caused by the catalytic effect of accumulated sewage sludge ash on NH_3 and HCN oxidation [167,189,248]. In fluidized bed combustion, the NO concentration is largely influenced by the CO concentration and temperature [220]. The results here indicate that the temperature and averaged CO concentration were comparable between experiments. Therefore, the observed reduction in fuel-N conversion to NO with an increase in fuel-N content was primarily caused by differences in the preferred oxidation pathway of fuel-N. These results are in agreement with previous studies [172,174], in which the explanation of the decreasing NO selectivity with increasing fuel-N content was attributed to the facilitation of thermal $DeNO_X$ reactions in the presence of higher concentrations of NH_i radicals. For a single fuel, the effluent CO and NO concentration may be correlated, as the former is an indication of reducing conditions and/or extent of mixing in the reactor. A brief investigation of this is summarized in Appendix A.4, showing that in some cases an inversely proportional relationship was observed for NO and CO, while in other cases a correlation was lacking. Moreover, as the NO emission from wood combustion was relatively low, a concern was raised to the contribution of prompt NO_X. The general consensus is that prompt NO_X can be neglected and that the major contributor to NO in fluidized bed combustion is from fuel-N [10–13]. However, some studies have reported the importance of prompt NO_X at fluidized bed conditions [255], e.g. lean CH_4 combustion in a fluidized bed combustor (few to 10 ppm NO from prompt NO_X) [256].

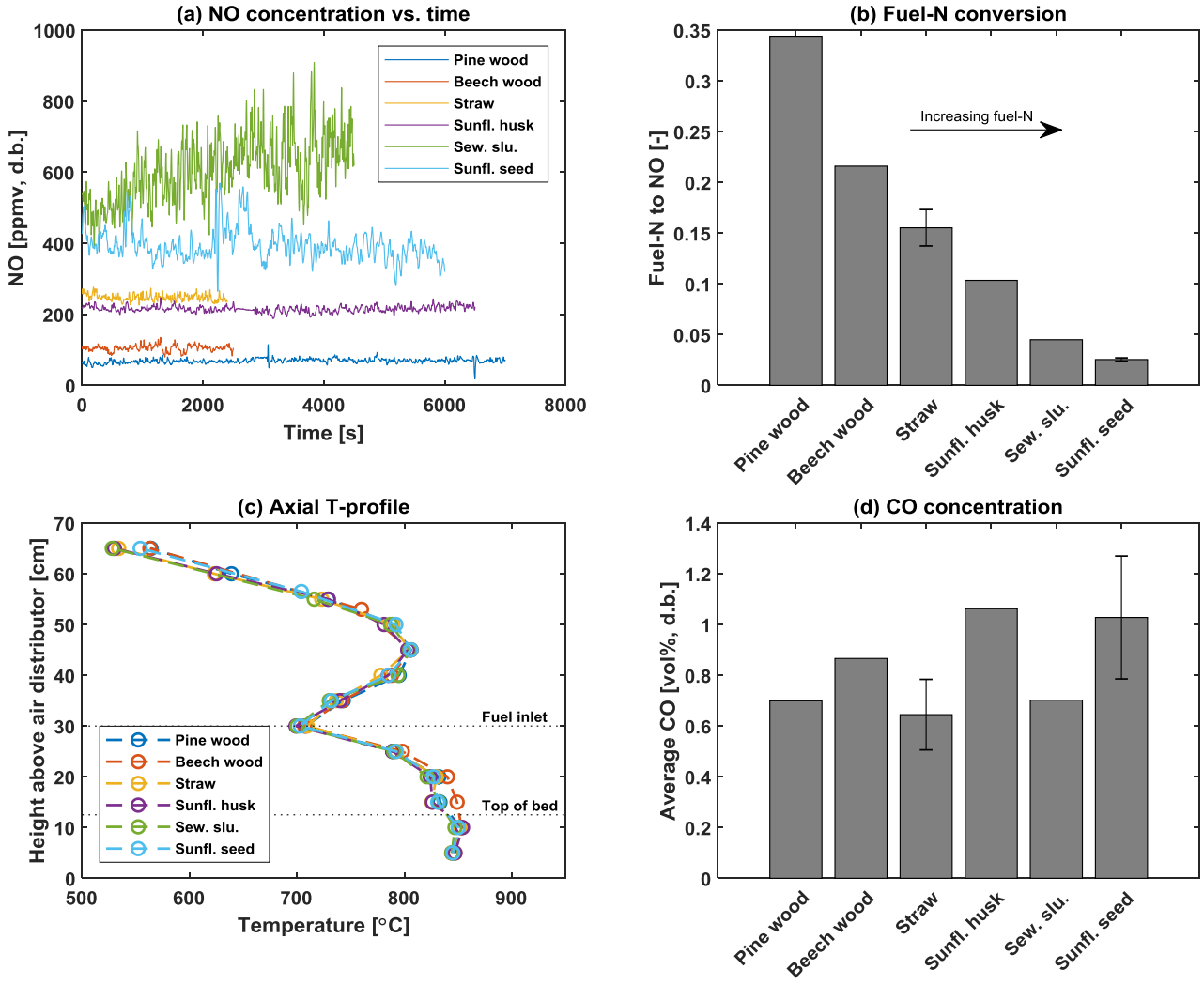

Figure 3.4: Effluent NO concentration (a), conversion of fuel-N to NO (b), axial temperature profile (c), and average CO concentration (d) during steady state fluidized bed mono-combustion of biomass. The error bars on straw and sunflower seed were determined from several repetitions. Conditions: T_{bed} = 850ºC; λ = 1.4; λ_1/λ = 1.

3.3.1.1 Local gas composition measurements

Figure 3.5 displays the axial concentration profiles of NO, N_2O, NH_3, HNCO, and CO during straw, sunflower husk, sewage sludge, and sunflower seed combustion. The profiles of the distinct fuels are in qualitative agreement, showing that the combustion reactions predominantly occurred between the top of the bed and fuel inlet. For sewage sludge combustion, the peaks of each species was shifted to a higher point in the reactor, most likely caused by the increase in bed height due to ash accumulation. During combustion, the relatively large fuel particles drop down to the bed surface from which they are rapidly heated, thereby undergoing drying, devolatilization, and later char combustion. The concentration of gaseous species in the bed was inhomogeneous, indicating that the turnover of fuel may be relatively low. Consequently, the gaseous species directly entered the freeboard from which NO was formed from volatile-N oxidation. The peak of NH_3 preceded that of NO, indicating that this may be an important contributor to NO formation. As the NO concentration is determined by the relative rates of formation and reduction, the NO reduction rate became dominant following the NO concentration peak. The reduction of NO may predominantly be ascribed to the presence of NH_3, HNCO, char, C_XH_Y compounds, and CO (cf. Chapter 2, Section 2.3.4). For the high-nitrogen fuels, considerably higher concentrations of NH_3 were observed, which may lead to a large reduction of NO by thermal deNO_X reactions. The profiles of important C_XH_Y compounds such as CH_4 and C_2H_4 were similar to that of CO as demonstrated in Appendix A.5. Therefore, reburning type reduction reactions could additionally destroy the formed NO above the bed surface. HNCO peaked at a similar location as CO and NO, indicating that this may be formed from secondary cracking reactions. The HNCO, NH_3, and CO concentrations exceeded the maximum range of the FTIR. Consequently, errors induced by extrapolation may obscure the absolute values of the concentration, while the qualitative trend is clear. Especially for HNCO, previous studies on urea decomposition showed that extrapolation above the maximum range of the FTIR would generally lead to an overestimation of the actual concentration [257]. Therefore, while the presence of the compound is undeniable, results above the maximum range (300 ppmv) must be viewed with care. The observed trends in Figure 3.5 are in qualitative agreement with that of other studies, showing a maximum in the CO and NO concentration profiles in the splash zone during bubbling fluidized bed combustion [185,258]. In addition, the emission of N_2O was relatively low in the case of straw and sunflower husk combustion, while considerably higher for sunflower seed and sewage sludge combustion. In sunflower seed combustion, N_2O was formed above the bed with slight change throughout the reactor. In the case of sewage sludge, N_2O was primarily formed in the gaseous phase by oxidation of NH_3 or possibly HCN, or partial reduction of NO, as negligible amounts of HNCO was observed above the fuel inlet.

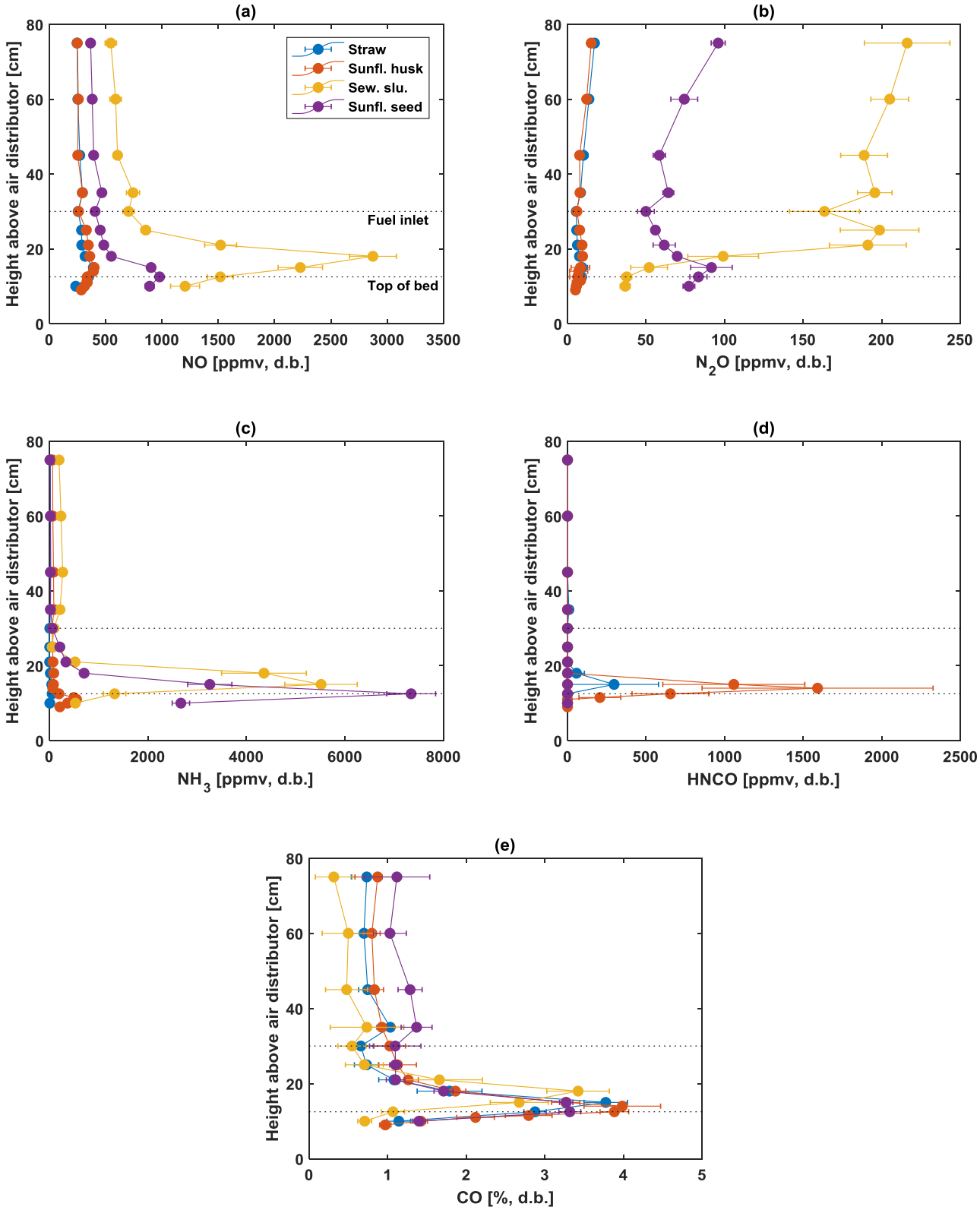

Figure 3.5: Axial NO (a), N_2O (b), NH_3 (c), HNCO (d), and CO (e) profiles during fluidized bed mono-combustion of selected biomass. The error bars indicate temporal fluctuations in the concentration. Conditions: T_{bed} = 850ºC; λ = 1.4; λ_1/λ = 1.

Although the local concentration of CO_2 could be measured in the FTIR, the raw data exhibited large fluctuations that necessitated comprehensive signal pre-treatment in order to obtain a concentration profile. The treatment of the CO_2 signal for the relevant fuels is demonstrated in Appendix A.6, and the resulting CO_2 and O_2 axial concentration is shown in Figure 3.6. The O_2 profile was obtained from the CO_2, NO, and CO data by Eq. 3.5 calculated at each height. It should be noted that due to the large error in the CO_2 measurement and the use of several signal processing techniques, the usability and credibility of the obtained data would be limited. However, with a priori knowledge of the CO and C_XH_Y profiles, a simplified expectation profile was constructed for CO_2 and O_2, additionally shown in Figure 3.6. The treated data qualitatively exhibit a similar tendency as the expectation, in which most of the combustion takes place in the top of the bed and freeboard sections. Although prone to error, the results here may be useful in the case of future modelling studies.

$$O_2 = 21 - CO_2 - \frac{1}{2}\,CO - \frac{1}{2}\,NO \qquad \text{Eq. 3.5}$$

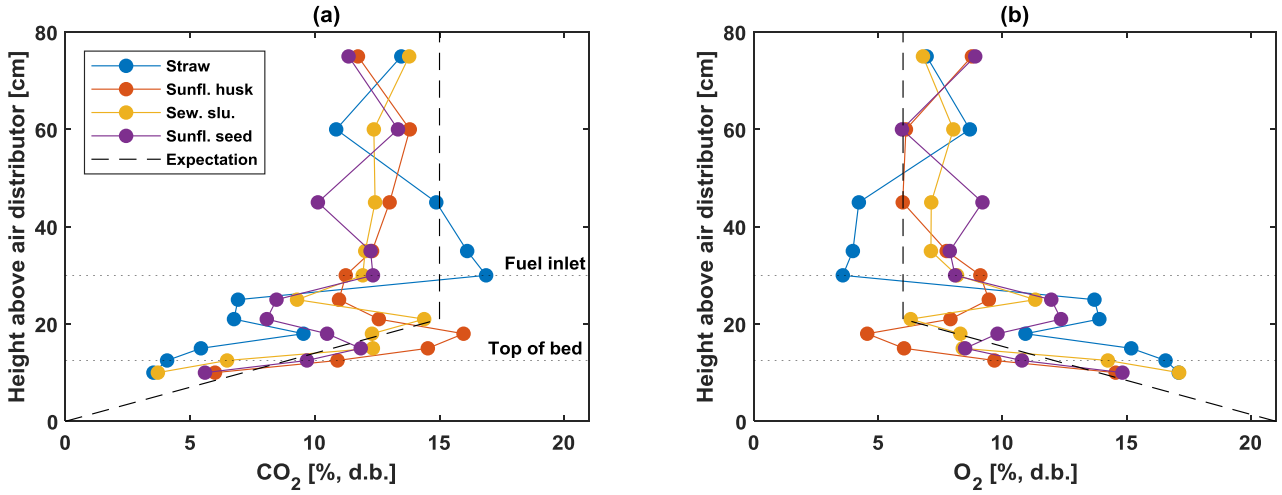

Figure 3.6: Axial CO_2 (a) and O_2 (b) profiles during fluidized bed mono-combustion of selected biomass. Conditions: T_{bed} = 850ºC; λ = 1.4; λ_1/λ = 1.

3.3.2 Un-staged co-combustion of selected biomass

Figure 3.7a-d summarize the experimental results from fluidized bed co-combustion. The averaged effluent NO concentration data indicate that straw-sunflower husk and straw-sunflower seed co-combustion were additive, as the NO concentration followed the linear trend line. In contrast to this, the NO emission from straw-sewage sludge co-combustion exhibited a strong promoting effect. A similar synergy effect was observed in sunflower seed-sewage sludge co-combustion, demonstrated in Appendix A.7. These observations were additionally visible from the fuel-N to NO conversion, in which the trend lines were calculated from the propensity of the pure fuels for forming NO, demonstrated in Eq. 3.6-3.7.

$$NO_{mix} = f_{sf}\, NO_{sf} + (1\text{-}f_{sf})\, NO_S \qquad \text{Eq. 3.6}$$

$$\eta_{mix} = \frac{f_{sf}\, w_{N,sf}\, \eta_{sf} + (1\text{-}f_{sf})\, w_{N,S}\, \eta_S}{f_{sf}\, w_{N,sf} + (1\text{-}f_{sf})\, w_{N,S}} \qquad \text{Eq. 3.7}$$

Here, f_{sf} is the fraction of secondary fuel, NO_{sf} and NO_S are the NO emissions (ppmv) during mono-combustion of the secondary fuel and straw, respectively, NO_{mix} is the NO emission (ppmv) during straw-secondary fuel co-combustion, w_{sf} and w_S are the nitrogen contents (kg N/kg fuel) in the secondary fuel and straw respectively, η_{sf} and η_S are the conversions of fuel-N to NO during mono-combustion of secondary fuel and straw respectively, and η_{mix} is the conversion of fuel-N to NO during straw-secondary fuel co-combustion based on the propensities of the individual fuels for forming NO.

The temperature during co-combustion was reasonably constant, while the CO concentration from sewage sludge co-combustion exhibited a minimum. The decrease in CO with increasing sewage sludge share from 0 to 50% may be caused by the catalytic effect of sewage sludge ash on CO oxidation [259] and/or by the capture of KCl from the gas phase. With an increase in the straw share, the concentration of KCl in the gas phase is expected to increase, which could inhibit CO oxidation (cf. Chapter 4, Section 4.3.2.1). As sewage sludge is rich in Al and Si, the produced ash may act as a sink for gas phase potassium [260,261], thereby lowering the CO emission indirectly. Above a sewage sludge fraction of 50%, the CO increased most likely due to the presence of smaller sewage sludge particles. Sewage sludge particles are brittle and may break upon feeding to the reactor, leading to fuel particle elutriation and incomplete combustion. The lower CO concentration along with the catalytic effect of sewage sludge ash on HCN and NH_3 oxidation could explain the increased emission of NO during straw-sewage sludge co-combustion [167,189,220,248]. The influence of sewage sludge ash on the nitrogen conversion during co-combustion was further investigated using model compounds, fuel fractionation, and local concentration measurements.

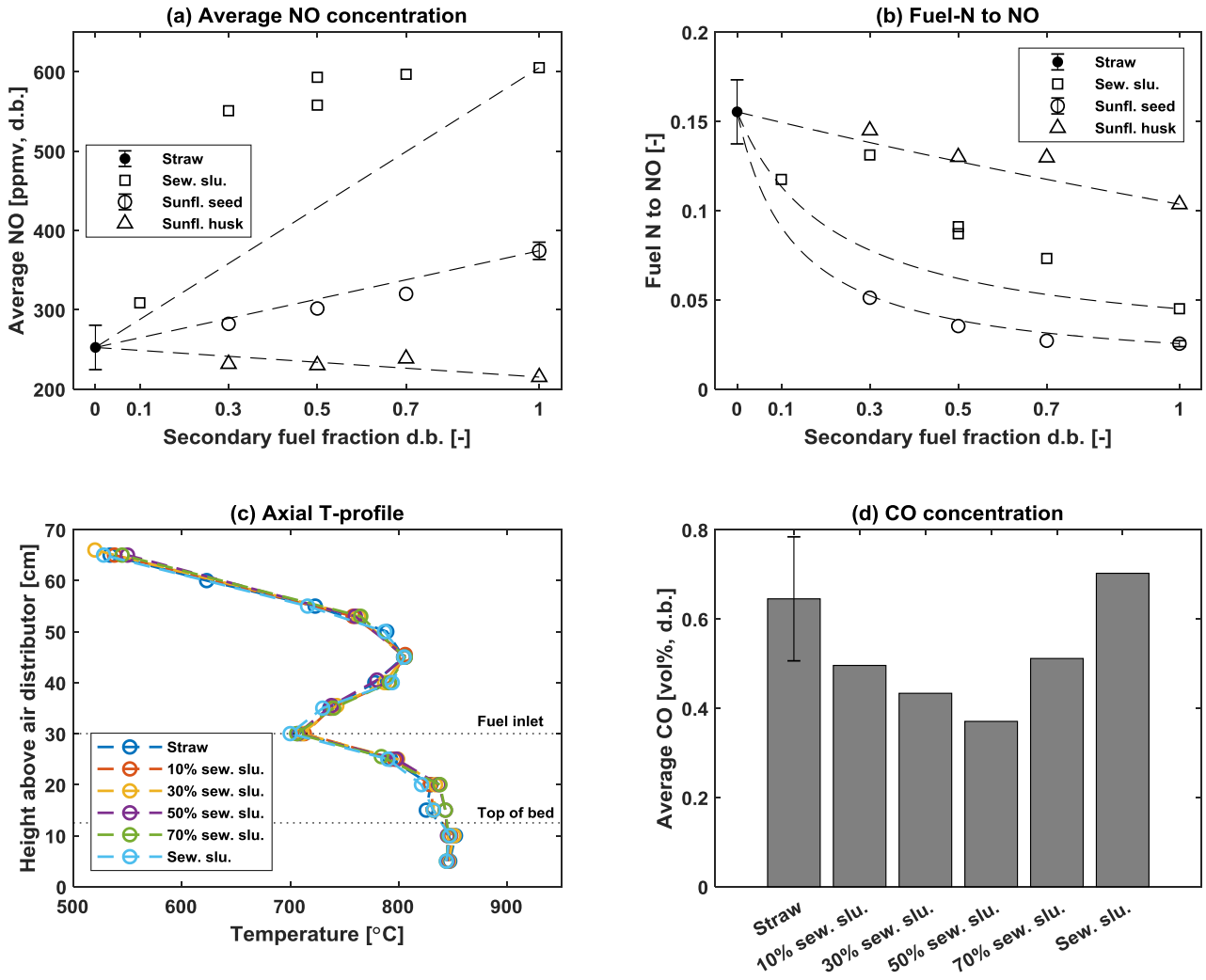

Figure 3.7: Averaged effluent NO concentration (a), conversion of fuel-N to NO (b), axial temperature profile (c), and averaged effluent CO concentration (d) during steady state, air un-staged fluidized bed co-combustion of biomass. Conditions: T_{bed} = 850ºC; λ = 1.4; λ_1/λ = 1.

3.3.2.1 Influence of sewage sludge ash

To investigate the catalytic effect of the sewage sludge ash, pellets of model compounds, urea and alanine, were fed batch wise to the fluid bed reactor before and after a combustion experiment. The bed before an experiment consisted of silica sand, while that after would additionally contain ash. Figure 3.8a and b show the conversion of model compound nitrogen to NO against the mass of sewage sludge ash theoretically added the reactor during combustion. At high heating rate, the decomposition of urea mainly yielded NH_3 and HNCO [262], while the major nitrogen product from alanine decomposition was NH_3 with a lesser amount of $CH_3CH_2NH_2$ [263–265]. The presence of ash increased the conversion to NO for both model compounds. In addition, no significant differences were observed for the ash from straw-sewage sludge and straw-sunflower seed. This was most likely due to the much larger ash content of sewage sludge (50.2 wt% d.b.) compared to that of straw (4.6 wt% d.b.) and sunflower seed (14 wt% d.b.). The influence of ash levelled off with the amount of ash added to the reactor.

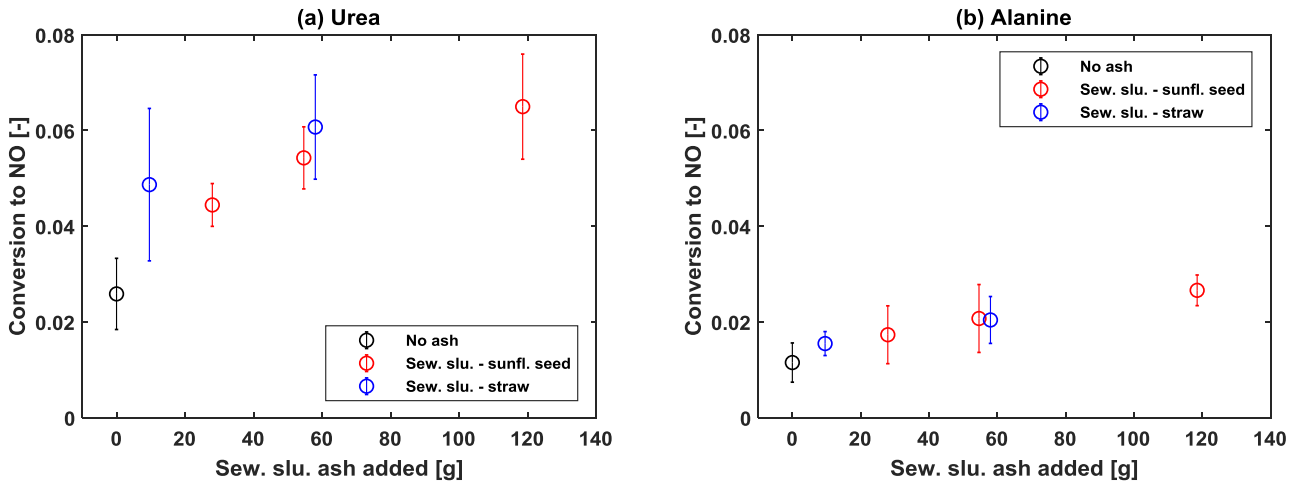

Figure 3.8: Conversion of nitrogen to NO during combustion of urea (a) and alanine (b) before and after continuous combustion experiments. No ash refers to a fluidized sand bed. The x-axis was calculated from the theoretical amount of sewage sludge ash added during experiments. Conditions: T_{bed} = 850ºC.

Figure 3.9a-d illustrates the results from combustion of straw with sewage sludge ash. The ash particles were added either batch wise from the top of the reactor or premixed with the fuel. The presence of sewage sludge ash increased the NO emission and consequently fuel-N to NO conversion during combustion. The influence of ash was highest when the ash was premixed with the fuel and prepared at lower temperatures. The explanation of the effect of ash preparation temperature could be related to physical and/or chemical differences. Consequently, the BET surface area and XRD spectra of the different ash were determined, shown in Appendix A.8. The surface area decreased with the severity of heat treatment due to the enhanced sintering, while the crystal structure of the ash prepared at 550ºC was different from the higher temperature ash. These differences may explain the lower catalytic effect of high temperature sewage sludge ash. However, while a lower surface area conceivably reduces the propensity for reaction, a deeper investigation into the effect of the crystalline composition of the ash on the catalytic properties should be performed. Besides ash preparation temperature, the ash introduction method was also of importance, as premixed ash increased the NO

emissions to a larger extent. Premixing would lead to a closer contact between the fuel and ash, thereby facilitating the catalytic conversion of fuel-N to NO. In addition, premixing led to lower CO emissions, which could additionally increase NO emission. This may again be attributed to the catalytic effect of sewage sludge ash on CO oxidation [259] or to the capture of KCl by sewage sludge ash [260,261]. Similar to the model compound study, the influence of ash on the NO emission reached a plateau after the introduction of a certain amount of ash, which in this case was approximately 10-20 g.

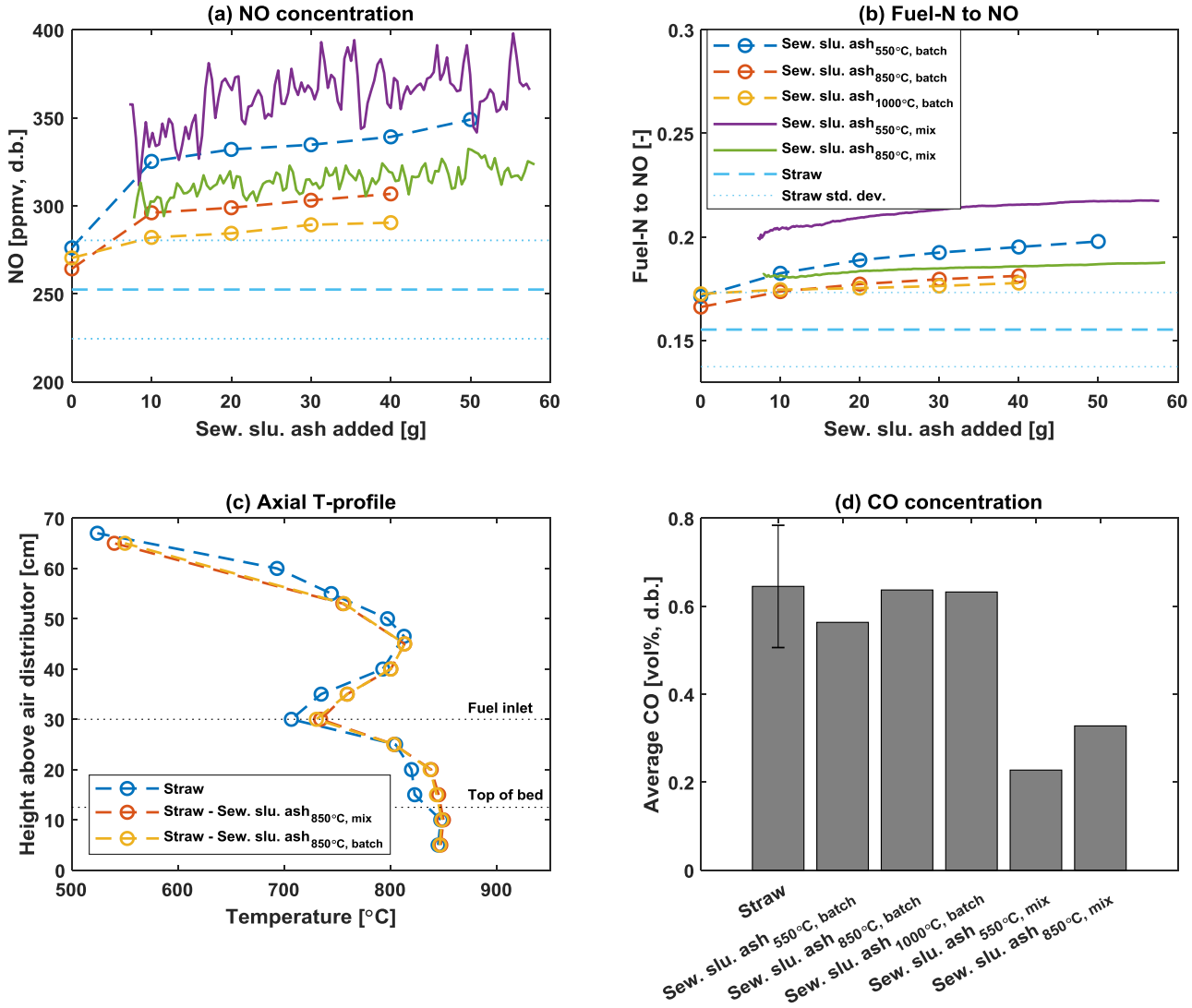

Figure 3.9: Effluent NO concentration (a), conversion of fuel-N to NO (b), axial temperature profile (c), and average CO concentration (d) during fluidized bed combustion of straw and sewage sludge ash. The ash was added either batch wise or premixed with the fuel, described in the legend. Conditions: T_{bed} = 850ºC; λ = 1.4; λ_1/λ = 1.

3.3.2.2 Influence of sewage sludge volatiles, char, and ash

Figure 3.10 displays the effluent NO emission against the theoretical amount of sewage sludge ash added to the reactor during co-combustion of straw with sewage sludge and its derivatives, i.e., ash and char. The fraction of char in the premixed fuel was calculated to ensure a constant sewage sludge ash feeding rate during experiment (around 29 wt% d.b. of char). The combustion of straw with sewage sludge char and ash reached steady state after the addition of approximately 10 g of sewage sludge ash. The NO emissions were clearly higher due to the catalytic effect of ash and the oxidation of sewage sludge char-N. In contrast to this, the NO emission during co-combustion of the two fuels exhibited a transient behavior showing initially a low NO emission followed by an increase with the addition of sewage sludge ash until reaching a plateau. It was therefore speculated that, at low concentrations of sewage sludge ash in the bed, the presence of volatiles, mainly a high concentration of NH_3 based on Figure 3.5, reduced the NO emission by thermal $DeNO_X$. With the accumulation of ash, the NO emission increased significantly, as the ash catalyzed the formation of NO from NH_3 originating from sewage sludge devolatilization. This in turn indicates that the interaction in the nitrogen chemistry during co-combustion occurred both by homogeneous gas phase reactions and heterogeneous gas-solid reactions. However, based on the effluent NO concentration and fuel-N to NO conversion during co-combustion (Figure 3.7a and b), no significant interaction was observed during straw-sunflower seed co-combustion, even though a large concentration of NH_3 was measured during sunflower seed mono-combustion. This was further investigated by determining the NO reduction reactivity of the fuels along with measurements of the local gas composition.

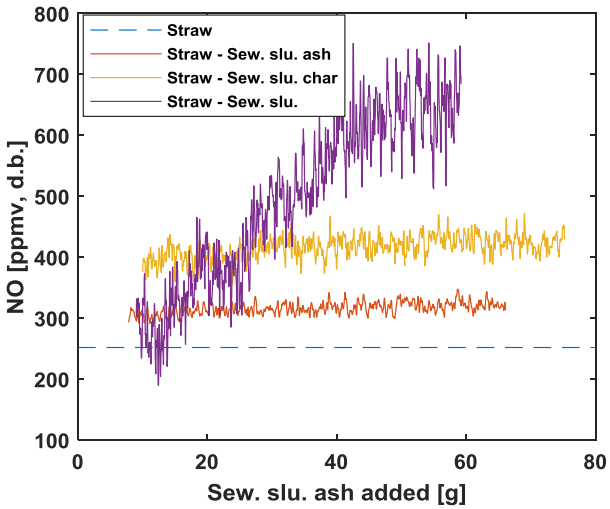

Figure 3.10: NO emission from straw combustion and co-combustion of straw with sewage sludge fuel, char, and ash. In the case of co-combustion, 50% straw and 50% sewage sludge was used. Conditions: T_{bed} = 850ºC; λ = 1.4; λ_1/λ = 1.

3.3.2.3 NO reduction reactivity

To investigate the reduction reactivity of the fuels and thereby gain insight into the fate of NO within the reactor, combustion experiments were performed with the introduction of NO with the primary gas. The raw and smoothened concentration measurements of NO in the outlet are demonstrated in Figure 3.11, along with the NO emission from combustion without external NO for comparison. The smoothened data were determined for the stable combustion regions, found from the outlet O_2 and CO_2 profiles. In the case of sunflower seed alone, the concentration of external NO was changed during experiment. The results show that the net reduction of NO was favored, as the outlet concentration of NO was lower than the sum of the NO introduced with the primary gas and that from combustion. This is similarly observed in NO_X minimization by flue gas recirculation, in which the reduction product from recirculation was generally N_2 with a lesser amount of N_2O [227,266]. During straw and sunflower seed combustion, the NO concentrations with and without external NO were more or less stable. In the case of sewage sludge and straw-sewage sludge combustion with and without external NO, the NO concentration increased with ash accumulation and time.

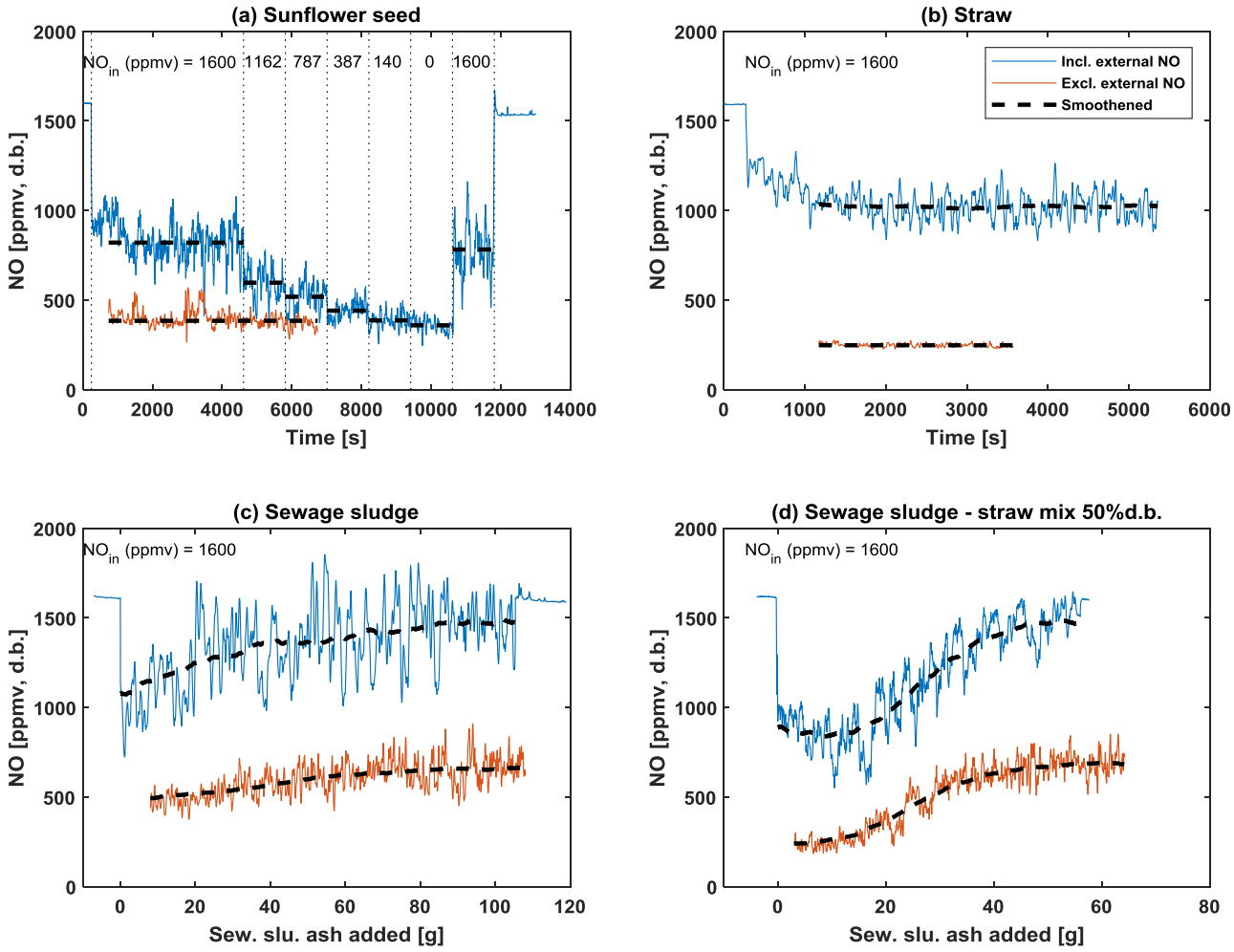

Figure 3.11: Effluent NO concentration during sunflower seed (a), straw (b), sewage sludge (c), and straw-sewage sludge combustion (d) with and without the addition of external NO with the primary gas. In the case of co-combustion, 50% straw and 50% sewage sludge was used. Note that the experiments including sewage sludge are plotted against the amount of ash added to the reactor. Conditions: T_{bed} = 850ºC; λ = 1.4; λ_1/λ = 1.

The fractional reduction of the external NO (R_{NO}) was quantified by Eq. 3.8 [227,266,267]. Here, NO_{in} (ppmv) is the initial concentration of NO, NO_b (ppmv) is the concentration of NO formed during combustion without external NO, and NO_{out} (ppmv) is the concentration of NO in the effluent.

$$R_{NO} = \frac{NO_{in} + NO_b - NO_{out}}{NO_{in}} \qquad \text{Eq. 3.8}$$

Figure 3.12a demonstrates R_{NO} against time for sunflower seed and straw, and against the amount of added sewage sludge ash for the experiments involving sewage sludge. The NO reduction reactivity of straw and sunflower seed was stable in the steady state combustion region. Sunflower seed showed the highest reduction reactivity, most likely due to the large concentration of NH_3 during its combustion (cf. Figure 3.5). In contrast to this, the fractional reduction of NO decreased for sewage sludge and showed a maximum during co-combustion. Consequently, the reduction propensity was higher in the reactor (bed and freeboard) at the early stages of combustion, i.e. lower ash content. The relevant NO reduction mechanisms are by char, combustibles (CO and C_XH_Y), and NH_3 or other N-containing light gaseous species. At low concentrations of ash in the reactor, the NH_3 (and possibly HCN) may favor the reduction of NO, thereby explaining the higher reduction reactivity. With the accumulation of ash, the light gaseous N-species are oxidized to NO under the catalysis of sewage sludge ash. The ash could possibly also influence the concentration of combustibles, e.g. by catalyzing oxidation reactions of CH_4 and CO [259], the presence of which could affect the NO reduction indirectly (change in thermal $DeNO_X$) or directly (reburning mechanism). After around 40 g of ash introduced to the reactor, the fractional reduction from sewage sludge and straw-sewage sludge combustion was similar. From Figure 3.12b, showing R_{NO} against the NO inlet concentration for sunflower seed combustion, R_{NO} decreased with an increase in NO inlet concentration, suggesting a concentration dependency of R_{NO}. Previous studies on flue gas recirculation revealed a negligible change in R_{NO} for different NO inlet concentrations [227,266]. Further study is necessary to elucidate the influence of NO concentration on R_{NO}.

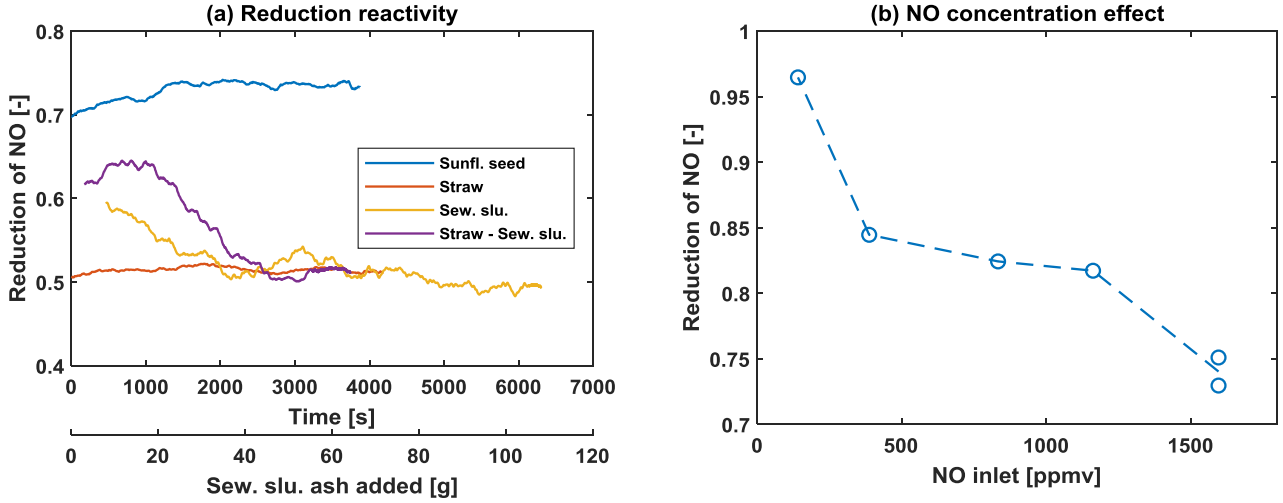

Figure 3.12: Fractional reduction of the fuels against time for sunflower seed and straw, and against sewage sludge ash added for experiments involving sewage sludge (a). Fractional reduction of the sunflower seed against NO inlet concentration (b). Conditions: T_{bed} = 850ºC; λ = 1.4; λ_1/λ = 1.

3.3.2.4 Local gas composition measurements

Figure 3.13 illustrates the NO, N_2O, NH_3, HNCO, and CO axial concentration profiles during combustion of straw, sewage sludge, and straw-sewage sludge. For the co-combustion, measurements were taken at the initial stages of combustion, corresponding to 2 – 25 g of sewage sludge ash added, while the late measurements were taken from 40 – 80 g sewage sludge ash added. The maximum in the NO, NH_3, and CO profiles shifted with the accumulation of ash, which was previously attributed to the increase in bed height during experiment. At low levels of ash in the reactor, a significantly larger amount of NH_3 and correspondingly lower concentration of NO were detected at the top of the bed. With ash accumulation, the formation of NO increased due to the catalytic activity of ash, thereby leading to higher emission of NO, comparable to that of the pure sewage sludge. Correspondingly, the concentration of NH_3 decreased along with the potential for thermal $DeNO_x$. The effect of sewage sludge ash accumulation on C_XH_Y species in co-combustion are summarized in Appendix A.9 (Figure A.22), showing that the accumulation of ash shifted the concentration profiles without significantly altering the magnitudes. In the initial stages of co-combustion, some HNCO was detected in the freeboard which was not present at later stages, most likely due to the catalytic effect of the sewage sludge ash on the HNCO reactions. The N_2O concentration decreased with ash accumulation, possibly due to the increased selectivity for forming NO and the ash-catalyzed destruction of N_2O (cf. Chapter 2, Section 2.3.5).

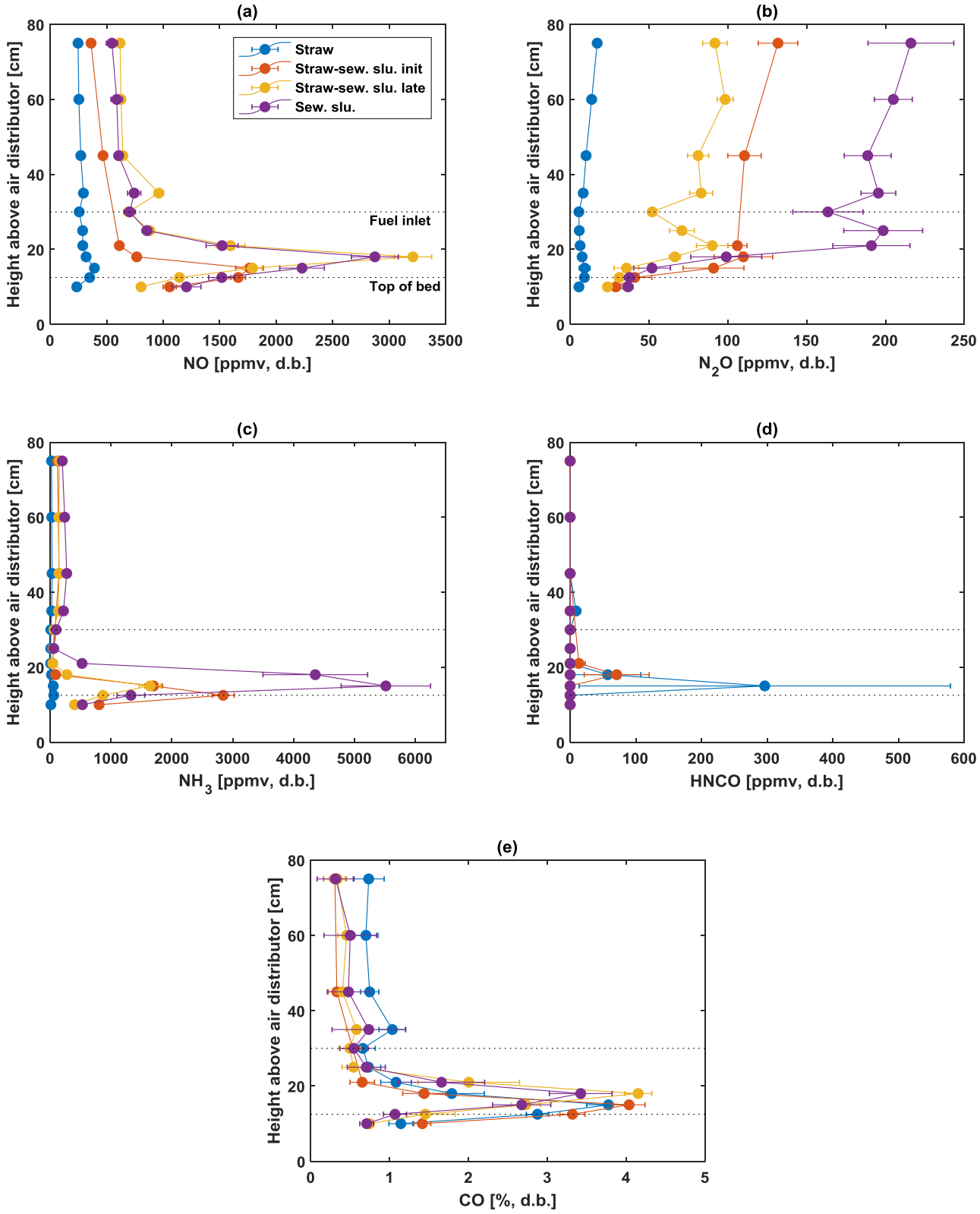

Figure 3.13: Axial NO (a), N_2O (b), NH_3 (c), HNCO (d), and CO (e) profiles during fluidized bed combustion of straw, sewage sludge, and straw-sewage sludge (50-50% d.b.). For the co-combustion, measurements were performed at the initial stages of combustion (init, corresponding to the addition of 2-25 g of ash to the reactor) and later stages (late, corresponding to the addition of 40-80 g of ash to the). Conditions: T_{bed} = 850ºC; λ = 1.4; λ_1/λ = 1.

Figure 3.14 shows the NO, N_2O, NH_3, HNCO, and CO axial concentration profiles during combustion of straw, sunflower seed, and straw-sunflower seed. Based on the outlet NO measurements of straw-sunflower seed co-combustion (cf. Figure 3.7a and b), it was hypothesized that no interaction occurred during co-combustion. However, in Figure 3.14, although the NO concentration in the outlet was close to the weighted average of the pure fuels, the concentration near the top of the bed was significantly higher than expected. In addition, a high concentration of NH_3 was observed at the top of the bed, which conceivably interacted with the nitrogen from straw. A large reduction of the formed NO occurred in the freeboard due to the high concentration of NH_3 released from sunflower seed and possibly due to the direct or indirect reduction by combustibles. Furthermore, the N_2O emission from co-combustion was significantly higher than that of the weighted average, additionally indicating that an interaction effect was prominent during straw-sunflower seed combustion. No HNCO was detected from the co-combustion, the explanation of which remains unknown. The CO concentration profiles in Figure 3.14e as well as the profiles of major C_XH_Y species such as CH_4 and C_2H_4 in Appendix A.10 from straw, sunflower seed, and straw-sunflower seed combustion were comparable.

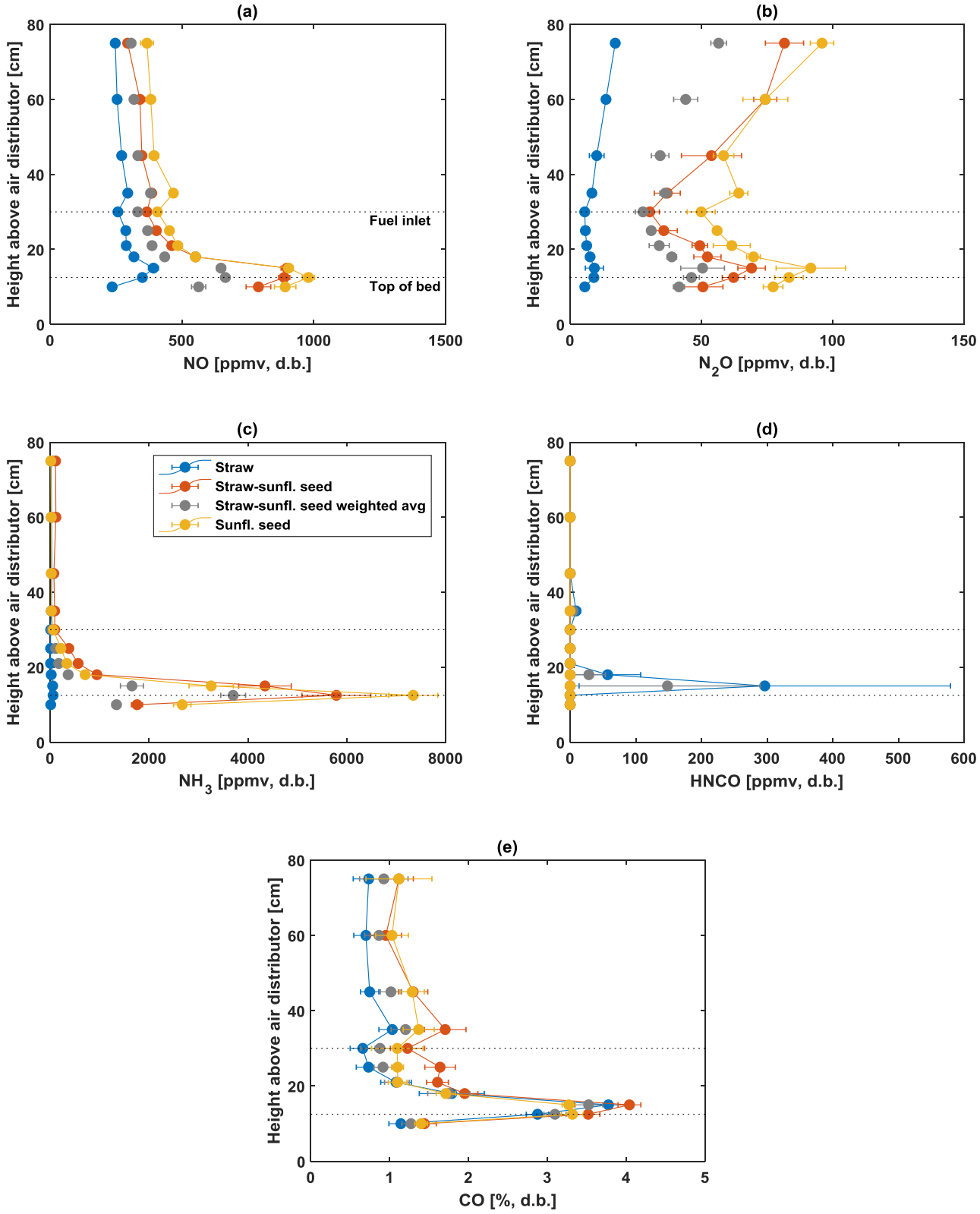

Figure 3.14: Axial NO (a), N_2O (b), NH_3 (c), HNCO, and CO (d) profiles during fluidized bed combustion of straw, sunflower seed, and straw-sunflower seed (50-50% d.b.). Conditions: T_{bed} = 850ºC; λ = 1.4; λ_1/λ = 1.

3.3.3 Air staged combustion of straw, sewage sludge, and their mixture

Figure 3.15a-d show the results from combustion of straw, sewage sludge, and the mixtures of these at air staged and un-staged conditions. The average NO concentration demonstrates the changes with time as calculated from Eq. 3.9. At air un-staged conditions, the NO concentration changed significantly with time. In comparison, the change was much less pronounced at air staged conditions, most likely due to the lower concentration of O_2 and thereby lower importance of NO forming reactions near the bed and freeboard. Air staging led to a significant reduction in the NO emission and thereby conversion of fuel-N to NO. The temperature profiles from air staged and un-staged combustion were similar, while the CO concentration in air staged combustion was slightly higher. In both cases, a minimum in the CO concentration was observed, explained in Section 3.3.2.

$$\text{Average NO(from 0 s to (1200·i) s)} = \sum_{i=1}^{k} \frac{\text{NO(from 0 s to (1200·i) s)}}{1200 \cdot i + 1} \qquad \text{Eq. 3.9}$$

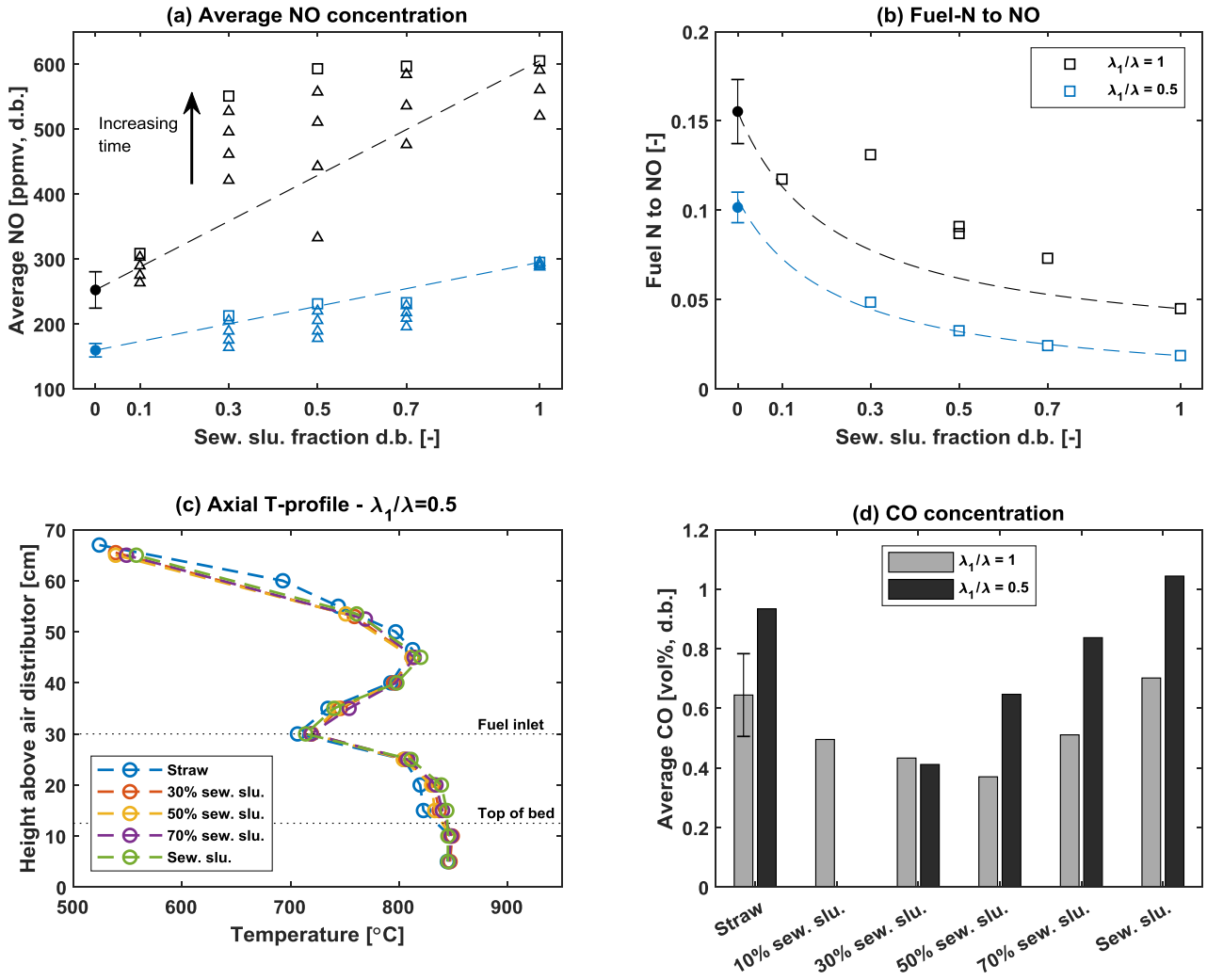

Figure 3.15: Averaged effluent NO concentration (a), conversion of fuel-N to NO (b), axial temperature profile (c), and averaged effluent CO concentration (d) during combustion of straw, sewage sludge, and mixtures at staged and un-staged conditions. Conditions: T_{bed} = 850ºC; λ = 1.4; λ_1/λ = 0.5 and 1.

3.3.3.1 Local gas composition measurements

The NO, N_2O, NH_3, HNCO, and CO axial concentration profiles during combustion of straw and straw-sewage sludge are depicted in Figure 3.16 and Figure 3.17, respectively, at air staged and un-staged conditions. The results indicate that the trends in both experiments were comparable. As the bottom section of the fluidized bed was kept under reducing conditions, the CO concentration was generally higher, while the NO concentration lower. The NH_3 and HNCO concentrations were higher at air staged conditions near the bed in consequence of the lower concentration of O_2. At the conditions of low O_2 and high H_2O concentrations, any formed HCN may additionally be hydrolyzed to NH_3 [183]. The high NH_3 and HNCO, and low O_2 concentrations in turn favored the reduction of NO over formation, leading to a lower concentration of NO in the effluent. While N_2O was lower at air staged conditions below the fuel inlet, the introduction of secondary air resulted in a negligible change in the outlet concentration. Similar trends were observed for sewage sludge combustion, demonstrated in Appendix A.11 (Figure A.26). In addition, the C_XH_Y and CH_2O profiles from air staged and un-staged combustion of straw and sewage sludge are shown in Appendix A.12, showing that the trends in the combustibles were similar to that of CO, i.e. generally higher in the reduction zone.

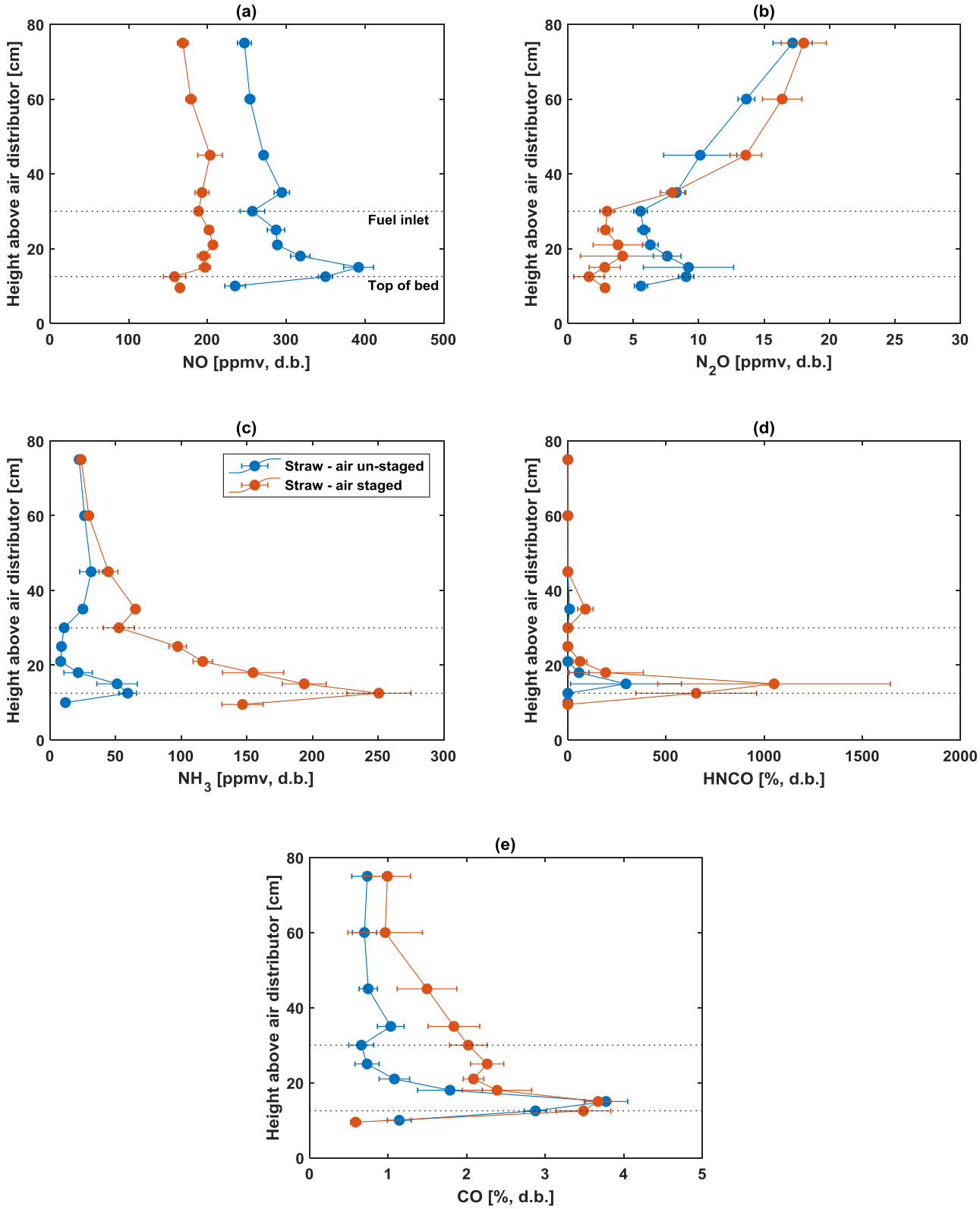

Figure 3.16: Axial NO (a), N_2O (b), NH_3 (c), HNCO (d), and CO (e) profiles during air staged and un-staged fluidized bed combustion of straw. Conditions: T_{bed} = 850ºC; λ = 1.4; λ_1/λ = 1 and 0.5.

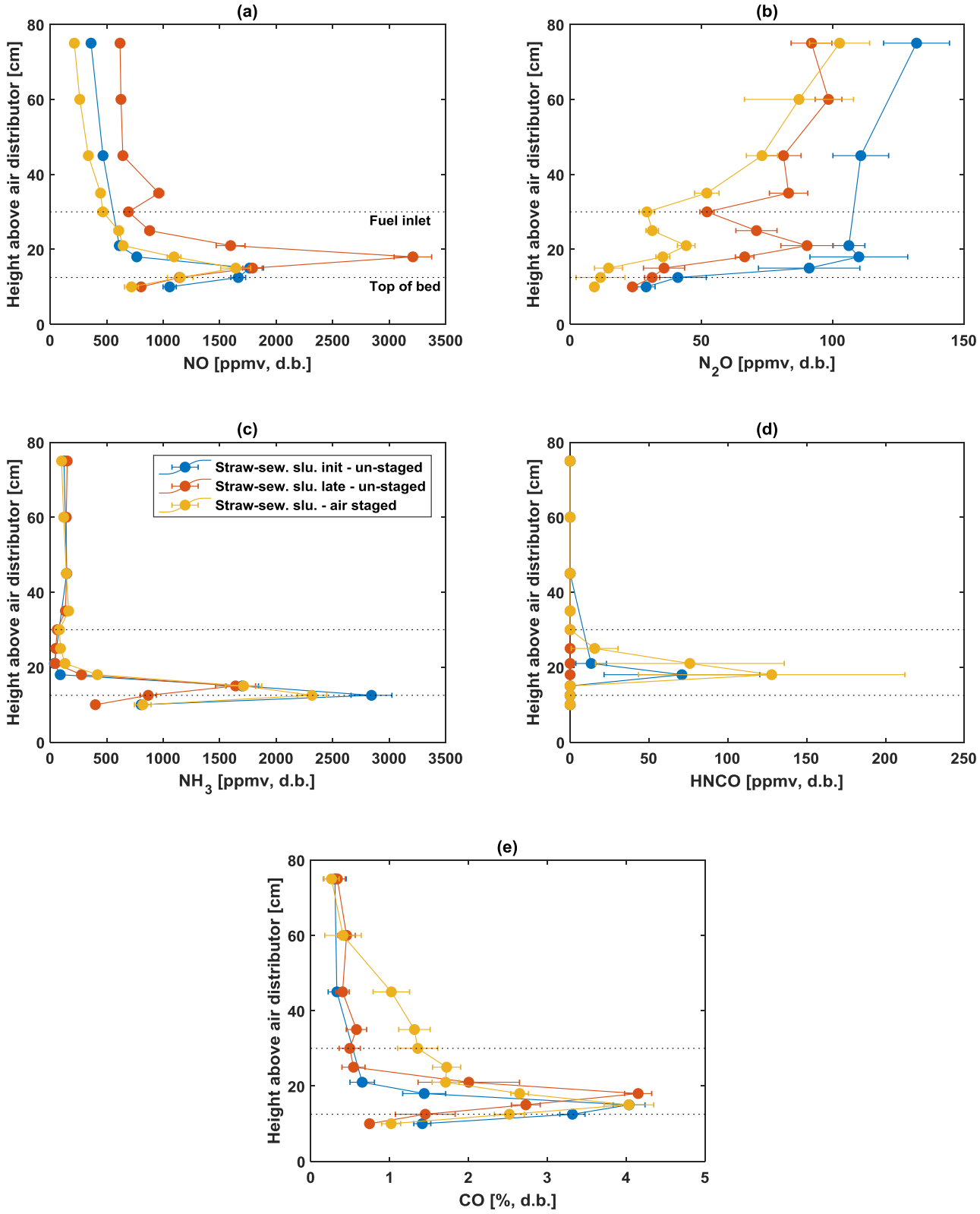

Figure 3.17: Axial NO (a), N_2O (b), NH_3 (c), HNCO (d), and CO (e) profiles during air staged and un-staged fluidized bed combustion of straw-sewage sludge (50-50% d.b.). Conditions: T_{bed} = 850ºC; λ = 1.4; λ_1/ λ = 1 and 0.5. For the un-staged co-combustion, measurements were performed at the initial stages of combustion (init, corresponding to the addition of 2-25 g of ash to the reactor) and later stages (late, corresponding to the addition of 40-80 g of ash to the).

3.4 Conclusions

In combustion of pine wood, beech wood, straw, sunflower husk, sewage sludge, and sunflower seed, the fuel-N to NO conversion decreased with an increase in fuel-N content, attributed to the larger release of nitrogen species (NH_3) thereby facilitating NO reduction by thermal $DeNO_X$.

A synergy effect was observed from the effluent NO concentration in straw-sewage sludge combustion, showing that the NO emission was higher than the weighted values. This was primarily caused by the promotional effect of sewage sludge ash on NO formation from NH_3 and HCN. The selectivity and reactivity of the ash towards NO formation increased with lower ash preparation temperature and a better mixing of ash with straw. This was attributed to the higher surface area of the low temperature ash and possibly to differences in the crystal composition as determined by XRD.

The NO emission from straw-sewage sludge combustion changed with time and ash accumulation. In the initial stages of combustion, the NH_3 released by sewage sludge reduced the NO emission, while at higher concentration of ash in the bed, the NH_3 was predominantly oxidized to NO. In the case of straw-sunflower seed combustion, although the effluent data did not reveal an interaction between the fuels, the local concentration measurements showed a synergy effect during combustion.

Air-staging significantly reduced the NO emissions from mono- and co-combustion. In addition, the interaction effect between straw-sewage sludge was less pronounced at air staged conditions. This was attributed to the lower concentration of O_2 near the bed and thereby lower importance of NO forming reactions.

4 Influence of fuel properties and operating conditions on NO_X emissions

Abstract: The nitrogen conversion behavior of pine wood, beech wood, straw, sunflower husk, sewage sludge, and sunflower seed was investigated by batch fluidized bed combustion and compared to results obtained from continuous combustion. In addition, the influence of ash forming elements, herein especially KCl, KOH, K_2CO_3, and KCl/K_2CO_3, on the NO emission was investigated during continuous combustion. Moreover, the effect of air staging (primary to total air ratio (λ_1/λ) from 0 to 1), temperature, type of bed material (CaO and kaolin), and gas phase composition (N_2 or CO_2) on the NO emission was examined. The fuel-N to NO conversion decreased with increasing fuel-N content and was lower in continuous combustion compared to batch combustion. Volatile-NO was generally the major contributor (45-75%) to NO_X emissions. Washing off ash forming elements from straw increased the fuel-N to NO conversion and decreased CO emission. KCl and KOH doping the washed straw increased CO emission, while lowering fuel-N to NO conversion. K_2CO_3 doping had a negligible effect on the fuel-N to NO conversion, while it increased CO emission. Compared to pine wood, KCl-doped pine wood increased the CO emission and did not change the fuel-N to NO conversion considerably. Batch addition of KCl during straw combustion led to increased CO and decreased NO emissions, which were more pronounced at air staged ($\lambda_1/\lambda = 0.04$) compared to un-staged ($\lambda_1/\lambda = 1$) conditions. The combustion of straw and sunflower husk showed a minimum in the NO emission and fuel-N to NO conversion in the range of $\lambda_1/\lambda = 0.5$-0.75. Increasing temperature increased the fuel-N to NO conversion for straw, while for KCl-doped washed straw, the fuel-N to NO conversion increased and levelled off, explained by the inverse trend in CO. Furthermore, the fuel-N to NO conversion and CO emission were unaffected by replacing the bed partially with kaolin and CaO, or complete by CaO at $\lambda_1/\lambda = 1$, or by changing the primary gas from N_2 to CO_2 at $\lambda_1/\lambda = 0$ and 0.04 during straw combustion

4.1 Introduction

NO emission from fluidized bed combustion is influenced by the fuel properties and operating conditions, summarized in Chapter 2, Section 2.4.1 and 2.4.2. Knowledge on the nitrogen chemistry during solid fuel combustion, i.e. fuel-N to NO conversion, and volatile- and char-NO contribution, is important for developing strategies for NO_X minimization. The existing studies typically involve a clear distinction of volatile and char combustion, and are predominantly performed for single particles or a narrow particle size range [84,95,172,174]. However, biomass used in fluidized bed combustors has a wide particle size range [9]. Insight into the conversion of biomass-N to NO and the relative contribution of volatile- and char-NO for a particle size distribution is desired.

Several studies have compared the combustion of raw and washed biomass [268–272]. These were mainly focused on the agglomeration and deposition behaviour. However, ash forming elements may affect the fuel-N conversion by interacting with gaseous species, or by changing the pyrolysis behaviour and char reactivity (cf. Chapter 2). The influence of ash forming elements on the nitrogen behaviour is predominantly studied under well controlled conditions (cf. Chapter 2, Section 2.4.1.3). Consequently, information from fluidized bed combustion of biomass is scarce.

In terms of operating conditions, no consensus exists on the importance of the bed temperature (cf. Chapter 2, Section 2.4.2.2). Moreover, alternative bed material and changing gas phase composition contain unexplored areas in terms of NO emission. While air staging has shown to be an effective technique for reducing NO emission [213,222,273–275], studies generally do not investigate secondary air ratios above 50%.

This study summarizes the results of an experimental study on the influence of fuel properties and operating conditions on NO_X emissions. Fundamental knowledge on the batch combustion behavior (fuel-N to NO conversion, and volatile- and char-NO contribution) of a particle size range of biomass was obtained using a methodology inspired by Konttinen et al. [172]. Moreover, the influence of ash forming elements was investigated by continuous combustion of straw, washed straw, pine wood, and potassium (KCl, KOH, K_2CO_3, and KCl/ K_2CO_3) doped pine wood and washed straw. In addition, the influence of temperature, air staging, type of bed material, and gas phase composition on the NO emission was examined during fluidized bed combustion of biomass.

4.2 Experimental section

Continuous and batch fluidized bed combustion of biomass was performed in the reactor described in Chapter 3, Section 3.2.3. The NO_2 concentration was insignificant in the continuous combustion experiments and was therefore not further investigated.

4.2.1 Fuels and their pre-treatment

The chemical composition and size range of the biomass used in the batch combustion experiments (pine wood, beech wood, straw, sunflower husk, sewage sludge, and sunflower seed) were shown in Table 3.1 (Chapter 3, Section 3.2.1).

Washing and K-doping of biomass were performed as described in [254]. Straw was washed with water in a pilot scale mixer using 20 mL water per gram of straw. The straw-water slurry was mixed for 24 h, after which the water was removed and the remaining straw filtered. The washed straw was dried in a vacuum oven for 24 h at 105ºC. After drying, the washed straw was sieved to a size range of 0.6-4 mm. Pine wood and washed straw were doped with KCl, KOH, K_2CO_3, and KCl/K_2CO_3 with a purity exceeding 99.9%. For water washed straw, it was assumed that 90% of the K was washed off and a similar amount of K was compensated for by the K model compounds. For pine wood, the amount of K model compound added was similar as in the case of washed straw. K-doping was performed by mixing model compounds with 4-6 g of water per gram of biomass, thereby forming a

slurry, which was stirred for 24 h. Subsequently, the doped biomass was dried at 70ºC for 24 h followed by 105ºC for 24 h and sieved to a size range of 0.6-4 mm. The chemical composition of the pine wood, straw, washed straw, and KCl doped pine wood and washed straw, determined by ICP-OES, are summarized in Table 4.1. The K-content of the KCl-doped fuels were reasonably close to the raw straw. Similarly, the K-content of the K_2CO_3 and KOH doped pine wood and washed straw were assumed to be in a similar range as the raw straw.

Table 4.1: Chemical composition of pine wood, straw, water washed straw, and KCl-doped pine wood and washed straw.

	Unit	Pine wood	KCl-doped pine wood	Straw	Washed straw	KCl-doped washed straw
Moisture	% wb	7.1	0.9	12.5	4.0	5.0
VM	% db	85.6	79.0	76.5	81.2	77.9
Ash		0.43	1.9	4.6	3.3	3.8
C		49.5	49.8	48.7	47.1	47.0
H		6.1	6.1	5.8	5.9	5.7
N		<0.1	0.1	0.69	0.6	0.5
S		0.006	< 0.005	0.08	0.042	0.046
Cl		0.02	0.66	0.18	0.021	0.58
O		43.8	42.1	40.0	43.1	42.8
Al	mg/kg db	90	11	230	180	150
Ca		950	770	3600	3700	3500
Fe		53	12	180	130	110
K		507	8300	8000	990	7700
Mg		94	130	630	530	500
Na		15	57	280	230	210
P		35	25	750	320	300
Si		299	57	11000	9500	8900
Ti		-	< 3	17	13	10

4.2.2 Batch combustion of a particle size range of biomass

Batch combustion experiments of the raw biomass were performed using the methodology illustrated in Figure 4.1, inspired by the work of Konttinen et al. [172]. The bed was fluidized by N_2 (6.2 NL/min), while air (10.1 NL/min) and N_2 (0.6 NL/min) were fed through the fuel feeding tube. Biomass (300-400 mg) was introduced to the pre-heated reactor at a stable O_2 outlet concentration (~12.5%). After biomass introduction, volatile combustion took place until the O_2 concentration reached its initial value. At this point, the introduction of air through the feeding tube was stopped and the concentration of O_2 in the outlet was monitored. When the O_2 outlet concentration was below around 0.5%, air was fed with the fluidizing gas, thereby commencing char combustion. The outlet concentrations of CO, CO_2, O_2, and NO (NGA2000, Fischer-Rosemount), and NO_2 (Eco Physics CLD 700 EL) were monitored with a sampling frequency of 0.5 Hz. The carbon closures, calculated from the outlet CO and CO_2 concentrations, ranged from 85-110% indicating a sufficient closure of the material balance of the system.

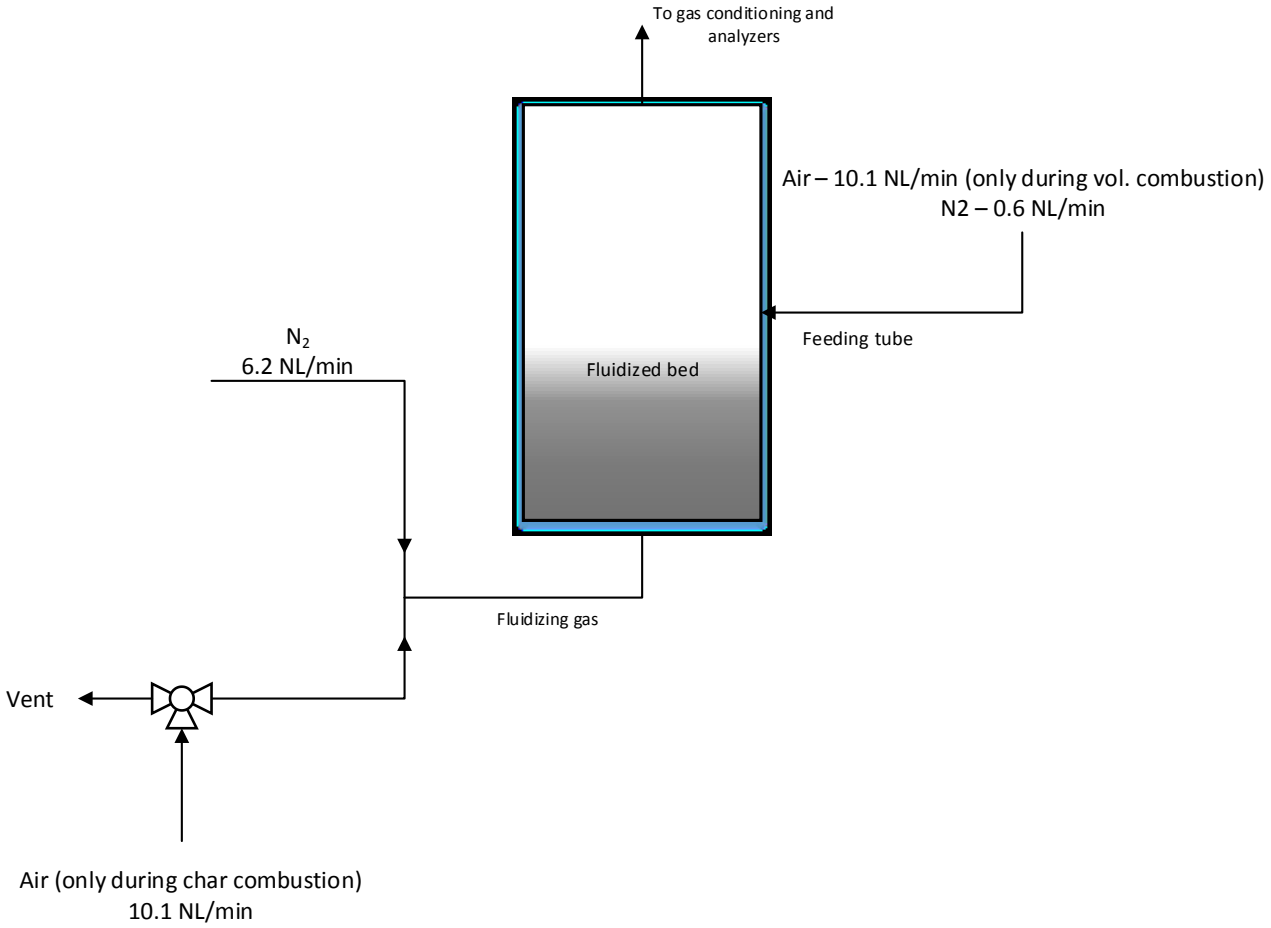

Figure 4.1: Setup of the batch combustion experiments.

Figure 4.2 depicts the axial temperature profile in the reactor without combustion at the conditions used in volatile and char combustion. For comparison, the temperature profile from continuous straw combustion is additionally shown, revealing that the profiles during volatile and char combustion were comparable to the continuous experiment. Optimally, the temperature profiles during volatile and char combustion would be similar and constant until the point of the last heating element, i.e. around 45 cm above the air distributor. However, the temperature in the freeboard during volatile combustion was lower, thereby slightly distorting the temperature at which volatile and char combustion occured. In future work, this should be optimized by varying the extent of external heating and by using pure O_2 to lower the total flow rate from the feeding tube.

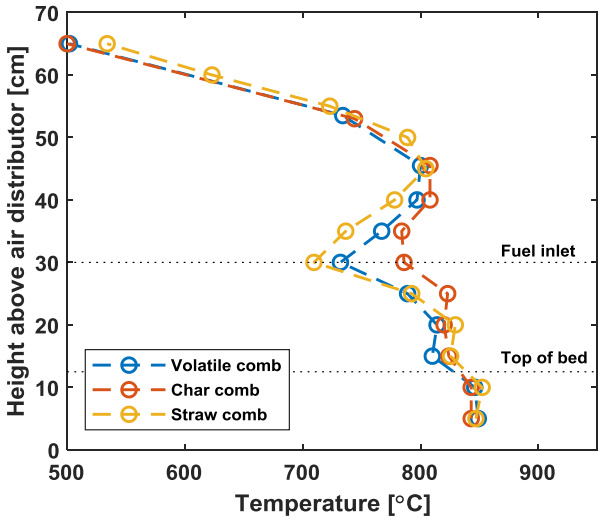

Figure 4.2: Axial temperature profile during volatile and char combustion configurations. For comparison, the profile from continuous straw combustion is additionally shown. The measurements were obtained without biomass introduction.

Figure 4.3 demonstrates the outlet concentrations of CO, CO_2, O_2, NO, and NO_2 from batch combustion of sunflower seed. The volatile and char combustion stages are separated by the dashed black line, showing a clear distinction between these two stages. The time difference between the onset of char combustion and the corresponding change in gas composition was caused by the delay in the gas analysis system. The outlet O_2 concentration did not decrease considerably during volatile combustion, indicating that the overall conditions in the reactor were oxidizing. However, some CO was formed during volatile combustion, which may be due to inadequate mixing and/or gas residence time, i.e. local redox conditions. Some NO_2 was measured in sunflower seed combustion, most likely formed in the gas analysis system downstream of the reactor. As high-nitrogen fuels release more NO and low-nitrogen fuels are sensitive towards small changes in NO_X concentration, the presence of NO_2 may be important for these two extremes.

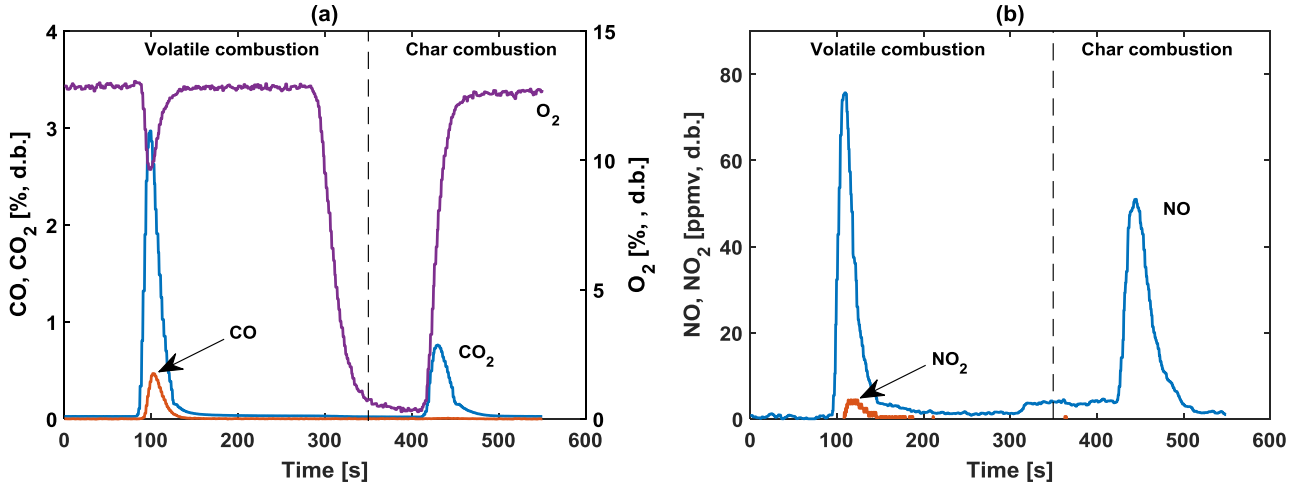

Figure 4.3: CO, CO_2, O_2 (a), NO, and NO_2 (b) concentration profiles during batch combustion of sunflower seed (323 mg). The separation between volatile and char combustion is illustrated by the dashed black line.

4.3 Results and discussion

4.3.1 Batch combustion of biomass

Figure 4.4 demonstrates the conversion of fuel-N to NO_X from batch and continuous fluidized bed combustion of biomass. The data from continuous combustion were described in Chapter 3, Section 3.3.1. The results show that the conversion of fuel-N to NO_X decreased with an increase in fuel-N content, explained by the higher concentration of N-intermediates released from high-nitrogen biomass, thereby leading to a larger reduction of NO [172]. The trends observed for batch combustion of biomass particles seem to resemble the data from single particle combustion studies [172,174]. In addition, the fuel-N to NO conversion was slightly higher during batch combustion compared to continuous combustion. As the temperature in the reactor during volatile and char combustion were comparable to the continuous experiments, the explanation for higher fuel-N to NO_X conversion is possibly due to more oxidizing conditions in the reactor during batch combustion, thereby suppressing the reduction of NO.

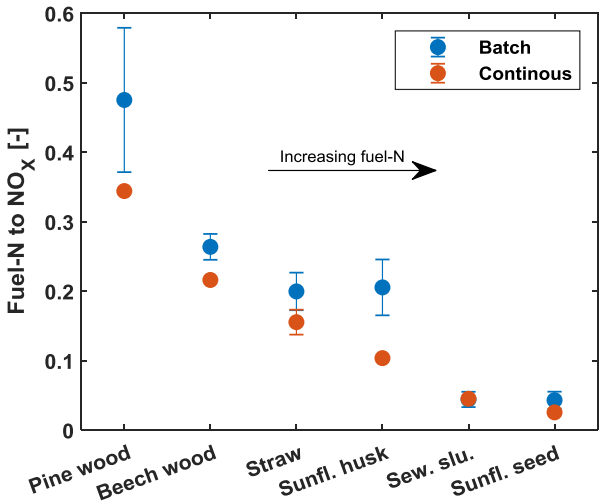

Figure 4.4: Fuel-N to NO_X conversion from batch and continuous combustion of biomass. The continuous combustion data were described in Chapter 3, Section 3.3.1. Conditions during continuous combustion: Conditions: T_{bed} = 850ºC; λ = 1.4; λ_1/λ = 1.

Figure 4.5 summarizes the relative contribution of volatile and char combustion to the total NO (a) and carbon (b). The volatile-NO contribution ranged from 45-75% for the investigated biomass. This indicates that volatile-NO was generally the major contributor to NO_X at temperatures relevant to fluidized bed combustion. However, char-NO may be of significance as well, as in the case of beech wood, showing that 55% of the NO was formed during char combustion. In contrast to this, most of the carbon was released during volatile combustion for all of the fuels, similar to single particle combustion studies [95,174].

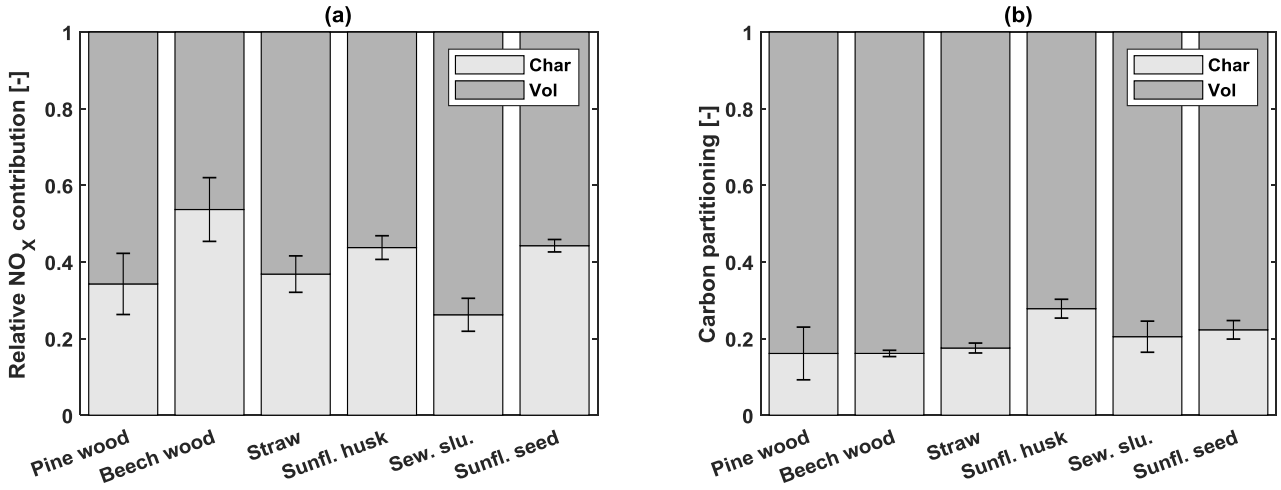

Figure 4.5: Relative contribution of volatile- and char-NO (a) and carbon partitioning between volatile and char (b).

4.3.2 Influence of ash forming elements on NO and CO emission

Figure 4.6 depicts the results from fluidized bed combustion of raw, washed, and K-doped washed straw, and raw and K-doped pine wood. Of the straw fuels, the conversion of fuel-N to NO was lowest for raw straw and highest for washed straw. KCl and KOH doping of washed straw decreased the fuel-N to NO conversion and increased the average CO emission. K_2CO_3 doping did not alter the fuel-N to NO conversion significantly, while also increasing the CO emission. For the pine wood, all K-compounds had a lesser effect on the fuel-N to NO conversion. The CO emission from KCl doped pine wood combustion was higher than the raw pine wood. However, caution must be taken when interpreting the presented results, as the axial temperature profiles were affected by the pre-treatment. A higher temperature near the fuel inlet was prominent for washed and KCl doped washed straw, due to the sticking of fuel particles to the reactor walls, which was confirmed visually. The influence of KCl on the combustion chemistry is further investigated in the following section.

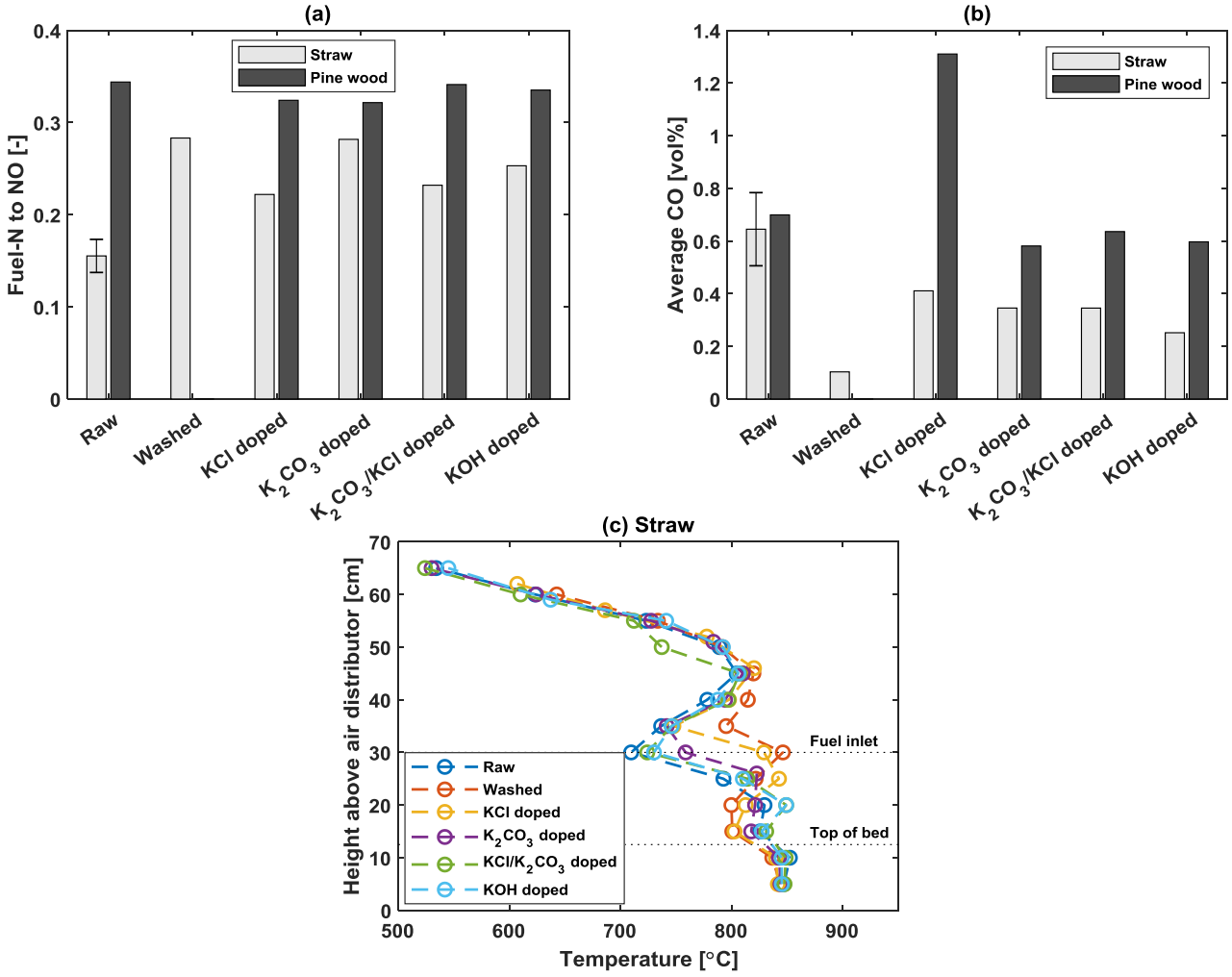

Figure 4.6: Fuel-N to NO conversion (a) and average CO concentration (b) during fluidized bed combustion of raw, washed, and K-doped washed straw, and raw and K-doped pine wood. Axial temperature profile (c) during combustion of raw, washed, and K-doped straw. Conditions: T_{bed} = 850ºC; λ = 1.4; λ_1/λ = 1.

4.3.2.1 Impact of KCl on NO emission

During continuous straw combustion at two different air staging configurations, 1.07 g of KCl (180-355 µm) was dropped into the reactor from the top. The effluent NO and CO concentrations are shown in Figure 4.7. When all the air was introduced as primary gas ($\lambda_1/\lambda = 1$), the CO concentration slightly increased and the NO concentration was unaffected by the addition of KCl. The influence of KCl was more pronounced when employing air staging. At λ_1/λ of 0.04, a significant increase in CO and decrease in NO was observed. Studies under well controlled conditions show that alkali metals could inhibit CO oxidation at reducing and to some extent at oxidizing conditions by radical recombination [171]. The inhibitory effect of KCl on CO oxidation at reducing conditions increased and levelled off with increasing KCl concentration [191]. The radical recombination effect of alkali species may additionally affect the nitrogen chemistry depending on the radical levels [147,152]. Projecting these results to those obtained in Figure 4.7 indicates that the CO oxidation was inhibited as KCl lowered the radical concentration in the reactor. The change in nitrogen combustion chemistry by radical recombination and the stronger reducing conditions caused a reduction in NO outlet concentration from KCl addition.

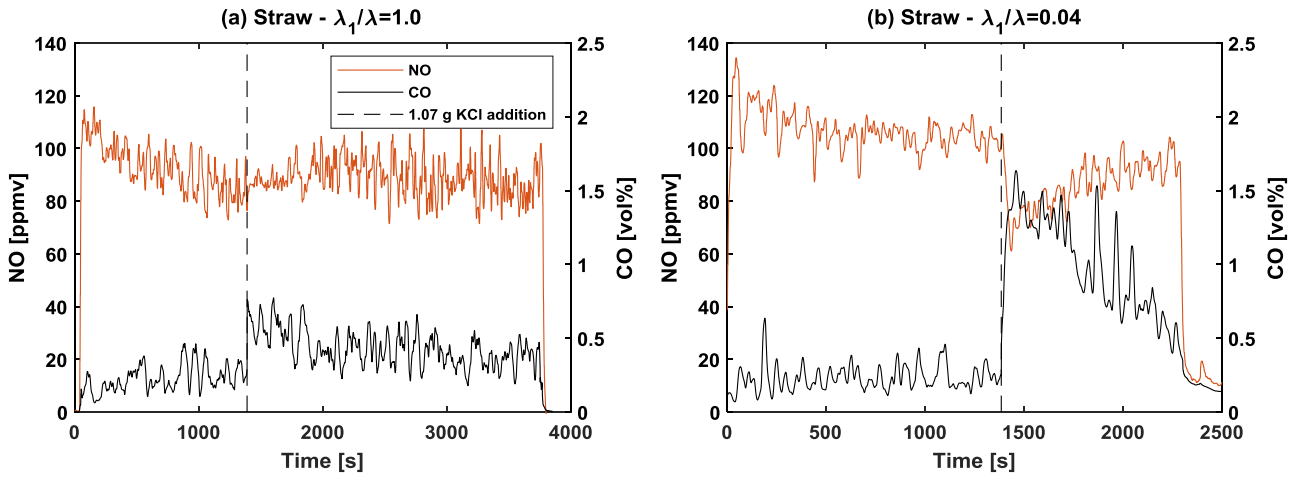

Figure 4.7: NO and CO effluent concentrations during straw combustion with batch addition of KCl at two air staging conditions, $\lambda_1/\lambda = 1.0$ (a) and 0.04 (b). Conditions: $T_{bed} = 850$ºC; $\lambda = 1.4$; $\lambda_1/\lambda = 1$ (a) and 0.04 (b).

4.3.3 Influence of air staging and temperature on NO emission

Figure 4.8 depicts the averaged effluent CO concentration (a) during straw and sunflower seed combustion, and the axial temperature profile (b) during straw combustion at different air staging configurations. The CO concentration of straw exhibited a maximum, while no clear trend was observed in sunflower husk combustion. Previous studies show that the CO concentration generally increases with higher secondary air ratio in consequence of the lower gas residence time in the oxidizing zone [222]. However, this may not always be the case as the CO concentration is a complex function of residence time, temperature, and excess air ratio in the reducing and oxidizing zones [213,234,274]. In addition, deviations in the feeding rate during and between experiments may influence the CO emission. The axial temperature profiles were comparable for $\lambda_1/\lambda = 0.5$-1.0. At $\lambda_1/\lambda < 0.5$, the temperature near the fuel inlet increased as a larger extent of combustion occurred around this point.

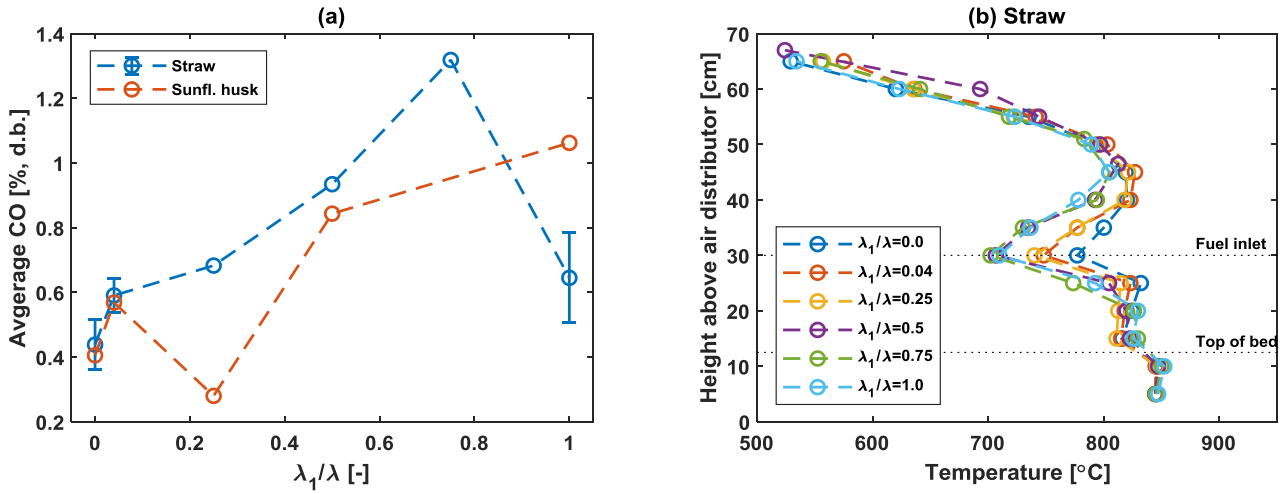

Figure 4.8: Averaged effluent CO concentration (a) during steady state combustion of straw and sunflower husk at different air staging configurations. Axial temperature profile during steady state straw combustion at different air staging configurations (b).

Figure 4.9 illustrates the averaged NO concentration (a) and fuel-N to NO conversion (b) during straw and sunflower husk combustion at different air staging configurations. The averaged NO concentrations were obtained from the steady state combustion region. In the case of $\lambda_1/\lambda = 0$ and 0.04, a considerable amount of char-N accumulated in the bed. Consequently, the fuel-N to NO conversion for these cases included the char-N combustion after the fuel feeding was stopped. The averaged NO concentration and fuel-N to NO conversion exhibited minima for both straw and sunflower husk combustion at $\lambda_1/\lambda = 0.5$-0.75. Air staging has been shown to be an efficient way of reducing NO emission in different combustors [213,222,273–275], some of which report the existence of an optimum secondary air ratio [222,235]. Studies on air staging rarely examine the extreme cases below $\lambda_1/\lambda < 0.5$. The results here indicate that the NO emission and fuel-N to NO conversion would increase when operating under these extreme cases, the reasoning of which requires further study.

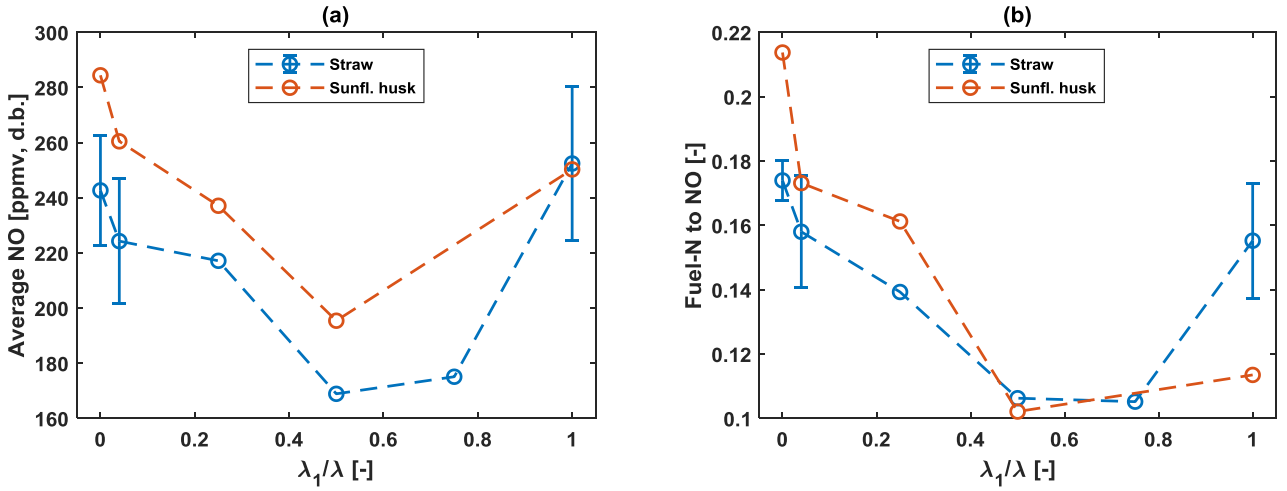

Figure 4.9: Averaged effluent NO concentration (a) and fuel-N to NO conversion (b) during continuous combustion of straw and sunflower husk at different air staging configurations. The averaged NO concentrations were obtained during steady combustion, while the fuel-N to NO conversion for $\lambda_1/\lambda = 0$ and 0.04 included the char combustion after the fuel feeding was stopped. Conditions: T_{bed} = 850ºC; λ = 1.4; λ_1/λ = 0-1.

Figure 4.10 shows the impact of bed temperature on the fuel-N to NO conversion (a) and averaged CO concentration (b) during fluidized bed combustion of straw and KCl-doped washed straw. For raw straw, the fuel-N to NO exhibited a slight increasing trend in the investigated temperature range. In the case of KCl doped washed straw, the fuel-N to NO conversion increased significantly from 650 to 770°C, while the difference from 810 to 850°C was negligible. The reasoning for this may be explained by the CO concentration, showing a large decrease from 650 to 770°C, while the difference from 810 to 850°C was less pronounced. Previous studies indicate similarly that NO emission increased or was unchanged by an increase in temperature (cf. Chapter 2, Section 2.4.2.2).

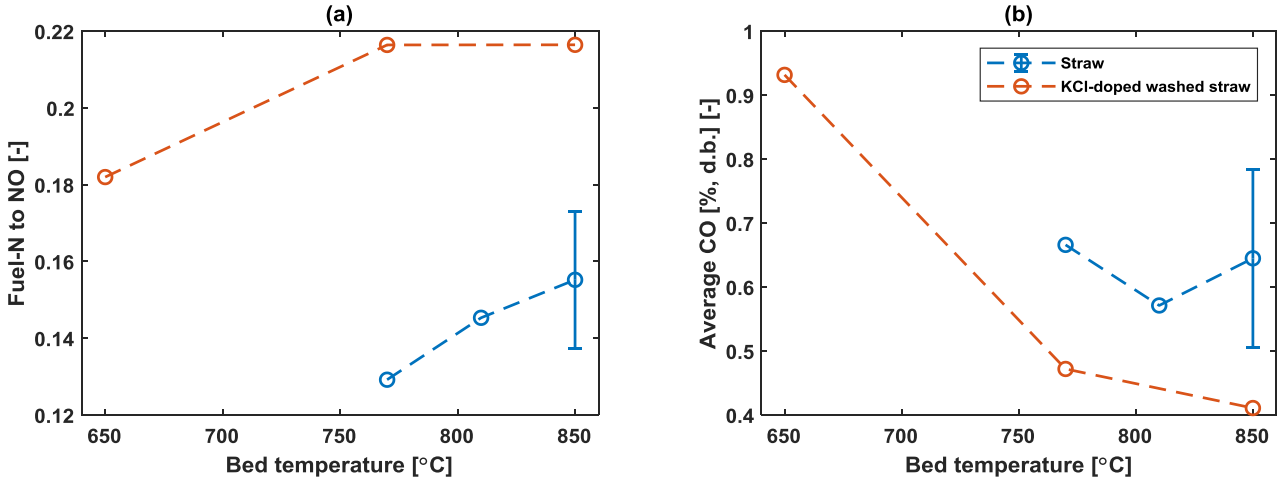

Figure 4.10: Fuel-N to NO conversion (a) and averaged effluent CO concentration (b) during combustion of straw and KCl doped washed straw at different bed temperatures. Conditions: T_{bed} = 650, 770, 810, and 850ºC; λ = 1.4; λ_1/λ = 1.

The temperature profiles from fluid bed combustion at different bed temperatures are illustrated in Figure 4.11. The temperature profiles below the fuel inlet were different, whereas the profiles above the fuel inlet were similar, due to safety issues caused by high CO concentrations. The temperature profile of the KCl doped straw was different below 850°C as less biomass stuck to the sides of the reactor, presumably related to the melting point of KCl, 771ºC [254].

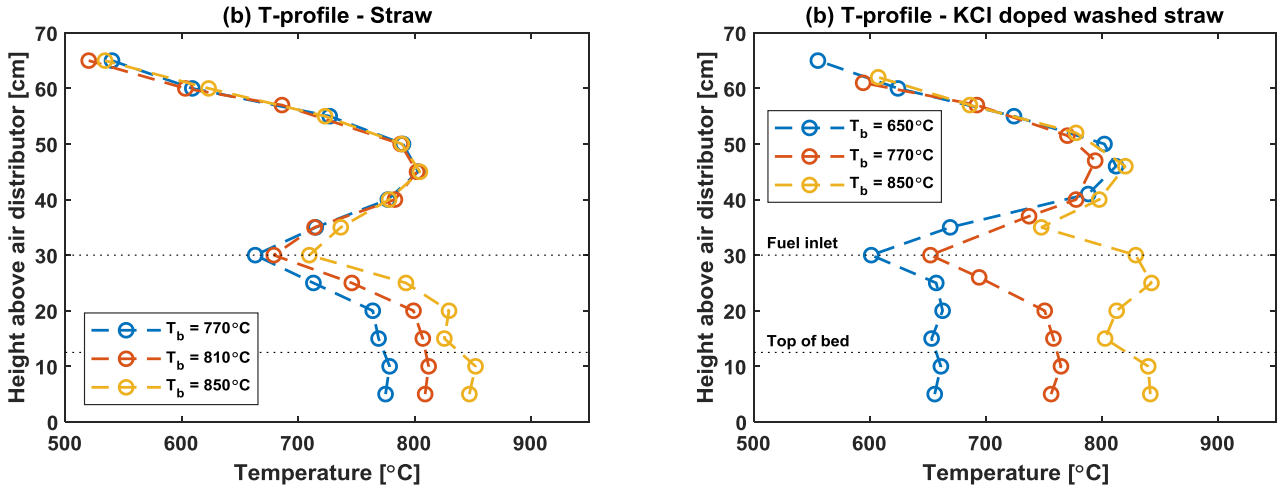

Figure 4.11: Axial temperature profile during combustion of straw and KCl doped washed straw at different bed temperatures (T_b). Conditions: T_{bed} = 650, 770, 810, and 850ºC; λ = 1.4; λ_1/λ = 1.

4.3.4 Influence of bed material and gas atmosphere on NO emission

The influence of bed material on the NO emission was investigated by partially or completely replacing the silica sand bed with kaolin or CaO. The resulting fuel-N to NO conversion (a) and averaged effluent CO concentration (b) are demonstrated in Figure 4.12. While Ca has been shown to increase fuel-N to NO conversion in fluid bed combustion (cf. Chapter 2, Section 2.4.1.3), the change in fuel-N to NO conversion with the addition of CaO to the bed was negligible. This may be explained by the lower importance of the bed chemistry as most of the combustion occurred above the bed during straw combustion (cf. Chapter 3, Section 3.3.1.1). In addition, kaolin did not alter the fuel-N to NO conversion significantly. The influence of the bed material on the CO emission was also negligible with the only exception being for 10%CaO-90%SiO_2. Here a slightly higher CO emission was observed, presumably due to a comparatively higher fuel feeding rate. The temperature profiles from the different experiments were comparable, demonstrated in Appendix B.1 (Figure B.1).

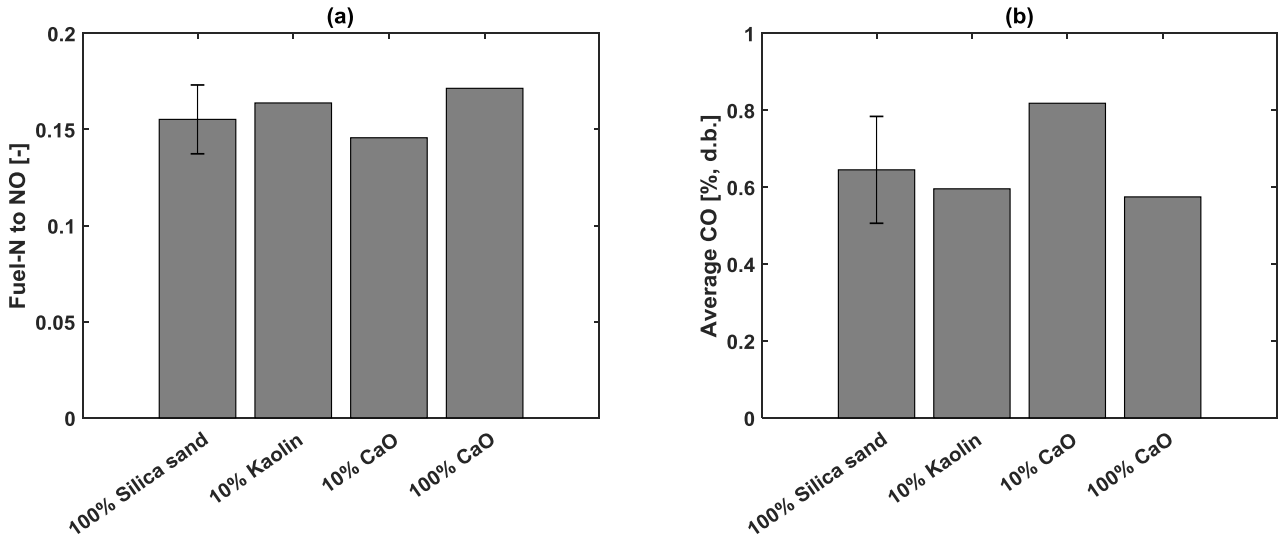

Figure 4.12: Fuel-N to NO conversion (a) and averaged effluent CO concentration (b) during combustion of straw with different bed material. The base case employed 100% silica sand. Conditions: T_{bed} = 850ºC; λ = 1.4; λ_1/λ = 1.

To investigate the influence of gas composition, the balance gas of the primary gas was changed between N_2 and CO_2 at λ_1/λ = 0 and 0.04. This means that at λ_1/λ = 0 and 0.04, besides the necessary amount of air, either N_2 or CO_2 was fed as primary gas, thereby forming $CO_2/O_2/N_2$ or O_2/N_2 systems. The fuel-N to NO conversion and averaged effluent CO concertation are demonstrated in Figure 4.13. A slightly lower fuel-N to NO conversion may be possible when using CO_2 at λ_1/λ = 0; however, the difference was small. In addition, no significant change was observed in the effluent CO concentration in the two systems. A high concentration of CO_2 may affect both the volatile- and char-N oxidation chemistry (cf. Chapter 2, Section 2.4.2.3). However, based on the conditions and results in this study, no obvious change was observed. The temperature profiles from the combustion tests at λ_1/λ = 0 were comparable, demonstrated in Appendix B.1 (Figure B.2).

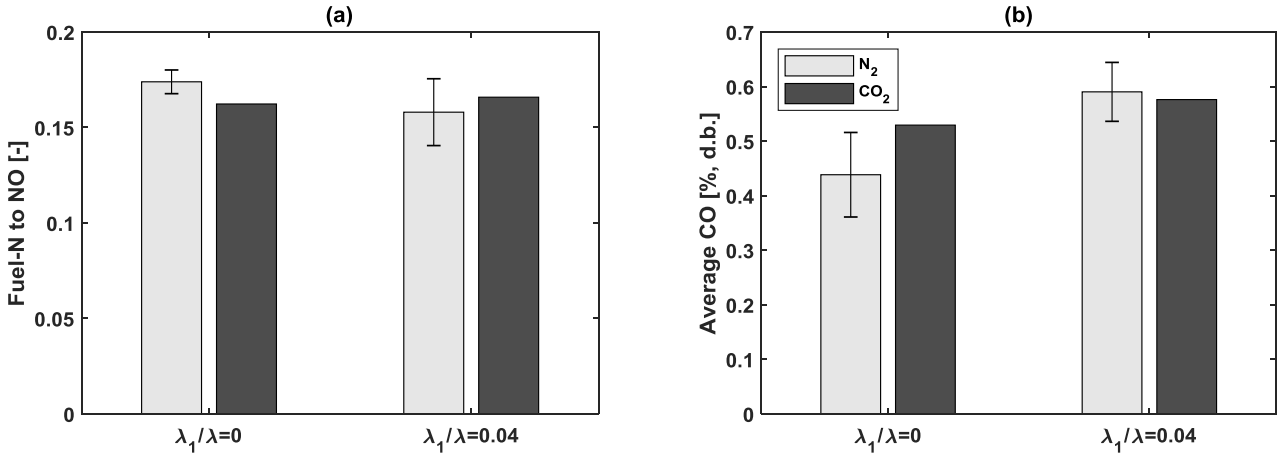

Figure 4.13: Fuel-N to NO conversion (a) and averaged effluent CO concentration (b) during combustion of straw with different primary gas composition at air staged conditions. Conditions: T_{bed} = 850ºC; λ = 1.4; λ_1/λ = 0 and 0.04.

4.4 Conclusions

The fuel-N to NO conversion decreased with an increase in fuel-N content during batch and continuous fluidized bed combustion of biomass particles with size ranges from 0.5-4 mm. The fuel-N to NO conversion was higher in the batch combustion experiments, due to the more oxidizing conditions. While volatile-NO (45-75%) was the major contributor for most biomass, char-NO could be of significance for some biomass. For beech wood, up to 55% of the NO was formed during char combustion.

The fuel-N to NO conversion increased and the averaged CO emission decreased when combusting washed straw. Doping washed straw with KCl, KOH, and K_2CO_3 increased CO emission. KCl and KOH doping decreased the fuel-N to NO conversion, while K_2CO_3 doping did not alter the fuel-N to NO conversion significantly. Compared to raw pine wood, KCl-doped pine wood significantly increased the CO emission, while having a negligible influence on the fuel-N to NO conversion. The effect of KCl on the CO and NO emissions was more pronounced during air staged ($\lambda_1/\lambda = 0.04$) compared to un-staged ($\lambda_1/\lambda = 1$) combustion. Batch addition of KCl during straw combustion at air staged conditions resulted in increased CO and decreased NO emissions, presumably due to the reduction of the radical concentration by recombination reactions.

By varying the primary air ratio (λ_1/λ) from 0 to 1, a minimum was observed for the NO emission and fuel-N to NO conversion during straw and sunflower husk combustion at $\lambda_1/\lambda = 0.5$-0.75. The CO concentration from straw combustion exhibited a maximum at $\lambda_1/\lambda = 0.75$, while no clear trend was observed for the CO concentration from sunflower husk combustion at the investigated conditions. Moreover, the fuel-N to NO conversion increased with temperature during straw combustion. For KCl-doped washed straw, the fuel-N to NO conversion increased first then levelled off with increasing temperature, explained by the inverse trend in the CO emission.

Replacing the bed partly with kaolin and CaO, or completely by CaO resulted in a negligible effect on the fuel-N to NO conversion and CO emission during straw combustion. In addition, changing the primary gas from N_2 to CO_2 had a negligible effect on the fuel-N to NO conversion and CO emission at $\lambda_1/\lambda = 0$ and 0.04.

5 Additives against NO_X emissions and bed agglomeration

Abstract: The influence of additives on NO_X emissions and bed agglomeration was investigated during continuous fluidized bed combustion of straw. The investigated additives included CaO, kaolin, $MgCO_3$, coal fly ash, clay, $(NH_4)_2Fe(SO_4)_2$, $NH_4Fe(SO_4)_2$, $(NH_4)_2SO_4$, NH_4MgPO_4, $AlNH_4(SO_4)_2$, $(NH_4)_2HPO_4$, $(NH_4)_3[Fe(C_2O_4)_3]$, and urea. The most effective additives were additionally employed in air staged straw combustion and un-staged sunflower husk combustion. Moreover, the influence of $(NH_4)_2SO_4$ particle size (<35 μm and <106 μm) and introduction method (batch addition or premixing with fuel) was investigated during straw combustion, while the effect of ash accumulation and bed agglomeration was studied during sunflower husk combustion. The results show that kaolin, CaO, $MgCO_3$, $(NH_4)_2Fe(SO_4)_2$, $NH_4Fe(SO_4)_2$, $AlNH_4(SO_4)_2$, and NH_4MgPO_4 prevented defluidization during straw combustion. Of these, $AlNH_4(SO_4)_2$, and NH_4MgPO_4 reduced the fuel-N to NO conversion by 40%. The mechanism of reduction was related to the facilitation of thermal $DeNO_X$ reactions by introduction of NH_3-releasing additives. However, the NH-based additives resulted in higher emissions of N_2O. The combustion behavior of straw was unaffected by the presence of additives, demonstrated by local CO concentration and temperature measurements. The larger particle size range of $(NH_4)_2SO_4$ increased the time before defluidization, while slightly increasing NO and lowering N_2O emissions, related to the different decomposition locations of $(NH_4)_2SO_4$. Larger particles tended to drop to the bed, while smaller particles would be elutriated and/or decompose upon introduction to the reactor. Moreover, no significant differences in the fuel-N to NO conversion and defluidization tendency were observed between the two additive introduction methods, possibly caused by differences in the release mechanism and location of $(NH_4)_2SO_4$. Air staging resulted in a 40% reduction of the fuel-N to NO conversion during straw combustion. The use of NH_4MgPO_4 and $AlNH_4(SO_4)_2$ under air staged conditions increased the NO emission slightly. This was predominantly caused by the combustion of NH_3 by the secondary air jet. In the case of un-staged sunflower husk combustion, NH_4MgPO_4 and $AlNH_4(SO_4)_2$ prevented defluidization, while reducing the conversion of fuel-N to NO by 30%. The behavior of the additives during sunflower husk combustion was similar to that of straw. The accumulation of ash increased NO and decreased NH_3 above the bed. This was related to the poorer mixing as the bed approached defluidization and to the catalytic effect of ash forming elements on the oxidation of NH_3 to NO.

5.1 Introduction

Two major operational issues in fluidized combustion of biomass are bed defluidization and increased NO_X emissions. The mechanisms of NO_X formation in fluidized bed combustion were described in Section 2.3. Bed agglomeration is generally caused by the interaction between the ash forming elements and bed material, leading to the formation of a molten viscous glassy phase such as K-silicates on bed particles. This sticky molten phase increases the propensity of bed particles to stick and form agglomerates, which ultimately leads to bed defluidization [276]. Measures for NO_X reduction were summarized in Section 2.5, while countermeasures against bed agglomeration include the use of alternative bed materials [276–278], additives [279,280], co-combustion [276,281], and biomass pre-treatment [269,282]. Techniques for overcoming these two issues mainly target each area independently. Hence, alternative methods aiming at reducing both NO_X emissions and bed agglomeration have, to the knowledge of the authors, not been studied.

This study investigates the impact of additives on NO_X emissions and bed agglomeration during fluidized bed combustion of straw. The additives are summarized in Figure 5.1 in three categories based on their hypothesized impact; de-agglomeration, de-NO_X, and multifunctional. The influence of additive particle size and additive introduction method was additionally examined in the case of $(NH_4)_2SO_4$. Selected additives were also used in air staged straw and un-staged sunflower husk combustion. Moreover, the impact of ash accumulation on NO_X emissions was investigated during un-staged sunflower husk combustion, as the defluidization time was longer for this fuel than for straw, which allowed measurements at the initial and later stages of combustion. While overall results of the influence of additives on bed agglomeration are presented in the following sections, the focal point of this work is on the NO_X emissions. A more thorough examination of the effect of kaolin, CaO, $MgCO_3$, clay, coal fly ash, and $(NH_4)_2SO_4$ addition on bed agglomeration can be found in [254].

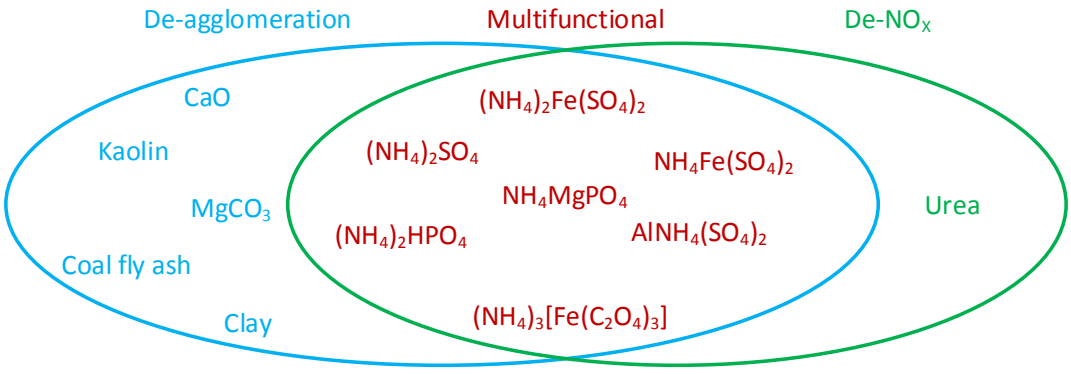

Figure 5.1: Illustration showing the three classes of additives employed in this study; de-agglomeration, de-NO_X, and multifunctional.

5.2 Experimental section

5.2.1 Materials

The chemical composition of the investigated biomass, wheat straw and sunflower husk, was shown in Table 3.1 in Section 3.2.1. The biomass particles were grinded and sieved to a size range of 0.6-4 mm to minimize fuel particle elutriation and ensure continuous feeding. Silica sand was used as bed material in the fluidized bed (D_{50} 273 μm, Geldart B). The particle size and crystalline phases of the additives are demonstrated in Table 5.1. Some of the additives were used as received, explaining the small differences in the used size ranges. Generally, smaller particles were chosen to ensure adequate adhesion to the biomass particles. Two different particle sizes (<35 and <106 μm) and additive introduction methods (batch addition or premixed with fuel) of $(NH_4)_2SO_4$ were investigated. The chemical composition of the additives are summarized in Table 5.2. All the compositional data for the de-agglomeration additives were extracted from [254]. Prior to combustion experiments, the additives were mixed with the fuel using a rotational mixer. For the de-agglomeration additives approximately 4.7 g additive was added per 100 g of biomass based on the potassium capture capability of kaolin [261,283]. For the additives with NH-functionality, the NH_3/fuel-N molar ratio was kept at 1.5. It was assumed that the one mol of NH_4 or urea released one mol of NH_3 [262].

Table 5.1: Particle size and crystalline phases of the additives. a: determined by XRD [254], b: determined from label.

Additive	Particle size [μm]	Crystalline phases
Kaolin [a]	< 85	$Al_2Si_2O_5(OH)_4$, SiO_2
Coal fly ash [a]	< 32	$2Al_2O_3 \cdot SiO_2$, SiO_2
Clay [a]	< 35	$CaCO_3$, SiO_2, Al_2SiO_5
$MgCO_3$ [a]	< 25	$MgCO_3$, MgO
CaO [a]	< 50	CaO
$(NH_4)_2SO_4$ [a]	< 35 and < 106	$(NH_4)_2SO_4$
$(NH_4)_2HPO_4$ [b]	< 106	$(NH_4)_2HPO_4$
$(NH_4)_2Fe(SO_4)_2$ [b]	< 106	$(NH_4)_2Fe(SO_4)_2 \cdot 6\ H_2O$
$NH_4Fe(SO_4)_2$ [b]	< 106	$NH_4Fe(SO_4)_2 \cdot 12\ H_2O$
NH_4MgPO_4 [b]	< 106	$NH_4MgPO_4 \cdot 6\ H_2O$
$AlNH_4(SO_4)_2$ [b]	< 106	$AlNH_4(SO_4)_2 \cdot 12\ H_2O$
$(NH_4)_3[Fe(C_2O_4)_3]$ [b]	< 106	$(NH_4)_3[Fe(C_2O_4)_3] \cdot 3\ H_2O$
Urea [b]	< 106	CH_4N_2O

Table 5.2: Chemical composition of the additives. a: oxygen determined by calculation while remaining elements from ICP-OES [254], b: calculated from the crystalline structure in Table 5.1.

	wt% d.b.										
Additives	**O**	**Si**	**Al**	**Fe**	**Ca**	**Mg**	**Na**	**K**	**P**	**S**	**N**
Kaolin [a]	56.9	22.0	19.0	0.47	0.10	0.14	0.10	1.10	0.05	0.02	-
Coal fly ash [a]	46.6	22.0	14.0	2.90	4.50	0.97	0.27	0.87	0.64	0.26	-
Clay [a]	54.4	28.0	4.2	1.8	8.4	0.45	0.84	1.9	0.05	-	-
$MgCO_3$ [a]	50.3	-	-	-	-	41.1	-	-	-	-	-
CaO [a]	31.0	-	-	-	69.0	-	-	-	-	-	-
$(NH_4)_2SO_4$ [a]	48.5	-	-	-	-	-	-	-	-	24.2	27.3
$(NH_4)_2HPO_4$ [b]	48.5	-	-	-	-	-	-	-	23.5	-	21.2
$(NH_4)_2Fe(SO_4)_2$ [b]	57.1	-	-	14.2	-	-	-	-	-	16.4	7.1
$NH_4Fe(SO_4)_2$ [b]	66.4	-	-	11.2	-	-	-	-	-	13.3	2.9
NH_4MgPO_4 [b]	65.2	-	-	-	-	9.9	-	-	12.6		5.7
$AlNH_4(SO_4)_2$ [b]	70.6	-	6.0	-	-	-	-	-	-	14.1	3.1
$(NH_4)_3[Fe(C_2O_4)_3]$ [b]	56.1	-	-	13.0	-	-	-	-	-	-	9.8
Urea [b]	26.6	-	-	-	-	-	-	-	-	-	46.6

5.2.2 Fluidized bed combustion of biomass and additives

Continuous fluidized bed combustion experiments were performed in the reactor described in Chapter 3, Section 3.2.3. As NO_2 was not detected in significant amounts, this was not further considered.

The experimental procedure was similar to that described in Chapter 3, Section 3.2.4. 0.5 kg of silica sand (10 cm static bed height) was used in each test. The temperature in the bed was kept at 850ºC and two different air staging configurations (λ_1/λ = 0.5 and 1) were examined for selected cases. Continuous combustion experiments were performed until the point of defluidization or until all the prepared fuel was burned out (0.3 kg for straw and 0.5 kg for sunflower husk). Stable combustion was achieved in most cases, observed from the temperature measurements, and O_2 and CO_2 effluent concentrations. However, the adhesion force of the additives complicated the fuel feeding. In one case (sunflower husk-$NH_4Al(SO_4)_2$), this led to pipe blockage and premature stop of the experiment. The repeatability of the straw-$(NH_4)_2SO_4$ combustion was examined showing a reasonable repeatability (Appendix C.1).

5.2.3 Thermogravimetric analyses (TGA) of additives

The decomposition of additives was investigated in a thermogravimetric analyzer (NETZSCH STA 449 F1). Approximately 2.5 mg of sample was heated from ambient temperature to 40 ºC and kept there for 20 min to remove moisture. A relative low temperature was chosen to remove moisture to avoid thermal decomposition of the additives. Following this, the sample was heated at 5 ºC/min to 1100 ºC. All the additives were tested under inert conditions (50 NmL/min of N_2). Additionally, the influence of $(NH_4)_2SO_4$ particle size on the mass loss behavior was investigated, while the effect of O_2 (20%) was examined for NH_4MgPO_4 and $AlNH_4(SO_4)_2$. The gaseous decomposition products were characterized during NH_4MgPO_4 and $AlNH_4(SO_4)_2$ decomposition in inert and oxidizing atmospheres by mass spectrometry.

5.3 Results and discussion

5.3.1 TGA results

Figure 5.2a-d summarize the weight loss data from TGA of the additives. The decomposition onset temperature varied for the additives, from around 70ºC for $(NH_4)_3[Fe(C_2O_4)_3]$ and $AlNH_4(SO_4)_2$ to around 250ºC for $(NH_4)_2SO_4$. Several of the additives exhibited plateaus indicating the formation of decomposition byproducts. From Figure 5.2c and d, the results show that the particle size and gas atmosphere were insignificant for the weight loss. In the case of NH_4MgPO_4 and $AlNH_4(SO_4)_2$, the decomposition products from TG experiments were analyzed by mass spectrometry, demonstrated in Appendix C.2. These show that the nitrogen in the additives were predominantly released as NH_3 with and without the presence of air. In addition, some NO and N_2O was observed for $AlNH_4(SO_4)_2$ under oxidizing conditions.

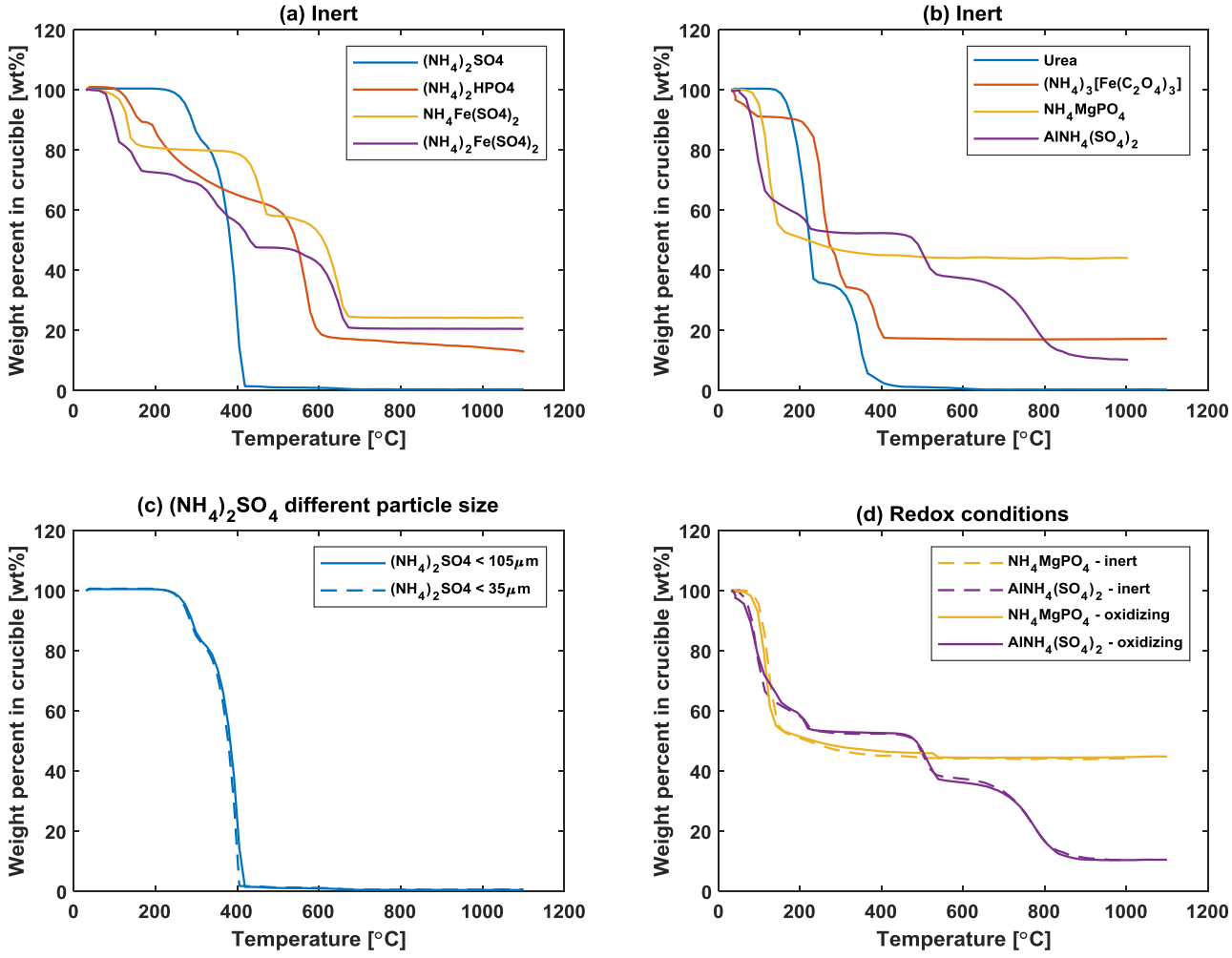

Figure 5.2: Weight loss data from TGA of additives in inert (a,b) atmosphere. Weight loss data from TGA of two different sizes of $(NH_4)_2SO_4$ under inert conditions (c). Weight loss data from TGA of NH_4MgPO_4 and $AlNH_4(SO_4)_2$ under inert and oxidizing conditions (d).

5.3.2 Straw-additives combustion

Figure 5.3 describes the conversion of fuel-N to NO (a) and the defluidization tendency (b) during straw combustion with additives. For the de-agglomeration additives, the results indicate that the fuel-N to NO conversion slightly increased when using CaO and $MgCO_3$, while coal fly ash, clay, and kaolin did not have a significant influence. CaO and possibly MgO have been suggested to increase NO emission in fluidized bed combustion by catalyzing the oxidation of NH_3 and HCN [167,187]. Of the NH-based additives, urea, $NH_4(SO_4)_2$, $AlNH_4(SO_4)_2$, and NH_4MgPO_4 decreased the fuel-N to NO conversion, while $(NH_4)_2HPO_4$, $(NH_4)_3[Fe(C_2O_4)_3]$, $(NH_4)_2Fe(SO_4)_2$, and $NH_4Fe(SO_4)_2$ had a negligible impact. The results show that the presence of a NH-functionality in the additives was necessary to reduce NO emission. In terms of defluidization tendency, kaolin, CaO, and $MgCO_3$ prevented defluidization, while coal fly ash and clay slightly prolonged the defluidization time. A deeper investigation of these is provided in [254], showing that kaolin captured fuel-K, preventing the formation of low melting K-silicates, whereas CaO and $MgCO_3$ increased the viscosity the melt, thereby decreasing the propensity for agglomerate formation. Urea had a negligible impact on the defluidization behaviour, since the decomposition products of urea (HNCO and NH_3 [262]) are not expected to alter the ash chemistry significantly. For the multifunctional additives, defluidization was prevented by $(NH_4)_2Fe(SO_4)_2$, $NH_4Fe(SO_4)_2$, $AlNH_4(SO_4)_2$, and NH_4MgPO_4, prolonged by $NH_4(SO_4)_2$ and $(NH_4)_3[Fe(C_2O_4)_3]$, and accelerated by $(NH_4)_2HPO_4$. Generally, phosphates have been shown to decrease the defluidization tendency by forming crystalline K-Ca/Mg-phosphates; however, at a high concentration, low-temperature-melting phosphates may promote defluidization [284–286]. The presence of S during combustion may convert the fuel-K to less harmful species such as K_2SO_4 [287]. In addition, Al and Fe may increase the melting point of the compounds leading to agglomeration [288]. Of the examined additives, $AlNH_4(SO_4)_2$, and NH_4MgPO_4 were capable of reducing NO emission (approximately 40% reduction) while preventing defluidization.

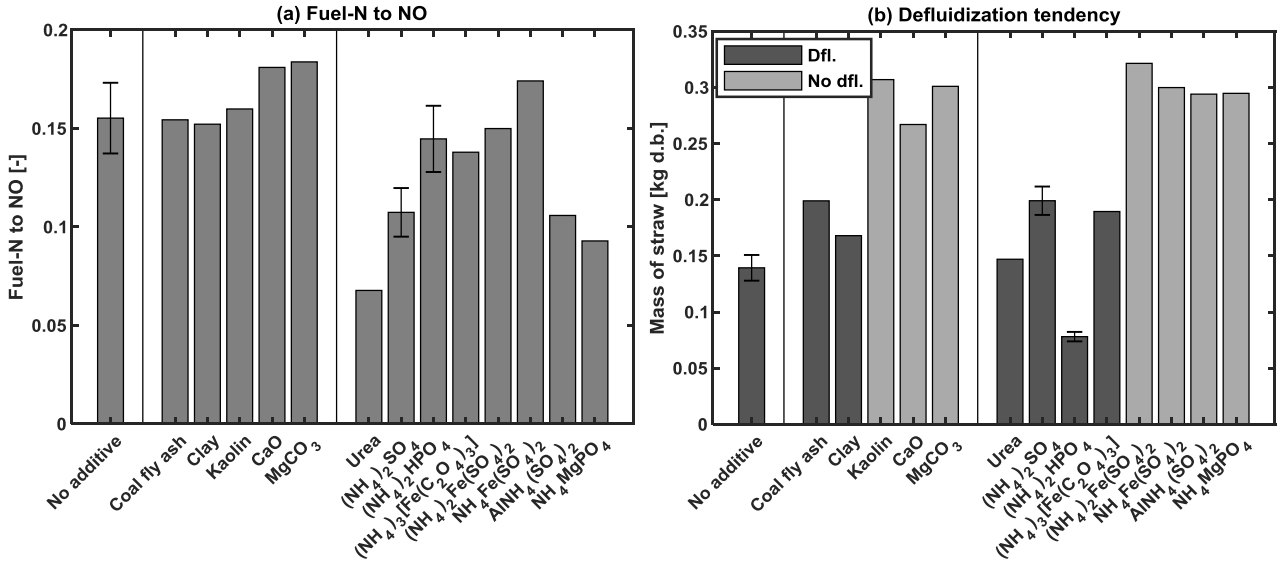

Figure 5.3: Fuel-N to NO conversion (a) and defluidization tendency, expressed in mass of straw combusted, (b) during straw combustion with additives. Nomenclature: dlf: defluidization, no dfl: no defluidization. Conditions: T_{bed} = 850ºC; λ = 1.4; λ_1/λ = 1.

5.3.2.1 Local gas composition and temperature measurements

Figure 5.4a-f illustrate the NO, NH_3, and HNCO axial concentration profiles from fluidized bed combustion of straw with additives. The figures on the left, i.e. a, c, and e, include the additives that led to a decrease in the fuel-N to NO conversion, while the figures on the right, i.e. b, d, and f, include the additives that had no significant influence the fuel-N to NO conversion (cf. Figure 5.3a). The NH_3 concentration in the reactor was significantly higher due to the decomposition of additives, which occurred predominantly above the fuel inlet and/or at the top of the fluid bed. The location of highest NH_3 concentration cannot be correlated to the decomposition onset temperatures determined in Section 5.3.1. This was most likely due to differences in heating rate and gas-particle flow for the two different reactors. In addition, the adhesion of the additives to the fuel particle may be important for the release location. While the outlet NO data of the Fe-based additives were comparable to that of raw straw, the local concentration measurements reveal a significantly higher concentration of NO near the bed. This was caused by the catalytic effect of Fe on the oxidation of NH_3 to NO [167]. Moreover, the combustion with $(NH_4)_2HPO_4$ increased the NO emission near the bed compared to straw combustion. While phosphorous may affect the combustion chemistry, the reasoning for the higher NO emission was presumably due to the poorer mixing as the bed approached defluidization, further explained in Section 5.3.5.1. The results indicate that the additives which did not substantially increase the NO concentration near the bed were capable of reducing NO emission relative to pure straw combustion. This was caused by the facilitation of thermal $DeNO_X$ reactions due to a higher concentration of NH_3 in the reactor, i.e. R5.1 > R5.2. The HNCO peak location was similar to that of NO, i.e., in the freeboard, indicating that HNCO was most likely formed from primary combustion products. For the Fe and Al-based additives no HNCO was observed during combustion, possibly due to the catalytic effect of these on the HNCO reactions [289]. Similar to the measurements in Section 3.3.1.1, while the presence and qualitative trend in HNCO are clear, the quantitative data must be viewed with care. Within the reactor, the presence of HNCO, NH_3, CO, and C_XH_Y in the freeboard accounted for the reduction observed in NO.

$$NH_3 + NO + \frac{1}{4}O_2 \rightarrow N_2 + \frac{3}{2}H_2O \qquad \text{R5.1}$$

$$NH_3 + \frac{5}{4}O_2 \rightarrow NO + \frac{3}{2}H_2O \qquad \text{R5.2}$$

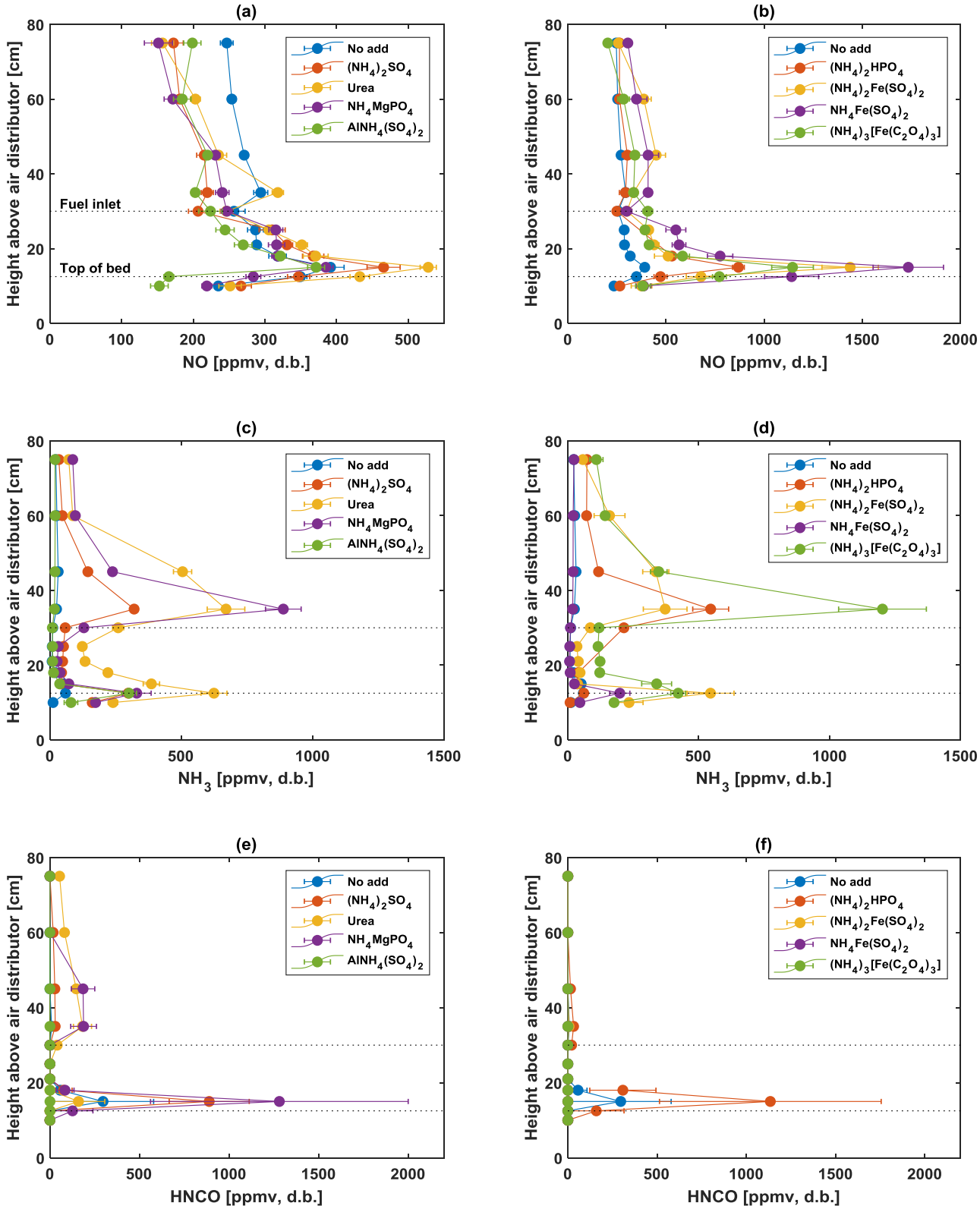

Figure 5.4: Axial NO (a,b), NH_3 (c,d), and HNCO (e,f) profiles during fluidized bed combustion of straw with different additives. For comparison the pure straw combustion profile is shown. The figures on the left (a,c,e) include the additives that led to a decrease in the fuel-N to NO conversion, while the figures on the right (b,d,f) include additives that did not alter fuel-N to NO conversion significantly (cf. Figure 5.3a). The error bars indicate the fluctuations in the measured concentrations. Conditions: T_{bed} = 850ºC; λ = 1.4; λ_1/λ = 1.

Figure 5.5a-d illustrate the N_2O and CO axial concentration profiles from fluidized bed combustion of straw with additives. The figures on the left, i.e. a and c, include the additives that led to a decrease in the fuel-N to NO conversion, while the figures on the right, i.e. b and d, include the additives that had no significant influence the fuel-N to NO conversion (cf. Figure 5.3a). All the additives increased the N_2O concentration within the reactor. The highest N_2O emission was observed for urea, most likely due to the release and combustion of HNCO. The higher N_2O emission for the other additives was predominantly related to the larger concentration of NH_3 in the reactor, which may form N_2O by R5.3 and R5.4. Moreover, the presence of inorganic material such as Fe and Al may affect the selectivity for forming NO, N_2O, and N_2. The CO profiles in Figure 5.5, and the C_XH_Y and CH_2O profiles in Appendix C.3 from straw-additive combustion were comparable, indicating that the additives had small influence on the combustion properties of straw.

$$NH_2 + NO_2 \rightarrow N_2O + H_2O \qquad \text{R5.3}$$

$$NH + NO \rightarrow N_2O + H \qquad \text{R5.4}$$

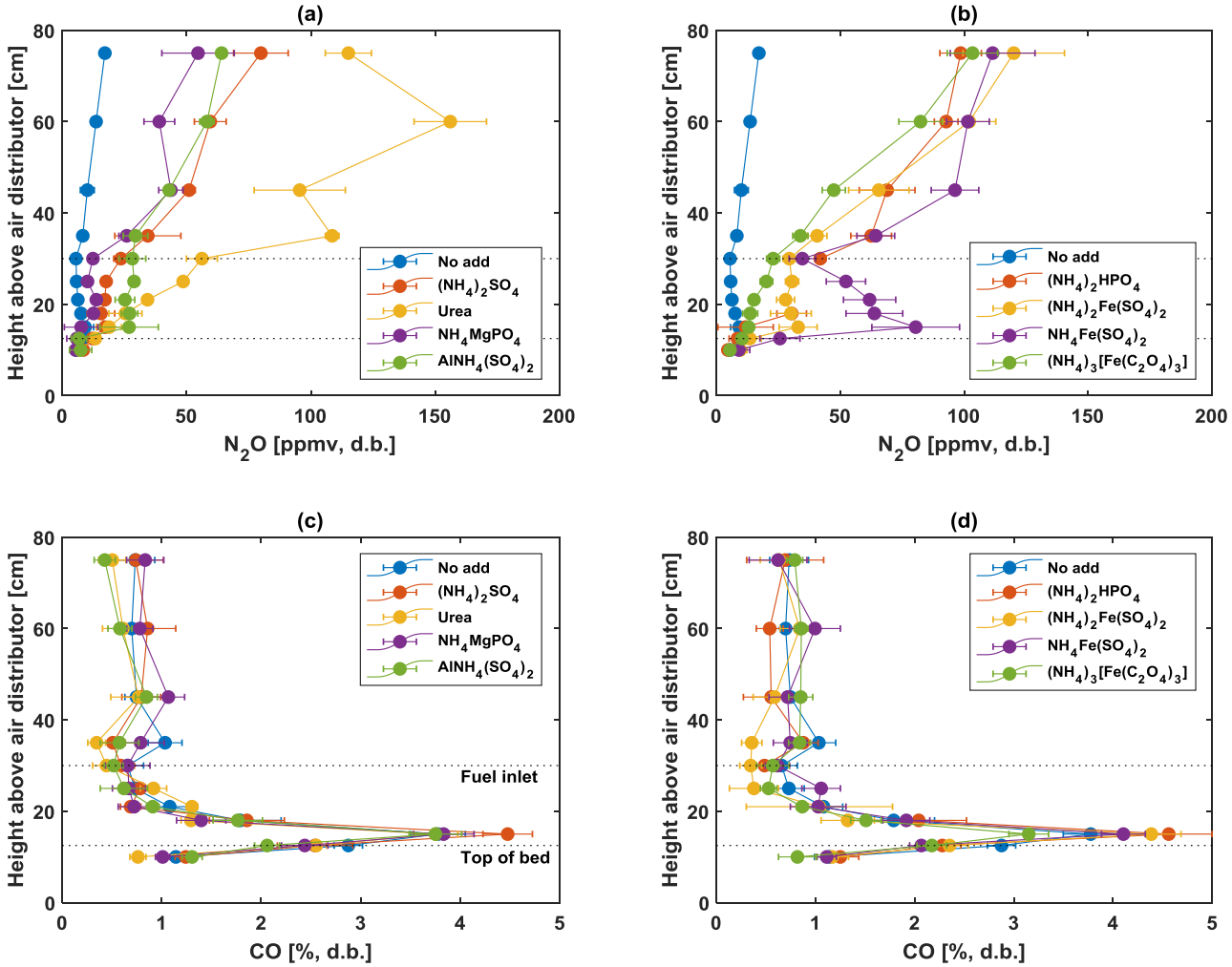

Figure 5.5: Axial N_2O (a,b) and CO (c,d) profiles during fluidized bed combustion of straw with different additives. The figures on the left (a,c) include the additives that led to a decrease in the fuel-N to NO conversion, while the figures on the right (b,d) include additives that did not alter fuel-N to NO conversion significantly (cf. Figure 5.3a). Conditions: T_{bed} = 850ºC; λ = 1.4; λ_1/λ = 1.

Figure 5.6 shows the temperature profile within the reactor during air un-staged fluidized bed combustion of straw with additives. The qualitative and quantitative trend in the data were similar between experiments. This again confirms that the combustion behavior of straw was not significantly affected by the presence of additives, and the observed differences in NO emission was predominantly related to the nitrogen chemistry.

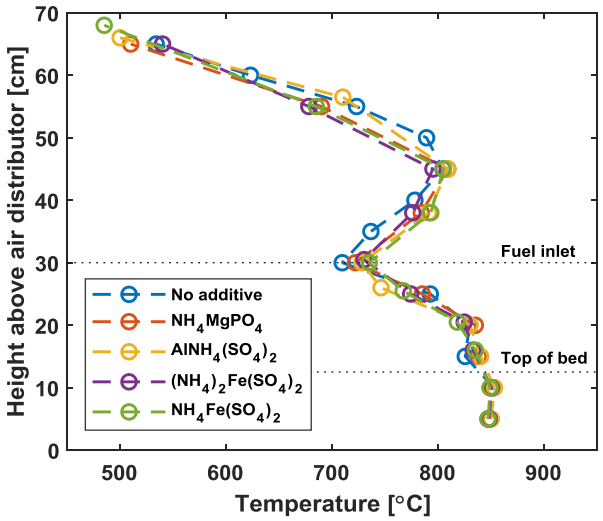

Figure 5.6: Temperature profile in air un-staged fluidized bed combustion of straw with different additives. Conditions: T_{bed} = 850ºC; λ = 1.4; λ_1/λ = 1.

5.3.3 Influence of $(NH_4)_2SO_4$ particle size and introduction method

Figure 5.7 summarizes the local concentration measurements during the combustion of straw with two different sizes of $(NH_4)_2SO_4$. No significant difference was measured in the effluent concentrations of NO and CO during combustion. However, slight differences are prominent from the local concentration data. For the smaller additive particle size range, more NH_3 was released above the fuel inlet, while for the larger range, NH_3 was released to a greater extent near the bed. The high NH_3 concentration above the fuel inlet led to a larger reduction of NO and higher concentration of N_2O for the smaller size range. In addition, the HNCO profiles of the two sizes of additive were similar and exhibited a maximum in the freeboard above the top of the bed. As the additives had a negligible influence on the combustion of straw, no significant changes were noted in the CO measurements. In terms of defluidization tendency, complete defluidization was observed after combustion of 0.23 kg and 0.20 kg of straw for the $(NH_4)_2SO_4$ size ranges <106 μm and <35 μm, respectively. As the slight increase in mass of fuel burned was higher than that of the standard deviation of several repetitions (±0.13 kg straw), the difference may be related to the larger proportion of additive reaching the bed. The concentrations of SO_2 and H_2SO_4 were similar in the reactor for the two additive size ranges, while a slightly higher SO_3 concentration was observed using the larger particle size range, seen in Appendix C.4. However, the differences are small and caution must be taken as fluctuations in the feeding rate may affect the results.

To investigate the influence of $(NH_4)_2SO_4$ addition method, $(NH_4)_2SO_4$ was added as pellets during straw combustion or premixed with straw. The results are summarized in Table 5.3, showing that the fuel-N to NO conversion, average CO concentration, and defluidization tendency were within the uncertainty determined from several repetition. Consequently, no significant differences were observed from the two addition methods. Based on the results in the previous paragraph, a larger particle size, in this case a pellet, would ensure that most of the $(NH_4)_2SO_4$ decomposed in the bed. Therefore, the amount of straw burned before defluidization would be expected to increase. The reason for the negligible difference between the two additive methods may be related to distinct additive decomposition locations and/or mechanisms. The premixed smaller particles adhere to the fuel thereby achieving a closer contact with ash and gas components produced from combustion. In comparison, in the case of the pellet, the contact with the fuel and release mechanism differ, which may lower the influence of the additive on the defluidization tendency. Further investigation would be necessary to elucidate the mechanisms of the two addition methods. For both addition methods, a reduction in fuel-N to NO conversion and increase in time before defluidization was observed relative to straw combustion.

Table 5.3: The influence of $(NH_4)SO_4$ addition method on the fuel-N to NO, average CO concentration, and defluidization tendency during straw combustion. For the premixed data, the $(NH_4)SO_4$ size was <35 μm.

Addition method	Fuel-N to NO [-]	Average CO [vol%, d.b.]	Defluidization tendency [kg straw d.b]
Batch (pellets)	0.0965	0.593	0.190
Premixed with straw	0.107 (± 0.0123)	0.801 (±0.261)	0.20 (± 0.13)

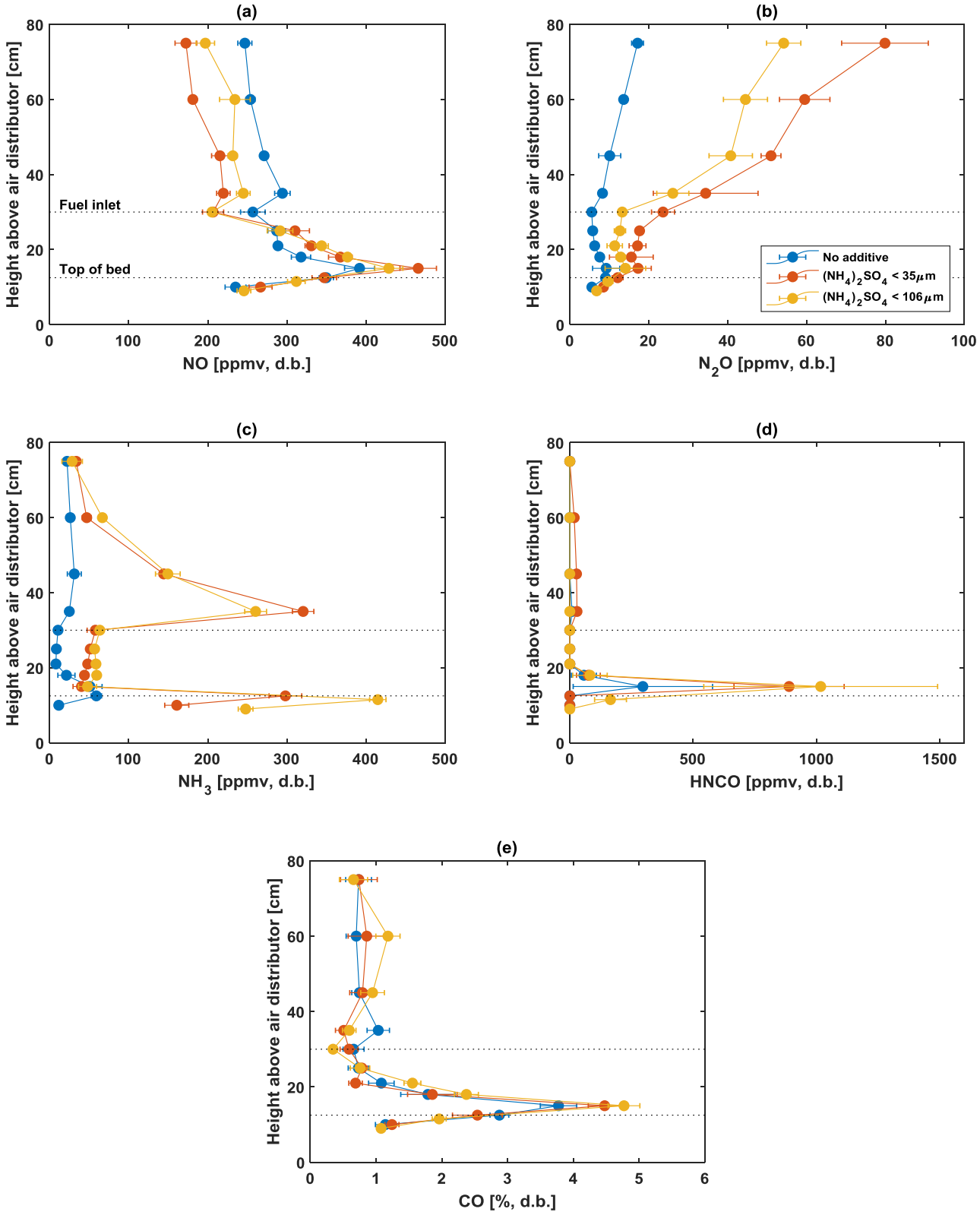

Figure 5.7: Axial NO (a), N_2O (b), NH_3 (c), HNCO (d), and CO (e) profiles during fluidized bed combustion of straw with two different sizes of $(NH_4)_2SO_4$. Conditions: T_{bed} = 850ºC; λ = 1.4; λ_1/λ = 1.

5.3.4 Influence of air staging

Figure 5.8 describes the conversion of fuel-N to NO (a) and the defluidization tendency (b) during straw combustion with additives under different air staging configurations. The results show that air staging is an effective way of reducing the fuel-N to NO conversion (40% reduction) during straw combustion. No synergy effect was observed during staged combustion with additives. On the contrary, a slightly higher fuel-N to NO conversion was observed during air staged combustion with $AlNH_4(SO_4)_2$. For both additives, no defluidization was observed during air staged and un-staged straw combustion. The axial temperature profiles of selected experiments are demonstrated in Appendix C.5 (Figure C.8), showing no significant influence of staging on the combustion properties.

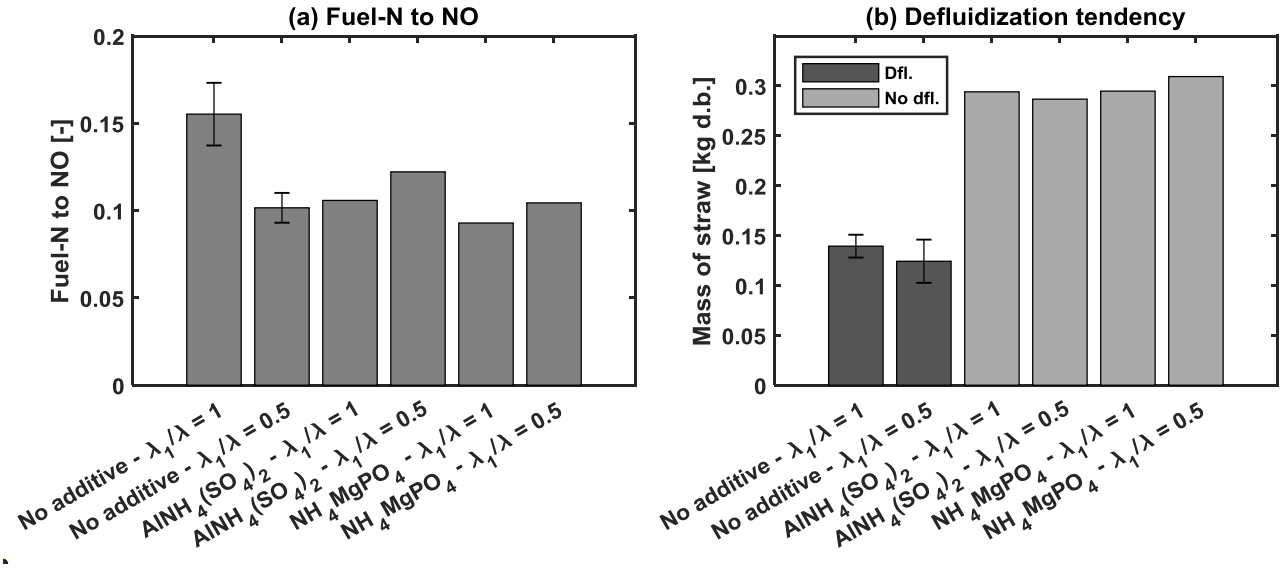

Figure 5.8: Fuel-N to NO conversion (a) and defluidization tendency, expressed in mass of straw combusted, (b) during straw combustion with additives with different staging configurations. Nomenclature: dlf: defluidization, no dfl: no defluidization. Conditions: T_{bed} = 850ºC; λ = 1.4; λ_1/λ = 0.5 and 1.

Figure 5.9 depicts the local concentration measurements during combustion of straw-NH_4MgPO_4 at air staged (λ_1/λ = 0.5) and un-staged (λ_1/λ = 1) conditions. The results show that during air staged combustion, the NO concentration was lower than the un-staged experiment below the secondary air injection point (fuel inlet). This was due to the facilitation of NO reducing reactions in a reducing atmosphere, indicated by the high CO concentration. Above the secondary air injection point, a comparable concentration of NH_3 was released to the freeboard. The fate of the NH_3 was determined by the mixing and O_2 concentration in the secondary jet. In air-staged combustion, the reduction of NO was less favored than in un-staged combustion. Consequently, the NO outlet concentration during air staged combustion with NH_4MgPO_4 surpassed the concentration from un-staged combustion. A similar trend was additionally observed for the N_2O emission, while the HNCO trends were more or less similar. The outlet CO concentration was higher in the air staged experiments, as the mixing and residence time in the reactor were inadequate for complete combustion. The results from straw-$AlNH_4(SO_4)_2$ combustion are illustrated in Appendix C.6, showing a similar trend in the observed results.

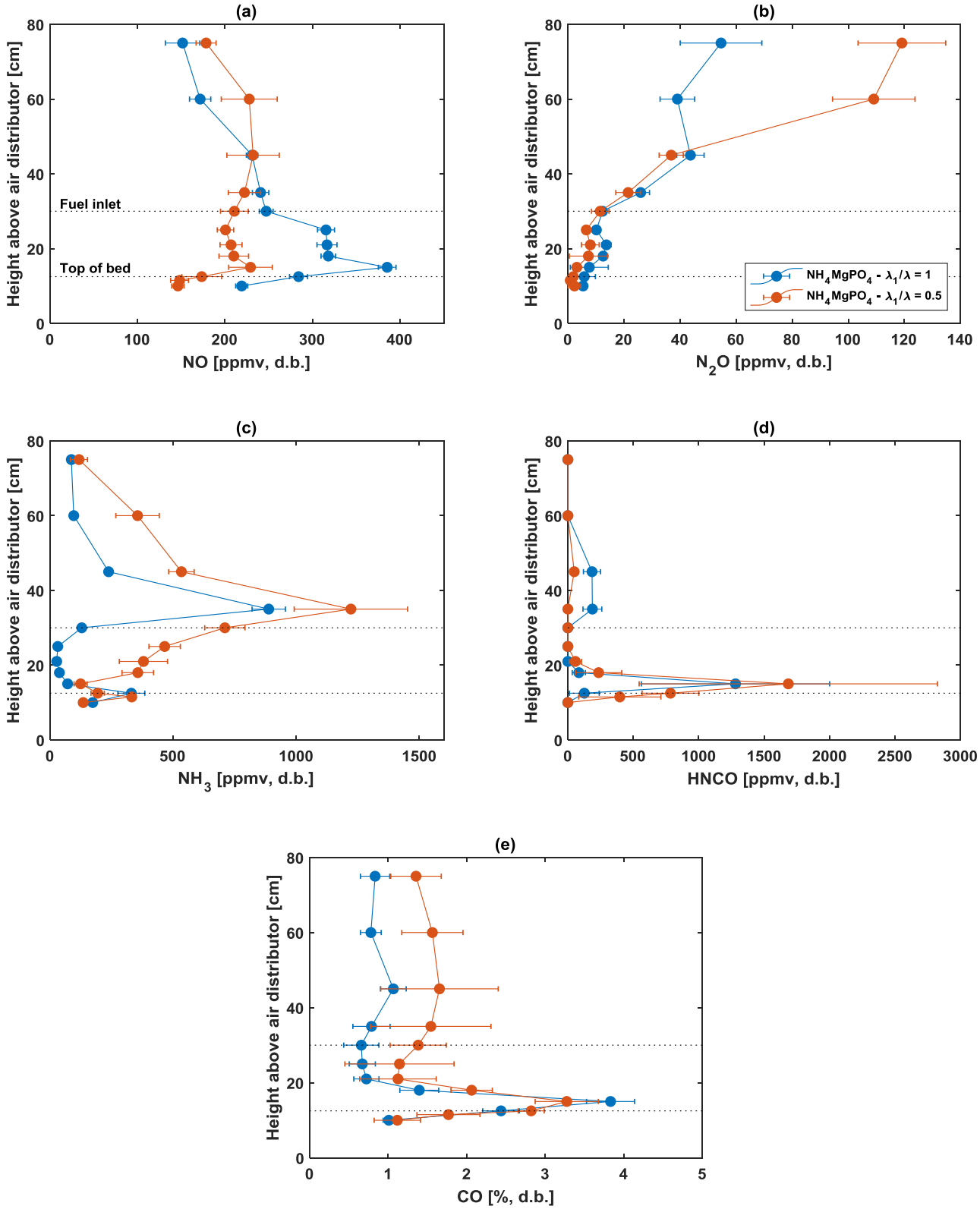

Figure 5.9: Axial NO (a), N_2O (b), NH_3 (c), HNCO (d), and CO (e) profiles during fluidized bed combustion of straw-NH_4MgPO_4 under air staged and un-staged conditions. Conditions: T_{bed} = 850ºC; λ = 1.4; λ_1/λ = 0.5 and 1.

5.3.5 Sunflower husk-additives combustion

Figure 5.10 depicts the conversion of fuel-N to NO (a) and the defluidization tendency (b) during sunflower husk combustion with additives. The de-agglomeration additives slightly increased the fuel-N to NO conversion, while the multifunctional additives reduced the fuel-N to NO conversion by 30%. Most additives prevented defluidization under the investigated conditions. In the case of $AlNH_4(SO_4)_2$, the experiment was stopped prematurely due to recurring blockage of the feeding pipe. However, it is suspected that $AlNH_4(SO_4)_2$ could prevent defluidization during sunflower husk combustion as well. The axial temperature profiles of selected experiments are demonstrated in Appendix C.5 (Figure C.9), showing no significant influence of the additives on the combustion of sunflower husk.

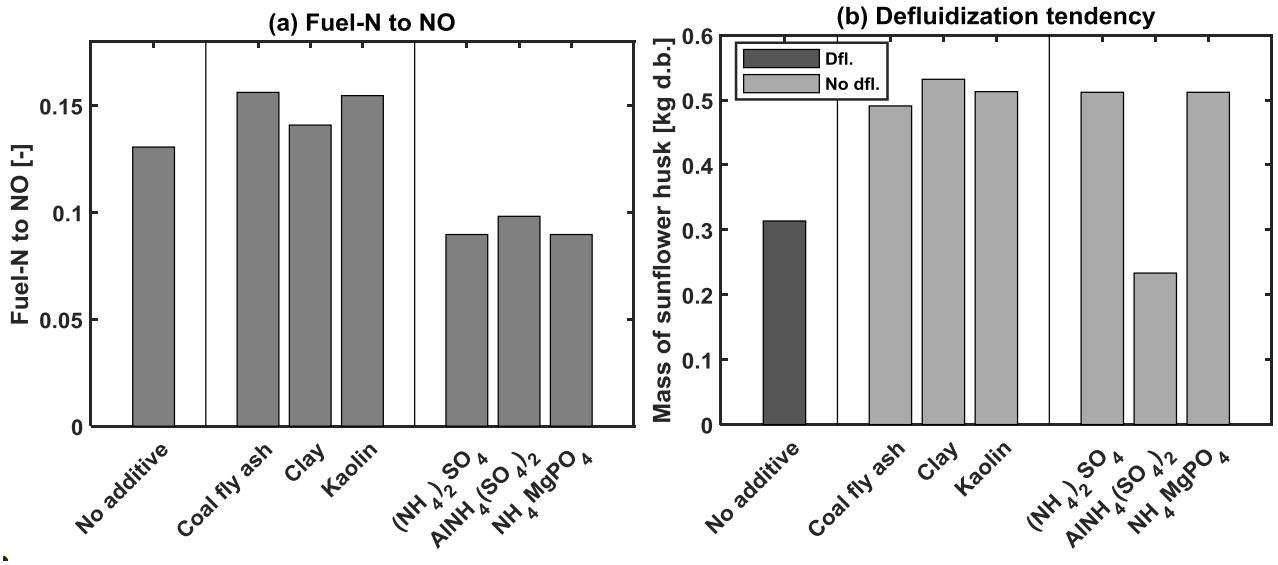

Figure 5.10: Fuel-N to NO conversion (a) and defluidization tendency, expressed in mass of sunflower husk combusted, (b) during sunflower husk combustion with additives. Experiment with $AlNH_4(SO_4)_2$ stopped prematurely due to feeding pipe blockage. Nomenclature: dlf: defluidization, no dfl: no defluidization. Conditions: T_{bed} = 850ºC; λ = 1.4; λ_1/λ = 1.

Figure 5.11 illustrates the results of the local concentration measurements during combustion of sunflower husk with additives. The release location of NH_3 of the additives was similar to the experiments with straw, showing that NH_4MgPO_4 released a larger quantity of NH_3 above the fuel inlet, while $AlNH_4(SO_4)_2$ predominantly released NH_3 at the top of the bed. Consequently, the reduction of NO above the fuel inlet was more prominent for NH_4MgPO_4, while the NO concentration near the bed region was lower for $AlNH_4(SO_4)_2$. The presence of HNCO during sunflower husk combustion was again prominent. However, similar to the straw combustion experiments, no HNCO was detected in the experiment with $AlNH_4(SO_4)_2$, possibly due to the catalytic effect of Al on the HNCO chemistry [289]. This may to some extent explain the higher N_2O concentration using $AlNH_4(SO_4)_2$. The CO profiles were comparable between experiments and to that of straw combustion in Figure 5.5, indicating similar combustion behavior of the fuels.

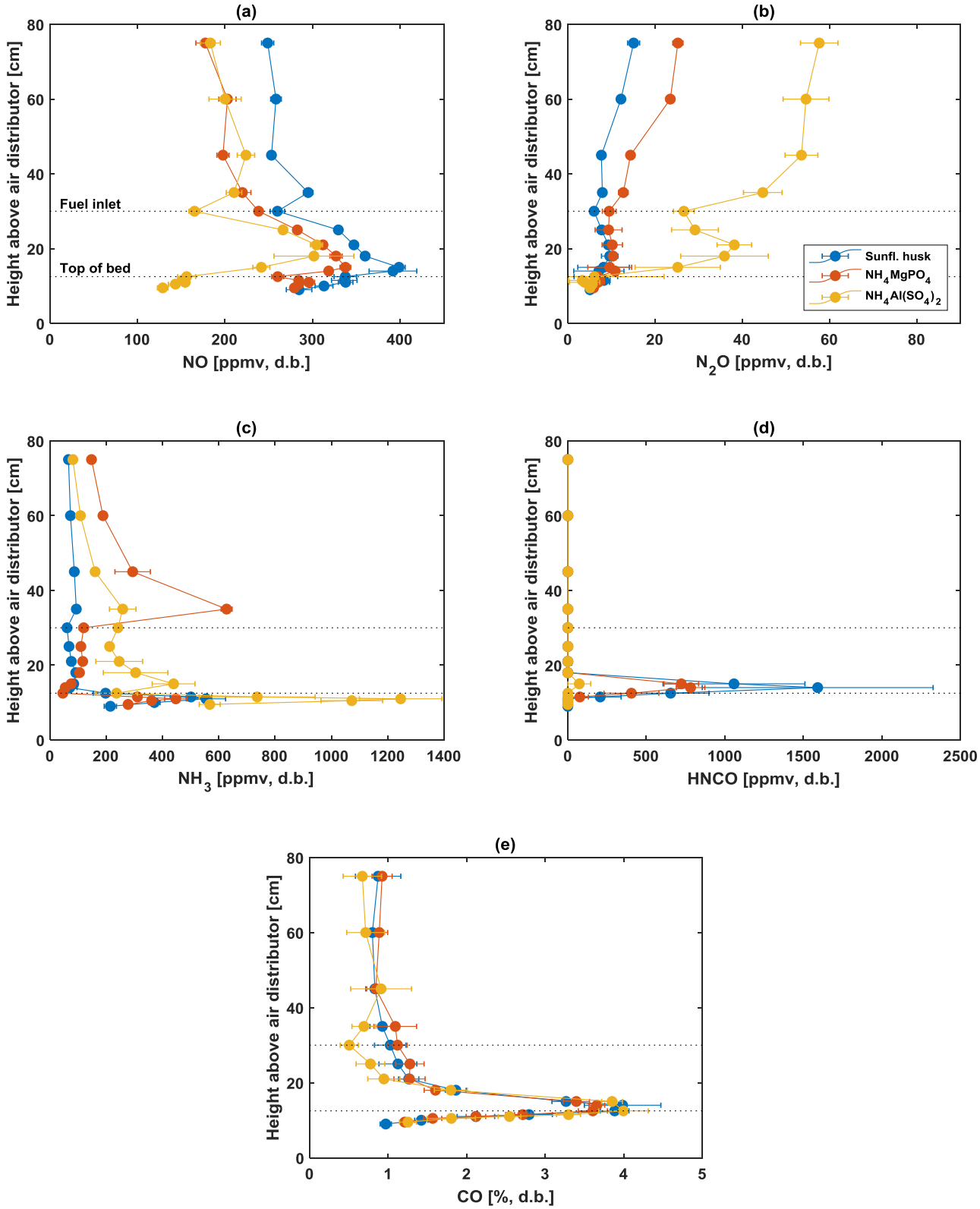

Figure 5.11: Axial NO (a), N_2O (b), NH_3 (c), HNCO (d), and CO (e) profiles during fluidized bed combustion of sunflower husk with NH_4MgPO_4 and $AlNH_4(SO_4)_2$. Conditions: T_{bed} = 850ºC; λ = 1.4; λ_1/λ = 1.

5.3.5.1 Influence of ash accumulation

The influence of ash accumulation and thereby bed agglomeration on the gaseous chemistry was investigated during sunflower husk combustion. Sunflower husk was chosen for this investigation, as it allowed measurements at the initial and late stages of combustion, since the time before defluidization was significantly longer than in straw combustion. The local concentration measurements are demonstrated in Figure 5.12. The initial stage (init) measurements were conducted during the feeding of 0.04-0.15 kg d.b. sunflower husk (1.3-4.8 g ash), whereas the late stage (late) measurements were performed between 0.23-0.30 kg d.b. sunflower husk (7.4-9.6 g ash). While the overall trend in NO was similar, a slightly higher concentration of NO above the fuel bed was prominent at later stages of combustion. This was to some extent reflected in a slightly lower concentration of NH_3 and HNCO at later stages of combustion. These differences may be attributed to the catalytic influence of ash on the NH_3 and HNCO oxidation and/or to mixing limitations. While the former was described in Chapter 2, Section 2.4.1.3, mixing limitations in the bed may be caused by the formation of a sticky molten layer and agglomerates in consequence of ash accumulation. This molten phase changes the fluid dynamics and thereby the extent of fluidization during combustion. This is to some extent reflected in the standard deviations of the concentration measurements near the top of the bed. In the early stages of combustion, larger temporal variations in the data (high standard deviation) were observed due to the burst of bubbles at the top of the bed. As the bed started to agglomerate and the fluid dynamics change, bubble bursting became less pronounced thereby dampening the temporal variation in the concentration measurements. Two mechanisms could explain the observed trends. Agglomerates formed during combustion could segregate and settle at the bottom of the bed [290], thereby effectively minimizing the bed height and ultimately diminishing bubble size [291]. This could reduce the fluctuations caused by bubble bursting above the bed. Alternatively, viewing the sand bed as a continuous fluid, ash accumulation would increase the viscosity of the fluid, thereby slowly and continuously shifting the gas flow behavior from bubbling fluidization to plug flow, i.e. changing from complete mixing to plug flow behavior. A similar reasoning, i.e. poor mixing, may explain the increased NO emission near the bed when employing $(NH_4)_2HPO_4$, described in Section 5.3.2.1. In addition, the accumulation of sunflower husk ash had a negligible influence on the major C_XH_Y species, demonstrated in Appendix C.7.

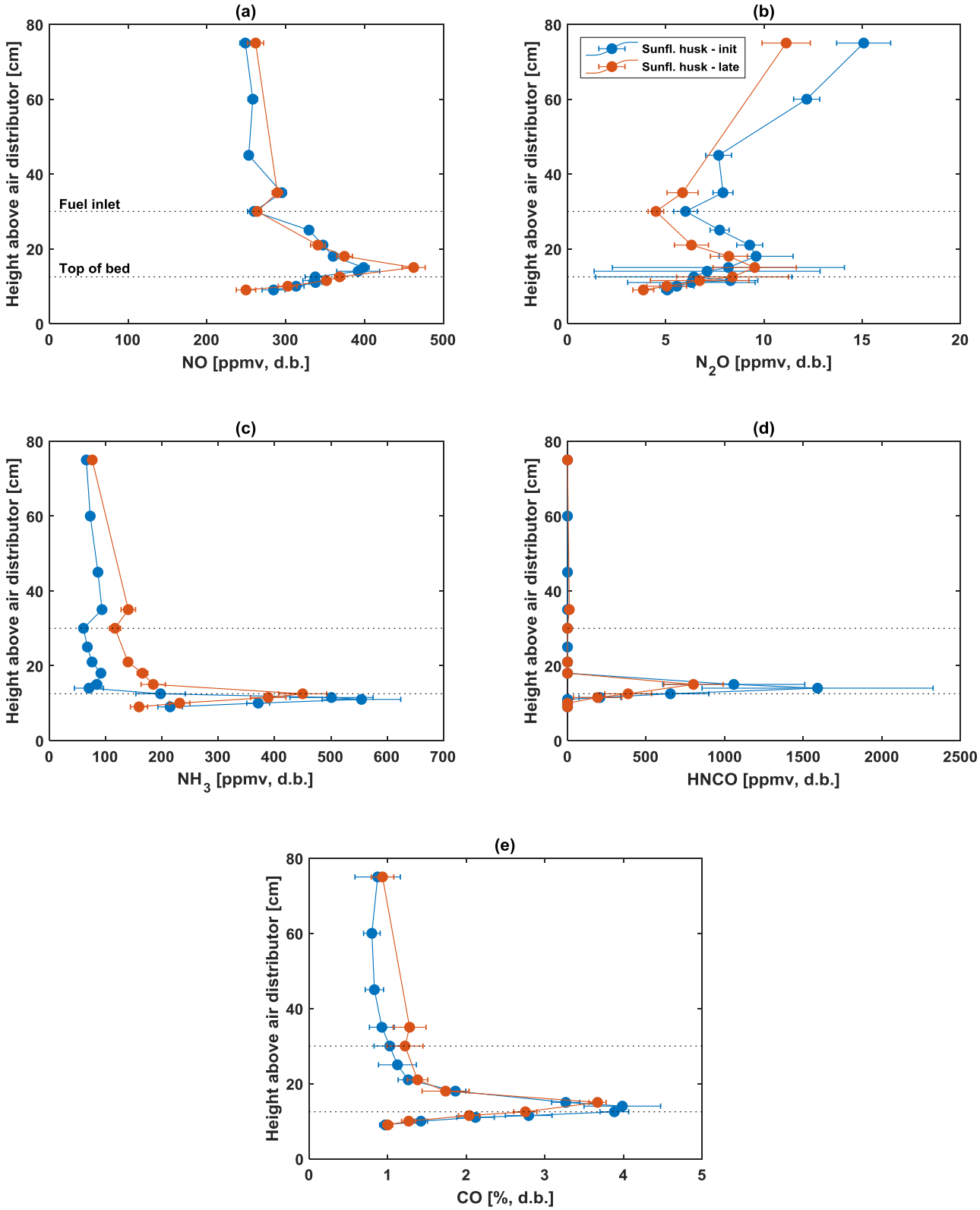

Figure 5.12: Axial NO (a), N_2O (b), NH_3 (c), HNCO (d), and CO (e) profiles during fluidized bed combustion of sunflower husk. Measurements were performed initial (init: 0.04-0.15 kg d.b. sunfl. husk) and late (init: 0.23-0.30 kg d.b. sunfl. husk) stages of combustion. Conditions: T_{bed} = 850ºC; λ = 1.4; λ_1/λ = 1.

5.4 Conclusions

The impact of a wide range of additives on NO_X emissions and bed agglomeration during continuous fluidized bed combustion of straw was investigated. Kaolin, CaO, and $MgCO_3$ addition prevented defluidization without reducing NO_X emissions. To reduce NO by additives, the NH-functionality was a necessity. Of the investigated additives, NH_4MgPO_4 and $AlNH_4(SO_4)_2$ prevented defluidization while reducing fuel-N to NO conversion by 40%.

Local gas composition measurements revealed that the NH-based additives released NH_3 above the fuel inlet and/or bubbling bed. Some additives favored the reduction of NO by thermal $DeNO_X$ while others increased NO emission near the bed either due to the catalytic oxidation of NH_3 (Fe-based additives) or by inducing poor mixing conditions caused by the ash chemistry ($(NH_4)_2HPO_4$). All NH-based additives increased N_2O emission possibly by oxidation of NH_3 and HNCO. The combustion of straw was unaffected by the mixing of additive to the fuel, notable from the local CO and C_XH_Y concentrations, and temperature measurements.

Larger particles of $(NH_4)_2SO_4$ dropped to the bed, increasing the NH_3 release above the fuel bed and prolonging the time for defluidization. For smaller particles, the concentration of NH_3 and N_2O was higher and that of NO was lower above the fuel inlet. In addition, no significant differences in the fuel-N to NO conversion, effluent CO concentration, and defluidization tendency were observed when introducing $(NH_4)_2SO_4$ as pellets dropped batch wise during combustion or as smaller particles premixed with fuel. This may be caused by differences in the release location and mechanism of $(NH_4)_2SO_4$.

Air staging was an effective way of reducing the fuel-N to NO conversion (40% reduction) during straw combustion. The use of NH_4MgPO_4 and $AlNH_4(SO_4)_2$ under air staged conditions did not lead to a further decrease in NO; instead, the NO emission slightly increased when employing these additives with air staging. The introduction of secondary air favored the oxidation of NH_3 to NO to a larger degree than in un-staged combustion. In addition, N_2O and CO effluent concentrations increased, while the local concentration of HNCO was unaffected by air staging.

NH_4MgPO_4 and $AlNH_4(SO_4)_2$ prevented defluidization during un-staged sunflower husk combustion while lowering the fuel-N to NO conversion by 30%. The behavior of NH_4MgPO_4 and $AlNH_4(SO_4)_2$ during combustion with sunflower husk was similar to that of straw. The accumulation of ash increased NO and decreased NH_3 concentration above the bed, presumably caused by the incipient defluidization leading to poorer mixing and the catalytic effect of ash forming elements on the nitrogen chemistry.

6 Formation of NO and N_2O during raw and demineralized biomass char combustion

This chapter has been written in a manuscript format. A slightly modified version has been published in the peer-reviewed journal *Energy & Fuels* as,

Ulusoy B., Lin W., Karlström O., Li S., Song W., Glarborg P., Dam-Johansen K., Wu H., *Formation of NO and N_2O during Raw and Demineralized Biomass Char Combustion*, Energy & Fuels 2019;33:5304-15. doi: 10.1021/acs.energyfuels.9b00622

Abstract: The formation of nitrogen oxides (NO and N_2O) during raw and demineralized biomass char combustion and the reduction of NO over biomass char were investigated. The biomass fuels were pine wood, straw, waste wood, bran, dried distillers grains with solubles (DDGS), and sunflower seed. Fixed bed combustion experiments were performed at 800°C in 10vol% O_2, while NO reduction experiments were conducted at temperatures from 800 to 900°C and NO inlet concentrations from 400 to 1500 ppmv. The chars were characterized by means of ICP-OES, BET, SEM-EDX, and XPS. The conversion of char-N to NO decreased with an increase in the initial char-N content, partly explained by the increased inherent conversion of char-N to N_2O. The reduction of NO over char exhibited no correlation to the surface functionalities and content of nitrogen and oxygen at the investigated conditions. The NO reduction reactivity was strongly dominated by the content and association of ash forming elements in the chars. The NO reduction reactivity of pine wood, waste wood, and straw chars correlated reasonably well with the (K+Ca)/C molar ratio, while the chars with a high phosphorous content, i.e., bran, DDGS, and sunflower seed chars, differed by showing a significantly lower reactivity. The inhibition effect of phosphorous on NO reduction reactivity was likely caused by the formation of less catalytically active potassium species (such as KPO_3) in biomass char.

6.1 Introduction

Minimizing NO_X emissions from industrial solid fuel combustion is important due to the harmful environmental impact and strict emission regulations. In fluidized bed combustion, NO_X primarily stems from the fuel bound nitrogen through volatile and char oxidation. While the gaseous nitrogen chemistry is fairly well established [17,18], the conversion of char-N to NO is less understood, especially in the case of high-nitrogen biomass fuels. During char combustion, NO is simultaneously formed from and reduced by char. The final emission of NO_X is determined by the competing NO_X formation and reduction reactions [131].

The products of char nitrogen combustion include primarily NO, N_2O, and N_2 [16]. During fixed bed coal char combustion at single particle conditions, the conversion of char-N to NO ranged from 75-100% [16,139]. Similar experiments employing biomass chars yielded char-N to NO conversions in a range of 25-75%, implying a significant reduction of NO during biomass char combustion [143]. The fractional conversion of char-N depends on the operating conditions (such as temperature and gas composition) and the fuel properties [16].

The proposed mechanism for the formation and reduction of NO during char combustion in an O_2/N_2 system is summarized in R6.1-R6.2 and R6.3-R6.9, respectively [61,98,154–156]. Here, (-CX) denotes a carbon surface complex of either nitrogen or oxygen, while (-C) is a free carbon active site and M is a catalytically active ash forming element. The dissociative chemisorption of NO occurs in R6.3 and R6.7 followed by reduction through R6.4 and R6.5, and active site regeneration by R6.8 and R6.9. Additionally, the presence of CO has been reported to enhance the reduction reaction [159], presumably by reaction with NO catalyzed by char, demonstrated by the non-elementary R6.6. Ultimately, the (-CO) is released to the gas phase as CO or CO_2, and a free active site is formed. Several reviews dealing with the reduction reaction between NO and coal char have been reported [16,131,136,292,293]. Compared to coal, biomass chars generally exhibit a higher reactivity towards NO reduction [155,159,294,295]. This has been attributed the higher potassium content and larger surface area of biomass chars. Besides these, other factors such as increased amounts of sodium [158], magnesium [161], calcium, and iron [162], and more effective porosity [163,296] have been shown to enhance the NO reduction reactivity.

$$O_2 + (\text{-C}) + (\text{-CN}) \rightarrow (\text{-CO}) + (\text{-CNO}) \quad \text{R6.1}$$

$$(\text{-CNO}) \rightarrow NO + (\text{-C}) \quad \text{R6.2}$$

$$NO + 2\,(\text{-C}) \rightarrow (\text{-CO}) + (\text{-CN}) \quad \text{R6.3}$$

$$2\,(\text{-CN}) \rightarrow N_2 + 2\,(\text{-C}) \quad \text{R6.4}$$

$$(\text{-CN}) + NO \rightarrow N_2 + (\text{-CO}) \quad \text{R6.5}$$

$$2\,NO + 2\,CO \rightarrow N_2 + 2\,CO_2 \quad \text{(over char)} \quad \text{R6.6}$$

$$(\text{-M}_x\text{O}_y) + (\text{-C}) + NO \rightarrow (\text{-M}_x\text{O}_{y+1}) + (\text{-CN}) \quad \text{R6.7}$$

$$(\text{-M}_x\text{O}_{y+1}) + (\text{-C}) \rightarrow (\text{-M}_x\text{O}_y) + (\text{-CO}) \quad \text{R6.8}$$

$$(\text{-CO}) \rightarrow CO + (\text{-C}) \quad \text{R6.9}$$

Studies have shown that the conversion of char-N to NO decreased with an increase in char-N content and external NO concentration [155,172,297]. This effect was more pronounced with demineralized biomass, wherein the influence of the inorganics was minimized [155]. These results indicate that the formation and reduction of NO are related to the initial char-N content and gas phase NO concentration. The reaction rate between char and NO was suggested to be proportionally correlated to the instantaneous NO and C(N) concentrations [154]. R6.3-R6.9 are indicative that higher contents of char-N and ash forming elements would lead to higher NO reduction rates. Consequently, the reactivity of high-nitrogen chars towards NO could conceivably be enhanced by the initial char-N

content. In addition, although the influence of the ash forming elements on the char NO reactivity has been well documented [155,159], the importance of their association in the raw biomass is still unclear.

To obtain an improved understanding of the declining tendency in char-N conversion to NO with an increase in char-N content, a thorough study of the NO formation and reduction during raw and demineralized biomass char combustion was conducted in a fixed bed reactor at conditions relevant to fluidized bed combustion. The product distribution from char-N oxidation was characterized and its dependency on the chemical composition of the chars was investigated. The NO reduction reactivity of the chars was examined at different temperatures and NO inlet concentrations. The results were interpreted based on analyses of the surface area, char-N content, nitrogen and oxygen surface functionality, and ash forming element content and association in biomass chars.

6.2 Experimental section

6.2.1 Fuels and their demineralization

Six types of biomass, pine wood, straw, waste wood, bran, dried distillers grains with solubles (DDGS), and sunflower seed, were employed in the experiments. Table 6.1 shows the composition of selected elements in the raw fuels. The complete compositions are given in Appendix D.1 (Table D.1). The nitrogen contents ranged from 0.2 to 6.14 wt%, thereby covering a wide range of nitrogen contents in biomass fuels.

Table 6.1: Chemical composition of the six biomass

	[wt% d.b]						[mg/kg d.b.]					
Fuel	**C**	**H**	**N**	**O**	**S**	**Ash**	**K**	**P**	**Mg**	**Ca**	**Fe**	**Na**
Pine wood	51.5	6.20	<0.20	41.9	0.007	0.2	480	52	140	950	26	95
Straw	46.9	6.00	0.56	42.2	0.120	4.2	14,000	910	960	2,300	41	230
Waste wood	49.0	6.13	1.33	41.8	0.037	1.7	703	93	443	3,200	363	326
Bran	45.0	6.30	2.65	40.6	0.19	5.3	13,000	11,000	3,800	920	210	50
Sunfl. seed	40.5	5.73	6.14	33.4	0.23	14	18,416	12,810	6,724	7,328	1,730	410
DDGS	43.7	6.55	5.13	37.8	0.41	6.4	11,723	10,204	3,442	1,105	91	3,255

The biomass samples were demineralized (DM) following the work of Aho et al. [298] Biomass was initially ground and sieved to a size range of 212-1000 μm and subsequently suspended in 500 mL of HNO_3 (Sigma Aldrich, CAS number: 7697-37-2) solution at pH 2 and heated to 60°C. The leaching was continued for one hour at 60°C under stirring at 750 rpm. After one hour, the solids were collected by filtration and the leaching process repeated. Then, the biomass was filtered with 250 mL demineralized water until the permeate pH was above 6.0. The obtained demineralized biomass was dried at 105°C for one day.

A chemical fractionation method was used to separate the different groups of ash forming elements in straw [299–302]. To eliminate the influence of water-soluble materials such as alkali sulfates, carbonates, chlorides, and to a lesser extent organically bound metals, 30-35 g of straw was washed in 500 mL deionized water at room temperature under stirring at 750 rpm for 24 h. Subsequently, the liquid was removed by filtration, and the extraction process repeated. After the second leaching, the suspended solids were washed several times with 250 mL deionized water until the permeate pH was above 6.0. Following this, half of the water washed (WW) straw was dried at 105°C for one day, while the other half was suspended in 150 mL 1 M ammonium acetate (Fluka Chemica, CAS number: 631-61-8) to remove ion-exchangeable cations in the form of organically bound metals. The ammonium acetate treatment was continued for one day under stirring at 750 rpm, after which the organic washed (OW) straw was washed using 100 mL, 1 M ammonium acetate for the first wash and 250 mL deionized water for the subsequent washes until the permeate pH was above 6.0. The filtered solids were dried at 105°C for one day.

6.2.2 Char preparation

Chars from raw and DM biomass were prepared in a horizontal oven at 800°C using a N_2 flow of 2.5 NL/min. The pyrolysis temperature was monitored through a thermocouple placed in the middle of the oven. Upon reaching the desired temperature, approximately 10-15 g of biomass was quickly pushed into the reactor. The pyrolysis was continued for 10 minutes, after which the sample was rapidly withdrawn to a water cooled section to ensure prompt cooling. The char samples were withdrawn from the reactor below a temperature of approximately 150°C. The char yield was determined from the biomass and char mass.

6.2.3 Experimental setup

Figure 6.1 illustrates the quartz fixed bed reactor used for char combustion and NO reduction experiments. The temperature in the bed was kept uniform by three independent heating elements and monitored by a thermocouple located 0.5 cm below the porous plate. Upon reaching the desired conditions, a solid feeding device enabled the introduction of a char-sand sample. In all experiments, 1.75 g quartz sand with a size of 250-355 µm, pre-treated at 800ºC, was added together with the char to facilitate sample admission and ensure a constant bed height. Blank tests confirmed that the sand itself had no reactivity towards NO reduction. NO reduction experiments were conducted at three temperatures (800, 850, 900 ºC) and NO inlet concentrations (400, 800, 1500 ppmv) using 20-50 mg char with a size of 125-180 µm to diminish mass transport resistances. The influence of external and internal mass transfer limitations during NO reduction over char were assessed based on the Maer and Weisz-Prater criteria, respectively [303]. The results, summarized in Appendix D.1 (Table D.2) for the most reactive biomass, straw, showed that the influence of mass transfer limitations was negligible at the highest applied temperature. Following a reduction experiment, 10% O_2 was introduced the reactor to burn the NO treated char. In addition, separate combustion experiments using 20 mg, 125-180 µm char were carried out at 800ºC in 10% O_2. The temperature in the sample bed was assumed constant during combustion in consequence of the low percentage of char in the bed and the high heat capacity of sand. In all experiments, the total volumetric flow rate was 1 NL/min

with the balance gas being N_2. The CO, CO_2, O_2, and NO concentrations in the dry flue gas were continuously monitored by a series of on-line gas analyzers (NGA2000, Fischer-Rosemount). Moreover, a Fourier Transform Infrared spectrometer (FTIR) (Multigas 2030 FTIR, MKS instruments) was employed in selected experiments to determine the distribution of nitrogen products during combustion and NO reduction.

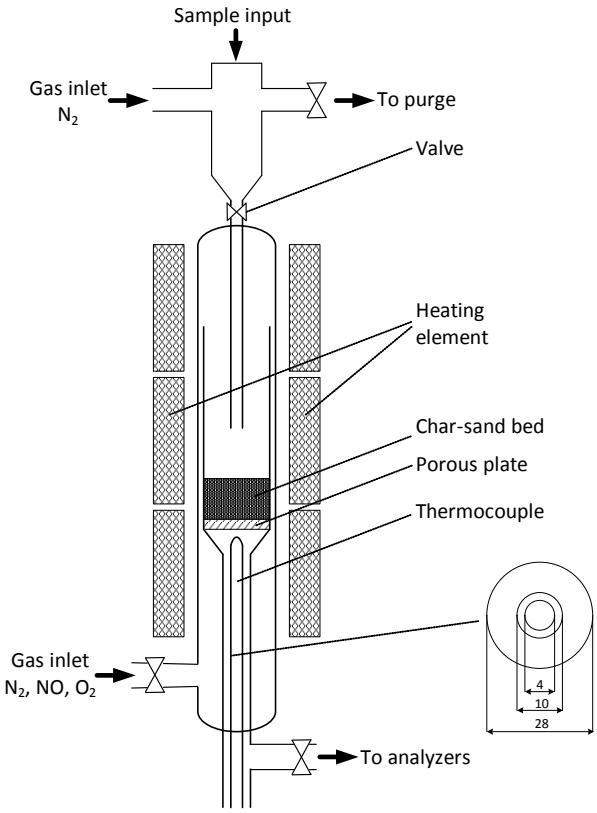

Figure 6.1: Schematic illustration of the fixed bed reactor.

A typical plot of the NO concentration versus time, depicting the complete steps in the NO reduction experiments, is shown in Figure 6.2. Each experiment involved four steps (S1-S4), NO signal stabilization (S1), char introduction and NO reduction (S2), NO cutoff and residual char combustion in 10vol% O_2 forming a NO concentration peak (S3), and NO signal stabilization (S4). The experiment was stopped when the NO concentration in S4 equaled that in S1. Little to no reduction of NO was observed over pure fuel ash.

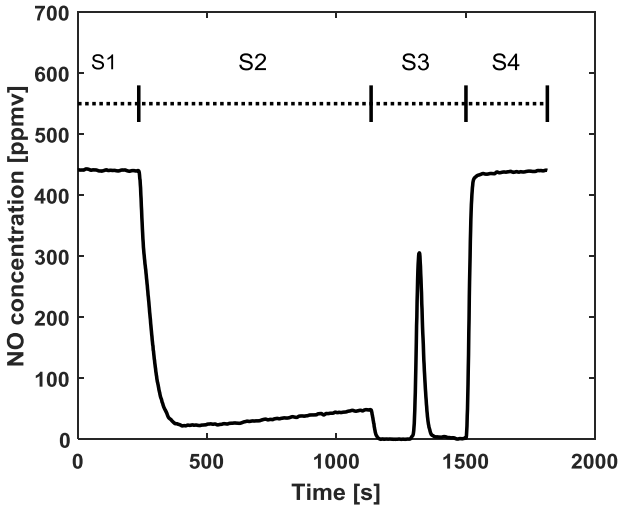

Figure 6.2: Example of a NO versus time curve, illustrating the steps during a reduction experiment. S1: stabilization of the NO signal, S2: introduction of char and NO reduction commences, S3: NO feeding is stopped, and 10vol% O_2 is introduced to burn residual char, and S4: stabilization of NO signal. The reduction was carried out at 800°C with an inlet concentration of 400 ppm NO using straw char.

The reactivities of solid fuel chars towards NO are commonly evaluated from globalized first [304–307] or fractional [159,308,309] order rate expressions, where the rate constant is most frequently based on the instantaneous mass of carbon in the char. To compare the reactivities between chars, the first order rate constant of the NO-char reaction was determined under the assumption of plug flow, shown in Eq. 6.1.

$$-\ln(1-X_{NO}) = \frac{k_{NO} \cdot W}{V_g} \qquad \text{Eq. 6.1}$$

Here, X_{NO} (-) is the instantaneous conversion of NO, W (kg C) the instantaneous char carbon mass in the bed, V_g (m^3/s) the volumetric gas flowrate, and k_{NO} ($m^3\ s^{-1}\ kgC^{-1}$) the first order carbon mass based rate constant. The instantaneous carbon mass was determined from the CO and CO_2 measurements during the reduction section, while the total C-content from a mass balance of the entire experiment.

6.2.4 Characterization of chars

The specific Brunauer-Emmett-Teller (BET) surface area and the Barrett-Joyner-Halenda (BJH) mesoporosity of the chars were determined from N_2 adsorption at its boiling point (77 K) in the p/p_0 range of 0.01-0.99 using a Quantachrome iO2 equipment. Prior to measurements, the samples were vacuum degassed at 300°C for 5 h. Scanning electron microscopy and energy dispersive x-ray (SEM-EDX) analysis was performed on a selected number of chars. In the pre-treatment, the chars were coated with platinum, after which they were dried at 105°C for one day. X-ray photoelectron spectroscopy (XPS) was conducted on selected chars to analyze the content and functionalities of nitrogen and oxygen on the char surface. The C1s and N1s peaks were deconvolved using XPS PEAK 4.1 software by subtracting a Shirley type background and fitting Gaussian-Lorentzian mix functions. The nitrogen functionality was determined from 395-408 eV, in which five distinct nitrogen peaks,

pyridinic N-6 (398.7±0.3), pyrrolic N-5 (400.3±0.3), quartenary N-Q (401.4±0.5), oxides N-X1 and N-X2 (402-405), were assigned [114]. The parameters used for the fitting were the peak width, position, and full-width-half-maximum (FWHM). The Gaussian-Lorentzian (G/L) mix, describing instrumental and metallic effects, was set at 0.7, i.e. 70% Gaussian and 30% Lorentzian for all nitrogen functionalities.

The chemical composition of the chars was analysed with a Thermo Scientific Flash 2000 Organic Elemental Analyser (Flash 2000) for the carbon, hydrogen, nitrogen, and sulphur content, while the inorganic contents were determined by inductively coupled plasma emission spectroscopy (ICP-OES).

Table 6.2 summarizes the chemical analyses of the chars, including selected ICP-OES results. The demineralized chars exhibited a lower ash content in comparison with the raw chars. Straw, bran, sunflower seed, and DDGS chars contained large amounts of potassium, which is presumably the most active catalytic element in the char-NO reaction. In comparison, the demineralized chars were largely depleted of elements presumed to have a catalytic effect on the NO reduction, i.e. potassium, iron, calcium, sodium, and magnesium.

Table 6.2: Elemental and proximate analyses of six raw and demineralized biomass chars

	[wt% d.b.]							[mg/kg d.b.]					
Char	**C**	**H**	**N**	**O**	**S**	**Ash**	**Char yield**	**K**	**P**	**Mg**	**Ca**	**Fe**	**Na**
Pine wood	85.7	1.48	0.11	9.12	0.0	3.59	20.5	1,083	210	515	4,008	223	373
Straw	71.2	1.18	0.50	8.42	0.0	18.7	25.8	43,642	2,789	2,329	4,459	<3	740
Waste wood	70.0	1.17	1.06	18.4	0.0	9.36	20.8	1,977	355	3,505	32,002	4,426	1,152
Bran	59.9	1.30	2.90	9.90	0.0	26.0	26.5	69,610	49,429	18,304	3,629	676	<120
Sunfl. seed	57.0	1.10	3.59	11.2	0.0	27.1	29.4	55,749	29,190	17,100	18,101	2,446	550
DDGS	59.0	1.30	5.36	13.2	0.0	21.1	26.9	31,430	31,355	11,779	3,758	443	11,697
DM pine wood	87.5	1.56	0.11	10.7	0.0	0.11	15.8	<20	<60	<0.2	90	442	<120
DM straw	82.2	1.53	0.83	7.04	0.0	8.40	16.9	76	450	<0.2	212	77	<120
DM waste wood	74.8	1.23	0.84	16.5	0.0	6.59	17.4	245	194	1,606	8,845	1,483	<120
DM bran	76.9	1.49	3.52	7.69	0.0	10.4	25.7	129	13,702	32	96	1,047	<120
DM sunfl. seed	71.7	1.24	4.50	8.26	0.0	14.3	25.0	874	14,327	485	1,400	2,275	<120
DM DDGS	73.3	1.35	6.92	9.58	0.0	8.85	23.8	<20	8,402	<0.2	87	540	<120

Table 6.3 shows the physical properties of the chars. In general, the surface area and pore volume were noted to increase due to demineralization. The only exception to this was in the case of pine wood, where demineralized pine wood char showed a significantly lower surface area and pore volume, the reasoning of which is unknown. The large pore volume in some chars was primarily due to the formation of micropores in addition to mesopores during charring. A wide range of surface areas and pore volumes are covered by the investigated chars.

Table 6.3: BET surface area (SA), pore volume (V_p), and mean pore diameter ($d_{p,mean}$) of the chars

Char	**SA [m^2/g]**	**V_P [cm^3/g]**	**$d_{p,mean}$ [nm]**
Pine wood	405	0.18	1.076/3.377
Straw	25	$2.4 \cdot 10^{-2}$	3.404
Waste wood	91	$5.8 \cdot 10^{-2}$	4.275
Bran	4.5	$6.1 \cdot 10^{-3}$	3.054
Sunfl. seed	1.2	$2.7 \cdot 10^{-3}$	3.855
DDGS	1.0	$1.2 \cdot 10^{-3}$	3.087
DM pine wood	4.5	$6.5 \cdot 10^{-3}$	3.059
DM straw	430	0.18	1.932/3.382
DM waste wood	415	0.18	1.178/3.383
DM bran	3.0	$3.1 \cdot 10^{-3}$	3.379
DM sunfl. seed	135	$6.8 \cdot 10^{-2}$	3.374
DM DDGS	4.6	$4.7 \cdot 10^{-3}$	3.440

6.3 Results

6.3.1 Conversion of char-N to NO

Figure 6.3 illustrates the conversion of char-N to NO during combustion of raw (a) and demineralized (b) chars in 10 % O_2, along with error bars depicting the deviations in the elemental analyses. The results indicate that the conversion of char-N to NO decreased with an increase in char-N content, in accordance with previous single particle combustion studies [155,172]. This trend was also observed for the demineralized chars at both investigated temperatures. At higher temperature, a slight increase in the conversion of char-N to NO was observed. Previous studies on coal chars showed that the effect of temperature was negligible when increased from 800 to 900°C [310], while it could be more pronounced when changing from 850 to 1150°C [139]. According to the mechanism shown in R6.1-R6.9, the observed trends are conceivably related to the NO formation and/or reduction reactions. In the demineralized chars, i.e., with a diminished impact of inorganic elements, it could be expected that R6.4 and R6.5 occur more rapidly when high local concentrations (-CN) and NO are prominent. Alternatively, nitrogen-rich compounds could form a higher concentration of alternative combustion products such as N_2O, N_2, and NO_2. Lastly, the lower conversion to NO could be caused by the combustion atmosphere, e.g. simultaneous presence of high O_2 and CO concentrations, thereby increasing the importance of R6.6 and R6.9, respectively. In the following sections, the combustion product distribution and NO reduction reactivity of the chars were examined to provide insight into the decreasing conversion of char-N to NO.

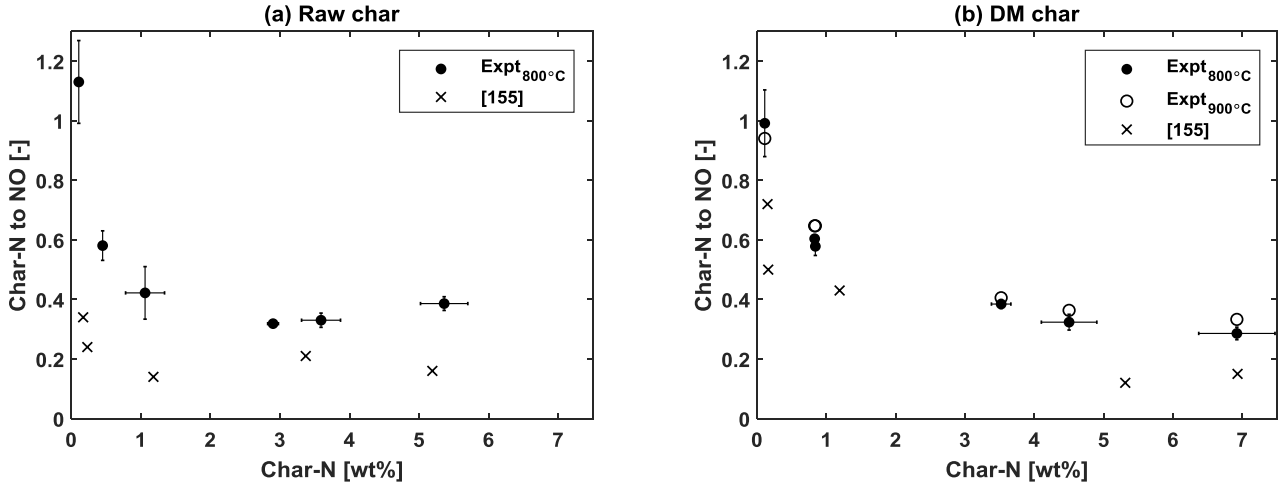

Figure 6.3: Conversion of char-N to NO during combustion of 20 mg raw (a) and DM (b) biomass char at 800°C in 10vol% O_2. The DM chars were additionally oxidized at 900°C. The measurement errors describe the deviations in the elemental analysis. For comparison, the data of Karlström et al. [155] at 900°C in 3vol% O_2 is shown.

6.3.2 Combustion product distribution of char-N

Figure 6.4 illustrates the FTIR determined nitrogen product distribution from raw and demineralized char combustion at 800°C in 10% O_2. The primary oxidation products were NO, N_2O, and a residual fraction, presumably consisting of N_2 and to lesser extent HCN, as negligible amounts of NH_3,

HNCO, and NO_2 were detected. The HCN concentrations were not measured in the present study. In a combustion atmosphere without the addition of radical quenching compounds, the presence of HCN is expected to be low [297,311,312]. Consequently, the residual fraction is presumed to consist predominantly of N_2. The results show that a significant amount of N_2O was formed during biomass char combustion at 800°C, especially for the high-nitrogen chars. This is consistent with reported coal char combustion studies [131,135]. In addition, a slightly higher conversion to N_2O was observed for the demineralized chars, presumably caused by the promoting effect of ash forming elements such as potassium on the N_2O reduction over char [313].

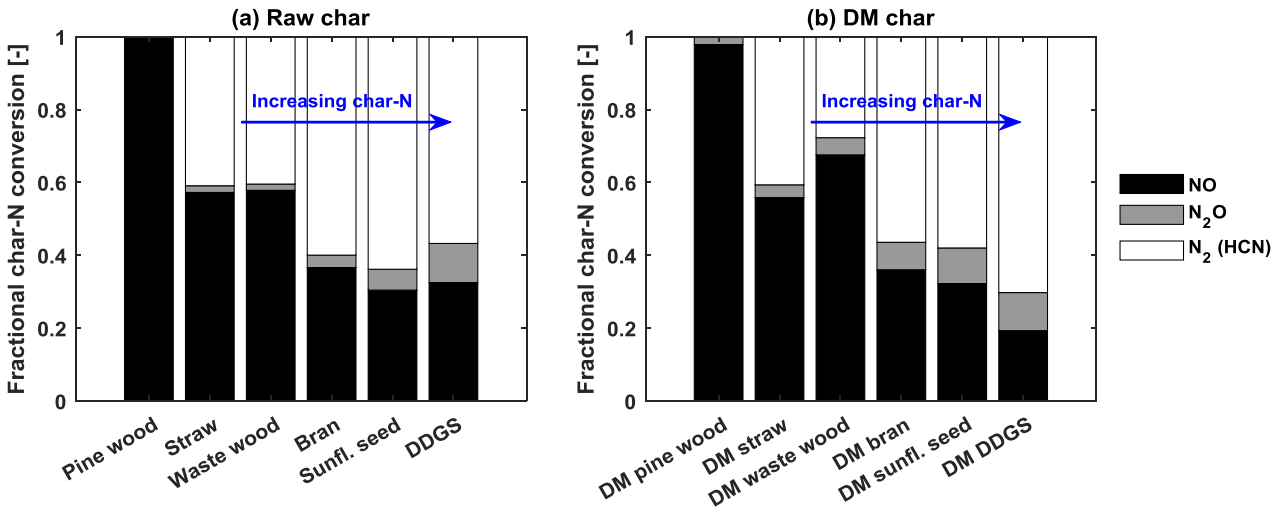

Figure 6.4: Distribution of nitrogen products from 20 mg char combustion at 800°C in 10vol% O_2.

Figure 6.5 illustrates the fractional conversion of char-N to NO and N_2O, and the ratio of N_2O to ($NO+N_2O$) during combustion of selected chars at varying char mass. By reducing the char mass, a smaller degree of reduction of the formed nitrogen oxidation products by secondary char particles is expected. The results show that high amounts of N_2O were formed during char combustion; in one case, as much as 25% of the char-N formed N_2O. The conversion of char-N to NO and N_2O generally increased with a decrease in char mass. In addition, the $N_2O/(NO+N_2O)$ ratio was higher for the high-nitrogen DDGS chars and decreased with an increase in char mass, due to the faster decomposition of N_2O to N_2 over char (R6.10 [135] and R6.11 [136]) compared to NO [314]. As the reduction of reactive nitrogen combustion products by secondary char particles was small at low char mass, the results indicate that the inherent conversion of char-N to N_2O increased for a char size range of 125-180 µm. For different char sizes, the reduction within the parent char particle could be affected [137]. Two mechanisms have been proposed for the formation of N_2O during char combustion [16]. In the homogeneous mechanism, HCN or HNCO is released during char combustion, followed by reaction of the NCO radical with NO to form N_2O (R6.12-R6.13) [237]. The heterogeneous mechanism involves the dissociative adsorption of O_2, followed by reaction of the surface complex (-CNO) with a (-CN) site (R6.14) or NO molecule (R6.15). Negligible amounts of N_2O was detected by the reaction between NO and (-CN) without the presence of O_2 [159,315,316]. This finding was additionally verified by selected reduction experiments in this study. The relative importance of R6.12-R6.13 and R6.14-R6.15 is yet unknown [136]. The larger amount of N_2O formed from combustion of high-

nitrogen chars could possibly be explained by the high local concentrations of HCN and NO, or NO, (-CN), and (-CNO). Consequently, with an increase in char-N a higher fraction of char-N is inherently converted to N_2O, which is more readily reduced over char, thereby partly explaining the decrease in char-N to NO conversion with increasing char-N content. Besides affecting NO formation, a higher char-N content could conceivably enhance the NO reduction reactivity of the chars, which was further examined.

$$N_2O + (\text{-C}) \rightarrow N_2 + (\text{-CO}) \quad \text{R6.10}$$

$$N_2O + CO \rightarrow N_2 + CO_2 \quad \text{(over char)} \quad \text{R6.11}$$

$$HCN + O, OH \rightarrow NCO + H, H_2O \quad \text{R6.12}$$

$$NCO + NO \rightarrow N_2O + CO \quad \text{R6.13}$$

$$(\text{-CN}) + (\text{-CNO}) \rightarrow N_2O + 2\,(\text{-C}) \quad \text{R6.14}$$

$$NO + (\text{-CNO}) \rightarrow N_2O + (\text{-CO}) \quad \text{R6.15}$$

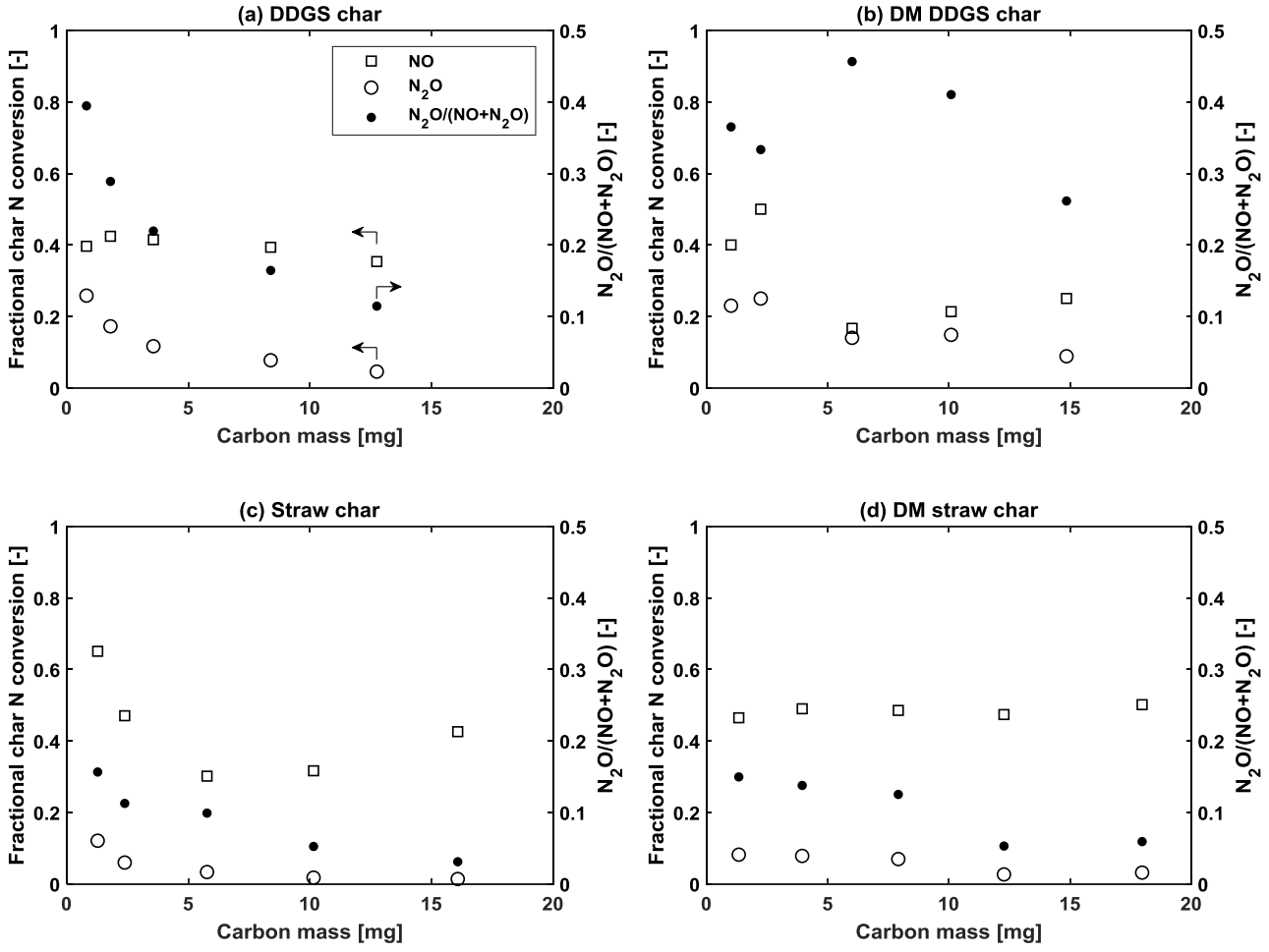

Figure 6.5: Conversion of char-N to NO and N_2O during combustion of DDGS (a), DM DDGS (b), straw (c), and DM straw (d) chars at varying mass at 800 ºC using 10vol% O_2.

6.3.3 Reduction of NO over raw and DM biomass chars

Figure 6.6 illustrates the conversion of 400 ppmv NO over the raw (a) and demineralized (b) biomass chars at 800°C. Of the raw biomass chars, the conversion of NO is high for straw, waste wood, and sunflower seed, while lower for bran, pine wood, and DDGS. The demineralized chars exhibited lower reduction in comparison to the raw chars and less discrepancy between different fuel chars. The maximum relative standard error between repetitions was determined to be 4%, demonstrated in Appendix D.2 (Figure D.1). Based on the inherent nitrogen content of the chars in Table 6.2 and the conversion of char-N to NO in Figure 6.3, it was suspected that the reduction reactivity of the demineralized chars in decreasing order would be DM DDGS, DM sunflower seed, DM bran, DM waste wood, DM straw, DM pine wood.

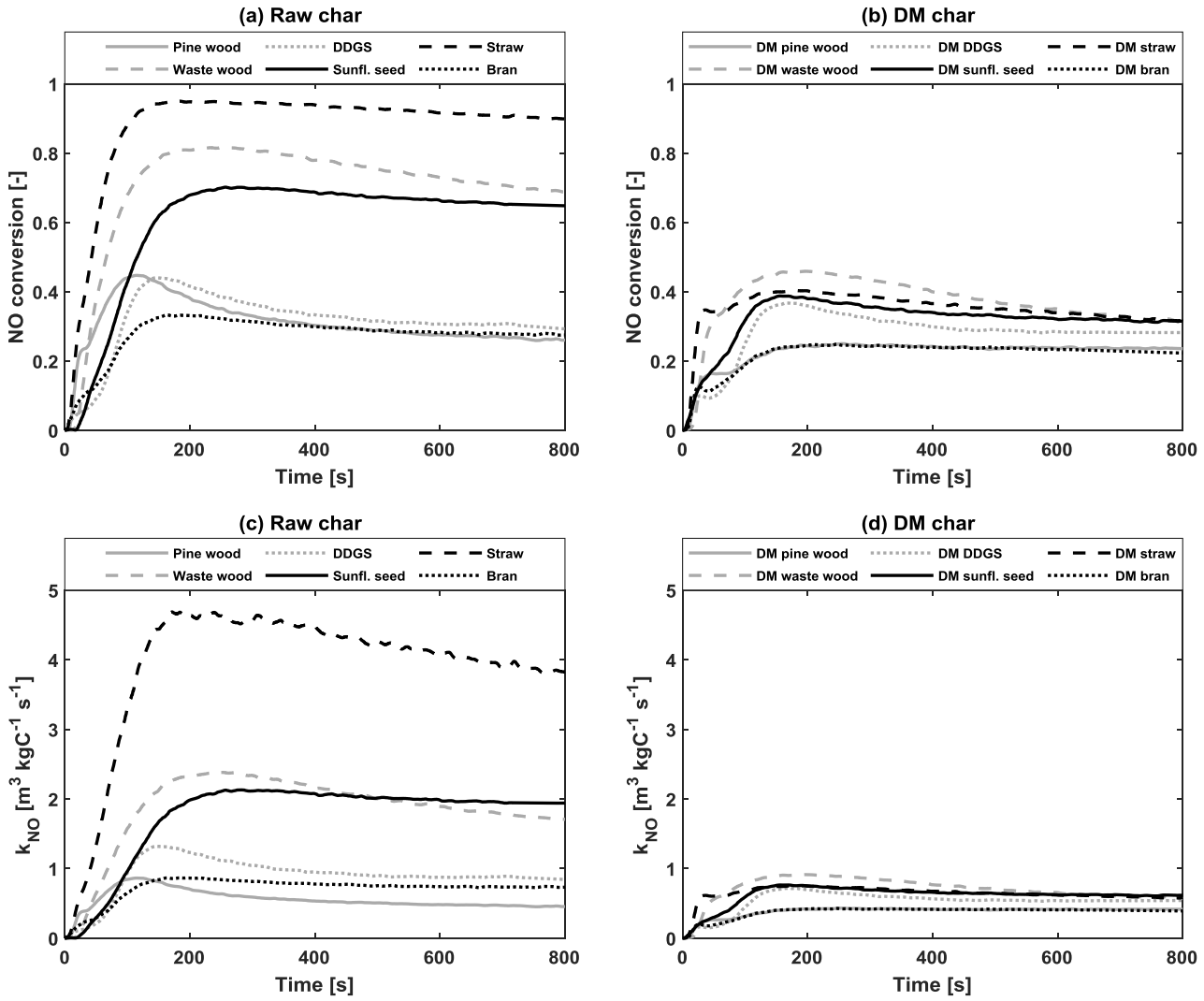

Figure 6.6: Conversion of NO over 50 mg raw (a) and DM (b) chars at 800°C using an NO inlet concentration of 400 ppmv NO. First order carbon mass based NO reduction rate constant (k_{NO}) against time for raw (c) and DM (d) chars at 800°C and 400 ppmv NO.

Figure 6.6c and d present the reactivity on a carbon mass basis of the chars at 800°C using 400 ppmv NO, calculated by Eq. 6.1. The difference in the raw chars was again more pronounced than that of

the demineralized chars. For a majority of the chars, a high transient reactivity followed by a steady state is observed. This has previously been attributed to thermal deactivation, initial accumulation of NO on the char surface, or formation of thermally stable surface oxides [16,308]. In addition, mixing and delay of the gas downstream of the reactor contribute to the duration of this phase. The straw displayed the highest reactivity towards NO, presumably due to the large potassium content. Although the potassium in bran exceeded that of the straw, their reactivities differed significantly; this is further examined in the following sections. In addition, different transient behaviors of the chars was observed. In some cases, a distinct steady state was observed, e.g. bran and pine wood, while for other chars, e.g., from straw and waste wood, the reactivity significantly decreased with time. This in turn suggests that some chars are more prone to deactivation, possibly related to the transformation of catalytic inorganic species, which needs to be further studied. To correlate the observed trends in reactivity with the physiochemical properties of the chars, the transient reactivity was defined as the maximum rate constant. This reactivity was preferred over the steady state reactivity to minimize effects from long term, high temperature exposure. However, the conclusions for the transient reactivity also apply to the steady state reactivity. In addition, the influence of temperature and inlet NO concentration on the NO reduction reactivity of the chars was investigated. The results are generally in consensus with previous studies [16,159] and can be seen in Appendix D.2 (Figure D.2 and Figure D.3). Although the reactivities were dependent on the NO inlet concentrations, the first order rate constant can be used as a qualitative comparison of the char reactivity under similar NO concentration. For modelling purposes, other rate expressions such as fractional order, concentration averaged, or mechanistic models may be used to capture the effect of NO inlet concentration.

6.3.4 Influence of initial surface area and char-N content on NO reduction

Figure 6.7 demonstrates the reactivity as a function of BET surface area. A direct correlation between the reactivity and the initial BET surface area was not observed for any of the chars. As the surface areas of the chars were prone to change during reaction either by thermal annealing or pore opening, it may not be possible to rule out the effect of surface area on the NO reduction. Therefore, the relevant or active instantaneous surface area could provide a better basis for reactivity especially for the non-catalytic, demineralized chars [317]. A previous study suggested that the reactivity of chars towards NO correlated better with the specific surface area of the meso and macropores (>50 nm) determined by mercury intrusion [163].

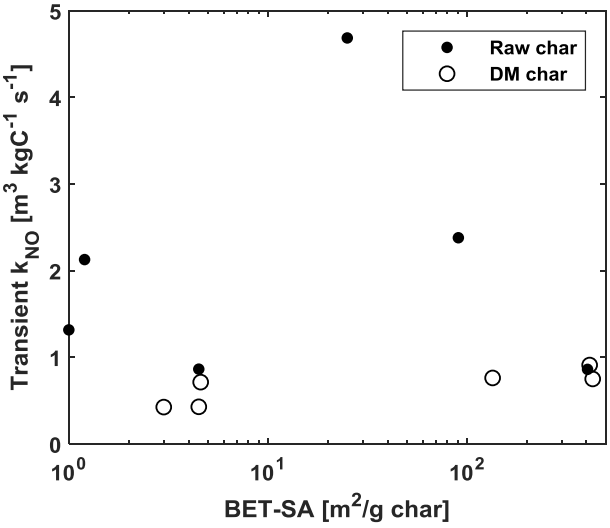

Figure 6.7: First order, transient NO reduction reactivity of DM and raw biomass chars against the BET surface area expressed in m^2/g. The rate constants were determined at 800°C using an NO inlet concentration of 400 ppmv.

Figure 6.8 demonstrates the reactivity of the demineralized and raw chars against the initial char-N content. No correlation was observed between the reactivity and the initial char-N content. In addition, no correlation was observed between the reactivity, and the product and ratio of char-N content and surface area, seen in Appendix D.3 (Figure D.4). For the raw chars, the reasoning for this is most likely due to the stronger impact of catalytic elements. In comparison, the demineralized chars showed a smaller discrepancy. The small differences in reactivity are presumably caused by distinct physical or chemical properties, all of which are prone to change during experimentation. Possible influential factors are the surface area, pore size distribution, and surface chemistry, the latter of which includes elemental population and functionality. Based on the results on the conversion of char-N to NO and the proposed reduction mechanism (R6.3-R6.9), it was hypothesized that a higher nitrogen content (-CN) would lead to a higher reduction reactivity of the demineralized chars through R6.4 and R6.5. The results here show no direct correlation between reactivity and initial char-N content. Although, the reactivities at 800°C are shown in Figure 6.7 and Figure 6.8, the conclusions drawn here also apply at 900°C. Pevida et al. [318] reported a similar observation in their study, noting that the reactivities of model chars with and without (-CN) were quite similar. Hence, they concluded that the inherent nitrogen content had a small effect on the reduction reaction. The reduction reactivity of the accumulated (-CN) sites could be different relative to the inherent (-CN) sites, thereby explaining why no correlation to the inherent char-N content was observed. The buildup of (-CN) sites during NO reduction was demonstrated in this study by the combustion of NO treated and untreated chars at 900ºC. From these experiments, it was noted that the conversion of char-N to NO systematically increased with the concentration of NO during reduction experimentation, seen in Figure 6.9. The systematic increase in conversion was most likely caused by surface enrichment of (-CN) and (-CO) species during the NO reduction. Previous studies indicated a temperature dependent buildup of both (-CN) and (-CO) species during the NO-char reaction, during which the accumulation of (-CN) was greater than (-CO) at temperatures above 750°C [154,319]. An increase in (-CN) would increase the amount of NO formed from combustion, while (-CO) could have a promoting or inhibiting effect on

the NO reduction, depending on the bond strength. In the following section, the type and importance of the inherent surface nitrogen functionality is discussed.

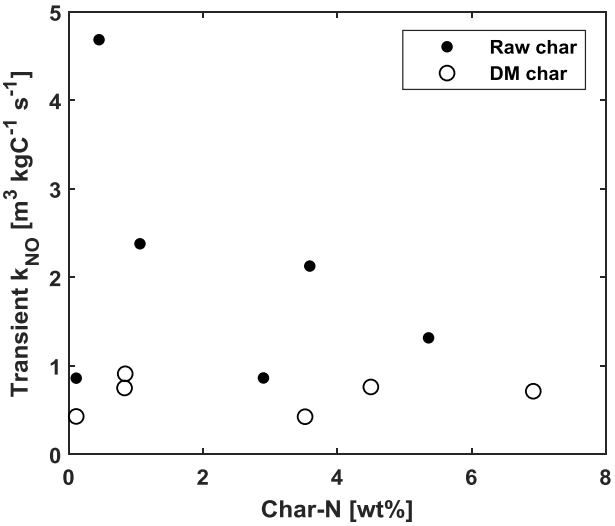

Figure 6.8: First order, transient NO reduction reactivity of DM and raw biomass chars against the initial nitrogen content. The rate constants were determined at 800°C using an NO inlet concentration of 400 ppmv.

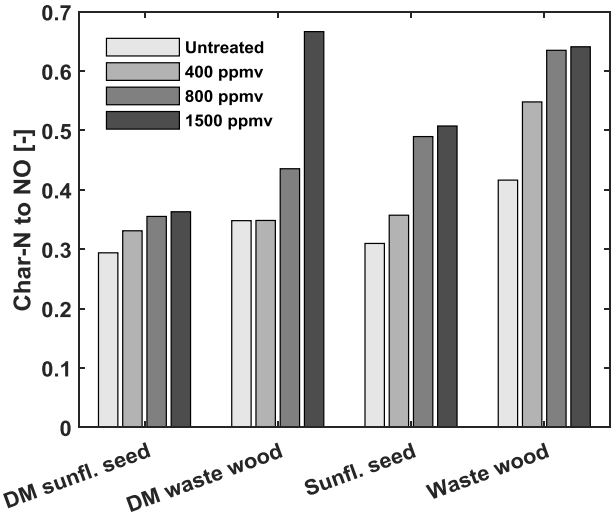

Figure 6.9: The conversion of char-N to NO (η_{NO}) from combustion of NO treated and untreated chars. $\eta_{NO} = \int_0^{t_{final}} NO\, dt / \left[\int_0^{t_{final}} CO+CO_2\, dt \cdot \left(\frac{N}{C}\right)_{char}\right]$. Conditions of combustion: 900°C, 10vol% O_2. Conditions of NO treatment: 900°C, [400;1500] ppmv NO.

6.3.5 Influence of char nitrogen and oxygen functionality on NO reduction

Figure 6.10 displays the nitrogen functionality as determined by XPS. All chars contained large amounts of pyridinic (N6), pyrrolic (N5), and quartenary (NQ) nitrogen with differences in the relative distributions of these. In general, the relative abundance of N6 and NQ in chars increases with the severity of heat treatment, i.e., temperature and holding time, due to the thermal stabilities of these compounds [109,114,115]. The results here show a small discrepancy between the demineralized samples with the only exception being DM pine wood. Notably, the nitrogen content

in this char was low, thereby raising question as to the usability of a deconvolution method for extracting functionality data, seen in Appendix D.4 (Figure D.5). Nonetheless, the results are shown here and treated critically in the correlation studies described below. In addition, the demineralization changed the nitrogen functionalities in the resulting char in the case of straw, while a lesser impact was observed for bran and sunflower seed. Previously, deashing of coals and their respective chars using stronger acids such as HCl and HF showed little or no change in the nitrogen functionality [110]. Thus, the change in nitrogen functionality for straw could therefore be due to the influence of ash forming elements on the pyrolysis, rather than the demineralization process itself.

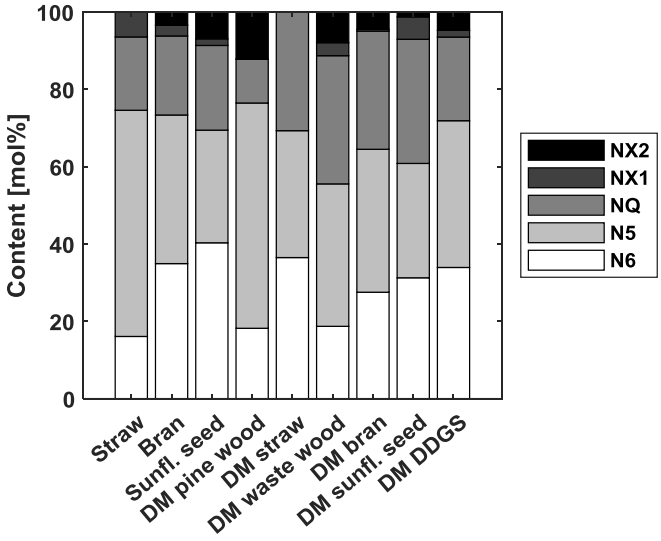

Figure 6.10: Surface nitrogen distribution as measured by XPS for selected raw and all demineralized chars.

Several studies have concluded that no correlation exists between the char-N functionality and NO emission in an oxidizing atmosphere [112,136,141,320,321]. This has primarily been attributed to the larger influence of other factors such as physical properties, catalytic effects, and NO reduction over char [136]. This study also implies a lack of correlations between the surface nitrogen/oxygen functionality and the measured NO formation and reduction properties, as shown in Appendix D.5 (Table D.3 and Table D.4, and Figure D.6 and Figure D.7). Instead the char-N content was again determining for the fractional conversion to NO and N_2O during char combustion (Appendix D.6, Figure D.8), further explained in the discussion section.

6.3.6 Influence of ash forming element content and association on NO reduction

It was previously stated that potassium, calcium, iron, magnesium, and sodium can catalyze the reduction of NO over char, most likely through reactions R6.7 and R6.8. Although, bran char contained considerably higher amounts of potassium and magnesium, and comparable amounts of calcium, iron, and sodium as straw char, the reactivity was significantly lower. A contributing factor to this could be the much larger phosphorous content in bran, which could capture the potassium and form presumably catalytically less active compounds, e.g. KPO_3 [322]. A similar reasoning would describe the observed differences between the high-phosphorous sunflower seed and DDGS chars,

and low-phosphorous straw char. To investigate this hypothesis, the surface composition of catalytic elements were examined using SEM-EDX measurements, illustrated in Figure 6.11 and Table 6.4. The straw char contained a rougher surface structure compared to the smoother bran char, thus explaining the smaller surface area of the latter. Both bran and straw char contained a large quantity of potassium on the surface, while bran char additionally showed a large phosphorous content. The ratio between these elements was approximately 1:1, thereby possibly indicating the presence of KPO_3 on the bran char surface, while the potassium in straw char was primarily present as organic-K, KCl, and to lesser extent K_2SO_4 and higher order minerals. As the magnitude of the surface areas of straw and bran char was comparable, the results here suggest that KPO_3 in bran char caused the lower NO reduction reactivity compared to straw char. However, further studies are necessary to clarify the influence of phosphorous on the NO reduction reactivity of chars.

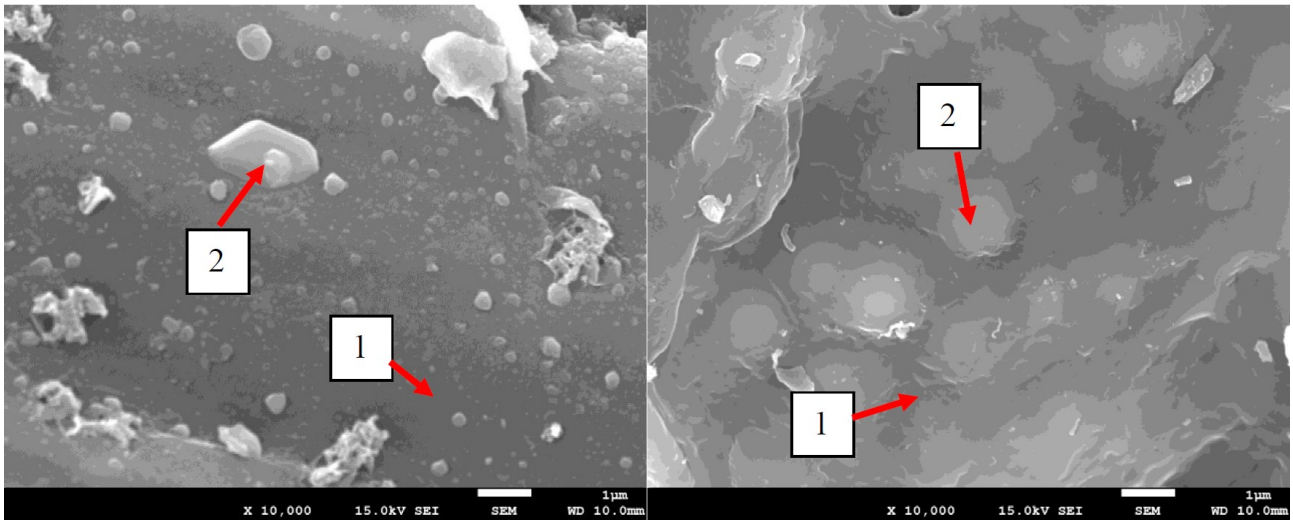

Figure 6.11: SEM-EDX measurements of straw (left) and bran (right)

Table 6.4: EDX results in connection to Figure 6.11.

	[at%]							
Char	**K**	**P**	**Mg**	**Ca**	**Fe**	**Na**	**Cl**	**S**
Straw 1	**6.7**	**1.7**	0.90	0.87	0.00	0.15	4.9	0.2
Straw 2	**3.5**	**0.1**	0.04	0.01	0.00	0.01	1.1	0.1
Bran 1	**7.0**	**7.1**	1.10	0.51	0.07	0.01	0.03	0.1
Bran 2	**4.6**	**5.8**	2.49	0.28	0.05	0.01	0.02	0.1

To determine the influence of ash forming element association in the raw straw, a sequential leaching method was employed. Table 6.5 summarizes selected chemical and physical properties of the raw and washed straw chars, along with the NO reduction reactivities. The results show that the ash content decreased with the severity of pre-treatment. Potassium, phosphorous, and sodium in the straw were predominately water soluble, while magnesium and to some extent calcium was

organically bound. In addition, the surface area increased from raw to demineralized straw char, most likely due to the formation of micropores as a consequence of pre-treatment. The contribution of water soluble, organically soluble, acid soluble, and insoluble ash forming elements to the total ash was 44.6%, 4.3%, 5.9%, and 45.2%, respectively. The presence of the ash forming elements on the surface was verified using SEM-EDX, which additionally showed little change in the morphology of the chars, seen in Appendix D.7 (Figure D.9 and Figure D.10). All char samples exhibited a rod shaped particle with a porous, tunnel-like structure. In addition, the reactivity decreased with the severity of pre-treatment. As the water soluble elements (secluded alkali or alkaline carbonates, chlorides, sulfates, and hydroxides) in straw had a large contribution to the total ash content, the influence of these on the reduction reactivity were higher. Moreover, the results show that the influence of ash forming elements dominates the reduction reactivity of the chars in comparison to other factors such as surface area and porosity.

Table 6.5: Chemical and physical properties of the sequentially leached chars. The reduction rate constants (k_{NO}) are the transient values from reduction experiments at 800°C using 400 ppmv NO.

Property	Unit	Straw char	WW straw char	OW straw char	DM straw char
C	[wt% d.b.]	71.2	78.9	71.7	82.2
H		1.18	1.36	1.29	1.53
N		0.50	0.41	0.50	0.83
O		8.42	8.93	16.9	7.04
S		0.0	0.0	0.0	0.0
Ash		18.7	10.4	9.6	8.4
K	[mg/kg d.b.]	43 642	3047	<20	76
P		2789	235	228	450
Mg		2329	2175	104	<0.2
Ca		4459	5714	1630	212
Fe		<3	92	154	77
Na		740	<120	<120	<120
BET-SA	[m^2/g]	25	296	421	430
V_P	[cm^3/g]	$2.4 \cdot 10^{-2}$	0.14	0.18	0.18
$d_{P,mean}$	[nm]	3.404	1.932/3.380	1.932/3.389	1.932/3.382
k_{NO}	[$m^3\ kgC^{-1}\ s^{-1}$]	4.7	2.1	0.97	0.75

The NO reduction reactivity of all studied chars as a function of the molar (K+Ca)/C ratio is shown in Figure 6.12. In Chapter 7, Section 7.4.2, the NO reduction reactivity of sewage sludge, RDF, and straw chars correlated well with the (Fe+K+Ca)/C molar ratio [61]. As the iron content in the biomass chars was very low, Fe was neglected in this study. The results show that the reactivities of the low-phosphorous (pine wood, waste wood, and straw) chars correlated reasonably well with the (K+Ca)/C molar ratio at two temperatures. The reactivities of the raw high-phosphorous (bran, sunflower seed, and DDGS) chars were lower than the regression line, the reasoning of which has been discussed in previous paragraphs. Demineralized chars exhibited a lower discrepancy, thereby showing a lesser impact of phosphorous.

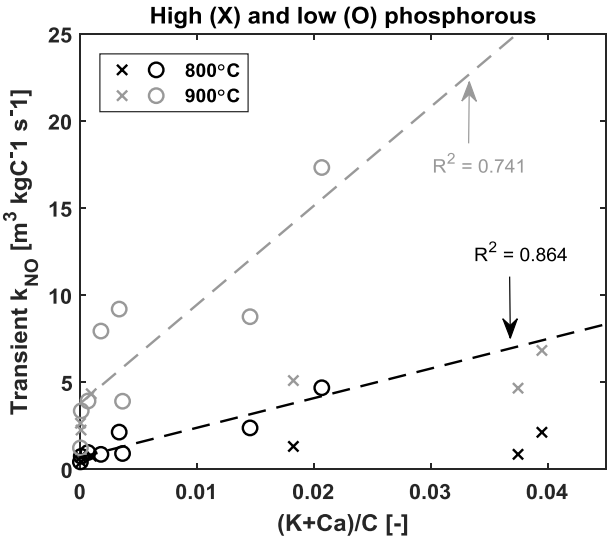

Figure 6.12: First order, transient NO reduction reactivity of all investigated chars at 800ºC and 900ºC using 400 ppmv NO against the molar ratio (K+Ca)/C. The regression lines were made solely on the low-phosphorous chars.

6.4 Discussion

Previous studies reported a decrease in the conversion of char-N to NO with an increase in char-N content, indicating that the reduction of the formed NO by char may be faster for high-nitrogen chars [155,172]. However, the conversion of char-N to NO did not correlate with the NO reduction reactivities of the chars as shown in Figure 6.13a. Combustion studies revealed a decreased formation of NO and an increased formation of N_2O with a higher char-N content at 800°C, seen in Figure 6.13b and c. During fixed bed combustion, the formed NO and N_2O could either react with the char from which it was produced or with other secondary char particles in the bed. To gain insight into the inherent conversion of char-N to NO and N_2O for a certain char particle size range, combustion experiments with varying char mass were conducted. The results revealed that the fractional conversion of char-N to N_2O increased with a decrease in char mass and an increase in char-N content. Hence, the investigated char particles inherently formed a large fraction of N_2O. This could to some extent explain the decreasing tendency of char-N to NO conversion with an increase in char-N, as the larger proportion of N_2O from combustion of high-nitrogen biomass chars is more readily reduced over char than NO. However, caution must be taken when interpolating these results obtained at 800°C to other temperatures, as the char-N conversion is temperature dependent [131]. The importance of N_2O has been shown to decrease with temperature, due to higher rates of competitive reactions and N_2O destruction [16].

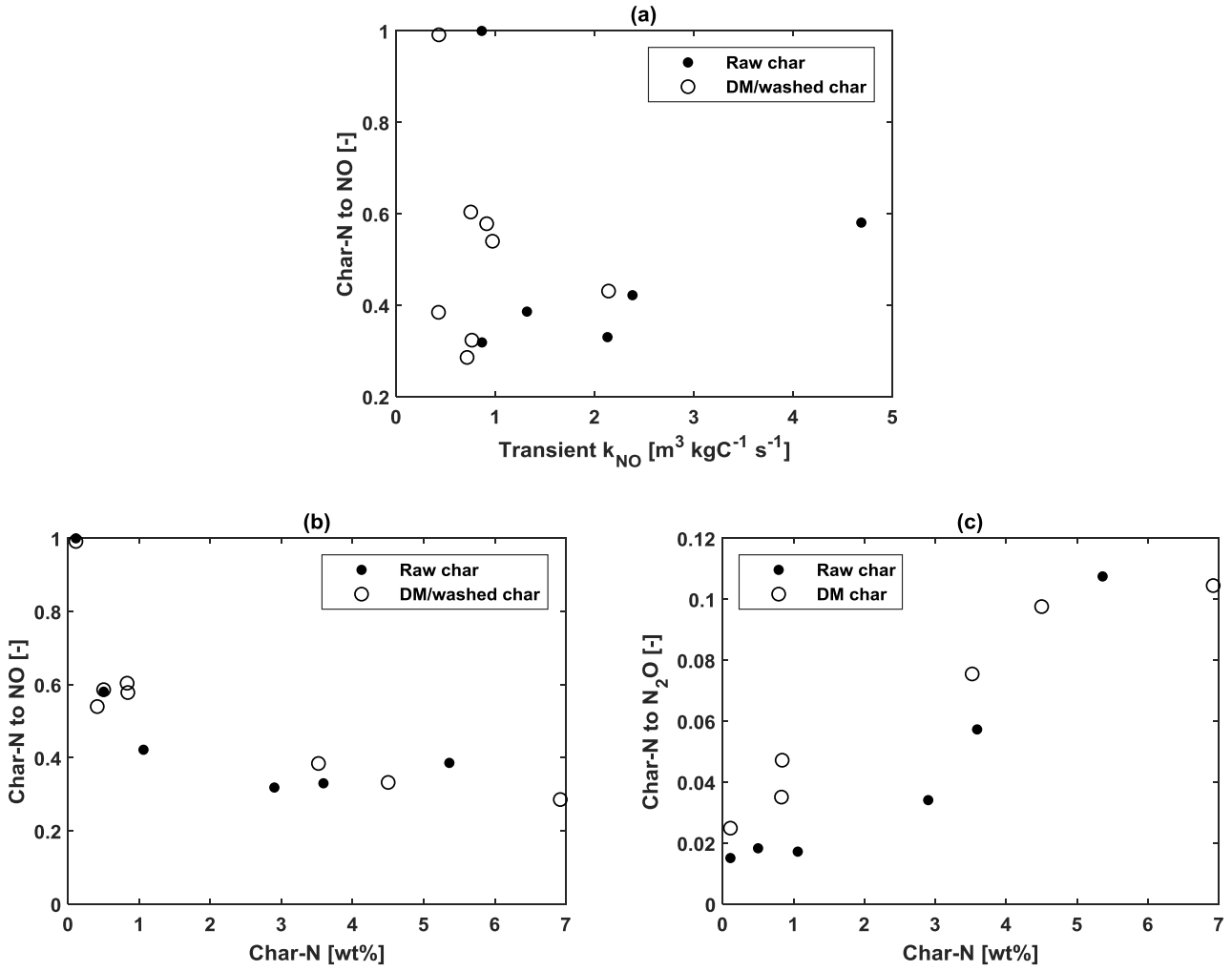

Figure 6.13: Char-N to NO conversion against the first order, transient NO reduction reactivity (a) and char-N content (b), and char-N to N_2O conversion against char-N content (c). The combustion properties were determined from 20 mg char combustion at 800°C in 10% O_2. The data for raw pine wood char has been corrected for fluctuations in the elemental analyses, i.e., set equal to 1.

While the formation of N_2O can partly explain the decreasing tendency of NO with the char-N content, additional factors could have a prominent effect. The most probable effects would be that of CO and O_2 on the NO reduction by R6.6 or R6.9, respectively. While the influence of CO on NO reduction in the inert NO reduction experiments was negligible due to the relatively low concentration, the contribution of this in a combustion atmosphere cannot be omitted. Effluent CO concentrations were around 4000 ppmv and likely much higher near the char particle surface. The local concentrations of NO in high-nitrogen chars could likewise be high, thereby increasing the relative importance of R6.6. However, additional investigations are necessary to clarify the influence of R6.6 on the overall reduction of NO from combustion. In the case of O_2, NO reduction has generally been reported to be enhanced in the presence of O_2 either by oxidative active site generation (R6.9) or activation of (-CN) [323]. Lastly, changes in surface properties and catalytic components with char conversion could have an important influence on the reactivities of the chars, which needs further study.

6.5 Conclusions

The conversion of char-N to NO during biomass char combustion decreased with an increase in the initial char-N content. As this trend did not correlate with the NO reduction reactivity of the chars, an important contributing factor may be the increased formation of N_2O with an increase in char-N content.

For NO reduction over biomass char, the reactivity was largely dominated by the association and content of ash forming minerals. The reactivities of chars containing a low content of phosphorous (pine wood, waste wood, and straw) correlated reasonably well with the (K+Ca)/C molar ratio. In comparison, the high-phosphorous (bran, DDGS, and sunflower seed) chars exhibited a lower NO reduction reactivity. A plausible explanation is that the potassium in chars with a high phosphorous content was bound in a catalytically less active form such as KPO_3. Other physical (initial surface area and porosity) and chemical (initial char-N content, and nitrogen and oxygen surface functionality and content) properties did not correlate with the NO reduction reactivity of the chars. During NO treatment, the char surface was enriched with (-CN) and/or (-CO). The accumulated (-CN) species may exhibit a different reactivity towards NO reduction compared to the inherent (-CN) sites.

7 Reactivity of sewage sludge, RDF, and straw chars towards NO

This chapter has been written in a manuscript format. A slightly modified version has been published in the peer-reviewed journal *Fuel* as,

Ulusoy B., Wu H., Lin W., Karlström O., Li S., Song W., Glarborg P., Dam-Johansen K., *Reactivity of sewage sludge, RDF, and straw chars towards NO*, Fuel 2019;236:297-305. doi: 10.1016/j.fuel.2018.08.164

Abstract: The reaction of NO with chars of sewage sludge, refuse derived fuel (RDF), and straw was investigated in a fixed bed reactor at temperatures from 800 to 900°C and NO inlet concentrations from 400 to 1500 ppmv. The effect of ash forming elements in the chars was examined by comparing the reactivity of raw and demineralized chars. Compared to straw char, the reaction rates of sewage sludge and RDF chars, at 800°C and 400 ppmv inlet NO, were an order of magnitude and a factor of six higher, respectively. The very high reactivity of the two waste chars was attributed to the catalytic effect of their large content of calcium and iron. A simple first order globalized rate expression was employed to describe the reactivity of waste chars toward NO, which predicted reasonably well the conversion of char nitrogen to NO during char combustion at 800°C in 10% O_2. A comparison with literature data revealed a higher reactivity of the waste chars towards NO compared to that of coal and biomass chars. The results in this work provide a simple and validated rate expression to simulate the waste char-NO reaction in boilers, and moreover facilitate a potential utilization of waste chars as primary or secondary measures for NO reduction.

7.1 Introduction

Waste fuels are increasingly used in utility and industrial boilers to reduce fuel costs and avoid landfilling [324]. Two widely used waste combustion technologies are fluidized bed combustion and grate-firing. In both processes, the NO primarily stems from the fuel bound nitrogen, either through volatile or char nitrogen oxidation [18], while the contribution of thermal and prompt NO is small or negligible [2,325,326]. Once formed, NO may be reduced through homogeneous reactions or by heterogeneous reduction over char [16]. The mechanism of NO formation and reduction during char combustion was described in Section 6.1, R6.1-R6.9. The reaction mechanism involves both catalytic and non-catalytic reaction steps. It indicates that larger contents of surface nitrogen and catalytic inorganic element may lead to a higher NO reduction reactivity. Waste fuels often have both high nitrogen and inorganic element content in the unreacted char. Consequently, these chars could be

expected to be very reactive towards NO reduction; however, this has to the knowledge of the authors not been examined.

The objective of the present work is to investigate the reduction of NO over sewage sludge, refuse derived fuel (RDF), and straw chars. The chars of raw and demineralized fuels were prepared in a horizontal oven and subsequently subjected to surface property and chemical composition characterization. NO reduction experiments were performed in a fixed bed reactor to investigate the reactivity of different chars towards NO. Based on the experiments, simple rate expressions that are applicable in large-scale simulations were provided for modelling the NO-char reduction reaction in combustion. Apart from providing an improved fundamental understanding of the char nitrogen to NO conversion and char-NO reduction reaction, the outcome of this study may facilitate the use of chars in NO reduction from boilers.

7.2 Experimental section

7.2.1 Materials

Two waste based fuels, sewage sludge and RDF, and one biomass, straw, were investigated. The employed demineralization (DM) and char preparation methods were described in Section 6.2.1 and 6.2.2, respectively. Notably, RDF was not demineralized due to the limited amount of available sample. Table 7.1 displays selected properties of the raw fuels. The complete ICP-OES results for the raw fuels and chars can be found in Appendix E.1 (Table E.1).

Table 7.1: Properties of the raw fuels.

	[wt% d.b.]					[mg/kg d.b.]					
Fuel	**C**	**H**	**N**	**S**	**Ash**	**K**	**P**	**Mg**	**Ca**	**Fe**	**Na**
Straw	46.9	6.0	0.56	0.12	4.2	14,000	910	960	2300	41	230
Sew. slu.	29.0	3.8	3.80	0.96	50.2	6300	34,000	4300	37,000	85,000	2400
RDF	48.7	6.6	1.16	0.28	16.4	1600	760	4440	37300	454	2000

7.2.2 Fixed bed reactor combustion and NO reduction

Char combustion and NO reduction experiments were performed in the fixed bed reactor described in Figure 6.1 in Section 6.2.3. Reduction experiments were carried out at three NO inlet concentrations [400,800,1500 ppmv] and temperatures [800,850,900 °C] using 20-50 mg char with a size of 125-180 µm to minimize mass transfer limitations and avoid issues in feeding fine particles. To extract kinetic information, the mass of sewage sludge and RDF char was reduced to avoid complete conversion of NO to N_2. Additional combustion experiments using 20 mg, 125-180 µm char were carried out at 800°C in 10% O_2. The total volumetric flow rate was 1 NL/min in both combustion and NO reduction experiments, with the balance being made up by N_2. The composition of the dry flue gas was continuously monitored by a series of on-line gas analysers (NGA2000, Fischer-

Rosemount); CO and CO_2 were measured by infrared-absorption, O_2 by a paramagnetic detector, and NO by an ultraviolet analyser. In addition, the nitrogen combustion product distribution was determined by a Fourier Transform Infrared spectrometer (FTIR) (Multigas 2030 FTIR, MKS instruments).

The influence of external and internal mass transfer limitations were assessed based on the Maer and Weisz-Prater criteria [303], respectively. The results are provided in Appendix E.1 (Table E.2) for the most reactive chars, sewage sludge and RDF. These indicate that the kinetics play a dominant role; hence, mass transport limitations were neglected in the estimation of kinetic parameters.

7.2.3 Physiochemical char properties

The carbon, hydrogen, nitrogen, and sulphur content, and inorganic element concentration of the raw fuels and chars were determined by standard CHNS and inductively coupled plasma emission spectroscopy (ICP-OES), respectively. Table 7.2 summarizes the ultimate analysis, char yield, and selected ash composition of the chars. The char yields of the demineralized fuels were lower than those of the raw fuels, as expected. Due to the large ash content, the waste chars contained a significantly lower carbon content in comparison with that of the biomass chars. Demineralization halved the ash content of the straw char, while only a small decrease was observed for sewage sludge char. Demineralization of sewage sludge removed a significant amount of calcium and to a lesser extent potassium and iron. Although dependent on the chemical association, previous studies have elucidated the catalytic importance of these elements and additionally that of sodium and magnesium in the NO-char reaction [161]. In this study, the major catalytic elements are expected to be potassium, calcium and iron.

Table 7.2: Elemental and proximate analysis of the chars.

	[wt% d.b.]						[mg/kg d.b.]					
Char	**C**	**H**	**N**	**S**	**Ash**	**Char Yield**	**K**	**P**	**Mg**	**Ca**	**Fe**	**Na**
Straw	72.38	1.42	0.45	0.029	18.7	25.8	43,642	2789	2329	4459	<3	740
Sew. slu.	17.91	0.52	1.37	0.188	79.4	56.7	5803	16,708	6745	61,579	39,697	1485
RDF	39.91	1.21	1.21	0.728	56.7	31.2	4314	1673	9778	95,688	9675	5880
DM straw	82.15	1.53	0.83	0.032	8.4	16.9	530	727	<0.2	283	<3	<120
DM sew. slu.	22.28	0.56	1.99	0.107	76.8	56.5	3090	10,614	4175	5698	33,059	603

The specific BET surface area and the mesoporosity (BJH) of the chars were determined from N_2 adsorption at its boiling point (77 K) in the p/p_0 range of 0.01-0.99. Table 7.3 shows the BET surface area, pore volume, and mean pore diameter of the chars. The demineralized and raw sewage sludge char surface areas were similar, while the RDF and straw chars displayed lower values. In comparison, demineralized straw char exhibited a high surface area and consequently pore volume; however, the volume and surface area mainly stem from micro- and some mesopores, leading to small pore diameters. Although some disagreement exists, it is widely accepted that surface area and pore structure play an important role in the NO reduction reaction [296]. While it has been difficult to

correlate the NO-char reaction rate with BET areas, incorporating the surface area associated with macro- and some mesopores (<20 nm by mercury porosimetry) yielded a better basis [16].

Table 7.3: BET surface area (SA), pore volume (V_p), and mean pore diameter ($d_{p,mean}$) of the chars. Note, demineralized straw char contained both micro- and mesopores.

Char	**SA [m^2/g]**	**V_P [cm^3/g]**	**$d_{p,mean}$ [nm]**
Straw	25.1	$2.4 \cdot 10^{-2}$	3.404
Sew. slu	66.0	$9.0 \cdot 10^{-2}$	4.856
RDF	43.2	$7.1 \cdot 10^{-2}$	3.385
DM straw	429.5	0.18	1.932/3.382
DM sew. slu.	55.8	$7.2 \cdot 10^{-2}$	4.852

7.3 NO reduction kinetics and char combustion model

The kinetic data for the NO-char reaction can be obtained from fixed bed reactor experiments under the assumption of plug flow in quasi steady state. The integral form of the design equation is shown in Eq. 7.1 for a first order rate expression.

$$-\ln(1-X_{NO}) = \frac{k_{NO} \cdot W}{V_g} \qquad \text{Eq. 7.1}$$

Here, X_{NO} (-) is the conversion of NO, k_{NO} ($m^3_{gas}\ s^{-1}\ kg\text{-}C^{-1}$) is the carbon mass based first order rate constant, W (kg-C) is the instantaneous carbon mass in the bed, and V_g (m^3_{gas}/s) is the volumetric gas flowrate. The instantaneous carbon mass was determined from the CO and CO_2 measurements during NO reduction experiments.

The conversion of char nitrogen to NO in fixed bed char combustion was investigated using a one-dimensional, transient, heterogeneous reactor model followed by a one-parameter description of the flue gas mixing in the downstream process using *n* stirred tank reactors in series. The residence time distribution methodology and results are demonstrated in Appendix E.2 (Figure E.1 and Table E.3). The main nitrogen products of char nitrogen oxidation are NO, N_2, HCN, and N_2O [16]. Based on FTIR measurements, the nitrogen combustion products by direct char oxidation were assumed to be NO with a fraction f_{NO} and N_2O with a fraction f_{N_2O}, while N_2 was formed by the reduction of NO over char, i.e. $f_{NO} + f_{N_2O} = 1$. The reduction of N_2O to N_2 over char was not examined in this work. The conservation equation for the gas and solid phase in the packed bed reactor are shown in Eq. 7.2 and 7.3, respectively [327], along with the initial and boundary conditions.

$$\frac{dC_{char}}{dt} = -\epsilon\, r_C \qquad \text{Eq. 7.2}$$

$$\frac{\delta C_i}{\delta t} = D_{ax}\, \frac{\delta C_i^2}{\delta x^2} - u_{int}\, \frac{\delta C_i}{\delta x} - r_C \qquad \text{Eq. 7.3}$$

$$C(t=0) = C_0 \text{ where } C_0 = \begin{bmatrix} C_{O_2,0} = 1.11\ \frac{mol}{m^3_{gas}} \\ C_{CO_2,0} = 0\ \frac{mol}{m^3_{gas}} \\ C_{CO,0} = 0\ \frac{mol}{m^3_{gas}} \\ C_{NO,0} = 0\ \frac{mol}{m^3_{gas}} \end{bmatrix}$$

$$C(x=0) = C_0$$

$$dC(x=h_{react}) = 0$$

Here, C_{char} ($mol/m^3_{reactor}$) is the molar concentration of carbon in the reactor, C_i (mol/m^3_{gas}) is the concentration of gas component i (i=CO, CO_2, O_2, NO), t (s) is the time, x (m) is the coordinate along the bed, ϵ (-) is the bed porosity, D_{ax} (m^2/s) is the axial dispersion coefficient, determined from the

Gunn correlation [328], u_{int} (m/s) is the interstitial gas velocity, and r_C (mol m^{-3}_{gas} s^{-1}) is the char oxidation rate.

The energy conservation equation and initial conditions for the solid phase are shown in Eq. 7.4. As the char constitutes 1% of the bed material, the energy equation was based on the silica sand. Hence, it is assumed that the temperature of the char equals that of the sand at any given time. Moreover, due to the heating elements around the reactor, the temperature of the gas phase was assumed to be constant. This assumption was validated by the thermocouple below the bed, showing a discrepancy of ±7°C. The energy equation includes effects from conductivity, convection, and char combustion. Radiation was neglected as the influence of this on the overall heat transfer was estimated to be around 10%.

$$C_{sand}\, C_{p,sand}\, \frac{\delta T_{sand}}{\delta t} = k_{eff}\, \frac{\delta T^2_{sand}}{\delta x^2} + h\, S\, \left(T_{gas}-T_{sand}\right) + \epsilon\, \Delta H_R\, r_C \qquad \text{Eq. 7.4}$$

$$T_{sand}(t=0) = T_0 \text{ where } T_0 = 298 \text{ K}$$

$$T_{sand}(x=0) = T_{gas,0} \text{ where } T_{gas,0} = 1073 \text{ K}$$

$$dT_{sand}(x=h_{react}) = 0$$

Here, C_{sand} (mol/$m^3_{reactor}$) is the molar concentration of sand in the reactor, C_p (kJ mol^{-1} K^{-1}) is the specific heat capacity of sand, T_{sand} (K) is the sand temperature, k_{eff} (kJ m^{-1} s^{-1} K^{-1}) is the effective thermal conductivity determined from [329], h (kJ m^{-2} s^{-1} K^{-1}) is the gas-solid heat transfer coefficient, S (m^2/m^3) is the volumetric solid surface area, and ΔH_R is the enthalpy of reaction between O_2 and char to form CO (-110.5 kJ/mol) and CO_2 (-396.6 kJ/mol). The fraction of CO_2 formed from char combustion was determined from the experimentally obtained concentration profiles. For straw, sewage sludge, and RDF chars, this parameter was set at 0.99, 0.95, and 0.97, respectively.

The char combustion rate (r_C) was simplified to an expression first order in oxygen and char concentration, Eq. 7.5. The formation of NO ($r_{NO,formed}$) was assumed proportional to r_C with the proportionality factor being the product of f_{NO} and the molar ratio between nitrogen and carbon in the char $\left(\frac{y_N}{y_C}\right)$, Eq. 7.6. The reduction of NO ($r_{NO,reduced}$) was determined from the experimentally obtained reduction rate constant, Eq. 7.7. The net formation of NO was ultimately calculated by the difference in formation and reduction, Eq. 7.8.

$$r_C = k_C \cdot C_{Char} \cdot C_{O_2}, \text{ where } k_C = A_C \cdot \exp(-E_{a,C}/R/T) \; [=] \; \frac{m^3_{reactor}}{mol\ s} \qquad \text{Eq. 7.5}$$

$$r_{NO,formed} = f_{NO}\, \frac{y_N}{y_C}\, r_C \; [=] \; \frac{mol}{m^3_{gas}\ s} \qquad \text{Eq. 7.6}$$

$$r_{NO,reduced} = k_{NO}\, C_{Char}\, C_{NO} \; [=] \; \frac{mol}{m^3_{gas}\ s} \qquad \text{Eq. 7.7}$$

$$r_{NO,net} = r_{NO,formed} - r_{NO,reduced} \qquad \text{Eq. 7.8}$$

To describe the dispersion downstream to the reactor, *n* stirred tank reactors in series were assumed. The number of reactors in series was determined from residence time distribution measurements. For each tank, the mass conservation equation assuming no reaction is shown in Eq. 7.9.

$$\frac{dC_i}{dt} = \frac{1}{\tau}\left(C_{i,in} - C_{i,out}\right) \qquad \text{Eq. 7.9}$$

Here, τ (s) denotes the residence time in one tank. The coupled differential equations were solved by discretizing in space using a central finite difference approximation followed by the solution of the coupled ordinary differential equations using a stiff ODE solver in MatLab. Figure 7.1 illustrates the steps in the combustion model. The values of the combustion parameters A_C and $E_{a,C}$ were fitted the experimentally obtained CO_2 and O_2 curves using a Maximum Likelihood Estimate (MLE) function following the previous work of Sin and Gernaey [330]. Subsequently, the NO and CO profiles were calculated based on the char combustion kinetics. The experimentally obtained reduction rate constant was used to describe the reduction of NO over char.

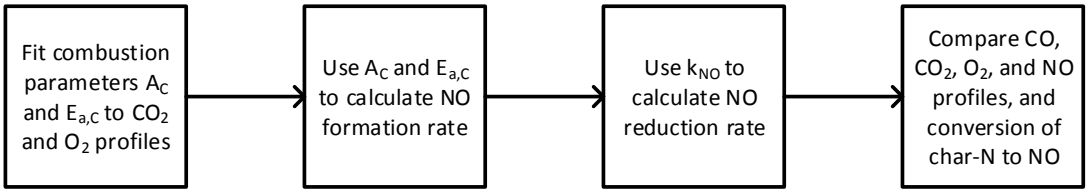

Figure 7.1: Schematic representation of the combustion model.

Since the optimization problem is non-convex, the MLE function depends on the starting values of the parameters to be optimized. The initial guess of the parameters were based on the previous study of Karlström et al. [331]. In the case of sewage sludge char combustion, a strong correlation was noted between the two kinetic parameters. This resulted in a large standard deviation, causing the lower limit of the pre-exponential factor to be negative, i.e. non-unique estimate of this parameters. Consequently, the activation energy was specified as a parameter and only the pre-exponential factor was fit to the data for sewage sludge char combustion. To get unique estimates of the activation energy and pre-exponential factor, additional experiments must be planned, e.g. combustion at different temperatures. An example of concentration plots from combustion modelling is illustrated in Appendix E.3 (Figure E.2).

$$A_{C,initial} = 100\ \frac{m^3_{react}}{mol\ s} \qquad E_{a,C,initial} = 50\text{-}60\ kJ/mol$$

7.4 Results and discussion

7.4.1 Reduction of NO over char

Figure 7.2a illustrates the conversion of 400 ppmv NO over 50 mg char at 800°C, while Figure 7.2b depicts the corresponding transient first order rate constant of the chars. The results in Figure 7.2a demonstrate that an almost complete reduction of NO was achieved for the raw sewage sludge and RDF chars, while the straw char showed a somewhat lower reduction of NO. The NO reduction was lower for the demineralized fuel chars as compared to the raw fuel chars. The results of Figure 7.2b indicate that the reactivities of the waste chars were significantly higher than those of the straw char. The NO reduction rate of the sewage sludge char was approximately 12 times that of the straw char, while the RDF char exhibited half the reactivity of the sewage sludge char and six times that of the straw char. From Table 7.2, it is observed that the straw char contained the highest amount of potassium, which is likely to be the most active element in catalyzing NO reduction [295]. In comparison, the waste based chars exhibited a larger content of iron, calcium, and sodium, all of which may catalyze the NO reduction and thereby compensate for the lower potassium content compared to straw char. In addition, although the conversion of NO of the demineralized sewage sludge char was lower than that of straw char in Figure 7.2a, it is suggested based on Figure 7.2b that the carbon in the former is more reactive than the latter, probably due to the larger content of iron. The demineralized straw char, showing the highest surface area and pore volume among the chars, displayed the lowest reactivity, as very small amounts of catalytic elements were present in the structure. Moreover, this char exhibited the lowest average pore diameter, which could be an additional contributing factor for the low reactivity. In several chars, a transient kinetic behavior followed by a steady state reduction rate was observed, similar to the observations of Garijo et al. [308,309] and Zhao et al. [143]. This behavior is further discussed in the following sections. The repeatability of the experimental results was examined, showing a relative standard error of maximum 4%, as seen in Appendix E.4 (Figure E.3).

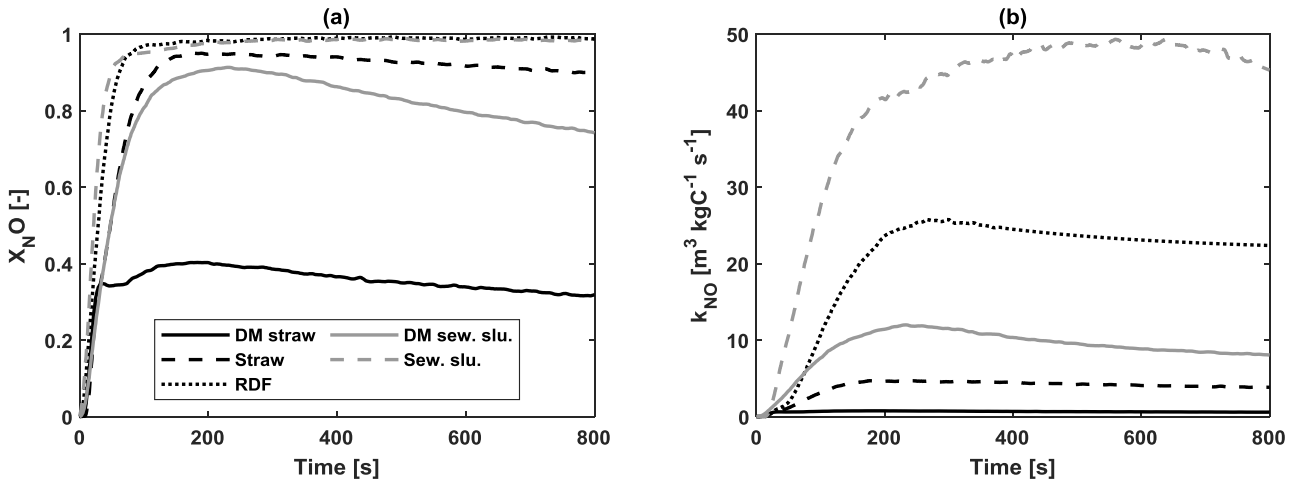

Figure 7.2: Conversion of NO (X_{NO}) (50 mg char) (a) and first order carbon mass based reaction rate constant (k_{NO}) for the NO reduction (b) versus reaction time for the five different chars at 800°C using an inlet NO concentration of 400 ppmv NO.

7.4.2 Effect of ash forming elements on reactivity

Figure 7.3 presents the maximum reduction rate constant at 800°C and 900°C using 400 ppmv NO as a function of the molar ratio of (Fe+Ca+K)/C (a) and the BET surface area (b) in the unreacted chars. Iron, calcium, and potassium may influence the catalytic activity through different pathways. However, for simplicity, the catalytic term was defined as the molar ratio (Fe+Ca+K)/C. The maximum rate constant was chosen to describe the initial reactivity, since the preliminary increase in reactivity was attributed to particle heating and NO accumulation, and therefore negligible deactivation was assumed prior to this point. The initial rate constant has typically been used in modelling of NO in fast char combustion [16]. The results indicate that the initial reactivity is proportional to the molar ratio of (Fe+Ca+K)/C in the unreacted chars. A higher content of calcium, iron, and potassium would conceivably enhance R6.7 and R6.8, thereby facilitating the NO reduction. Given the variable chemical and physical properties of the waste based fuels, this observation provides a method of classifying the fuel chars in terms of their reactivity towards NO. Although the molar ratio could be used as a basis to describe the reactivity prior to deactivation of the chars, the long-term reactivity cannot purely be based on this due to the complicated transient char structure change and ash transformation. Moreover, there appears to be no direct correlation between the surface area and reactivity even when neglecting DM straw, presumably due to the significant effect of ash forming elements and narrow surface area sample size [296].

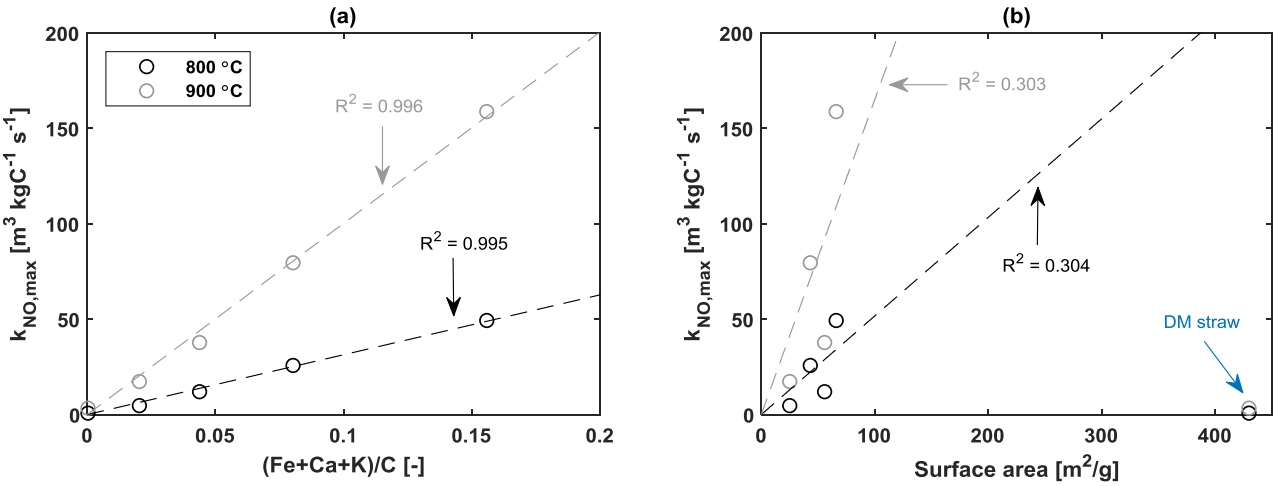

Figure 7.3: Maximum first order reaction rate constant ($k_{NO,max}$) of the examined chars against the initial concentration of iron, calcium, and potassium expressed in mol element per mol carbon (a) and the BET surface area. (b) The rate constant was determined from reduction experimentation at 800°C and 400 ppmv NO.

7.4.3 Influence of temperature and NO inlet concentration

Figure 7.4 depicts $k_{NO,max}$ against 1/T at varying NO inlet concentrations for sewage sludge and RDF chars. In agreement with previous studies, the reactivity increased with temperature [332]. The results show that the rate constant depends on the NO inlet concentration, thereby indicating a fractional dependence on the NO concentration. However, a reliable estimate of the reaction order and rate constant could not be made using a global fractional order rate expression, as the reaction order was strongly dependent on the temperature and carbon conversion. More complex models are necessary

to fully describe the char reactivity, as discussed further in the following sections. However, for simplicity and as a first attempt to provide a rate expression for NO reaction with sewage sludge/RDF char in large-scale simulations, e.g. in CFD modelling [333], concentration averaged rate constants were derived using the results shown in Figure 7.4. For the averaged $k_{NO,max}$, the recommended kinetic parameters to be used for modelling purposes are summarized in Table 7.4.

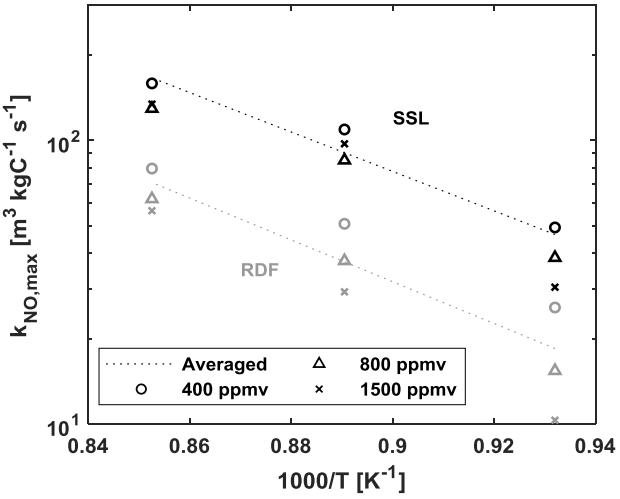

Figure 7.4: Arrhenius plot of the maximum carbon mass based reaction rate constant ($k_{NO,max}$) for NO reduction over RDF and sewage sludge chars at varying NO inlet concentrations. The symbols in black and grey refer to sewage sludge and RDF chars, respectively, while the dotted lines represent the averaged rate constants.

Table 7.4: Pre-exponential factor A (m^3 kgC^{-1} s^{-1}) and activation energy E_a (kJ/mol) for reduction of NO over char.

Char	A	E_a
Straw	$3.91 \cdot 10^7$	145
Sew. slu.	$1.39 \cdot 10^8$	133
Refuse derived fuel (RDF)	$1.35 \cdot 10^8$	141

7.4.4 Formation and reduction of NO in char combustion

The form of the char nitrogen combustion product distribution, determined by FTIR, is illustrated in Figure 7.5. As it was not possible to measure N_2 and HCN, these were calculated as a rest fraction based on the material balance. The presence of HCN during char combustion has previously been reported [136,195]. However, unless radical quenching compounds such as iodine are added, the amount is often small in a combustion atmosphere [312]. Consequently, the rest fraction was presumed to consist mainly of N_2. The results show that the majority of the emitted nitrogen was in the form of NO and N_2 with a smaller quantity of N_2O. In addition, no significant amounts of NH_3, HNCO, and NO_2 were detected. It has previously been suggested that the fractional conversion of char nitrogen to N_2O increased with the char nitrogen content or the NO concentration [131]. In agreement with this, the straw, RDF, and sewage sludge chars exhibited a fractional conversion to

N_2O of 1%, 2%, and 7%, respectively. The formation mechanisms of N_2O during char combustion were suggested to be by direct char nitrogen oxidation (R7.1 and R7.3), reaction between char nitrogen and NO (R7.4, R7.2 and R7.3, or direct reaction between NO and (-CN) [323]), or release and subsequent homogeneous oxidation of HCN. In general, the reaction between (-CN) and NO can be disregarded [16], since no N_2O was detected without the presence of oxygen [159,315,316]. This was additionally verified in this study, where the products of NO reduction over char were investigated using the FTIR, showing that no significant amounts of N_2O, HNCO, NH_3, and NO_2 were formed. The relative importance of the homogeneous and heterogeneous mechanisms of N_2O formation is as of yet unknown [136]. In the combustion model, N_2O was presumed to form primarily by direct oxidation of char nitrogen, with a fractional conversion f_{N_2O} equal to that measured by FTIR. This would lead to an overestimation of the actual NO fractional conversion f_{NO}, as N_2O is believed to decompose over the char at an even faster rate than NO reduction [314].

$$O_2 + (\text{-C}) + (\text{-CN}) \rightarrow (\text{-CO}) + (\text{-CNO}) \quad \text{R7.1}$$

$$NO + (\text{-C}) \rightarrow (\text{-CNO}) \quad \text{R7.2}$$

$$(\text{-CN}) + (\text{-CNO}) \rightarrow N_2O + 2\,(\text{-C}) \quad \text{R7.3}$$

$$NO + (\text{-CNO}) \rightarrow N_2O + (\text{-CO}) \quad \text{R7.4}$$

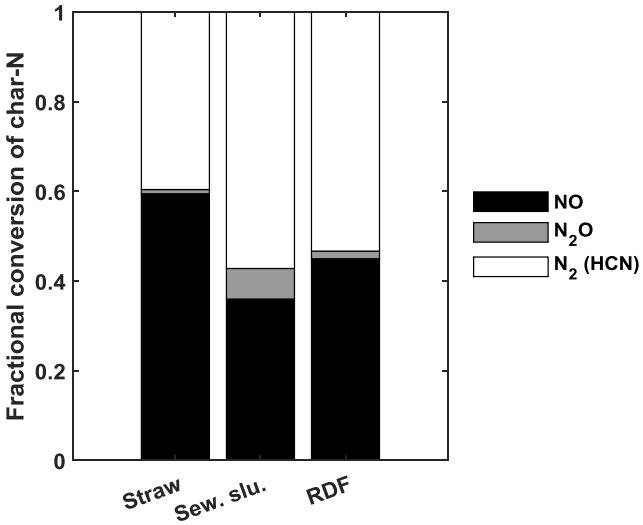

Figure 7.5: Nitrogen product distribution from char combustion at 800°C in 10% O_2. NH_3, HNCO, and NO_2 were not detected in significant quantities and therefore not shown here.

Figure 7.6 presents the experimental and modelled NO combustion selectivity (a) and concentration profiles (b) from fixed bed char combustion at 800°C in 10 vol% O_2. Although the nitrogen content in the RDF and sewage sludge chars were higher than in straw char, the experimental selectivity to form NO was lower. The concentration averaged $k_{NO,max}$ were used in the computations since the time for complete combustion of the chars was short, i.e., 20-30 s. A reasonable prediction of the conversion of char nitrogen to NO was achieved for the straw and RDF chars, while the conversion of sewage sludge char nitrogen to NO was slightly overestimated. This was additionally reflected in the concentration plots, wherein the qualitative trend of the data was well described with minor

quantitative differences. In the case of sewage sludge and RDF char, a slight overestimation of the NO release near the maximum was observed. As the formation of by-products were not the cause between model and experiment, the discrepancies were apparently a consequence of NO reduction by CO over char and ash (R6.6) [334] or reactivity enhancement in the presence of O_2 [143]. In addition to this, the experimental release of NO in RDF char was higher than predicted at later stages in the combustion. This could be caused by the assumption that the NO formation is proportional to the carbon burnout. Although, this is a common simplification in several char-NO modelling studies [156,332,335], the proportionality between the rates for coal chars is not always prominent [16], especially at temperatures around 600°C [136]. For the purposes of this study, the simplified combustion model provided reasonable predictions of the NO concentration profile and the conversion of char nitrogen to NO during combustion of straw and RDF chars. For the sewage sludge chars, the reduction rate constant was two times lower in an inert atmosphere, as compared to the combustion atmosphere. The results here indicate that the averaged rate constants could be useful in predicting the reactivity of the raw chars towards NO, and therefore potentially be implemented in large-scale simulations. However, it should be taken into consideration that the results provided here are based on a limited range of operating conditions as well as on several assumptions, which would require further evaluation. Some of these are discussed in the following section.

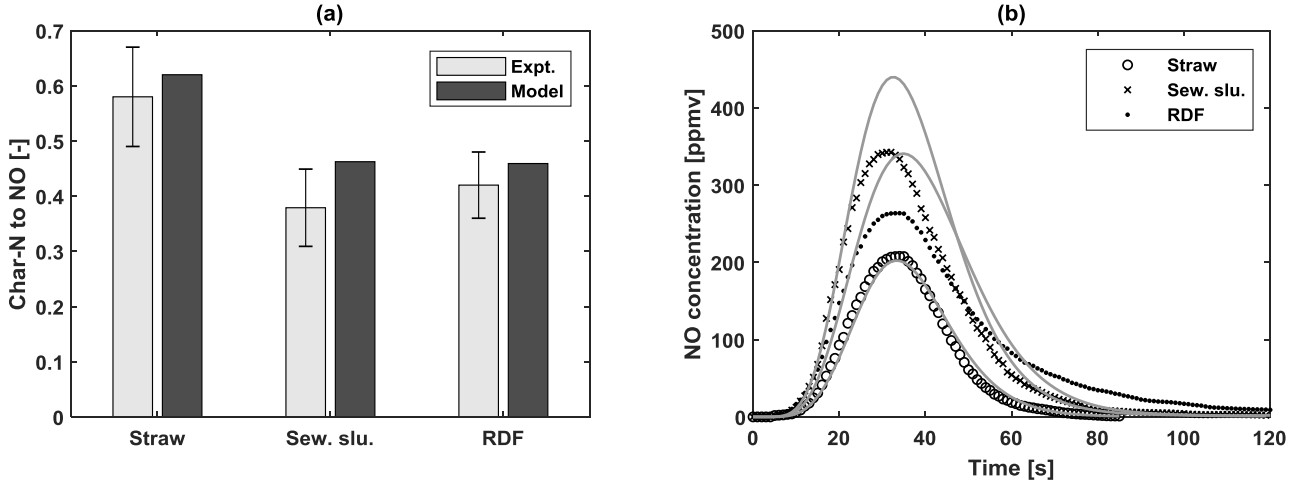

Figure 7.6: Experimental and predicted NO selectivity (a) and concentration profiles (b) from the combustion raw chars at 800°C in 10vol% O_2. The error bars depict the repeatability of the experiments. The predictions were made using a concentration averaged first order reaction rate in the combustion model presented in Eq. 7.2-7.9.

7.4.5 Assessment of rate expression

Figure 7.7 illustrates the first order rate constant against the reaction time (a) and carbon conversion (b) for sewage sludge, RDF, and straw chars. Unless otherwise stated in the legend, the data are extracted from the 900°C and 1500 ppmv NO experiments. In Figure 7.7a, all chars exhibited a maximum reactivity followed by a steady decline, the slope of which differed depending on temperature and NO inlet concentration. It became obvious that the reactivity decrease was not caused by carbon depletion, as illustrated in Figure 7.7b. Possible explanations for the declining reactivity are deactivation due to a long char residence time, formation of thermally stable oxides, and change in carbon active sites [16,308]. As thermal annealing is expectedly of smaller importance at the investigated temperatures, the dominating deactivation mechanism from long char residence times may be caused by transformation of catalytic ash species, e.g. evaporation of potassium or formation of possibly less-catalytic silicates of calcium and iron. Additionally, the production of surface complexes could lead to a blockage of the pores or active sites, thereby inhibiting reactions R6.8 and R6.9, wherein the catalytic site is regenerated and a new carbon site is formed. Further, the internal surface area may increase or decrease during carbon conversion, thus influencing the availability and number of active sites for NO reduction. To capture the effects of NO concentration and carbon conversion, fractional order and Random Pore Model (RPM) [336] rate expressions were employed; however, none of these yielded obvious advantages in comparison with the simple first order equation, as seen in Appendix E.5 (Figure E.4). In future work, a more thorough understanding of the deactivation mechanism, i.e. change in surface structure and ash forming element content, as a function of time and carbon conversion is needed to describe the reduction reactivity of waste chars.

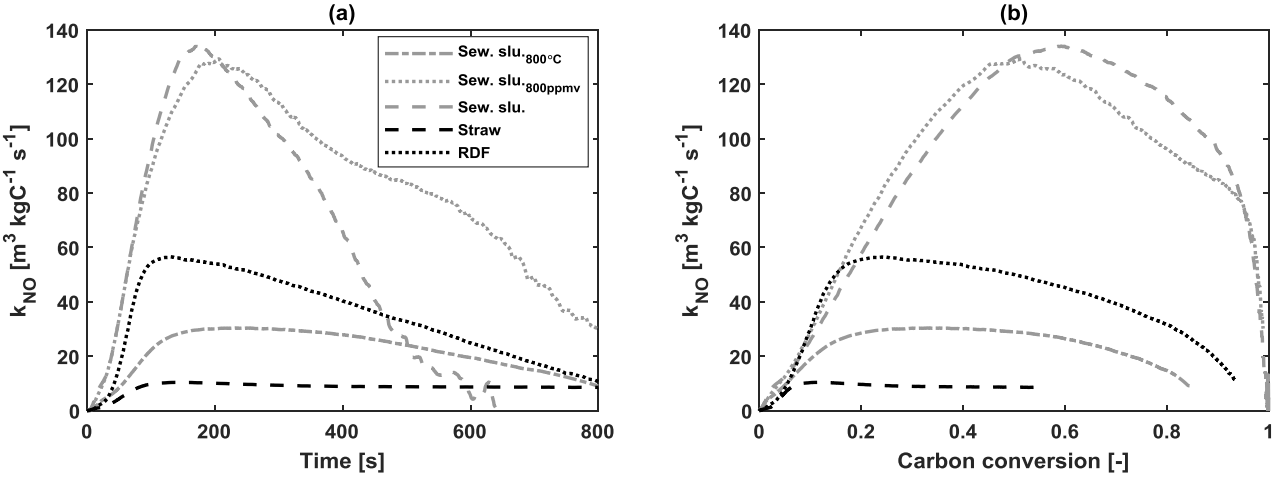

Figure 7.7: First order carbon mass based rate constant (k_{NO}) versus time on stream (a) and carbon conversion (b) at 900°C and 1500 ppmv NO. Additional data for sewage sludge from 900°C and 800 ppmv NO, and 800°C and 1500 ppmv NO.

7.4.6 Comparison of reactivity with literature data

Figure 7.8 compares the obtained reaction rates with selected literature values. The results indicate that the waste chars in general exhibited a higher reactivity than biomass chars and significantly higher than the rate constant recommended by Levy et al. [304] for coal char, the default choice for char + NO in ANSYS Fluent 18.0. Although the chars employed in this study were to some extent deactivated by the pyrolysis in the horizontal oven, the obtained rate of sewage sludge char was higher than and the RDF char comparable to that of bark and straw char reported by Zhao et al. [143], wherein the pyrolysis time was minimized and oxygen was introduced to enhance the kinetics. Similarly, the reactivity of the waste chars exceeded the rates reported by Garijo et al. [308], who performed in-situ pyrolysis to minimize the thermal deactivation.

The results of the present study provide an indication of the potential utilization of waste char in the reduction of NO in thermal conversion processes. This could possibly be by primary measures if the fuel and air feeding is controlled in such a way that the more reactive chars are present at reducing conditions within the boiler or through secondary techniques, if the char is employed subsequent to the combustion chamber, e.g. char bed or direct injection to the cyclone.

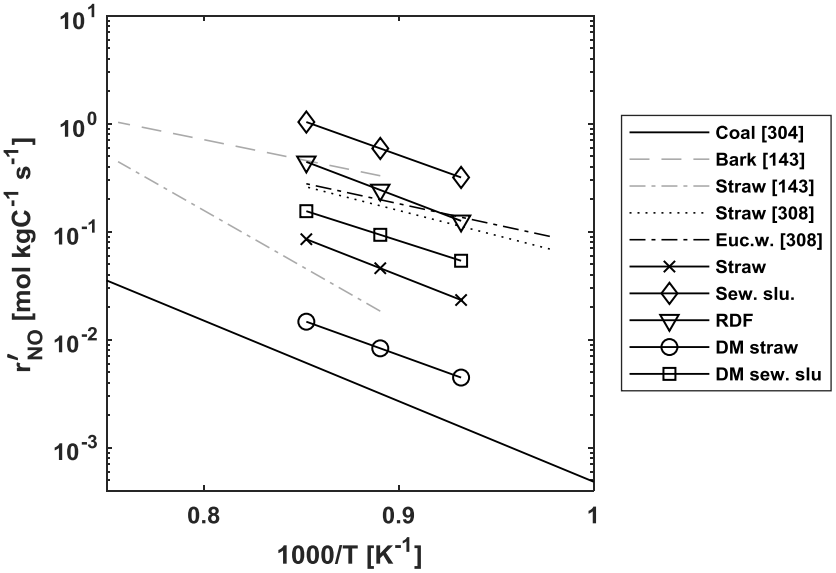

Figure 7.8: Comparison of carbon mass based NO reduction rates (r'_{NO}) obtained in this work with that from other studies [143,304,308]. The assumed properties and conditions were 100 m^2/g, 1.2 atm and NO inlet concentration of 500 ppmv.

Additionally, simple globalized rates are useful in Computational Fluid Dynamic (CFD) simulations [333], since more detailed schemes require extensive computational requirements. Consequently, the obtained concentration-averaged first order kinetic data can be used in modelling studies to evaluate pollutant formation from waste combustion, where interaction between waste char and NO is expected to be prominent, i.e. in fluidized bed combustors.

7.5 Conclusions

The reactivities of sewage sludge, refuse derived fuel (RDF), and straw chars towards NO were investigated in a fixed bed reactor at temperatures between 800 and 900°C using NO inlet concentrations from 400 to 1500 ppmv. On a carbon mass basis, the reactivities of sewage sludge and RDF chars were one order of magnitude and six-fold higher than that of straw char, respectively. A demineralization study indicated that the high reactivity could be attributed primarily to the high content of calcium and iron in the waste chars. The initial reactivities correlated well with the (Ca+K+Fe)/C molar ratio of the unreacted chars, implying that calcium, potassium, and iron played an important role in char reactivity towards NO.

During combustion of straw, RDF, and sewage sludge chars at 800°C in 10% O_2 in the fixed bed reactor, the char nitrogen was primarily converted to NO and N_2, and to a lesser extent N_2O (<7%). A mathematical model based on a first order reaction rate expression for NO reduction over char was able to provide a reasonable prediction of the conversion of char nitrogen to NO in the combustion experiments.

The high reactivity of waste chars towards NO indicates a potential utilization of the chars in the reduction of NO emission from combustion systems. Moreover, the simplified, concentration averaged, first order rate expression for NO reduction over straw, RDF, and sewage sludge chars can be implemented in large scale simulations of combustion plants.

8 Concluding remarks and Future work

8.1 Summary of conclusions

Chapter 2 provides an overview of the nitrogen conversion in fluidized bed combustion of biomass. The mechanisms of NO_X and N_2O formation and reduction from combustion, along with the influence of fuel properties and operating conditions on NO_X and N_2O emissions in fluidized bed combustion were reviewed. In addition, countermeasures for NO_X reduction from combustion were described.

Chapter 3 presents the experimental results on NO_X and N_2O emission from continuous fluidized bed mono- and co-combustion of biomass (pine wood, beech wood, straw, sunflower husk, sewage sludge, and sunflower seed) at air staged and un-staged conditions. The observed trends were explained based on effluent and local concentration data. From this work, the following conclusions can be drawn:

- The fuel-N to NO conversion decreased with an increase in fuel-N content, attributed to the larger amount of nitrogen species (e.g. NH_3) released with the volatiles thereby facilitating thermal $DeNO_X$ reactions.
- Based on the effluent data, straw-sewage sludge co-combustion exhibited a synergy effect, while the NO emission from straw-sunflower husk and straw-sunflower seed co-combustion were additive. The higher NO emission during straw-sewage sludge co-combustion was caused by the catalytic effect of sewage sludge ash on the oxidation of NH_3 and possibly HCN to NO.
- The catalytic effect of sewage sludge ash on NO forming reactions during straw combustion increased with a lower ash preparation temperature and a better mixing of the ash with straw. This was attributed to the higher surface area of the low temperature ash and possibly also to the differences in the crystalline structure.
- The mechanism of the interaction in straw-sewage sludge co-combustion was elucidated by measuring the NO reduction potential and local gas composition in the reactor. At a low ash content of 2-25 g, the NH_3 released from sewage sludge facilitated thermal $DeNO_X$ reactions, resulting in low NO emission. At later stages, the oxidation of NH_3 catalyzed by ash reduced the NO reduction potential in the reactor and increased NO emission.
- In straw-sunflower seed co-combustion, local concentration measurements indicated a synergy effect of the nitrogen chemistry, which was otherwise hidden in the effluent data. The

effluent NO concentration during co-combustion was approximated well by the weighted averages from pure straw and sunflower seed combustion, whereas the NH_3 and NO concentrations near the bed were significantly higher than the weighted values.

- Air-staging was an effective way of reducing NO emission from mono- and co-combustion. The influence of sewage sludge ash on the NO emission from straw-sewage sludge co-combustion was less pronounced at air staged conditions, due to the lower importance of NO forming reactions in the reducing zone, i.e. near the bed.

Chapter 4 presents an experimental study on the influence of fuel properties and operating conditions on NO_X emissions during fluidized bed combustion. Batch combustion experiments of biomass (pine wood, beech wood, straw, sunflower husk, sewage sludge, and sunflower seed) in a size range from 0.5-4 mm were conducted to investigate the relative contribution of volatile- and char-NO. To elucidate the influence of ash forming elements, pine wood, straw, washed straw, and potassium (KCl, KOH, K_2CO_3) doped pine wood and washed straw were continuously combusted in a fluidized bed reactor. In addition, the influence of air staging, temperature, type of bed material, and gas phase composition on NO_X emissions was investigated. The main conclusions from this investigation are:

- The fuel-N to NO conversion decreased with an increase in fuel-N content during batch combustion of biomass particles with size ranges from 0.5-4 mm.
- Volatile-NO was generally the main contributor to the total NO during batch combustion. However, char-NO may be important as well; in the case of beech wood, up to 55% of the NO was released during char combustion.
- Compared to raw straw, the fuel-N to NO conversion was higher and the CO emission was lower during washed straw combustion. KCl, K_2CO_3, and KOH doping washed straw increased CO emission. KCl and KOH doping of washed straw decreased the fuel-N to NO conversion, while K_2CO_3 had a negligible influence. KCl doping of pine wood increased CO emission, while having a negligible effect on the fuel-N to NO conversion. The increased CO and decreased NO emissions by KCl addition were more pronounced at air staged conditions (primary to total air ratio (λ_1/λ) of 0.04) compared to un-staged ($\lambda_1/\lambda = 1$) combustion, related to the radical recombination effect of KCl.
- The NO emission and fuel-N to NO conversion exhibited minima for λ_1/λ values between 0.5-0.75 during straw and sunflower husk combustion.
- The fuel-N to NO conversion increased slightly with increasing temperature for straw combustion. For KCl-doped washed straw, the fuel-N to NO conversion first increased then levelled off with increasing temperature, explained by the opposite trend in the CO emission.
- The fuel-N to NO conversion and CO emission were unaffected by changes to the bed composition (CaO, kaolin, and silica sand) at $\lambda_1/\lambda = 1$ and primary gas composition (N_2 and CO_2) at $\lambda_1/\lambda = 0$ and 0.04 during straw combustion.

Chapter 5 summarizes the results of an experimental investigation on the influence of additives (CaO, kaolin, $MgCO_3$, coal fly ash, clay, $(NH_4)_2Fe(SO_4)_2$, $NH_4Fe(SO_4)_2$, $(NH_4)_2SO_4$, NH_4MgPO_4, $AlNH_4(SO_4)_2$, $(NH_4)_2HPO_4$, $(NH_4)_3[Fe(C_2O_4)_3]$, and urea) on NO_X and N_2O emissions, and bed agglomeration during air un-staged fluidized bed combustion of straw. The influence of $(NH_4)_2SO_4$ particle size and introduction method was additionally examined. Selected additives were also employed in air staged straw and un-staged sunflower husk combustion. Furthermore, the influence of ash accumulation and bed agglomeration was investigated during sunflower husk combustion. The main conclusions from this study are:

- During straw combustion, kaolin, CaO, and $MgCO_3$ prevented defluidization without changing the fuel-N to NO conversion, while urea reduced NO emission without affecting bed agglomeration. To reduce NO_X emissions by thermal $DeNO_X$, the NH-functionality was a necessity. NH_4MgPO_4 and $AlNH_4(SO_4)_2$ prevented defluidization while reducing the fuel-N to NO conversion by 40% in straw and 30% in sunflower husk combustion.
- Local gas composition measurements revealed that the NH-based additives released NH_3 above the fuel inlet and/or the bubbling bed. Some additives (urea, $(NH_4)_2SO_4$, NH_4MgPO_4, and $AlNH_4(SO_4)_2$) favored the reduction of NO by thermal $DeNO_X$, whereas additives that contained Fe ($(NH_4)_2Fe(SO_4)_2$, $NH_4Fe(SO_4)_2$, and $(NH_4)_3[Fe(C_2O_4)_3]$) or facilitated bed agglomeration, i.e. induced poor mixing, ($(NH_4)_2HPO_4$) increased NO emission near the bed and led to a negligible change in the fuel-N to NO conversion. All NH-based additives increased N_2O emission possibly by oxidation of NH_3 and HNCO. The local CO and C_XH_Y concentrations, and temperature measurements were unaffected by the use of additives.
- When premixing additive and fuel, larger particles of $(NH_4)_2SO_4$ dropped to the bed, increasing the NH_3 release above the bubbling bed and prolonging the time for defluidization. In addition, no significant differences were observed when feeding $(NH_4)_2SO_4$ batch wise as pellets or premixed with straw.
- Air staging ($\lambda_1/\lambda = 0.5$) reduced the fuel-N to NO conversion by 40% in straw combustion.
- The use of NH_4MgPO_4 and $AlNH_4(SO_4)_2$ under air staged conditions did not lead to a further decrease in NO; instead the NO emission slightly increased when employing these additives with air staging. The introduction of secondary air favored the oxidation of NH_3 to NO to a larger degree than in un-staged combustion. In addition, N_2O and CO effluent concentrations increased, while the local concentration of HNCO was unaffected by air staging.
- The accumulation of sunflower husk ash increased NO and decreased NH_3 concentration above the bed. In addition, the temporal variations above the bed were dampened at higher ash content. These differences were attributed to the incipient defluidization leading to poorer mixing and the catalytic effect of ash forming elements on the nitrogen chemistry.

Chapter 6 presents the experimental results of an investigation on the conversion of char-N during raw and demineralized biomass char combustion in a fixed bed reactor. The formation of nitrogen combustion products and the reduction of NO over char were investigated. The main conclusions from this study are:

- The conversion of char-N to NO decreased with an increase in char-N content during raw and demineralized biomass char combustion. This trend did not correlate with the NO reduction reactivity of the chars. Consequently, a contributing factor may be the increased yield of N_2O for high-N chars.
- The NO reduction reactivity of raw and demineralized biomass chars were largely dominated by the association and content of ash forming elements. The NO reduction reactivity of chars with a low char-P content correlated reasonably well with the (K+Ca)/C molar ratio. Chars with high char-P generally showed a lower NO reduction reactivity. This was possibly caused by the formation of less catalytically active species such as KPO_3.
- The nitrogen functionality in the chars were predominantly pyridinic, pyrrolic, and quartenary with smaller amounts of oxides.
- The NO reduction reactivity of raw and demineralized chars did not correlate with the initial surface area, porosity, char-N content, or nitrogen and oxygen functionality or content of the chars.
- From combustion of NO treated and un-treated chars, the char-N to NO conversion was higher for the NO treated chars. This indicates that the surface was enriched by (-CN) and/or (-CO). The accumulated (-CN) sites may lead to a different reactivity towards NO reduction than the inherent (-CN) sites.

Chapter 7 presents the experimental results of an investigation on the conversion of char-N during sewage sludge, refuse derived fuel (RDF), and straw char combustion in a fixed bed reactor. Demineralization was employed to study the influence of ash forming elements. The formation of nitrogen combustion products and the reduction of NO over char were investigated. The obtained NO reduction reactivity was used in a simplified, one-dimensional, transient packed bed reactor model to predict the conversion of char-N to NO. The main inferences from this study are:

- The reactivity of sewage sludge char was an order magnitude higher while that of RDF char was six-fold higher than that of straw char. This was attributed to the high content of Ca and Fe in the waste chars.
- The initial reactivities correlated well with the (K+Fe+Ca)/C molar ratios of the chars.
- A simple concentration-averaged, first order reaction expression was used to describe the char-NO reaction. Employing fractional order or random pore model expressions did not yield any obvious advantages to the simple model.
- The products from fixed bed char combustion at 800ºC in 10% O_2 were NO, N_2, and to a lesser extent N_2O. A mathematical model, using the experimentally obtained, concentration-averaged, first order NO reduction rate constant, predicted reasonably well the conversion of char-N to NO during combustion.
- The reactivities of waste chars exceeded that of coal and biomass char found in literature.

8.2 Suggestions for future work

The results in this work provide an improved understanding of the nitrogen chemistry during combustion of biomass and waste fuels at fluidized bed conditions. However, additional work could be performed in this field to further improve the understanding and thereby aid in NO_X emission control. A few suggestions are described below.

Additional fluidized bed combustion experiments with local gas composition measurement
The current fluidized bed setup allows for local gas composition measurements and thereby the possibility of a deeper understanding of the combustion process, which may not be visible from the effluent measurements. In addition, the temporal concentration variations of certain spatial points can be obtained, which may be of importance as well. Using the current setup, experiments could be conducted on the influence of the most important parameters affecting NO_X and N_2O emissions, including the effect of fuel type (RDF, algae, washed fuels, etc.), staging (air and fuel), and gas composition (H_2O, CO_2, etc.).

Fundamental understanding of the nitrogen chemistry from batch fluidized bed combustion
Many studies focus on the conversion of nitrogen during single particle combustion. In comparison, less emphasis has been put on the nitrogen conversion during combustion of a group of particles, which may be more representative of industrial conditions. Therefore, the fundamental understanding of the influence of fuel type, particle size, and operating conditions (temperature, gas composition etc.) on NO_X needs to be improved. This can be done using the current methodology for batch combustion of a group of biomass particles. Besides NO_X, N_2O may also be considered for this type of study, as this becomes increasingly important for high-nitrogen fuels.

Further work on the use of additives for NO_X and bed agglomeration minimization
As a first attempt to reduce NO_X emissions and bed agglomeration simultaneously, a variety of additives was screened. The focal point of this work was on the NO_X emissions; hence, the mechanism of the interaction between additive and bed material has yet to be elucidated. While several of the additives prevented defluidization and/or reduced NO_X emissions, further investigation may be necessary to obtain data outside of the investigated conditions such as varying temperature, fuel type, additive amount, additive particle size etc. Moreover, a fundamental understanding of the decomposition of the additives needs to be obtained. In addition, large-scale tests and cost-benefit analyses may be considered to identify and propose effective and cheap countermeasures.

Quantitative description of the fluidized bed experimental results
Local gas and temperature measurements from fluidized bed combustion of biomass were obtained, which may be used as validation in computational fluid dynamic (CFD) or chemical engineering models. Different models may be considered with detailed fluid dynamics and/or chemical kinetics, thereby providing a predictive tool, which may aid in understanding, and potentially upscaling or extrapolation.

Measurement of instantaneous char properties during NO gasification
No correlation was found between the NO reduction reactivity, and the chemical and physical properties of biomass char. This may conceivably be related to the changes in these properties during experimentation. Therefore, measurements of instantaneous char properties such as nitrogen content and functionality, ash forming element content, surface area etc. may provide a better basis for reactivity correlation and moreover an improved understanding of the char-NO reaction.

Influence of O_2, CO, and char-P on the char-NO reactivity
The results presented in Chapter 6 indicate that the presence of char-P may decrease the NO reduction reactivity. However, further work is necessary before any conclusions can be drawn. In addition, the role and importance of CO and O_2 in the char-NO reaction must be established.

Quantitative description of the char-NO reaction
While a qualitative understanding of the char-NO reaction and char-N to NO conversion has been obtained, quantitative descriptions of the ongoing reactions are based on globalized expressions. Consequently, a universally accepted mechanism has yet to be elucidated. Compared to the volatile-N chemistry, the fundamental understanding of the char-N chemistry is lacking and requires further study.

Proposals for NO reduction based on this work
Waste chars with high ash forming element content exhibited a high reactivity towards NO reduction. In addition, fuels such as sewage sludge and sunflower seed released large amounts of NH_3 during combustion. At high O_2 concentration, these may contribute to a net increase in NO emission. However, at air or fuel staged conditions, these compounds could possibly reduce the net NO emission, which would require further study and possibly tests on a larger scale. In addition, alternative processes taking advantage of the high NH_3 release and/or waste char NO reduction reactivity may be explored and tested.

References

[1] Ravishankara AR, Daniel JS, Portmann RW. Nitrous Oxide (N_2O): The Dominant Ozone-Depleting Substance Emitted in the 21st Century. Science (80-) 2009;326:123–5. doi:10.1126/science.1176985.

[2] Frank A, Castaldi MJ. CFD analysis of municipal solid waste combustion using detailed chemical kinetic modelling. Waste Manag Res 2014;32:745–54. doi:10.1177/0734242X14538305.

[3] Environmental health criteria 188: Nitrogen Oxides. Chemical Safety Information from Intergovernmental (INCHEM) organizations. n.d. http://www.inchem.org/documents/ehc/ehc/ehc188.htm#PartNumber:1 (accessed March 18, 2019).

[4] Air pollution from the main sources - Air emissions from energy and industrial sources. Eur Com 2018. http://ec.europa.eu/environment/air/sources/energy.htm (accessed July 16, 2019).

[5] Ågren C. Tighter emission limits for EU power plants. Air Pollut Clim 2017. http://www.airclim.org/acidnews/tighter-emission-limits-eu-power-plants (accessed March 20, 2019).

[6] Best Available Techniques (BAT) Reference Document for Waste Incineration by the Joint Research Centre 2018. http://eippcb.jrc.ec.europa.eu/reference/BREF/WI/WI_BREF_FD_Black_Watermark.pdf.

[7] Directive 2010/75/EU of the European Parliament and of the Council of 24 November 2010 on industrial emissions (integrated pollution prevention and control) by The European Parliament and The Council of The European Union 2010. https://eur-lex.europa.eu/legal-content/EN/TXT/?uri=CELEX:32010L0075.

[8] COMMISSION IMPLEMENTING DECISION (EU) 2017/1442 of 31 July 2017 establishing best available techniques (BAT) conclusions, under Directive 2010/75/EU of the European Parliament and of the Council, for large combustion plants by the European Commision by th 2017. https://eur-lex.europa.eu/legal-content/EN/TXT/HTML/?uri=CELEX:32017D1442&from=EN.

[9] Basu PP. Combustion and gasification in fluidized beds. Taylor & Francis Group; 2006.

[10] Khan AA, de Jong W, Jansens PJ, Spliethoff H. Biomass combustion in fluidized bed boilers: Potential problems and remedies. Fuel Process Technol 2009;90:21–50. doi:10.1016/j.fuproc.2008.07.012.

[11] Leckner B, Karlsson M. Gaseous emissions from circulating fluidized bed combustion of wood. Biomass and Bioenergy 1993;4:379–89.

[12] Werther J, Saenger M, Hartge EU, Ogada T, Siagi Z. Combustion of agricultural residues. Prog Energy Combust Sci 2000;26:1–27. doi:10.1016/S0360-1285(99)00005-2.

[13] Chyang CS, Qian FP, Lin Y-C, Yang S-H. NO and N2O emission characteristics from a pilot scale vortexing fluidized bed combustor firing different fuels. Energy and Fuels 2008;22:1004–11. doi:10.1016/j.fuel.2015.02.023.

[14] Hayhurst AN, Vince IM. Nitric oxide formation from N2 in flames: The importance of "prompt" NO. Prog Energy Combust Sci 1980;6:35–51. doi:10.1016/0360-1285(80)90014-3.

[15] Jonke AA, Carls EL, Jarry RL, Haas M, Murphy WA. Reduction of atmospheric pollution by the application of fluidized bed combustion, Annual report, July 1968-June 1969, by Chemical Engineering Division, Argonne National Laboratory, Illinois, Report No. ANL/ES/-CEN-1001. 1969.

[16] Glarborg P, Jensen AD, Johnsson JE. Fuel nitrogen conversion in solid fuel fired systems. Prog Energy Combust Sci 29 2003;29:89–113. doi:10.1016/S0360-1285(02)00031-X.

[17] Glarborg P, Miller JA, Ruscic B, Klippenstein SJ. Modeling nitrogen chemistry in combustion. Prog Energy Combust Sci 2018;67:31–68. doi:10.1016/j.pecs.2018.01.002.

[18] Hupa M, Karlström O, Vainio E. Biomass combustion technology development - It is all about chemical details. Proc Combust Inst 2017;36:113–34. doi:10.1016/j.proci.2016.06.152.

[19] Vassilev S V, Baxter D, Andersen LK, Vassileva CG. An overview of the chemical composition of biomass. Fuel 2010;89:913–33. doi:10.1016/j.fuel.2009.10.022.

[20] Nakhaei M, Pedersen MN, Wu H, Skaarup Jensen L, Glarborg P, Jensen PA, et al. Aerodynamic and Physical Characterization of Refuse Derived Fuel. Energy and Fuels 2018;32:7685–700. doi:10.1021/acs.energyfuels.8b01359.

[21] Krüger B, Mrotzek A, Wirtz S. Separation of harmful impurities from refuse derived fuels (RDF) by a fluidized bed. Waste Manag 2014;34:390–401. doi:10.1016/j.wasman.2013.10.021.

[22] Hansson KM, Åmand LE, Habermann A, Winter F. Pyrolysis of poly-L-leucine under combustion-like conditions. Fuel 2003;82:653–60. doi:10.1016/S0016-2361(02)00357-5.

[23] Hansson KM, Samuelsson J, Tullin C, Åmand LE. Formation of HNCO, HCN, and NH3from the pyrolysis of bark and nitrogen-containing model compounds. Combust Flame 2004;137:265–77. doi:10.1016/j.combustflame.2004.01.005.

[24] Chen H, Wang Y, Xu G, Yoshikawa K. Fuel-N evolution during the pyrolysis of industrial biomass wastes with high nitrogen content. Energies 2012;5:5418–38. doi:10.3390/en5125418.

[25] Curran PJ, Dungan JL, Peterson DL. Estimating the foliar biochemical concentration of leaves with reflectance spectrometry: Testing the Kokaly and Clark methodologies. Remote Sens Environ 2001;76:349–59. doi:10.1016/S0034-4257(01)00182-1.

[26] Wei L, Wen L, Yang T, Zhang N. Nitrogen Transformation during Sewage Sludge Pyrolysis. Energy and Fuels 2015;29:5088–94. doi:10.1021/acs.energyfuels.5b00792.

[27] Marschner H. Nitrogen Fixation. Miner. Nutr. High. Plants. 2nd ed., Academic Press; 1995.

[28] Marschner H. Functions of Mineral Nutrients: Macronutrients. Miner. Nutr. High. Plants. 2nd ed., Academic Press; 1995.

[29] Ren Q, Zhao C. Evolution of fuel-N in gas phase during biomass pyrolysis. Renew Sustain Energy Rev 2015;50:408–18. doi:10.1016/j.rser.2015.05.043.

[30] Hansson KM. Principles of biomass pyrolysis with emphasis on the formation of the nitrogen-containing gases HNCO, HCN and NH3. Chalmers University of Technology, 2003.

[31] Åbo Akademi. Åbo Akademi Chemical Fractionation Database n.d. https://web.abo.fi/fak/tkf/ook/bransle/ (accessed March 1, 2019).

[32] Anca-Couce A, Sommersacher P, Evic N, Mehrabian R, Scharler R. Experiments and modelling of NOx precursors release (NH_3 and HCN) in fixed-bed biomass combustion conditions. Fuel 2018;222:529–37. doi:10.1016/j.fuel.2018.03.003.

[33] Chen W, Yang H, Chen Y, Li K, Xia M, Chen H. Influence of Biochar Addition on Nitrogen Transformation during Copyrolysis of Algae and Lignocellulosic Biomass. Environ Sci Technol 2018;52:9414–521. doi:10.1021/acs.est.8b02485.

[34] Sander B. Properties of Danish Biofuels and the Requirements for Power Production. Biomass and Bioenergy 1997;12:177–83.

[35] Spliethoff H, Hein KRG. Effect of co-combustion of biomass on emissions in pulverized fuel furnaces. Fuel Process Technol 1998;54:189–205.

[36] Werther J, Ogada T. Sewage sludge combustion. Prog Energy Combust Sci 1999;25:55–116. doi:10.1016/S0140-6701(99)91279-1.

[37] Yang Z, Zhang Y, Liu L, Wang X, Zhang Z. Environmental investigation on co-combustion of sewage sludge and coal gangue: SO2, NOx and trace elements emissions. Waste Manag 2016;50:213–21. doi:10.1016/j.wasman.2015.11.011.

[38] Åmand L-E, Westberg H, Karlsson M, Leckner B, Coda B, Hocquel M, et al. Co-Combustion of dried sewage sludge and coal/wood in CFB-A Search for Factors Inluencing Emissions. Proc. 16th Int. Conf. Fluid. Bed Combust., Reno, Nevada, USA: n.d.

[39] ECN, Phyllis2: Databse for biomass and waste n.d. https://www.ecn.nl/phyllis2/ (accessed March 1, 2019).

[40] Zhou H, Jensen AD, Glarborg P, Kavaliauskas A. Formation and reduction of nitric oxide in fixed-bed combustion of straw. Fuel 2006;85:705–16. doi:10.1016/j.fuel.2005.08.038.

[41] Demirbas A. Carbonization ranking of selected biomass for charcoal , liquid and gaseous products. Energy Convers Manag 2001;42:1229–38.

[42] Lang T, Jensen AD, Jensen PA. Retention of Organic Elements during Solid Fuel Pyrolysis with Emphasis on the Peculiar Behavior of Nitrogen. Energy & Fuels 2005;19:1631–43.

[43] Yuan S, Chen X, Li W, Liu H, Wang F. Nitrogen conversion under rapid pyrolysis of two types of aquatic biomass and corresponding blends with coal. Bioresour Technol 2011;102:10124–30. doi:10.1016/j.biortech.2011.08.047.

[44] Meesuk S, Cao J, Sato K, Hoshino A. Nitrogen Conversion of Pig Compost during Pyrolysis. J Chem Eng Japan 2013;46:556–61. doi:10.1252/jcej.12we262.

[45] Singh K, Risse LM, Das KC, Worley J, Risse LM, Das KC, et al. Effect of Fractionation and Pyrolysis on Fuel Properties of Poultry Litter. J Air Waste Manag Assoc 2010;60:875–83. doi:10.3155/1047-3289.60.7.875.

[46] Zheng Y, Jensen AD, Glarborg P, Sendt K, Haynes BS. Heterogeneous fixation of N2: Investigation of a novel mechanism for formation of NO. Proc Combust Inst 2009;32 II:1973–80. doi:10.1016/j.proci.2008.06.187.

[47] Pohl JH, Sarofim AF. Devolatilization and oxidation of coal nitrogen. Symp Int Combust 1977;16:491–501.

[48] Leppälahti J, Koljonen T. Nitrogen evolution from coal , peat and wood during gasification : Literature review. Fuel Process Technol 1995;43:1–45.

[49] Wu W, Yang M, Feng Q, Mcgrouther K, Wang H, Lu H, et al. Chemical characterization of rice straw-derived biochar for soil amendment. Biomass and Bioenergy 2012;47:268–76. doi:10.1016/j.biombioe.2012.09.034.

[50] Peng X, Ye LL, Wang CH, Zhou H, Sun B. Temperature- and duration-dependent rice straw-derived biochar : Characteristics and its effects on soil properties of an Ultisol in southern China. Soil Tillage Res 2011;112:159–66. doi:10.1016/j.still.2011.01.002.

[51] Cai H-Y, Güell AJ, Dugwell DR, Kandiyoti R. Heteroatom distribution in pyrolysis products as a function of heating rate and pressure. Fuel 1993;72:321–7.

[52] Karaosmanoglu F, Isigigur-Ergudenler A, Sever A. Biochar from the Straw-Stalk of Rapeseed Plant. Energy & Fuels 2000;21:336–9. doi:10.1021/ef9901138.

[53] Shen J, Wang X, Garcia-perez M, Mourant D, Rhodes MJ, Li C. Effects of particle size on the fast pyrolysis of oil mallee woody biomass. Fuel 2009;88:1810–7. doi:10.1016/j.fuel.2009.05.001.

[54] Slaughter DM, Overmoe BJ, Pershing DW. Inert pyrolysis of stoker-coal fines. Fuel 1988;67:482–9.

[55] Samuelsson J. Conversion of nitrogen in a fixed burning biofuel bed. Chalmers University of Technology, 2006.

[56] Cheng S, Qiao Y, Huang J, Wang W, Wang Z, Yu Y, et al. Effects of Ca and Na acetates on nitrogen transformation during sewage sludge pyrolysis. Proc Combust Inst 2019;37:2715–22. doi:10.1016/j.proci.2018.08.018.

[57] Trubetskaya A, Arendt P, Degn A, David A, Llamas G, Umeki K, et al. Effect of fast pyrolysis conditions on biomass solid residues at high temperatures. Fuel Process Technol 2016;143:118–29. doi:10.1016/j.fuproc.2015.11.002.

[58] Ohtsuka Y, Zhiheng W, Furimsky E. Effect of alkali and alkaline earth metals on nitrogen release during temperature programmed pyrolysis of coal. Fuel 1997;76:1361–7.

[59] Ren Q, Zhao C, Wu X, Liang C, Chen X, Shen J, et al. Effect of mineral matter on the formation of NO_X precursors during biomass pyrolysis. J Anal Appl Pyrolysis 2009;85:447–53. doi:10.1016/j.jaap.2008.08.006.

[60] Blasi C Di, Signorelli G, Russo C Di, Rea G. Product Distribution from Pyrolysis of Wood and Agricultural Residues. Ind Eng Chem Res 1999;38:2216–24. doi:10.1021/ie980711u.

[61] Ulusoy B, Wu H, Lin W, Karlström O, Li S, Song W, et al. Reactivity of sewage sludge, RDF, and straw chars towards NO. Fuel 2019;236:297–305. doi:10.1016/j.fuel.2018.08.164.

[62] Ulusoy B, Lin W, Karlström O, Li S, Song W, Glarborg P, et al. Formation of NO and N_2O during raw and demineralized biomass char combustion. Energy & Fuels 2019. doi:10.1021/acs.energyfuels.9b00622.

[63] Abelha P, Gulyurtlu I, Cabrita I. Release of nitrogen precursors from coal and biomass residues in a bubbling fluidized bed. Energy and Fuels 2008;22:363–71. doi:10.1021/ef700430t.

[64] Farrow TS, Sun C, Snape CE. Impact of CO_2 on biomass pyrolysis , nitrogen partitioning , and char combustion in a drop tube furnace. J Anal Appl Pyrolysis 2015;113:323–31. doi:10.1016/j.jaap.2015.02.013.

[65] Ratcliff MA, Medley EE, Simmonds PG. Pyrolysis of Amino Acids. Mechanistic Considerations. J Org Chem 1976;39:1481–90.

[66] Simmonds PG, Medley EE. Thermal Decomposition of Aliphatic Monoamino-Monocarboxylic Acids. Anal Chem 1972;44:2060–6. doi:10.1021/ac60320a040.

[67] Johnson WR, Kang JC. Mechanisms of Hydrogen Cyanide Formation from the Pyrolysis of Amino Acids and Related Compounds1. J Org Chem 1971;36:189–92. doi:10.1021/jo00800a038.

[68] Hansson KM, Samuelsson J, Åmand LE, Tullin C. The temperature's influence on the selectivity between HNCO and HCN from pyrolysis of 2,5-diketopiperazine and 2-pyridone. Fuel 2003;82:2163–72. doi:10.1016/S0016-2361(03)00206-0.

[69] Zhang J, Tian Y, Cui Y, Zuo W, Tan T. Bioresource Technology Key intermediates in nitrogen transformation during microwave pyrolysis of sewage sludge : A protein model compound study. Bioresour Technol 2013;132:57–63. doi:10.1016/j.biortech.2013.01.008.

[70] Ren Q, Zhao C, Chen X, Duan L, Li Y, Ma C. NO_x and N_2O precursors (NH_3 and HCN) from biomass pyrolysis: Co-pyrolysis of amino acids and cellulose , hemicellulose and lignin. Proc Combust Inst 2011;33:1715–22. doi:10.1016/j.proci.2010.06.033.

[71] Ren Q, Zhao C. NO_X and N_2O Precursors from Biomass Pyrolysis : Role of Cellulose , Hemicellulose and Lignin. Environ Sci Technol 2013:8955–61. doi:10.1021/es4017574.

[72] Ren Q, Zhao C. NOx and N2O precursors (NH3 and HCN) from biomass pyrolysis: Interaction between amino acid and mineral matter. Appl Energy 2013;112:170–4. doi:10.1016/j.apenergy.2013.05.061.

[73] Zhou J, Gao P, Dong C, Yang Y. Effect of Temperature and Mineral Matter on the Formation of NOx Precursors during Fast Pyrolysis of 2,5-Diketopiperazine. Energies 2018;11:629–38.

doi:10.3390/en11030629.

[74] Yi L, Liu H, Lu G, Zhang Q, Wang J, Hu H, et al. Effect of Mixed Fe/Ca Additives on Nitrogen Transformation during Protein and Amino Acid Pyrolysis. Energy and Fuels 2017;31:9484–90. doi:10.1021/acs.energyfuels.7b01413.

[75] Hu J, Yu W, Guan R, Liu B, Li H, Yang J, et al. Effects of red mud on emission control of NOx precursors during sludge pyrolysis: A protein model compound study. Waste Manag 2019;85:452–63. doi:10.1016/j.wasman.2019.01.014.

[76] Liu G, Wright MM, Zhao Q, Brown RC, Wang K, Xue Y. Catalytic pyrolysis of amino acids : Comparison of aliphatic amino acid and cyclic amino acid. Energy Convers Manag 2016;112:220–5. doi:10.1016/j.enconman.2016.01.024.

[77] Wei F, Cao J, Zhao X, Ren J, Gu B, Wei X. Formation of aromatics and removal of nitrogen in catalytic fast pyrolysis of sewage sludge : A study of sewage sludge and model amino acids. Fuel 2018;218:148–54. doi:10.1016/j.fuel.2018.01.025.

[78] Ren Q, Zhao C, Wu X, Liang C, Chen X, Shen J, et al. Formation of NOx precursors during wheat straw pyrolysis and gasification with O_2 and CO_2. Fuel 2010;89:1064–9. doi:10.1016/j.fuel.2009.12.001.

[79] Hämäläinen JP, Aho MJ, Tummavuori JL. Formation of nitrogen oxides from fuel-N through HCN and NH3: a model-compound study. Fuel 1994;73:1894–8. doi:10.1016/0016-2361(94)90218-6.

[80] Hämäläinen JP, Aho MJ. Effect of fuel composition on the conversion of volatile solid fuel-N to N2O and NO. Fuel 1995;74:1922–4. doi:10.1016/0016-2361(95)80030-L.

[81] Jie L, Yuwen L, Jingyan S, Zhiyong W, Ling H, Xi Y, et al. The investigation of thermal decomposition pathways of phenylalanine and tyrosine by TG-FTIR. Thermochim Acta 2007;467:20–9. doi:10.1016/j.tca.2007.10.014.

[82] Zhou J, Masutani SM, Ishimura DM, Turn SQ, Konishita CM, Kinoshita CM. Release of fuel-bound nitrogen in biomass during high temperature pyrolysis and gasification. Proc. 1997 32nd Intersoc. Energy Convers. Eng. Conf. Part 1 (of 4), Honolulu, HI, USA: 1997, p. 1785–90. doi:10.1109/IECEC.1997.656693.

[83] Stubenberger G, Scharler R, Zahirovic S, Obernberger I. Experimental investigation of nitrogen species release from different solid biomass fuels as a basis for release models. Fuel 2008;87:793–806. doi:10.1016/j.fuel.2007.05.034.

[84] Aho MJ, Hämäläinen JP, Tummavuori JL. Importance of solid fuel properties to nitrogen oxide formation through HCN and NH3 in small particle combustion. Combust Flame 1993;95:22–30. doi:10.1016/0010-2180(93)90049-9.

[85] Becidan M, Skreiberg Ø, Hustad JE. NO_x and N_2O Precursors (NH_3 and HCN) in Pyrolysis of Biomass Residues. Energy & Fuels 2007;21:1173–80. doi:10.1021/ef060426k.

[86] Liu X, Luo Z, Yu C, Jin B, Tu H. Release Mechanism of Fuel-N into NO_x and N_2O Precursors during Pyrolysis of Rice Straw. Energies 2018;11:1–13. doi:10.3390/en11030520.

[87] Zhan H, Yin X, Huang Y, Yuan H, Xie J, Wu C, et al. Comparisons of Formation Characteristics of NO x Precursors during Pyrolysis of Lignocellulosic Industrial Biomass Wastes. Energy & Fuels 2017;31:9557–67. doi:10.1021/acs.energyfuels.7b01559.

[88] Giuntoli J, Gout J, Verkooijen AHM, de Jong W. Characterization of Fast Pyrolysis of Dry Distiller ' s Grains (DDGS) and Palm Kernel Cake Using a Heated Foil Reactor : Nitrogen Chemistry and Basic Reactor Modeling. Ind Eng Chem Res 2011;50:4286–300. doi:10.1021/ie101618c.

[89] Chen W, Yang H, Chen Y, Xia M, Chen X, Chen H. Transformation of Nitrogen and Evolution of N ‐ Containing Species during Algae Pyrolysis. Environ Sci Technol 2017;51:6570–9. doi:10.1021/acs.est.7b00434.

[90] Zhang J, Tian Y, Zhu J, Zuo W, Yin L. Characterization of nitrogen transformation during microwave-induced pyrolysis of sewage sludge. J Anal Appl Pyrolysis 2014;105:335–41. doi:10.1016/j.jaap.2013.11.021.

[91] Zhan H, Yin X, Huang Y, Zhang X, Yuan H, Xie J, et al. Characteristics of NO_X precursors and their formation mechanism during pyrolysis of herb residues. J Fuel Chem Technol 2017;45:279–88. doi:10.1016/s1872-5813(17)30017-8.

[92] Tchapda AH, Pisupati S V. A Review of Thermal Co-Conversion of Coal and Biomass/Waste. Energies 2014;7:1098–148. doi:10.3390/en7031098.

[93] Jensen AD. Nitrogen chemistry in fluidized bed combustion of coal. Technical University of Denmark, 1996.

[94] Winter F, Wartha C, Hofbauer H. The relative importance of radicals on the N2O and NO formation and destruction paths in a quartz CFBC. J Energy Resour Technol 1999:131–6.

[95] Winter F, Wartha C, Hofbauer H. NO and N_2O formation during the combustion of wood, straw, malt waste and peat. Bioresour Technol 1999;70:39–49. doi:10.1021/ef301383g.

[96] Tian FJ, Yu JL, Mckenzie LJ, Hayashi JI, Chiba T, Li CZ. Formation of NOx precursors during the pyrolysis of coal and biomass. Part VII. Pyrolysis and gasification of cane trash with steam. Fuel 2005;84:371–6. doi:10.1016/j.fuel.2004.09.018.

[97] Tian FJ, Yu J, McKenzie LJ, Hayashi JI, Li CZ. Conversion of fuel-N into HCN and NH_3 during the pyrolysis and gasification in steam: A comparative study of coal and biomass. Energy and Fuels 2007;21:517–21. doi:10.1021/ef060415r.

[98] Karlström O, Wu H, Glarborg P. Influence of H_2O on NO formation during char oxidation of biomass. Fuel 2019;235:1260–5. doi:10.1016/j.fuel.2018.08.156.

[99] Wei L, Wen L, Liu M, Yang T. Interaction Characteristics of Mineral Matter and Nitrogen during Sewage Sludge Pyrolysis. Energy & Fuels 2016;30:10505–10. doi:10.1021/acs.energyfuels.6b02146.

[100] Tsubouchi N, Ohshima Y, Xu C, Ohtsuka Y. Enhancement of N 2 Formation from the Nitrogen in Carbon and Coal by Calcium 2001:158–62. doi:10.1021/ef000090t.

[101] Lu G, Liu H, Zhang Q, Wang J, Yi L, Hu H, et al. Nitrogen conversion during the homogeneous

and heterogeneous stages of sludge steam gasi fi cation : Synergistic e ff ects of Fenton ' s reagent and CaO conditioner. Fuel 2019;241:1109–16. doi:10.1016/j.fuel.2018.12.109.

[102] Liu H, Zhang Q, Hu H, Liu P, Hu X. Catalytic role of conditioner CaO in nitrogen transformation during sewage sludge pyrolysis. Proc Combust Inst 2015;35:2759–66. doi:10.1016/j.proci.2014.06.034.

[103] Mori H, Asami K, Ohtsuka Y. Role of iron catalyst in fate of fuel nitrogen during coal pyrolysis. Energy & Fuels 1996;10:1022–7. doi:10.1021/ef960035d.

[104] Ren Q, Zhao C, Wu X, Liang C, Xiaoping C, Shen J, et al. Catalytic effects of Fe, Al and Si on the formation of NO_X precursors and HCl during straw pyrolysis. J Therm Anal Calorim 2010;99:301–6. doi:10.1007/s10973-009-0150-0.

[105] Wu Z, Ohtsuka Y. Key Factors for Formation of N 2 from Low-Rank Coals during Fixed Bed Pyrolysis : Pyrolysis Conditions and Inherent Minerals. Energy & Fuels 1997;11:902–8. doi:10.1021/ef9700238.

[106] Yuan S, Zhou Z, Li J, Chen X, Wang F. Pyrolysis HCN and NH_3 (NO_x precursors) released under rapid pyrolysis of biomass / coal blends. J Anal Appl Pyrolysis 2011;92:463–9. doi:10.1016/j.jaap.2011.08.010.

[107] Di Nola G, de Jong W, Spliethoff H. TG-FTIR characterization of coal and biomass single fuels and blends under slow heating rate conditions: Partitioning of the fuel-bound nitrogen. Fuel Process Technol 2010;91:103–15. doi:10.1016/j.fuproc.2009.09.001.

[108] Wang Q, Liu Q, Wang Z, Liu H, Bai J, Ye J. Characterization of organic nitrogen and sulfur in the oil shale kerogens. Fuel Process Technol 2017;160:170–7. doi:10.1016/j.fuproc.2017.02.031.

[109] Pels JR, Kapteijn F, Moulijn JA, Zhu Q, Thomas KM. Evolution of nitrogen functionalities in carbonaceous materials during pyrolysis. Carbon N Y 1995;33:1641–53. doi:10.1016/0008-6223(95)00154-6.

[110] Phiri Z, Everson RC, Neomagus HWJP, Wood BJ. The effect of acid demineralising bituminous coals and de-ashing the respective chars on nitrogen functional forms. J Anal Appl Pyrolysis 2017;125:127–35. doi:10.1016/j.jaap.2017.04.009.

[111] Phiri Z, Everson RC, Neomagus HWJP, Wood BJ. Transformation of nitrogen functional forms and the accompanying chemical-structural properties emanating from pyrolysis of bituminous coals. Appl Energy 2018;216:414–27. doi:10.1016/j.apenergy.2018.02.107.

[112] Darvell LI, Brindley C, Baxter XC, Jones JM, Williams A. Nitrogen in biomass char and its fate during combustion: A model compound approach. Energy and Fuels 2012;26:6482–91. doi:10.1021/ef201676t.

[113] Liu X, Luo Z, Yu C, Xie G. Conversion mechanism of fuel-N during pyrolysis of biomass wastes. Fuel 2019;246:42–50. doi:10.1016/j.fuel.2019.02.042.

[114] Kapteijn F, Moulijn JA, Matzner S, Boehm H. The development of nitrogen functionality in model chars during gasification in CO2 and O2.pdf 1999;37:1143–50.

[115] Xu J, Sun R, Ismail TM, Sun S, Wang Z. Effect of Char Particle Size on NO Release during Coal Char Combustion. Energy and Fuels 2017;31:13406–15. doi:10.1021/acs.energyfuels.7b02580.

[116] Kelemen SR, Gorbaty ML, Kwiatek PJ, Fletcher TH, Watt M, Solum MS, et al. Nitrogen Transformations in Coal during Pyrolysis. Energy & Fuels 1998;12:159–73. doi:10.1021/ef9701246.

[117] Burchill P, Herod AA. Investigation of nitrogen compounds tar products . 2 . Basic fractions in coal. Fuel 1983;62:20–9.

[118] Růžičková J, Kucbel M, Raclavská H, Barbora Š, Raclavský K, Juchelková D. Comparison of organic compounds in char and soot from the combustion of biomass in boilers of various emission classes. J Environ Manage 2019;236:769–83. doi:10.1016/j.jenvman.2019.02.038.

[119] Dabros TMH, Stummann MZ, Høj M, Jensen PA, Grunwaldt J-D, Gabrielsen J, et al. Transportation fuels from biomass fast pyrolysis , catalytic hydrodeoxygenation , and catalytic fast hydropyrolysis. Prog Energy Combust Sci 2018;68:268–309. doi:10.1016/j.pecs.2018.05.002.

[120] Sun S, Tian H, Zhao Y, Sun R, Zhou H. Experimental and numerical study of biomass flash pyrolysis in an entrained flow reactor. Bioresour Technol 2010;101:3678–84. doi:10.1016/j.biortech.2009.12.092.

[121] Chen Y, Matsuda H, Mori S, Hasatani M. Behaviors of Coal Nitrogen Converted to Tar. Energy & Fuels 1995:866–9. doi:10.1021/ef00053a019.

[122] Cao J, Li L, Morishita K, Xiao X, Zhao X, Wei X. Nitrogen transformations during fast pyrolysis of sewage sludge. Fuel 2013;104:1–6. doi:10.1016/j.fuel.2010.08.015.

[123] Pecha MB, Arbelaez JIM, Garcia-Perez M, Chejne F, Ciesielski PN. Progress in understanding the four dominant intra-particle phenomena of lignocellulose pyrolysis: chemical reactions, heat transfer, mass transfer, and phase change. Green Chem 2019:1–31. doi:10.1039/C9GC00585D.

[124] Okumura Y. Effect of heating rate and coal type on the yield of functional tar components. Proc Combust Inst 2017;36:2075–82. doi:10.1016/j.proci.2016.09.020.

[125] Hayashi J, Takahashi H, Doi S, Kumagai H, Tadatoshi C, Yoshida T, et al. Reactions in Brown Coal Pyrolysis Responsible for Heating Rate Effect on Tar Yield. Energy & Fuels 2000;14:400–8. doi:10.1021/ef9901490.

[126] Inc F. 18.1.4 Prompt NOx Formation n.d. http://jullio.pe.kr/fluent6.1/help/html/ug/node625.htm (accessed May 17, 2019).

[127] Zhong BJ, Roslyakov P V. Study on prompt NOX emission in boilers. J Therm Sci 1996;5:143–7.

[128] Semakula M, Inambao PF. The Formation , Effects and Control of Oxides of Nitrogen in Diesel Engines. Int J Appl Eng Res 2018;13:3200–9.

[129] Bulewicz EM. Free radicals, combustion and fludized beds n.d.:1–11.

[130] Wartha C, Winter F, Hofbauer H. The Trade-Off Between N_2 , NO, and N_2O Under Fluidized Bed Combustor Conditions. J Energy Resour Technol 2000;122:94–100.

[131] Johnsson JE. Formation and reduction of nitrogen oxides in fluidized-bed combustion. Fuel 1994;73:1398–415.

[132] Mendiara T, Glarborg P. Ammonia chemistry in oxy-fuel combustion of methane. Combust Flame 2009;156:1937–49. doi:10.1016/j.combustflame.2009.07.006.

[133] Glarborg P, Marshall P. Importance of the Hydrogen Isocyanide Isomer in Modeling Hydrogen Cyanide Oxidation in Combustion. Energy & Fuels 2016:2156–63. doi:10.1021/acs.energyfuels.6b02085.

[134] Svoboda K, Cermak J, Hartman M. Chemistry and Emission of Nitrogen Oxides (NO, NO_2, N_2O) in Combustion of Solid Fuels II. Heterogeneous Reactions. Chem Pap 2000;54:118–30.

[135] Feng B, Liu H, Yuan J, Lin Z, Liu D, Leckner B. Mechanisms of N_2O Formation from Char Combustion. Energy & Fuels 1996:203–8. doi:10.1021/ef9500898.

[136] Molina A, Eddings EG, Pershing DW, Sarofim AF. Char nitrogen conversion: implications to emissions from coal-fired utility boilers. Prog Energy Combust Sci 2000;26:507–31.

[137] Karlström O, Brink A, Hupa M. Biomass Char Nitrogen Oxidation - Single Particle Model. Energy & Fuels 2013;27:1410–8.

[138] Xu J, Sun R, Ismail TM, Sun S, Wang Z. Effect of Oxygen Concentration on NO Formation during Coal Char Combustion. Energy & Fuels 2017;31:7502–9. doi:10.1021/acs.energyfuels.7b00293.

[139] Jensen L, Jannerup H, Glarborg P, Jensen A, Dam-Johansen K. Experimental investigation of NO from pulverized char combustion. Proc Combust Inst 2000;28:2271–8. doi:10.1016/S0082-0784(00)80637-2.

[140] Zhou H, Li Y, Li N, Qiu R, Meng S, Cen K. Experimental study of the NO and N 2 O emissions during devolatilization and char combustion of a single biomass particle in O 2 / N 2 and O 2 / H 2 O under low temperature condition. Fuel 2017;206:162–70. doi:10.1016/j.fuel.2017.05.089.

[141] Liu X, Luo Z, Yu C. Conversion of char-N into NOx and N2O during combustion of biomass char. Fuel 2019;242:389–97. doi:10.1016/j.fuel.2019.01.061.

[142] Nelson PF, Nancarrow PC, Bus J, Prokopiuk A. Fractional conversion of char N to NO in an entrained flow reactor. Proc Combust Inst 2002;29:2267–74.

[143] Zhao K, Glarborg P, Jensen AD. NO Reduction over Biomass and Coal Char during Simultaneous Combustion. Energy & Fuels 2013;27:7817–26.

[144] Morf PO. Secondary Reactions of Tar during Thermochemical Biomass Conversion. 2001.

[145] Svoboda K, Hartman M. Formation of NO_x in fluidized bed combustion of model mixtures of liquid organic compounds containing nitrogen. Fuel 1991;70:865–71. doi:10.1016/0016-2361(91)90197-I.

[146] Duan F, Chyang CS, Zhang L hui, Chi YT. Effect of the molecular structure of nitrogen compounds on the pollutant formation in a bubbling fluidized-bed combustor. Energy 2015;83:394–402. doi:10.1016/j.energy.2015.02.037.

[147] Hao J, Yu W, Lu P, Zhang Y, Zhu X. The effects of Na/K additives and flyash on NO reduction in a SNCR process. Chemosphere 2015;122:213–8. doi:10.1016/j.chemosphere.2014.11.055.

[148] Gasnot L, Dao DQ, Pauwels JF. Experimental and kinetic study of the effect of additives on the ammonia based SNCR process in low temperature conditions. Energy and Fuels 2012;26:2837–49. doi:10.1021/ef300310c.

[149] Materials NSF, Company M. Rapid reduction of nitrogen oxides in exhaust gas streams. Nature 1986;324:657–8.

[150] Muzio LJ, Arand JK, Teixeira DP. Gas phase decomposition of nitric oxide in combustion products. Symp Combust 1977;16:199–208. doi:10.1016/S0082-0784(77)80325-1.

[151] Yang W, Zhou J, Zhou Z, Chen Z, Liu J, Cen K. Action of oxygen and sodium carbonate in the urea-SNCR process. Combust Flame 2009;156:1785–90. doi:10.1016/j.combustflame.2009.06.008.

[152] Wu X, Song Q, Zhao H, Yao Q. Synergetic effect of biomass volatiles on NO reduction and the influence of K/Na on it. Fuel 2015;158:634–40. doi:10.1016/j.fuel.2015.06.029.

[153] Tsukahara H, Ishida T, Mayumi M. Gas-phase oxidation of nitric oxide: Chemical kinetics and rate constant. Nitric Oxide - Biol Chem 1999;3:191–8. doi:10.1006/niox.1999.0232.

[154] Chambrion P, Kyotani T, Tomita A. Role of N-containing surface species on NO reduction by carbon. Energy & Fuels 1998;12:416–21.

[155] Karlström O, Perander M, DeMartini N, Brink A, Hupa M. Role of ash on the NO formation during char oxidation of biomass. Fuel 2017;190:274–80. doi:10.1016/j.fuel.2016.11.013.

[156] De Soete GG. Heterogeneous N_2O and NO formation from bound nitrogen atoms during coal char combustion. Symp Combust 1991;23:1257–64. doi:10.1016/S0082-0784(06)80388-7.

[157] Zevenhoven R, Hupa M. The reactivity of chars from coal, peat and wood towards NO, with and without CO. Fuel 1998;77:1169–76.

[158] Zhong BJ, Tang H. Catalytic NO reduction at high temperature by de-ashed chars with catalysts. Combust Flame 2007;149:234–43. doi:10.1016/j.combustflame.2006.04.004.

[159] Sørensen CO, Johnsson JE, Jensen A. Reduction of NO over wheat straw char. Energy and Fuels 2001;15:1359–68. doi:10.1021/ef000223a.

[160] Zhong BJ, Zhang HS, Fu WB. Catalytic effect of KOH on the reaction of NO with char. Combust Flame 2003;132:364–73. doi:10.1016/S0010-2180(02)00480-7.

[161] Wu X, Song Q, Zhao H, Zhang Z, Zhang L, Yao Q. Influence of mineral transformation on the reactivity evolution during rice straw char-NO reaction. Fuel 2013;113:553–9. doi:10.1016/j.fuel.2013.05.102.

[162] Zhao Z, Li W, Li B. Catalytic reduction of NO by coal chars loaded with Ca and Fe in various

atmospheres. Fuel 2002;81:1559–64. doi:10.1016/S0016-2361(02)00077-7.

[163] Commandré J-M, Stanmore BR, Salvador S. The High Temperature Reaction of Carbon with Nitric Oxide. Combust Flame 2002;128:211–6.

[164] Illán-Goméz MJ, Linares-Solano A, Salinas-Martínez de Lecea C. NO Reduction by Activated Carbons . 1 . The Role of Carbon Porosity and Surface Area. Energy & Fuels 1993;7:146–54.

[165] Galle M, Agar DW, Watzenberger O. Thermal N_2O decomposition in regenerative heat exchanger reactors. Chem Eng Sci 2001;56:1587–95.

[166] Vermeulen I, Block C, Vandecasteele C. Estimation of fuel-nitrogen oxide emissions from the element composition of the solid or waste fuel. Fuel 2012;94:75–80. doi:10.1016/j.fuel.2011.11.071.

[167] Shimizu T, Toyono M, Ohsawa H. Emissions of NO_X and N_2O during co-combustion of dried sewage sludge with coal in a bubbling fluidized bed combustor. Fuel 2007;86:957–64. doi:10.1016/j.fuel.2006.10.001.

[168] Liu H, Feng B, Lu J, Zheng C. COAL PROPERTY EFFECTS ON N2O AND NOx FORMATION FROM CIRCULATING FLUIDIZED BED COMBUSTION OF COAL. Chem Eng Commun 2005;192:1482–9. doi:10.1080/009864490896043.

[169] Ogunsola O, Herath B, No F. Use of multivariate analysis to determine the influence of some liquid-fuel properties on fuel-bound. Fuel 1990;69:1483–9.

[170] Pedersen LS, Morgan DJ, Kamp WL Van De, Christensen J, Jespersen P. Effects on SOx and NOx Emissions by Co-Firing Straw and Pulverized Coal. Energy & Fuels 1997;11:439–46. doi:10.1021/ef960110k.

[171] Glarborg P. Hidden interactions-Trace species governing combustion and emissions. Proc Combust Inst 2007;31 I:77–98. doi:10.1016/j.proci.2006.08.119.

[172] Konttinen J, Kallio S, Hupa M, Winter F. NO formation tendency characterization for solid fuels in fluidized beds. Fuel 2013;108:238–46. doi:10.1016/j.fuel.2013.02.011.

[173] Bai J, Yu C, Li L, Wu P, Luo Z, Ni M. Experimental Study on the NO and N_2O Formation Characteristics during Biomass Combustion. Energy & Fuels 2012;27:515–22. doi:10.1021/ef301383g.

[174] Giuntoli J, De Jong W, Verkooijen AHM, Piotrowska P, Zevenhoven M, Hupa M. Combustion characteristics of biomass residues and biowastes: Fate of fuel nitrogen. Energy and Fuels 2010;24:5309–19. doi:10.1021/ef100571n.

[175] Li P, Chyang C. A comprehensive study on NOx emission and fuel nitrogen conversion of solid biomass in bubbling fl uidized beds under staged combustion. J Energy Inst 2019. doi:10.1016/j.joei.2019.02.007.

[176] Qian FP, Chyang CS, Huang KS, Tso J. Combustion and NO emission of high nitrogen content biomass in a pilot-scale vortexing fluidized bed combustor. Bioresour Technol 2011;102:1892–8. doi:10.1016/j.biortech.2010.08.008.

[177] Werther J, Ogada T. Sewage sludge combustion. Prog Energy Combust Sci 1999;25:55–116. doi:10.1016/S0360-1285(98)00020-3.

[178] Hampartsoumian E, Gibbs BM. NOX formation and reduction in fluidized bed combustors. J Energy Inst 1987;57:402–10.

[179] Hill SC, Smoot LD. Modeling of nitrogen oxides formation and destruction in combustion systems. Prog Energy Combust Sci 2000;26:417–58. doi:10.1016/S0360-1285(00)00011-3.

[180] Gibbs BM, Hedley AB. A pilot plant study of large coal combustion in a fluidised bed. Proc Combust Inst 1978;17:211–20.

[181] Jensen A, Johnsson JE. Modelling of NOx emissions from pressurized fluidized bed combustion--a parameter study. Chem Eng Sci 1997;52:1715–31.

[182] Duan F, Chen J, Zhang L, Li P, Chyang C. Investigation of the Vortexing Effect on Sawdust Combustion in a Fluidized Bed Combustor. Energy & Fuels 2016:1701–7. doi:10.1021/acs.energyfuels.5b01976.

[183] Leckner B. Fluidized bed combustion: Mixing and pollutant limitation. Prog Energy Combust Sci 1998;24:31–61. doi:10.1016/S0360-1285(97)00021-X.

[184] Kouprianov VI, Permchart W. Emissions from a conical FBC fired with a biomass fuel. Appl Energy 2003;74:383–92. doi:10.1016/S0306-2619(02)00194-0.

[185] Kuprianov VI, Kaewklum R, Chakritthakul S. Effects of operating conditions and fuel properties on emission performance and combustion ef fi ciency of a swirling fl uidized-bed combustor fi red with a biomass fuel. Energy 2011;36:2038–48. doi:10.1016/j.energy.2010.05.026.

[186] Escandon LS, Ordonez S, Dies F V., Sastre H. Ammonia oxidation over conventional combustion catalysts. React Kinet Catal Lett 2002;76:61–8.

[187] Shimizu T, Satoh M, Fujikawa T, Tonsho M. Simultaneous Reduction of SO2 , NOX , and N2O Emissions from a Two-Stage Bubbling Fluidized Bed Combustor. Energy & Fuels 2000;14:862–8. doi:10.1021/ef9902202.

[188] Åmand L-E, Leckner B, Dam-Johansen K. Influence of SO_2 on the NO/N_2O chemistry in fluidized bed combustion. Fuel 1993;72:557–64. doi:10.1016/0016-2361(93)90116-J.

[189] Cammarota A, Chirone R, Salatino P, Solimene R, Urciuolo M. Particulate and gaseous emissions during fluidized bed combustion of semi-dried sewage sludge: Effect of bed ash accumulation on NOx formation. Waste Manag 2013;33:1397–402. doi:10.1016/j.wasman.2013.02.016.

[190] Ninduangdee P, Kuprianov VI. Bioresource Technology Combustion of an oil palm residue with elevated potassium content in a fluidized-bed combustor using alternative bed materials for preventing bed agglomeration. Bioresour Technol 2015;182:272–81. doi:10.1016/j.biortech.2015.01.128.

[191] Hindiyarti L, Frandsen F, Livbjerg H, Glarborg P. Influence of potassium chloride on moist CO oxidation under reducing conditions: Experimental and kinetic modeling study. Fuel

2006;85:978–88. doi:10.1016/j.fuel.2005.10.021.

[192] Babushok VI, Linteris GT, Hoorelbeke P, Roosendans D, van Wingerden K. Flame Inhibition by Potassium-Containing Compounds. Combust Sci Technol 2017;189:2039–55. doi:10.1080/00102202.2017.1347162.

[193] Wang J, Anthony EJ. CO oxidation and the inhibition effects of halogen species in fluidised bed combustion. Combust Theory Model 2009;13:105–19. doi:10.1080/13647830802444093.

[194] Wei X, Schnell U, Han X, Hein KRG. Interactions of CO, HCl, and SOxin pulverised coal flames. Fuel 2004;83:1227–33. doi:10.1016/j.fuel.2003.12.004.

[195] Winter F, Wartha C, Löffler G, Hofbauer H. The NO and N_2O formation mechanism during devolatilization and char combustion under fluidized-bed conditions. Symp Combust 1996;26:3325–34. doi:10.1016/S0082-0784(96)80180-9.

[196] Anthony E. Chemical links between different pollutant emissions from a small bubbling FBC. Fuel 1998;77:713–28. doi:10.1016/S0016-2361(97)00225-1.

[197] Julien S, Brereton CMH, Lim CJ, Grace JR, Anthony EJ. The effect of halides on emissions from circulating fluidized bed combustion of fossil fuels. Fuel 1996;75:1655–63. doi:10.1016/S0016-2361(96)00135-4.

[198] Wei X, Wang Y, Liu D, Sheng H. Influence of HCl on CO and NO emissions in combustion. Fuel 2009;88:1998–2003. doi:10.1016/j.fuel.2009.03.009.

[199] Wei X, Han X, Schnell U, Maier J, Wörner H, Hein KRG. The effect of HCl and SO2 on NOx formation in coal flames. Energy and Fuels 2003;17:1392–8. doi:10.1021/ef030010w.

[200] Valk M, Bramer EA, Tossaint HHJ. Optimal staged combustion conditions in a fluidised bed for simultaneous low NOX and SO2 emission levels. 1989 Int. Conf. Fluid. Bed Combust. Fbc - Technol. Today, 1989, p. 995–1001.

[201] Shimizu T, Han J, Choi S, Kim L, Kim H. Fluidized-Bed Combustion Characteristics of Cedar Pellets by Using an Alternative Bed Material. Energy & Fuels 2006;20:2737–42. doi:10.1021/ef0601723.

[202] Han J, Kim H. The effect of the particle size of alumina sand on the combustion and emission behavior of cedar pellets in a fluidized bed combustor. Bioresour Technol 2008;99:3782–6. doi:10.1016/j.biortech.2007.07.010.

[203] Jensen A, Johnsson JE, Andries J, Laughlin K, Read G, Mayer M, et al. Formation and Reduction of Nox in Pressurized Fluidized-Bed Combustion of Coal. Fuel 1995;74:1555–69. doi:10.1016/0016-2361(95)00155-x.

[204] Kuprianov VI, Permchart W, Janvijitsakul K. Fluidized bed combustion of pre-dried Thai bagasse. Fuel Process Technol 2005;86:849–60. doi:10.1016/j.fuproc.2004.09.002.

[205] Kuprianov VI, Janvijitsakul K, Permchart W. Co-firing of sugar cane bagasse with rice husk in a conical fluidized-bed combustor. Fuel 2006;85:434–42. doi:10.1016/j.fuel.2005.08.013.

[206] Findlay K, Probert SD. Limiting NO_X and SO_2 emissions from an industrial-size fluidised bed

combustor. Appl Energy 1993;45:1–99.

[207] Skopec P, Hrdlička J, Opatřil J, Štefanica J. NO_X emissions from bubbling fluidized bed combustion of lignite coal. Acta Polytech 2015;55:275–81. doi:10.14311/AP.2015.55.0275.

[208] Armesto L, Bahillo A, Veijonen K, Cabanillas A, Otero J. Combustion behaviour of rice husk in a bubbling uidised bed. Biomass and Bioenergy 2002;23:171–9.

[209] Shahzad K, Saleem M, Kazmi M, Ali Z, Hussain S, Akhtar NA, et al. Effect of Hydrodynamic Conditions on Emissions of NO_X , SO_2 , and CO from Co-Combustion of Wheat Straw and Coal Under Fast Fluidized Bed Condition and CO from Co-Combustion of Wheat Straw and Coal Under. Combust Sci Technol 2016;188:1303–18. doi:10.1080/00102202.2016.1190344.

[210] de Diego LF, Londonot CA, Wang XS, Gibbs BM. Influence of operating parameters on NOx and N20 axial profiles in a circulating fluidized bed combustor. Fuel 1996;75:971–8.

[211] Duan F, Liu J, Chyang C, Hu C, Tso J. Combustion behavior and pollutant emission characteristics of RDF (refuse derived fuel) and sawdust in a vortexing fl uidized bed combustor. Energy 2013;57:421–6. doi:10.1016/j.energy.2013.04.070.

[212] Tarelho LAC, Matos MAA, Pereira FJMA. Axial concentration profiles and N2O flue gas in a pilot scale bubbling fluidised bed coal combustor. Fuel Process Technol 2005;86:925–40. doi:10.1016/j.fuproc.2004.10.003.

[213] Sher F, Pans MA, Afilaka DT, Sun C, Liu H. Experimental investigation of woody and non-woody biomass combustion in a bubbling fluidised bed combustor focusing on gaseous emissions and temperature profiles. Energy 2017;141:2069–80. doi:10.1016/j.energy.2017.11.118.

[214] Toftegaard MB, Brix J, Jensen PA, Glarborg P, Jensen AD. Oxy-fuel combustion of solid fuels. Prog Energy Combust Sci 2010;36:581–625. doi:10.1016/j.pecs.2010.02.001.

[215] Hashemi H, Hansen S, Toftegaard MB, Pedersen KH, Jensen AD, Dam-Johansen K, et al. A model for nitrogen chemistry in oxy-fuel combustion of pulverized coal. Energy and Fuels 2011;25:4280–9. doi:10.1021/ef200853t.

[216] Park D-C, Day SJ, Nelson PF. Nitrogen release during reaction of coal char with O2, CO2, and H2O. Proc Combust Inst 2005;30:2169–75. doi:10.1016/j.proci.2004.08.051.

[217] Anthony EJ, Lu Y. Relationship between so 2 and other pollutant emissions from fluidized-bed combustion. Combustion 1998;2:3093–101. doi:10.1016/S0082-0784(98)80171-9.

[218] Zhang G, Liu H, Ge Y, Gao S. Gaseous emission and ash characteristics from combustion of high ash content antibiotic mycelial residue in fluidized bed and the impact of additional water vapor. Fuel 2017;202:66–77. doi:10.1016/j.fuel.2017.04.028.

[219] Zhu C, Liu S, Liu H, Yang J, Liu X, Xu G. NOx emission characteristics of fluidized bed combustion in atmospheres rich in oxygen and water vapor for high-nitrogen fuel. Fuel 2015;139:346–55. doi:10.1016/j.fuel.2014.08.058.

[220] Hartman M, Svoboda K, Pohořelý M, Trnka O. Combustion of dried sewage sludge in a fluidized-bed reactor. Ind Eng Chem Res 2005;44:3432–41. doi:10.1021/ie040248n.

[221] Åmand LE, Leckner B. Influence of fuel on the emission of nitrogen oxides (NO and N2O) from an 8-MW fluidized bed boiler. Combust Flame 1991;84:181–96. doi:10.1016/0010-2180(91)90047-F.

[222] Okasha F. Staged combustion of rice straw in a fluidized bed. Exp Therm Fluid Sci 2007;32:52–9. doi:10.1016/j.expthermflusci.2007.01.006.

[223] Shimizu T, Tachiyama Y, Souma M, Inagaki M. Emission control of NOX and N2O of bubbling fluidized bed combustor. Proc. Int. Conf. Fluid. Bed Combust., vol. 2, 1991, p. 695–700.

[224] Gibbs BM, Salam TF, Sibtain SF, Pragnell RJ, Gauld DW. The reduction of NOx emissions from a fluidized bed combustor by staged combustion combined with ammonia addition. Twenty-Second Symp Combust 1988:1147–54. doi:10.1016/S0082-0784(89)80125-0.

[225] Sirisomboon K, Kuprianov VI. Effects of fuel staging on the NO emission reduction during biomass-biomass co-combustion in a fluidized-bed combustor. Energy and Fuels 2017;31:659–71. doi:10.1021/acs.energyfuels.6b02622.

[226] Kuprianov VI, Ninduangdee P, Suheri P. Co-firing of oil palm residues in a fuel staged fluidized-bed combustor using mixtures of alumina and silica sand as the bed material. Appl Therm Eng 2018;144:371–82. doi:10.1016/j.applthermaleng.2018.08.089.

[227] de Diego LF, de las Obras-Loscertales M, Rufas A, García-Labiano F, Gayán P, Abad A, et al. Pollutant emissions in a bubbling fluidized bed combustor working in oxy-fuel operating conditions: Effect of flue gas recirculation. Appl Energy 2013;102:860–7. doi:10.1016/j.apenergy.2012.08.053.

[228] Kim HY, Baek SW, Lee CY. Effects of hybrid reburning system with SNCR and air staging on NO x reduction and thermal characteristics in oxygen-cnhanced combustion. Combust Sci Technol 2009;181:1289–309. doi:10.1080/00102200903074246.

[229] Xu H, Smoot LD, Hill SC. Computational model for NOx reduction by advanced reburning. Energy and Fuels 1999;13:411–20. doi:10.1021/ef980090h.

[230] Mahmoudi S, Baeyens J, Seville JPK. NOx formation and selective non-catalytic reduction (SNCR) in a fluidized bed combustor of biomass. Biomass and Bioenergy 2010;34:1393–409. doi:10.1016/j.biombioe.2010.04.013.

[231] Smoot LD, Hill SC, Xu H. NOx control through reburning. Prog Energy Combust Sci 1998;24:385–408. doi:10.1016/S0360-1285(97)00022-1.

[232] Speth K, Murer M, Spliethoff H. Experimental Investigation of Nitrogen Species Distribution in Wood Combustion and Their Influence on NOx Reduction by Combining Air Staging and Ammonia Injection. Energy and Fuels 2016;30:5816–24. doi:10.1021/acs.energyfuels.6b00943.

[233] Miroslav R. Reduction of nitrogen oxides in flue gases. Environ Pollut 1998;102:685–9. doi:10.1016/S0269-7491(98)80099-7.

[234] Spliethoff H, Greul U, Rdiger H, Hein KRG. Basic effects on NOx emissions in air staging and reburning at a bench-scale test facility. Fuel 1996;75:560–4.

[235] Spliethoff H, Scheurer W, Hein KRG. Effect of co-combustion of sewage sludge and biomass on emissions and heavy metals behaviour. Process Saf Environ Prot 2000;78:33–9. doi:10.1205/095758200530420.

[236] Bowman CT. Control of combustion-generated nitrogen oxide emissions: technology driven by regulation. Proc Combust Inst 1992;24:859–78.

[237] Hayhurst AN, Lawrence AD. Emissions of Nitrous Oxide from Combustion Sources. Prog Energy Combust Sci 1992;18:529–52.

[238] Lyngfelt A, Amand L, Leckner B. Reversed air staging - a method for reduction of N20 emissions from fluidized bed combustion of coal. Fuel 1998;77:953–9.

[239] Hou X, Zhang H, Pilawska M, Lu J, Yue G. The formation of N 2 O during the reduction of NO by NH 3. Fuel 2008;87:3271–7. doi:10.1016/j.fuel.2008.05.009.

[240] Mendoza-covarrubias C, Romero CE, Hernandez-rosales F, Agarwal H. N 2 O Formation in Selective Non-Catalytic NO x Reduction Processes. J Environ Prot (Irvine, Calif) 2011;2:1095–100. doi:10.4236/jep.2011.28126.

[241] Gao F, Tang X, Yi H, Zhao S, Li C, Li J, et al. A Review on Selective Catalytic Reduction of NO x by NH3 over Mn-Based catalyst at Low Temperatures: Catalysts, Mechnaisms, Kinetics and DFT Calculations. Catalysts 2017:1–32. doi:10.3390/catal7070199.

[242] Zhu M, Lai J, Wachs IE. Environmental Formation of N 2 O greenhouse gas during SCR of NO with NH 3 by supported vanadium oxide catalysts. Appl Catal B Environ 2018;224:836–40. doi:10.1016/j.apcatb.2017.11.029.

[243] Liu DC, Mi T, Shen BX, Feng B, Franz W. Reducing N2O emission by Co-combustion of coal and biomass. Energy and Fuels 2002;16:525–6. doi:10.1021/ef010108f.

[244] Lu L, Jin Y, Liu H, Ma X, Yoshikawa K. Nitrogen evolution during the co-combustion of hydrothermally treated municipal solid waste and coal in a bubbling fluidized bed. Waste Manag 2014;34:79–85. doi:10.1016/j.wasman.2013.08.025.

[245] Areeprasert C, Scala F, Coppola A, Urciuolo M, Chirone R, Chanyavanich P, et al. Fluidized bed co-combustion of hydrothermally treated paper sludge with two coals of different rank. Fuel Process Technol 2016;144:230–8. doi:10.1016/j.fuproc.2015.12.033.

[246] Åmand L, Miettinen-Westberg H, Karlsson M. Co-combustion of sewage sludge with wood/coal in a circulating fluidised bed boiler - A study of NO and N2O emissions. Proc. 3rd Int. Symp. Inciner. Flue Gas Treat. Technol., Bryssels, Belgium: 2001, p. Session 5.

[247] Åmand LE, Svärd SH, Eskilsson D, Leckner B, Gyllenhammar M, Tuillin C. Co-combustion of pulp- and paper sludge with wood - emissions of nitrogen, sulphur and chlorine compounds. 17th Int. Fluid. bed Combust. Conf., Jacksonville, Florida, USA: 2003.

[248] Shimizu T, Toyono M. Emissions of NOx and N2O during co-combustion of dried sewage sludge with coal in a circulating fluidized bed combustor. Fuel 2007;86:2308–15. doi:10.1016/j.fuel.2007.01.033.

[249] Duan L, Duan Y, Zhao C, Anthony EJ. NO emission during co-firing coal and biomass in an

oxy-fuel circulating fluidized bed combustor. Fuel 2015;150:8–13. doi:10.1016/j.fuel.2015.01.110.

[250] Pedersen LS, Nielsen HP, Kiil S, Hansen LA, Dam-Johansen K, Kildsig F, et al. Full-scale co-firing of straw and coal. Fuel 1996;75:1584–90. doi:10.1016/0016-2361(96)82642-1.

[251] Robinson AL, Junker H, Buckley SG, Sclippa G, Baxter LL. Interactions between coal and biomass when cofiring. Symp Combust 1998;27:1351–9. doi:10.1016/S0082-0784(98)80540-7.

[252] Nadziakiewicz J, Kozioł M. Co-combustion of sludge with coal. Appl Energy 2003;75:239–48. doi:10.1016/S0306-2619(03)00037-0.

[253] Jin Y, Li Y, Liu F. Combustion effects and emission characteristics of SO2, CO, NOx and heavy metals during co-combustion of coal and dewatered sludge. Front Environ Sci Eng 2016;10:201–10. doi:10.1007/s11783-014-0739-9.

[254] Aničić B. Agglomeration Mechanisms during Fluidized Bed Combustion of Biomass. Technical University of Denmark, 2018.

[255] Grass SW, Jenkins BM. Biomass fueled fluidized bed combustion: Atmospheric emissions, emission control devices and environmental regulations. Biomass and Bioenergy 1994;6:243–60. doi:10.1016/0961-9534(94)90064-7.

[256] Pilawska M, Butler CJ, Hayhurst AN, Chadeesingh DR. The production of nitric oxide during the combustion of methane and air in a fluidized bed. Combust Flame 2001;127:2181–93. doi:10.1016/S0010-2180(01)00319-4.

[257] Krum K. Decomposition of urea. Technical University of Denmark, 2017.

[258] Li PW, Chyang CS, Ni HW. An experimental study of the effect of nitrogen origin on the formation and reduction of NOx in fluidized-bed combustion. Energy 2018;154:319–27. doi:10.1016/j.energy.2018.04.141.

[259] Löffler G, Wargadalam VJ, Winter F. Catalytic effect of biomass ash on CO , CH4 and HCN oxidation under fluidised bed combustor conditions 2002;81.

[260] Wang G, Jensen PA, Wu H, Frandsen FJ, Laxminarayan Y, Sander B, et al. Potassium capture by coal fly ash: K2CO3, KCl and K2SO4. Fuel Process Technol 2019;194:106–15. doi:10.1016/j.fuproc.2019.05.038.

[261] Wang G, Jensen PA, Wu H, Frandsen FJ, Sander B, Glarborg P. Potassium Capture by Kaolin, Part 2: K2CO3, KCl, and K2SO4. Energy and Fuels 2018;32:3566–78. doi:10.1021/acs.energyfuels.7b04055.

[262] Koebel M, Strutz EO. Thermal and hydrolytic decomposition of urea for automotive selective catalytic reduction systems: Thermochemical and practical aspects. Ind Eng Chem Res 2003;42:2093–100. doi:10.1021/ie020950o.

[263] LIEN YC, NAWAR WW. THERMAL DECOMPOSITION OF SOME AMINO ACIDS. Alanine and β-Alanine. J Food Sci 1974;39:914–6. doi:10.1111/j.1365-2621.1974.tb07275.x.

[264] Sato N, Quitain AT, Kang K, Daimon H, Fujie K. Reaction Kinetics of Amino Acid Decomposition in High-Temperature and High-Pressure Water. Ind Eng Chem Res 2004;43:3217–22. doi:10.1021/ie020733n.

[265] Yablokov VY, Smel'tsova IL, Zelyaev IA, Mitrofanova S V. Studies of the rates of thermal decomposition of glycine, alanine, and serine. Russ J Gen Chem 2009;79:1704–6. doi:10.1134/S1070363209080209.

[266] Hosoda H, Hirama T, Azuma N, Kuramoto K, Hayashi J, Chiba T. NO_X and N_2O Emission in Bubbling Fluidized-Bed Coal Combustion with Oxygen and Recycled Flue Gas: Macroscopic Characteristics of Their Formation and Reduction. Energy & Fuels 1998;12:102–8. doi:10.1021/ef970075x.

[267] Lin W, Dam-Johansen K. NO emissions in fluidized bed combustion of biomass. Proc. 4th Int. Conf. Technol. Combust. a Clean Environ., 1997, p. 13–9.

[268] Arvelakis S, Vourliotis P, Kakaras E, Koukios EG. Effect of leaching on the ash behavior of wheat straw and olive residue during fuidized bed combustion. Biomass and Bioenergy 2001;20:459–70.

[269] Bakker RR, Jenkins BM, Williams RB. Fluidized Bed Combustion of Leached Rice Straw. Energy & Fuels 2002;16:356–65. doi:10.1021/ef010197w.

[270] Karnowo, Zahara ZF, Kudo S, Norinaga K, Hayashi JI. Leaching of alkali and alkaline earth metallic species from rice husk with bio-oil from its pyrolysis. Energy and Fuels 2014;28:6459–66. doi:10.1021/ef501748h.

[271] Liu H, Zhang L, Han Z, Xie B, Wu S. The effects of leaching methods on the combustion characteristics of rice straw. Biomass and Bioenergy 2013;49:22–7. doi:10.1016/j.biombioe.2012.12.024.

[272] Yu C, Thy P, Wang L, Anderson SN, Vandergheynst JS, Upadhyaya SK, et al. Influence of leaching pretreatment on fuel properties of biomass. Fuel Process Technol 2014;128:43–53. doi:10.1016/j.fuproc.2014.06.030.

[273] Weidong F, Zhengchun L, Youyi L, Jinguo K, Mingchuan Z. Effect of air-staging on anthracite combustion and NOx formation. Energy & Fuels 2009;23:111–20. doi:10.1021/ef800343j.

[274] Chyang CS, Duan F, Lin SM, Tso J. A study on fluidized bed combustion characteristics of corncob in three different combustion modes. Bioresour Technol 2012;116:184–9. doi:10.1016/j.biortech.2012.04.041.

[275] Lupiáñez C, Díez LI, Romeo LM. Influence of gas-staging on pollutant emissions from fluidized bed oxy-firing. Chem Eng J 2014;256:380–9. doi:10.1016/j.cej.2014.07.011.

[276] Hupa M. Ash-related issues in fluidized-bed combustion of biomasses: Recent research highlights. Energy and Fuels 2012;26:4–14. doi:10.1021/ef201169k.

[277] Chaivatamaset P, Tia S. The characteristics of bed agglomeration during fl uidized bed combustion of eucalyptus bark. Appl Therm Eng 2015;75:1134–46. doi:10.1016/j.applthermaleng.2014.10.046.

[278] Arromdee P, Kuprianov VI. Combustion of peanut shells in a cone-shaped bubbling fluidized-bed combustor using alumina as the bed material. Appl Energy 2012;97:470–82. doi:10.1016/j.apenergy.2012.03.048.

[279] Öhman M, Nordin A. The Role of Kaolin in Prevention of Bed Agglomeration during Fluidized Bed Combustion of Biomass Fuels. Energy & Fuels 2000:618–24. doi:10.1021/ef990198c.

[280] Billen P, Costa J, Aa L Van Der, Westdorp L, Caneghem J Van, Vandecasteele C. An Agglomeration Index for CaO Addition (as CaCO 3) to Prevent De fl uidization : Application to a Full-Scale Poultry Litter Fired FBC. Energy & Fuels 2014;28:5455–62. doi:10.1021/ef500621w.

[281] Teixeira P, Lopes H, Gulyurtlu I, Lapa N, Abelha P. Evaluation of slagging and fouling tendency during biomass co-firing with coal in a fluidized bed. Biomass and Bioenergy 2012;39:192–203. doi:10.1016/j.biombioe.2012.01.010.

[282] Vamvuka D, Zografos D, Alevizos G. Control methods for mitigating biomass ash-related problems in fluidized beds. Bioresour Technol 2008;99:3534–44. doi:10.1016/j.biortech.2007.07.049.

[283] Wang G, Jensen PA, Wu H, Frandsen FJ, Sander B, Glarborg P. Potassium Capture by Kaolin, Part 1: KOH. Energy & Fuels 2018;32:1851–62. doi:10.1021/acs.energyfuels.7b03645.

[284] Grimm A, Skoglund N, Boström D, Boman C, Öhman M. Influence of phosphorus on alkali distribution during combustion of logging residues and wheat straw in a bench-scale fluidized bed. Energy and Fuels 2012;26:3012–23. doi:10.1021/ef300275e.

[285] Piotrowska P, Grimm A, Skoglund N, Boman C, Öhman M, Zevenhoven M, et al. Fluidized-bed combustion of mixtures of rapeseed cake and bark: The resulting bed agglomeration characteristics. Energy and Fuels 2012;26:2028–37. doi:10.1021/ef300130e.

[286] Billen P, Creemers B, Costa J, Van Caneghem J, Vandecasteele C. Coating and melt induced agglomeration in a poultry litter fired fluidized bed combustor. Biomass and Bioenergy 2014;69:71–9. doi:10.1016/j.biombioe.2014.07.013.

[287] Wu H, Pedersen MN, Jespersen JB, Aho M, Roppo J, Frandsen FJ, et al. Modeling the use of sulfate additives for potassium chloride destruction in biomass combustion. Energy and Fuels 2014;28:199–207. doi:10.1021/ef4015108.

[288] Olofsson G, Ye Z, Bjerle I, Andersson A. Bed agglomeration problems in fluidized-bed biomass combustion. Ind Eng Chem Res 2002;41:2888–94. doi:10.1021/ie010274a.

[289] Chen Z, Yang W, Zhou J, Lv H, Liu J, Cen K. HNCO hydrolysis performance in urea-water solution thermohydrolysis process with and without catalysts. J Zhejiang Univ A 2010;11:849–56. doi:10.1631/jzus.a0900798.

[290] Balland M, Froment K, Ratel G, Valin S, Roussely J, Michel R, et al. Biomass Ash Fluidised-Bed Agglomeration: Hydrodynamic Investigations. Waste and Biomass Valorization 2017;8:2823–41. doi:10.1007/s12649-017-9853-9.

[291] Rowe PN. Prediction of bubble size in a gas fluidised bed. Chem Eng Sci 1976;31:285–8.

doi:10.1016/0009-2509(76)85073-7.

[292] Thomas KM. The release of nitrogen oxides during char combustion. Fuel 1997;76:457–73. doi:10.1016/S0016-2361(97)00008-2.

[293] Aarna I, Suuberg EM. A review of the kinetics of the nitric oxide-carbon reaction. Fuel 1997;76:475–91. doi:10.1016/S0016-2361(96)00212-8.

[294] Dong L, Gao S, Song W, Xu G. Experimental study of NO reduction over biomass char. Fuel Process Technol 2007;88:707–15. doi:10.1016/j.fuproc.2007.02.005.

[295] Wu X, Song Q, Zhao H, Yao Q. Catalytic Mechanism of Inherent Potassium on the Char-NO Reaction. Energy and Fuels 2015;29:7566–71. doi:10.1021/acs.energyfuels.5b01550.

[296] Calo JM, Suuberg EM, Aarna I. The Role of Surface Area in the NO-Carbon Reaction. Energy & Fuels 1999;13:761–2.

[297] Molina A, Murphy JJ, Winter F, Haynes BS, Blevins LG, Shaddix CR. Pathways for conversion of char nitrogen to nitric oxide during pulverized coal combustion. Combust Flame 2009;156:574–87. doi:10.1016/j.combustflame.2008.11.012.

[298] Aho A, DeMartini N, Pranovich A, Krogell J, Kumar N, Eränen K, et al. Pyrolysis of pine and gasification of pine chars - Influence of organically bound metals. Bioresour Technol 2013;128:22–9. doi:10.1016/j.biortech.2012.10.093.

[299] Zevenhoven M, Yrjas P, Skrifvars BJ, Hupa M. Characterization of ash-forming matter in various solid fuels by selective leaching and its implications for fluidized-bed combustion. Energy and Fuels 2012;26:6366–86. doi:10.1021/ef300621j.

[300] Khazraie Shoulaifar T, Demartini N, Zevenhoven M, Verhoeff F, Kiel J, Hupa M. Ash-forming matter in torrefied birch wood: Changes in chemical association. Energy and Fuels 2013;27:5684–90. doi:10.1021/ef4005175.

[301] Benson SA, Holm PL. Comparison of Inorganic Constituents in Three Low-Rank Coals. Ind Eng Chem Prod Res Dev Chem Prod Res Dev 1985;2:145–9.

[302] Tchoffor PA, Moradian F, Pettersson A, Davidsson KO, Thunman H. Influence of Fuel Ash Characteristics on the Release of Potassium, Chlorine, and Sulfur from Biomass Fuels under Steam-Fluidized Bed Gasification Conditions. Energy and Fuels 2016;30:10435–42. doi:10.1021/acs.energyfuels.6b01470.

[303] Wu SL, Iisa K. Kinetics of NO Reduction by Black Liquor Char. Energy & Fuels 1998;12:457–63.

[304] Levy JM, Chan LK, Sarofim AF, Beér JM. NO/char reactions at pulverized coal flame conditions. Symp Combust 1981;18:111–20. doi:10.1016/S0082-0784(81)80016-1.

[305] Guo F, Hecker WC. Effects of CaO and burnout on the kinetics of NO reduction by Beulah Zap char. Symp Combust 1996;26:2251–7.

[306] Guo F, Hecker WC. Kinetics of NO reduction by char: Effects of coal rank. Symp Combust 1998;27:3085–92. doi:10.1016/S0082-0784(98)80170-7.

[307] Schönenbeck C, Gadiou R, Schwartz D. A kinetic study of the high temperature NO-char reaction. Fuel 2004;83:443–50. doi:10.1016/j.fuel.2003.08.007.

[308] Garijo EG, Jensen AD, Glarborg P. Kinetic Study of NO Reduction over Biomass Char under Dynamic Conditions. Energy & Fuels 2003;17:1429–36.

[309] Garijo EG, Jensen AD, Glarborg P. Reactivity of coal char in reducing NO. Combust Flame 2004;136:249–53. doi:10.1016/j.combustflame.2003.09.007.

[310] Ninomiya Y, Yokoi K, Arai N, Hasatani M. Characteristics of emission of char NO during the combustion of a single particle of coal char. Int Chem Eng 1989;29:512–6.

[311] Winter F, Löffler G, Wartha C, Hofbauer H, Preto F, Anthony EJ. The NO and N20 Formation Mechanism under Circulating Fluidized Bed Combustor Conditions: from the Single Particle to the Pilot-Scale. Can J Chem Eng 1999;77:275–83.

[312] Molina A, Sarofim AF, Ren W, Lu J, Yue G, Beér JM, et al. Effect of boundary layer reactions on the conversion of CHAR-N to NO, N 2 O, and HCN at fluidized-bed combustion conditions. Combust Sci Technol 2002;174:43–71. doi:10.1080/713712945.

[313] López D, Calo J. The N2O-carbon reaction: The influence of potassium and CO on reactivity and populations of oxygen surface complexes. Fuel 2007;86:1900–7. doi:10.1021/ef070034t.

[314] Johnsson JE, Jensen A. Effective diffusion coefficients in coal chars. Proc Combust Inst 2000;28:2353–9. doi:10.1016/S0082-0784(00)80647-5.

[315] Dong L, Gao S, Song W, Xu G. Experimental study of NO reduction over biomass char. Fuel Process Technol 2007;88:707–15. doi:10.1016/j.fuproc.2007.02.005.

[316] Guerrero M, Millera Á, Alzueta MU, Bilbao R. Experimental and Kinetic Study at High Temperatures of the NO Reduction over Eucalyptus Char Produced at Different Heating Rates. Energy & Fuels 2011;25:1024–33.

[317] Wu XY, Song Q, Zhao HB, Zhang ZH, Yao Q. Kinetic modeling of inherent mineral catalyzed No reduction by biomass char. Environ Sci Technol 2014;48:4184–90. doi:10.1021/es405521k.

[318] Pevida C, Arenillas A, Rubiera F, Pis JJ. Heterogeneous reduction of nitric oxide on synthetic coal chars. Fuel 2005;84:2275–9. doi:10.1016/j.fuel.2005.06.003.

[319] Chambrion P, Orikasa H, Suzuki T, Kyotani T, Tomita A. A study of the C-NO reaction by using isotopically labelled C and NO. Fuel 1997;76:493–8.

[320] Stańczyk K. Nitrogen oxide evolution from nitrogen-containing model chars combustion. Energy and Fuels 1999;13:82–7. doi:10.1021/ef9801017.

[321] Stańczyk K. Temperature-time sievei - A case of nitrogen in coal. Energy and Fuels 2004;18:405–9. doi:10.1021/ef034018h.

[322] Wu H, Castro M, Jensen PA, Frandsen FJ, Glarborg P, Dam-Johansen K, et al. Release and transformation of inorganic elements in combustion of a high-phosphorus fuel. Energy and Fuels 2011;25:2874–86. doi:10.1021/ef200454y.

[323] Chambrion P, Kyotani T, Tomita A. C-NO reaction in the presence of O_2. Symp Combust 1998;27:3053–9.

[324] Seeker WR. Waste Combustion. Proc Combust Inst 1990;23:867–85.

[325] Rogaume T, Auzanneau M, Jabouille F, Goudeau JC, Torero JL. The effects of different airflows on the formation of pollutants during waste incineration. Fuel 2002;81:2277–88. doi:10.1016/S0016-2361(02)00151-5.

[326] Rogaume T, Jabouille F, Torero JL. Effect of excess air on grate combustion of solid wastes and on gaseous products. Int J Therm Sci 2009;48:165–73. doi:10.1016/j.ijthermalsci.2008.02.003.

[327] Zhou H, Jensen AD, Glarborg P, Jensen PA, Kavaliauskas A. Numerical modeling of straw combustion in a fixed bed. Fuel 2005;84:389–403. doi:10.1016/j.fuel.2004.09.020.

[328] Gunn DJ. On axial dispersion in fixed beds. Chem Eng Process 1993;32:333–8. doi:10.1016/0255-2701(93)80020-H.

[329] Fjellerup J, Henriksen U, Jensen AD, Jensen PA, Glarborg P. Heat transfer in a fixed bed of straw char. Energy and Fuels 2003;17:1251–8. doi:10.1021/ef030036n.

[330] Sin G, Gernaey K. Data handling and parameter estimation. In: Van Loosdrecht MCM, Nielsen PH, Lopez-Vazquez DM, Brdjanovic D, editors. Exp. Methods Wastewater Treat., London: IWA Publishing; 2016, p. 201–34.

[331] Karlström O, Brink A, Hupa M, Tognotti L. Multivariable optimization of reaction order and kinetic parameters for high temperature oxidation of 10 bituminous coal chars. Combust Flame 2011;158:2056–63. doi:10.1016/j.combustflame.2011.03.003.

[332] Karlström O, Brink A, Hupa M. Time dependent production of NO from combustion of large biomass char particles. Fuel 2013;103:524–32. doi:10.1016/j.fuel.2012.06.030.

[333] Nikolopoulos A, Malgarinos I, Nikolopoulos N, Grammelis P, Karrelas S, Kakaras E. A decoupled approach for NOx-N2O 3-D CFD modeling in CFB plants. Fuel 2014;115:401–15. doi:10.1016/j.fuel.2013.06.036.

[334] Barišić V, Kilpinen P, Hupa M. Comparison of the catalytic activity of bed materials from the combustion of biomass and waste fuels in a circulating fluidized bed boiler toward NO reduction by CO. Energy and Fuels 2006;20:1925–32. doi:10.1021/ef060094j.

[335] Jones JM, Patterson PM, Pourkashanian M, Williams a. Approaches to Modelling Heterogenous Char NO Formation/Destruction during Pulverised Coal Combustion. Carbon N Y 1999;37:1545–52.

[336] Bhatia SK, Perlmutter DD. A Rondom Pore Model for Fluid-Solid Reactions:1. Isothermal, Kinetic Control. AIChE J 1980;26:379–86.

[337] Makepeace JW, Wood TJ, Hunter HMA, Jones MO, David WIF. Ammonia decomposition catalysis using non-stoichiometric lithium imide. Chem Sci 2015;6:3805–15. doi:10.1039/c5sc00205b.

[338] David WIF, Makepeace JW, Callear SK, Hunter HMA, Taylor JD, Wood TJ, et al. Hydrogen production from ammonia using sodium amide. J Am Chem Soc 2014;136:13082–5. doi:10.1021/ja5042836.

[339] Duo W, Dam-Johansen K, Østergaard K. Kinetics of the gas-phase reaction between nitric oxide, ammonia, and oxygen. Can J Chem Eng 1992;70:1014–20.

[340] Dwivedi PN, Upadhyay SN. Particle-Fluid Mass Transfer in Fixed and Fluidized Beds. Ind Eng Chem Process Des Dev 1977;16:157–65. doi:10.1021/i260062a001.

[341] Figueiredo JL, Pereira MFR. The role of surface chemistry in catalysis with carbons. Catal Today 2010;150:2–7. doi:10.1016/j.cattod.2009.04.010.

Appendix A

A.1 NO_2 contribution to total NO_X

Figure A.1 depicts the NO and NO_2 effluent concentrations during fluidized bed mono-combustion of biomass. The maximum contribution of NO_2 was 95% in the case of pine wood. For the other fuels, negligible amounts of NO_2 were detected. The insignificance of NO_2 within the combustion chamber was additionally verified from local concentration measurements.

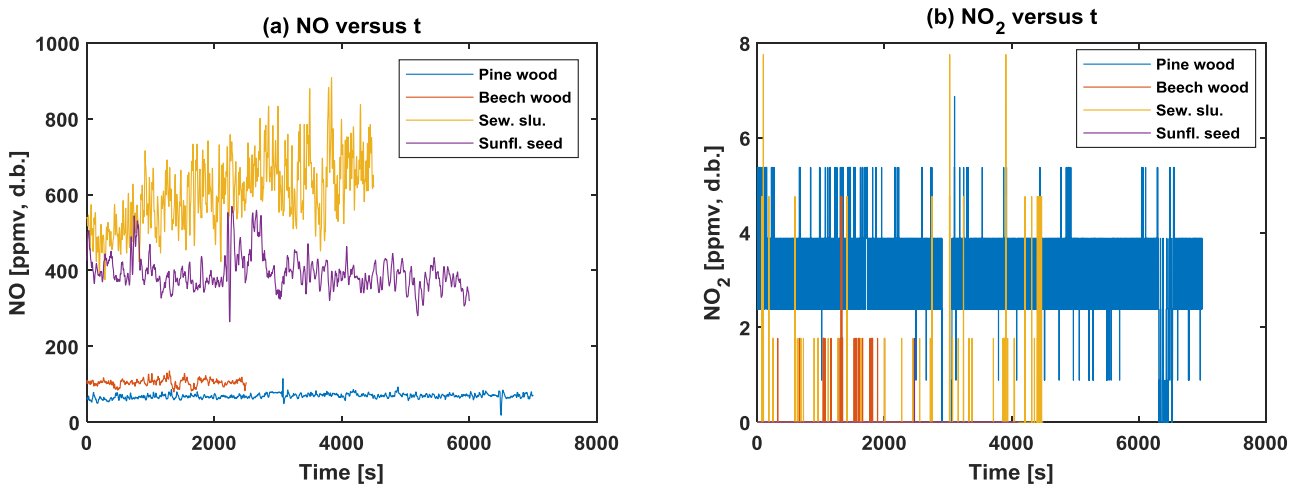

Figure A.1: Steady state NO (a) and NO_2 (b) effluent concentration against time during fluidized bed mono-combustion of biomass. Conditions: T_{bed} = 850ºC; λ = 1.4; λ_1/λ = 1.

A.2 Gas sampling probe commissioning and measurement procedure

Figure A.2 demonstrates the working principle of the water cooled probe used for local gas concentration measurements during fluidized bed combustion. A quartz wool filter was placed at the sample gas inlet of the probe to keep out solid material from entering and blocking the probe.

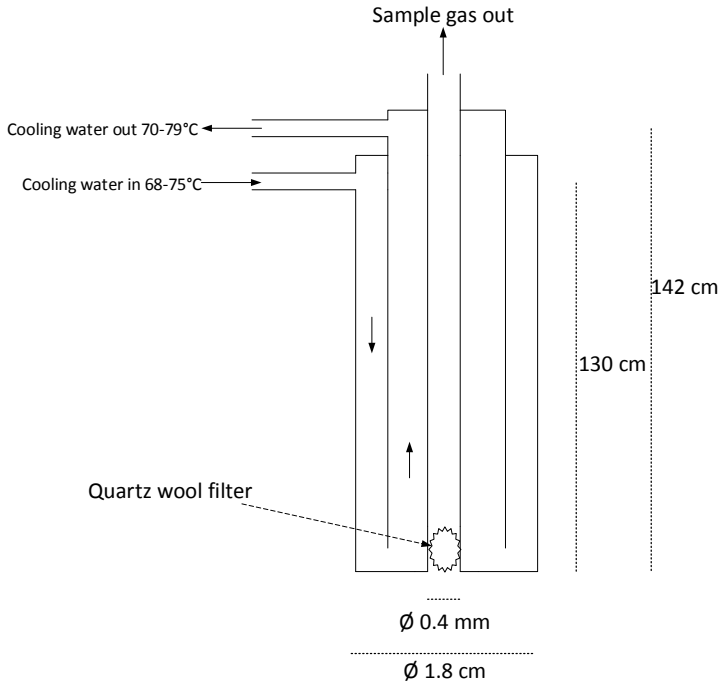

Figure A.2: Design and working principle of the water cooled probe used for local gas composition measurements in during fluid bed combustion.

Commissioning

When measuring the local gas composition, the temperature of the sample gas should be quenched to minimize secondary reactions within the probe. However, a minimum temperature exists below which the water in the flue gas may start condensing, thereby capturing some of the soluble species such as NH_3, HNCO etc. This minimum temperature corresponds to the point of highest H_2O concentration, which should appear below the secondary gas injection point. Based on combustion calculations and the fuel properties, the highest H_2O concentration for each fuel can be determined, as summarized Table A.1. Taking a safety margin and assuming that the maximum concentration of H_2O in the flue gas is 15%, the minimum temperature of the flue gas can be calculated as the dewpoint temperature using the Antoine equation. The results are summarized in Figure A.3, showing that the minimum temperature of the sample gas is 54.3ºC.

Table A.1: Theoretical maximum fraction of H_2O in the sample gas below the secondary gas feeding ($\mathbf{y_{H_2O,max}}$) during fluid bed combustion of biomass

Fuel	Pine wood	Beech wood	Straw	Sunfl. husk	Sew. slu.	Sunfl. seed
$\mathbf{y_{H_2O,max}}$	11	10.3	12	10.2	11.2	11.5

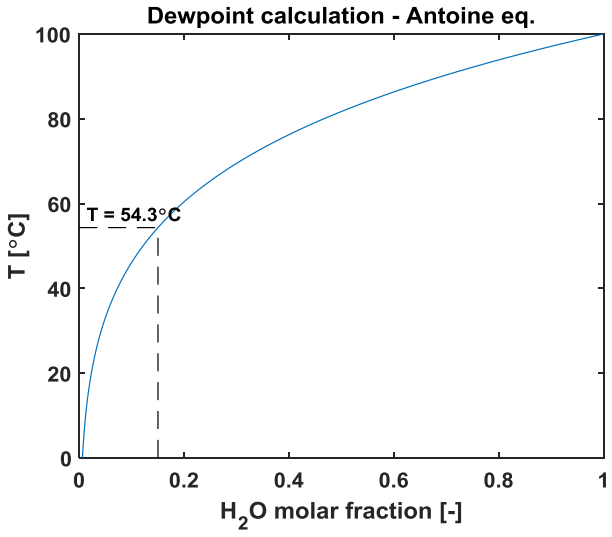

Figure A.3: Dewpoint against the molar fraction of H_2O calculated from the Antoine equation. The dewpoint at a H_2O molar fraction of 0.15 is 54.3ºC.

As NH_3 is to be measured in the local concentration measurements, the maximum temperature of the sample gas is limited by the reactivity of NH_3. The main reactions considered are the thermal decomposition of NH_3 and its reactions with O_2 and NO, demonstrated by non-elementary A.2-R1 – A.2-R3. The thermal decomposition (A.2-R3) was negligible below approximately 400ºC in a stainless steel tank reactor [337,338]. Little information is available on the catalytic effect of stainless steel on the NH_3 reactions. To investigate the reactions of NH_3 with O_2 and NO, the rate constants for A.2-R1 and A.2-R2 were extracted [339] and multiplied by a catalytic factor (fa_{cat}) to take into account the effect of stainless steel. Assuming a plug flow reactor, the concentration of NH_3 as a function of residence time for parametized values of T and fa_{cat} is summarized in Figure A.4. The results indicate that temperature and residence time must be carefully controlled to minimze secondary reactions within the probe. For simplicity it is here assumed that, below 400ºC, the reactions of NH_3 are quenched. However, a further investigation of this may be necessary either by experiment or modelling, as temperatures around 400ºC, corresponds to the temperature during Selective Catalytic Reduction (SCR) (cf. Chapter 2, Section 2.5.2).

$$NH_3 + \frac{5}{4} O_2 \rightarrow NO + H_2O \qquad \text{A.2-R1}$$

$$NH_3 + NO + \frac{1}{4} O_2 \rightarrow N_2 + \frac{3}{2} H_2O \qquad \text{A.2-R2}$$

$$NH_3 \rightarrow \frac{1}{2} N_2 + \frac{3}{2} H_2 \qquad \text{A.2-R3}$$

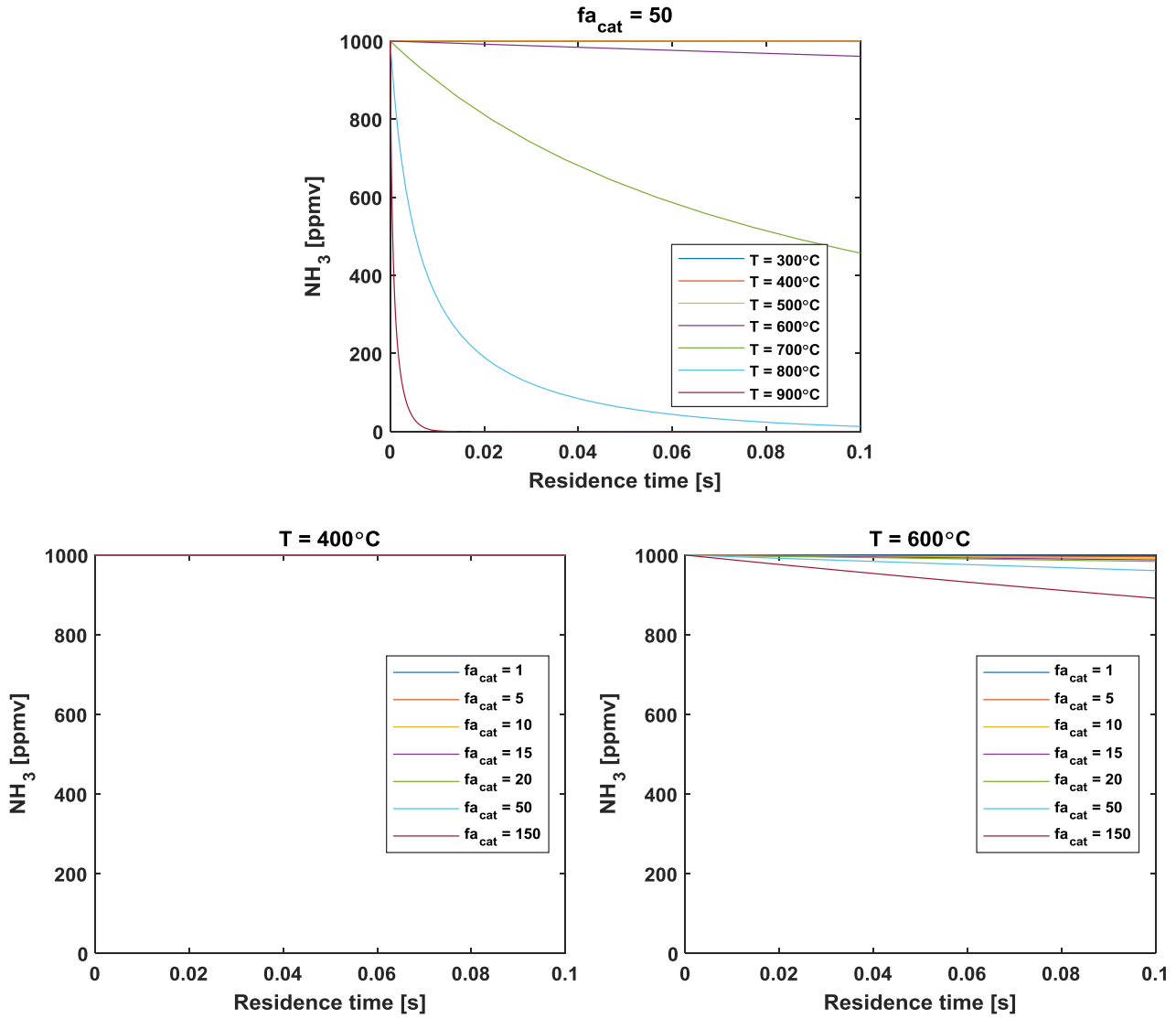

Figure A.4: Outlet concentration of NH_3 from a plug flow reactor including reactions B-R1 and B-R2 against residence time for discrete values of temperature (T) and catalytic factor (fa_{cat}), the latter of which was multiplied on the rate constant of both reactions.

The cooling capability of two different cooling media, air and water, were investigated. The temperature profile within the probe using each method is summarized in Figure A.5. The temperature profiles were extracted 12 cm above the air distributor, corresponding to the highest temperature gas sample, i.e. gas temperature of around 850ºC. To ensure adequate cooling of the sample gas, water cooling was used in the local concentration measurements. However, to ensure that no water condenses within the probe the cooling water was heated to around 68-75ºC.

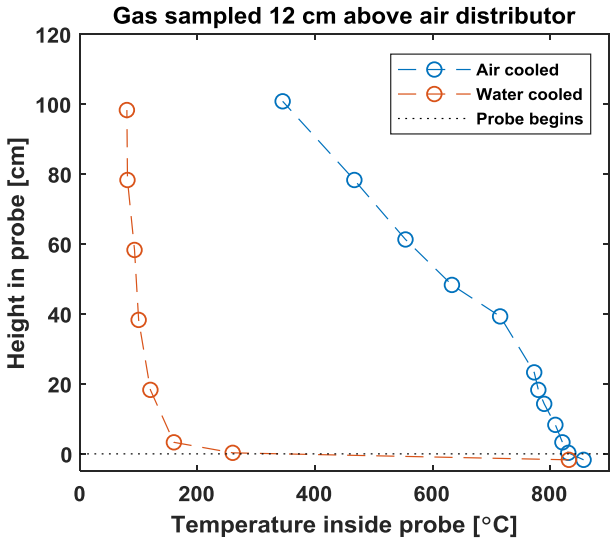

Figure A.5: Temperature profile of sample gas within the probe using two different cooling media. The gas was sampled at a point 12 cm above the air distributor.

The introduction of secondary gas resulted in a dilution of the measured sample gas. The dilution was corrected for by performing experiments in which a known concentration of NO was introduced with the primary gas under conditions resembling that of combustion. The axial NO concentration profile, dilution factor (fa_{dil}), and corrected concentrations are shown in Figure A.6.

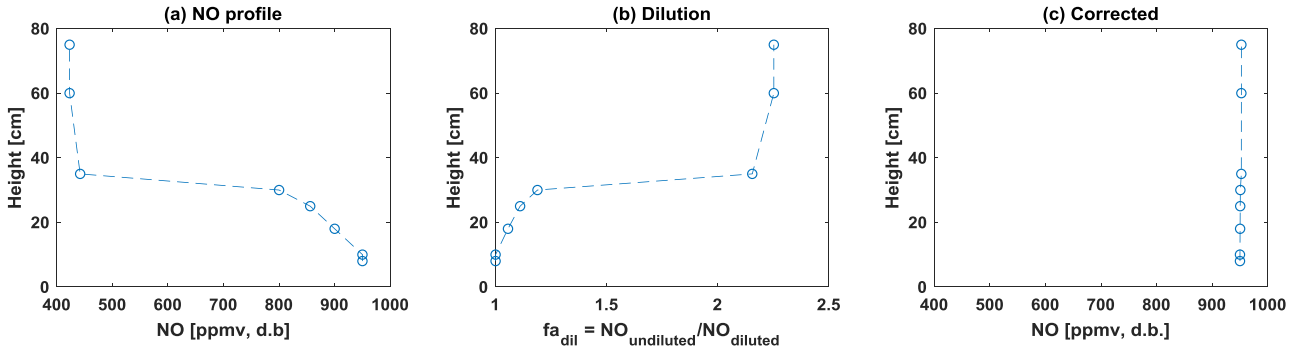

Figure A.6: Axial NO concentration (a), dilution factor (fa_{dil}) (b), corrected concentration (c) in experiments with tracer NO gas in the primary air.

Local gas concentration measreument procedure

Local concentration measurements during combustion were performed by insertion of the probe from the top of the reactor and moving it down through pre-defined points. At each point, a total of 3-6 minutes of measurements were obtained. The first 30-60 seconds were discarded due to the transient change in the results. The remaining data were used for average and standard deviation calculations. The temperature of the cooling water was monitored when changing the probe position to ensure that H_2O did not evaporate inside the probe. The mass flow of H_2O was approximately 40-60 g/s, while the sample gas flow was around 200-500 NmL/min. The probe setup is demonstrated in Figure A.7. A pump, placed between two Swagelok filters, provided the driving force for transfer of sample gas to the FTIR spectrometer.

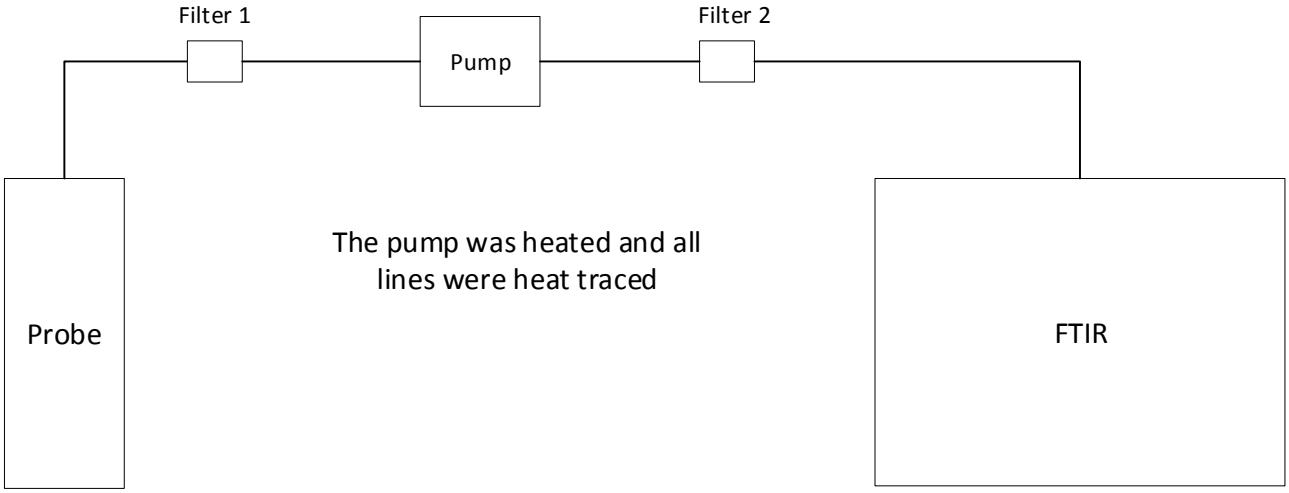

Figure A.7: Setup and connection of probe to FTIR.

A.3 Repeatability of local gas concentration measurements during straw combustion

The repeatability of the local gas concentration measurements of straw combustion at air un-staged and staged conditions are demonstrated in Figure A.8 and Figure A.9, respectively. The repeatability of the measurements are reasonable. In the case of NH_3 and HNCO, some differences were observed, while the qualitative trend was consistent. The measurements of HNCO above the maximum range generally lead to an overestimation of the concentration based on previous experience with the FTIR spectrometer.

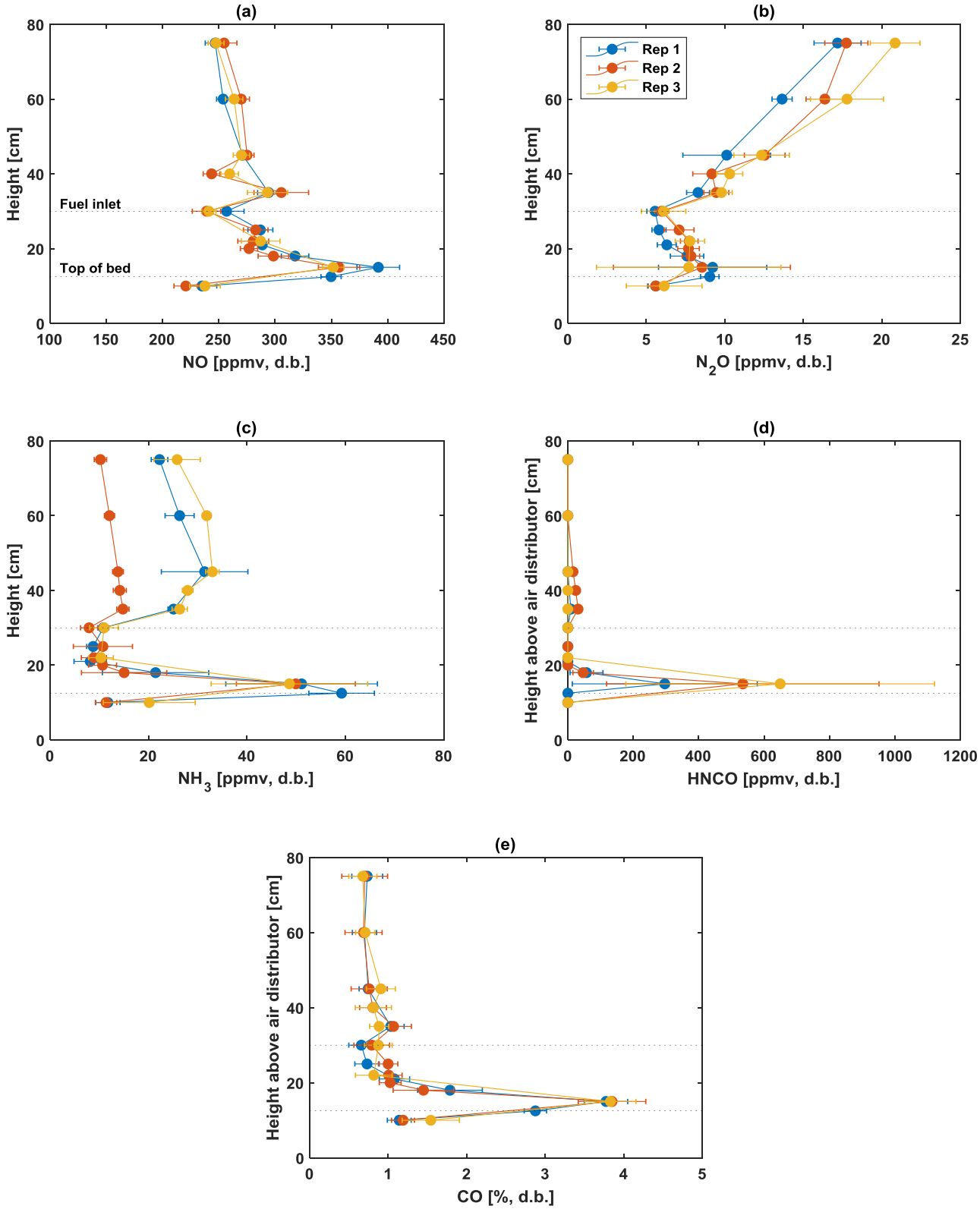

Figure A.8: Axial NO (a), N_2O (b), NH_3 (c), HNCO (d), and CO (e) profiles during fluidized bed mono-combustion of straw. Three repetitions are shown. Conditions: T_{bed} = 850ºC; λ = 1.4; λ_1/λ = 1.

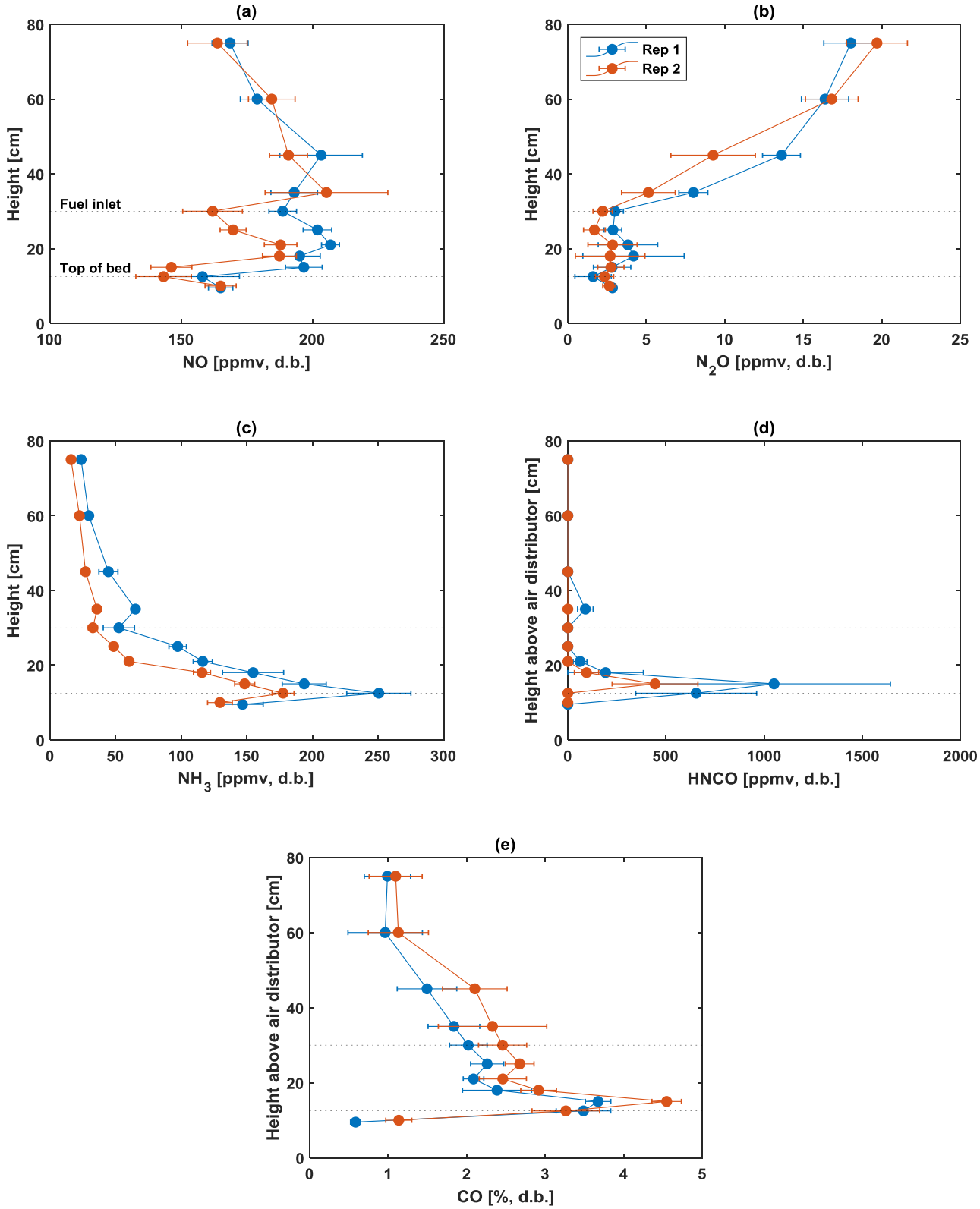

Figure A.9: Axial NO (a), N_2O (b), NH_3 (c), HNCO (d), and CO (e) profiles during fluidized bed mono-combustion of straw. Two repetitions are shown. Conditions: T_{bed} = 850ºC; λ = 1.4; λ_1/λ = 0.5.

A.4 CO and NO correlation during fluidized bed mono-combustion of biomass

Figure A.10 demonstrates the measured NO, CO, O_2, and CO_2 concentrations from fluidized bed combustion of biomass in the time domain extracted in a time range of 200 s during steady state conditions. The NO and CO peaks were adjusted to take into account the time delay in the analyzers. In the case of straw, sunflower husk, and to some extent sunflower seed combustion, a maximum in NO was accompanied by a minimum in CO and maximum in O_2. However, this trend was not prominent in pine wood, beech wood, and sewage sludge combustion.

Figure A.11 demonstrates the outlet concentration of NO versus CO. As stated previously, in some cases the NO decreased with an increase in CO, while in other cases no correlation was observed.

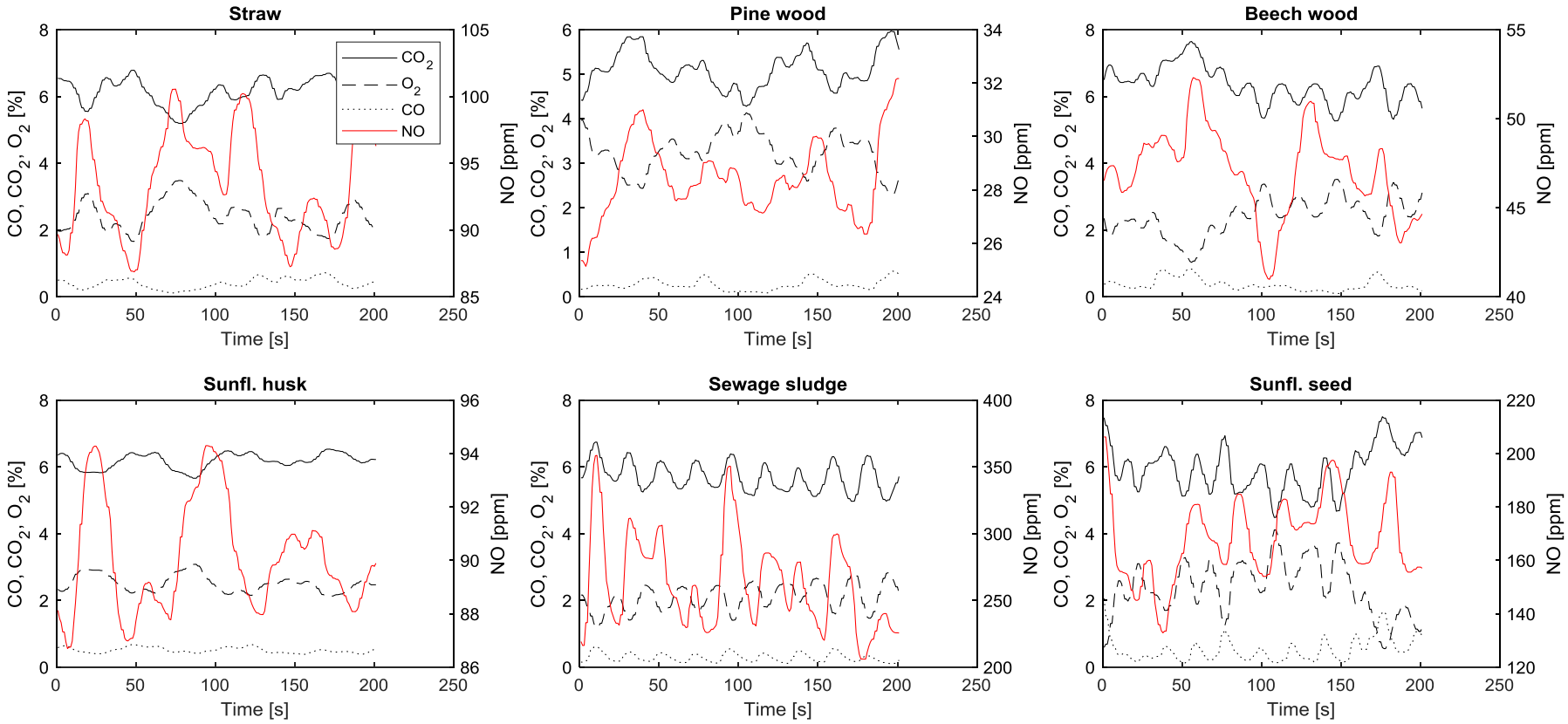

Figure A.10: CO_2, O_2, CO, and NO concentration plots versus time during steady stage combustion of straw, pine wood, beech wood, sunflower husk, sewage sludge, and sunflower seed.

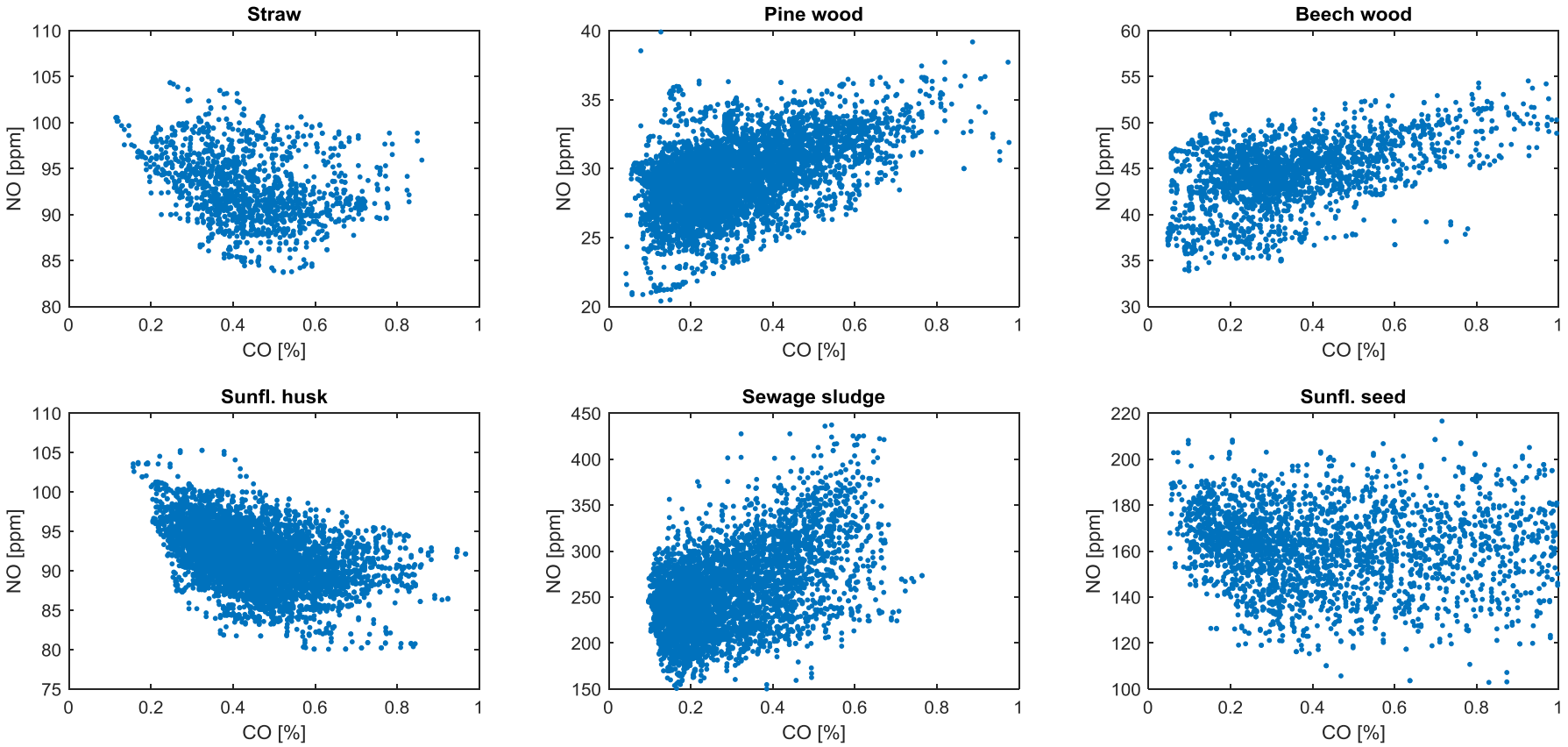

Figure A.11: Scatter plots of NO versus CO during steady stage combustion of straw, pine wood, beech wood, sunflower husk, sewage sludge, and sunflower seed.

A.5 CO, C_xH_y, CH_2O, H_2SO_4, and SO_x – un-staged mono-combustion

The local gas concentration measurements of the relevant species are demonstrated for the combustion of biomass at air un-staged conditions.

CO and CH_2O

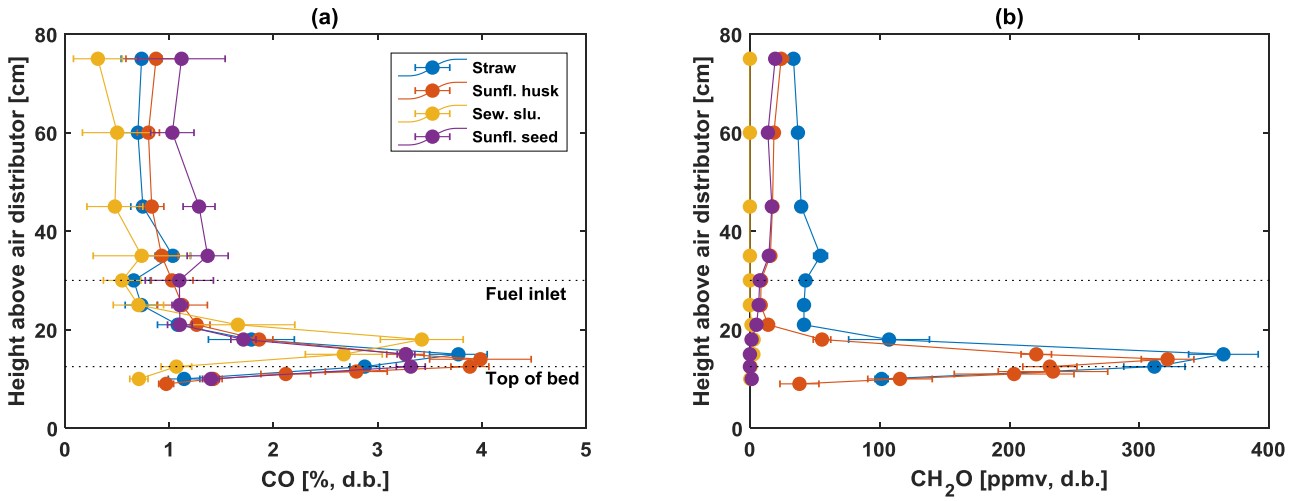

Figure A.12: Axial CO (a) and CH_2O b) profiles during un-staged fluidized bed mono-combustion biomass. Conditions: T_{bed} = 850ºC; λ = 1.4; λ_1/λ = 1 and 0.5.

CxHy

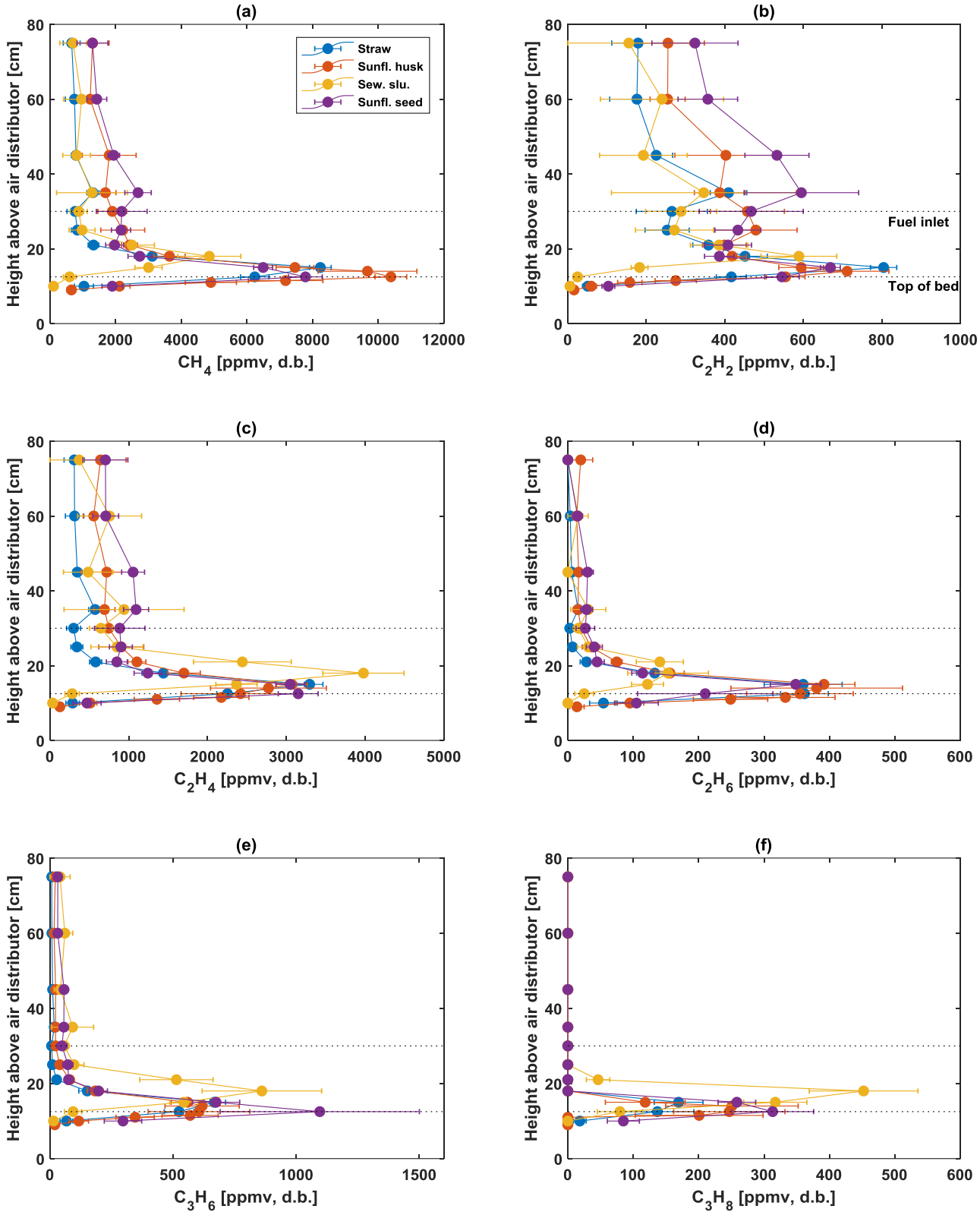

Figure A.13: Axial CH_4 (a), C_2H_6 (b), C_2H_4 (c), C_2H_2 (d), C_3H_8 (e), and C_3H_6 (f) profiles during un-staged fluidized bed combustion of biomass. Conditions: T_{bed} = 850ºC; λ = 1.4; λ_1/λ = 1 and 0.5.

A.6 CO_2 and O_2 local concentration

The raw CO_2 data from local measurements during sewage sludge combustion are illustrated in Figure A.14 in the case of high and low CO concentration. While a large degree of scatter is prominent, some underlying trends may be obtained by various signal processing techniques.

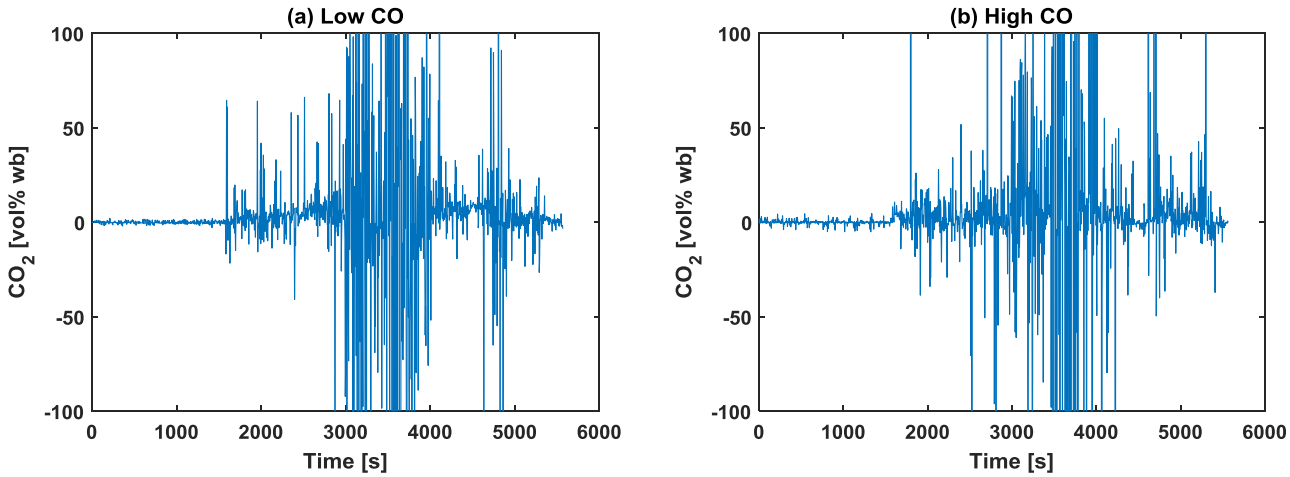

Figure A.14: Raw CO_2 concentration data from local concentration measurement during fluidized bed mono-combustion of sewage sludge. The calibration of CO_2 was obtained at low (a) and high (b) concentrations of CO. Conditions: T_{bed} = 850ºC; λ = 1.4; λ_1/λ = 1.

Initially, the peaks above 21% and below 0% are identified and removed. The identified peaks are demonstrated in Figure A.15, while the plots after removal of the outlier peaks are shown in Figure A.16. As the CO concentration was high near the bed, the CO_2 concentration obtained from the low CO calibration was inaccurate.

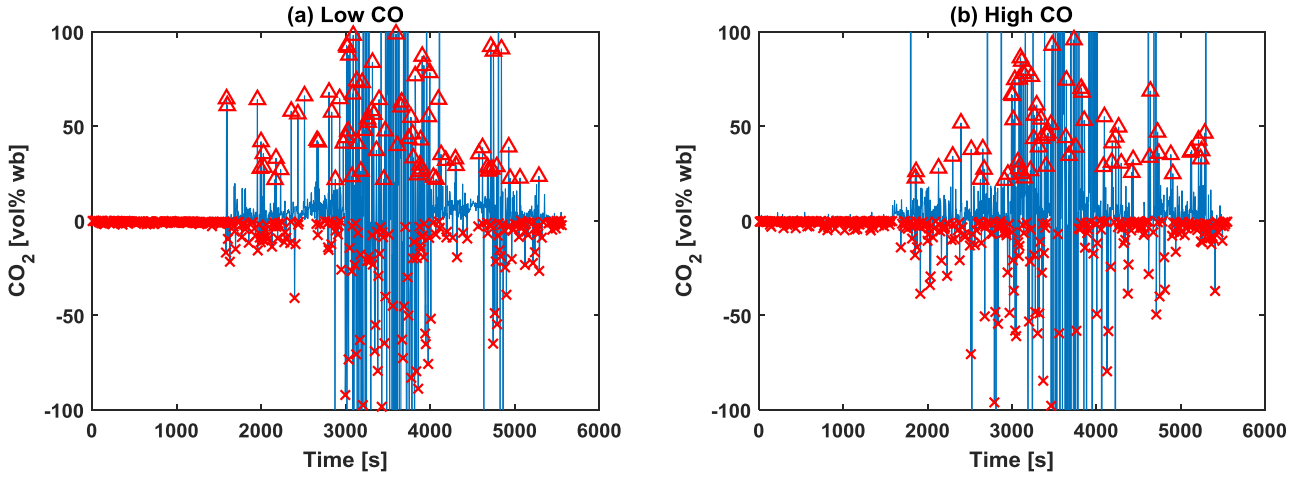

Figure A.15: Concentration plots in which the peaks above 21% (triangle) and below 0% (cross) are identified.

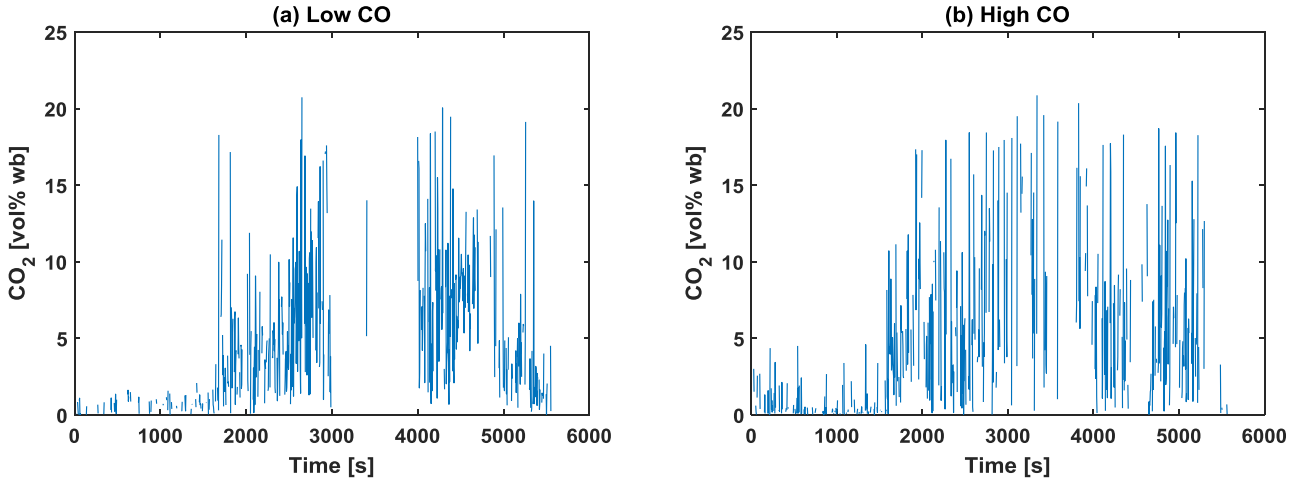

Figure A.16: Concentration plots without peaks above 21% and below 0%.

To treat the data, different smoothing techniques were used, including median filtering, moving average, and smoothing spline, each of which are demonstrated in Figure A.17 for the low (a, b, c) and high (d, e, f) CO data.

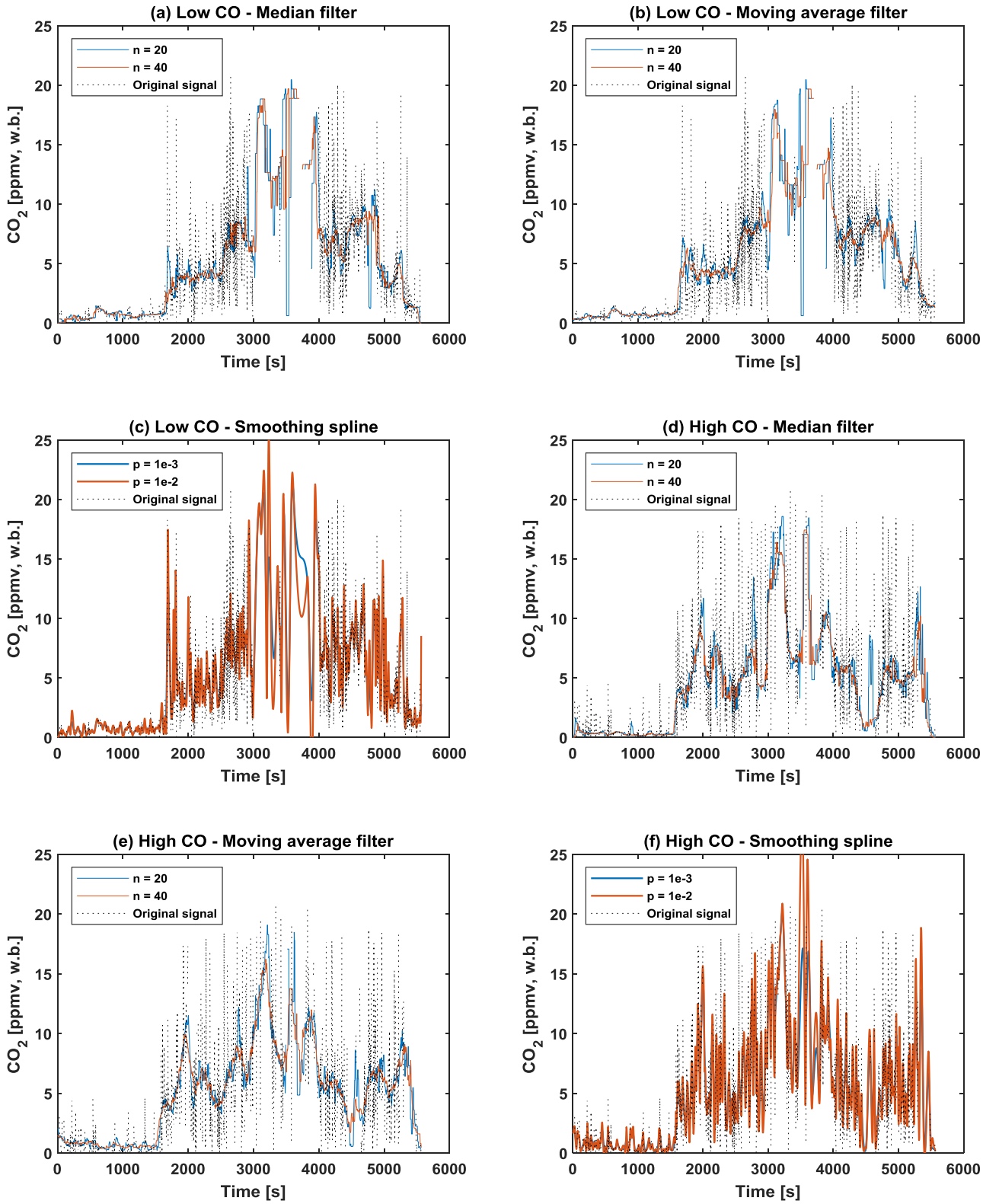

Figure A.17: Raw and smoothened data using median, moving average, and smoothing spline filtering for the low (a, b, c) and hig (d, e, f) CO data.

The CO_2 profiles using the different smoothing methods were determined for high and low CO as demonstrated in Figure A.18. As the outlet concentration of CO_2 should be around 15%, a moving average based filtering of the low CO data was deemed appropriate for points above the fuel inlet. Below the fuel inlet, the CO concentration was high; consequently, the high-CO data were used employing a moving average based filtering. The resultant CO_2 and O_2 ($O_2 = 21 - CO_2 - ½\ CO - ½\ NO$) profiles are demonstrated in Figure A.19.

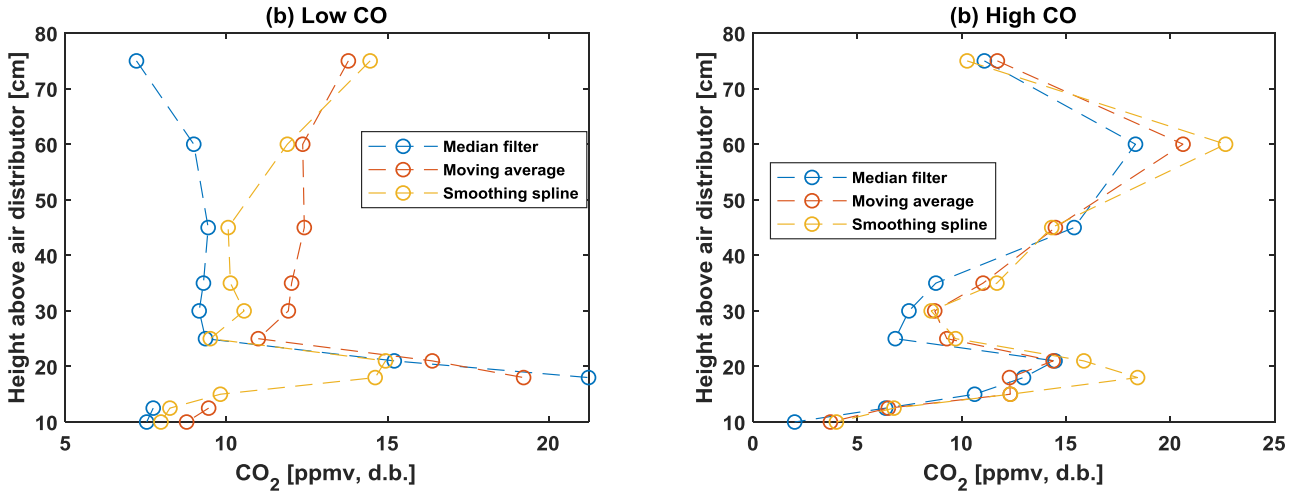

Figure A.18: CO_2 profiles from smoothening of low and high CO data.

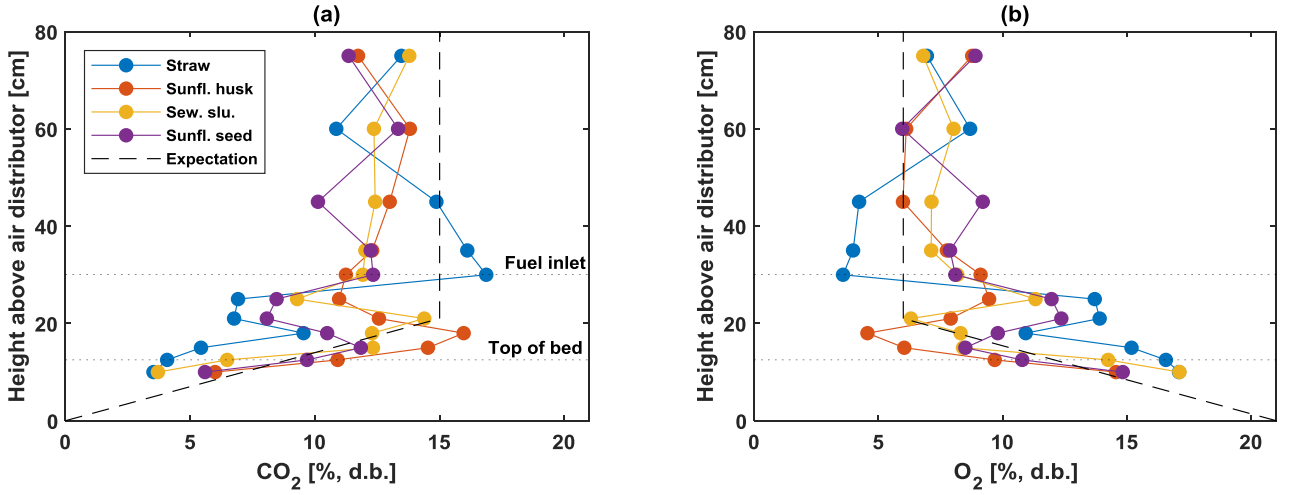

Figure A.19: CO_2 (a) and O_2 (b) profiles for the relevant fuels obtained from moving average smoothening of the low CO data above the fuel inlet and high CO data below the fuel inlet.

A.7 Sunflower seed-sewage sludge un-staged co-combustion

Figure A.20 depicts the averaged NO and CO concentrations from co-combustion of sunflower seed and sewage sludge. While the NO concentration exhibited a similar trend as in straw-sewage sludge co-combustion, the CO concentration slightly decreased with the share of sewage sludge, possibly due to the catalytic effect of sewage sludge ash on the oxidation of combustibles.

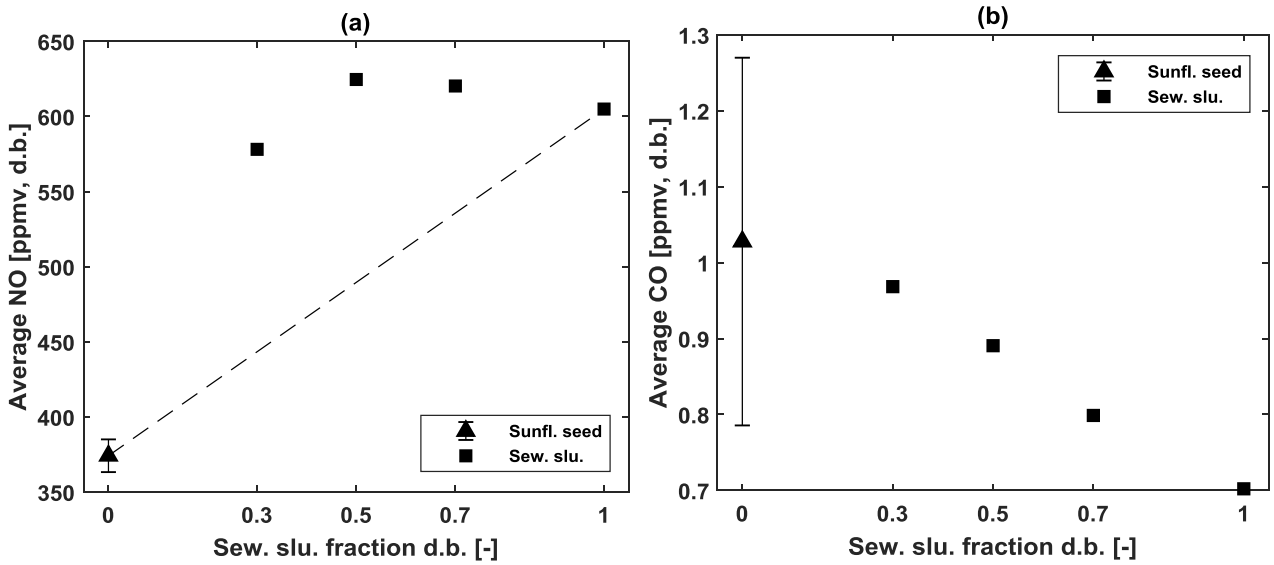

Figure A.20: Average effluent NO (a) and average effluent CO (b) concentration during fluidized bed co-combustion of sunflower seed and sewage sludge. Conditions: T_{bed} = 850ºC; λ = 1.4; λ_1/λ = 1. The error bars on sunflower seed results were determined from several repetitions.

A.8 BET surface area and XRD analysis of sewage sludge ash

Table A.2 summarizes the BET surface area of the sewage sludge ash prepared at different temperatures, while Figure A.21 depicts the XRD results with most of the peaks identified. The surface area decreased with the severity of heat treatment. In addition, the crystal phases were different for the ash prepared at 550ºC, compared to that of the higher temperature ashes, i.e. 850ºC and 1000ºC. A deeper investigation is necessary to unravel how the catalytic reactivity of the ash changes with the chemical structure.

Table A.2: BET surface area of sewage sludge ash prepared at different temperatures.

Material	Sew. slu. ash 550ºC	Sew. slu. ash 850ºC	Sew. slu. ash 1000ºC
BET [m^2/g]	17.8	2.9	1.5

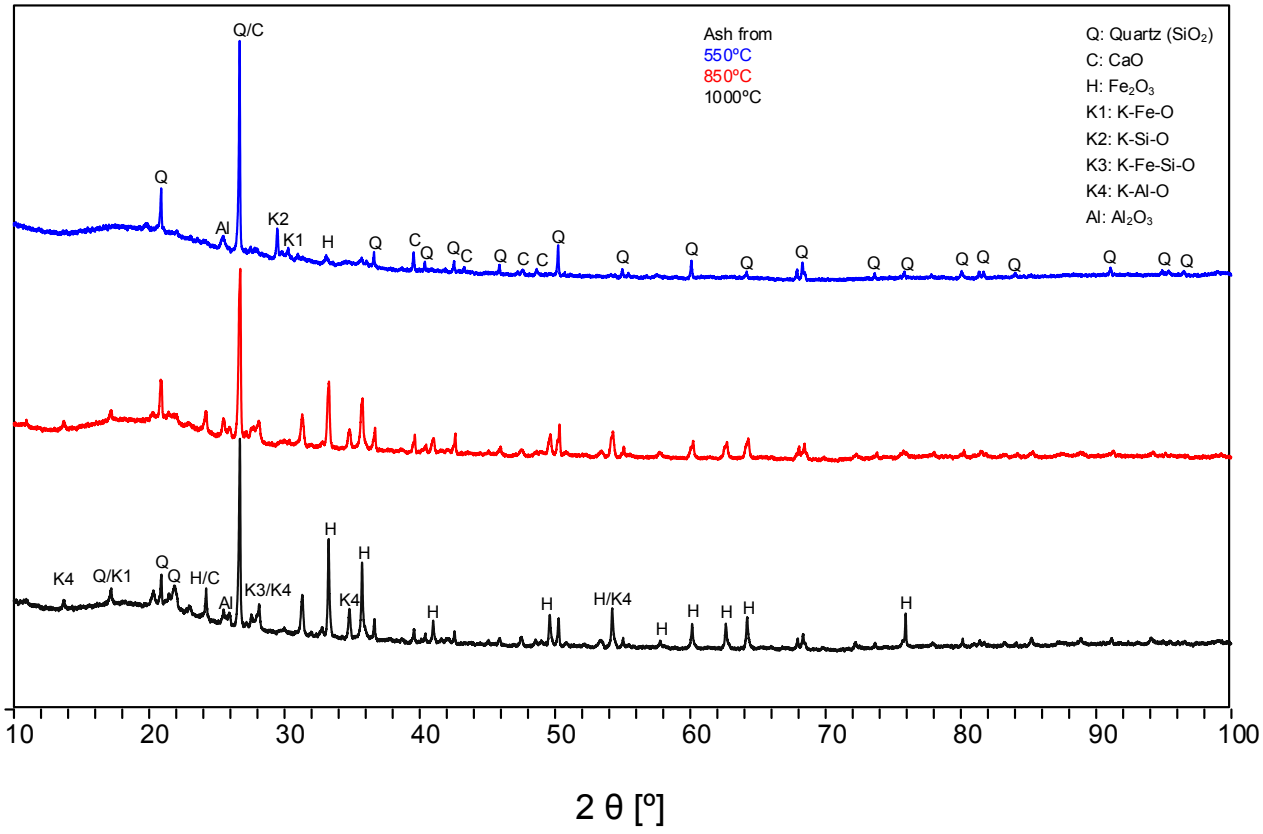

Figure A.21: XRD data of sewage sludge ash prepared at different temperatures.

A.9 C_XH_Y – straw-sewage sludge co-combustion – influence of ash accumulation

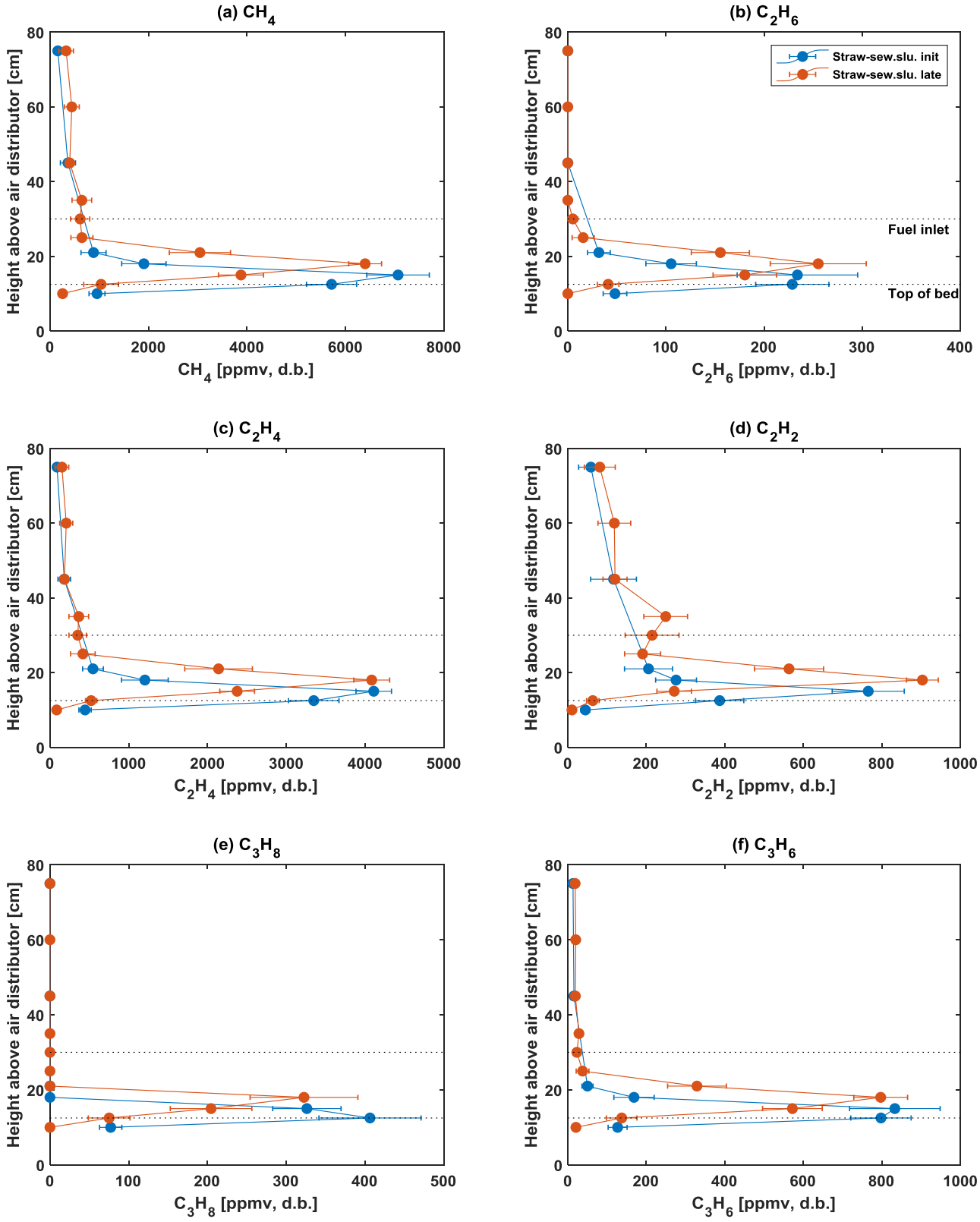

Figure A.22: Axial CH_4 (a), C_2H_6 (b), C_2H_4 (c), C_2H_2 (d), C_3H_8 (e), and C_3H_6 (f) during fluidized bed straw-sewage sludge co-combustion. Definitions: init = 2-25 g of ash to the reactor, late = 40-80 g of ash to the reactor. Conditions: T_{bed} = 850ºC; λ = 1.4; λ_1/λ = 1.

A.10 C_XH_Y – straw-sunflower seed co-combustion

The local gas concentration measurements of the relevant species are demonstrated for the combustion biomass at air un-staged conditions.

CO and CH_2O

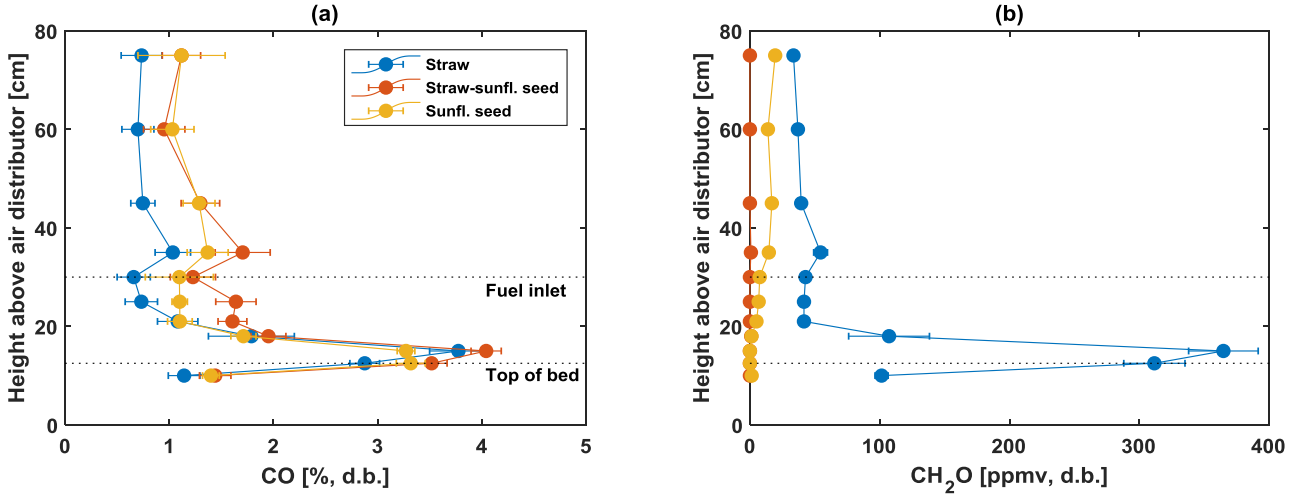

Figure A.23: Axial CO (a) and CH_2O b) profiles during un-staged fluidized bed combustion of straw, sunflower seed, and straw-sunflower seed. Conditions: T_{bed} = 850ºC; λ = 1.4; λ_1/λ = 1.

CxHy

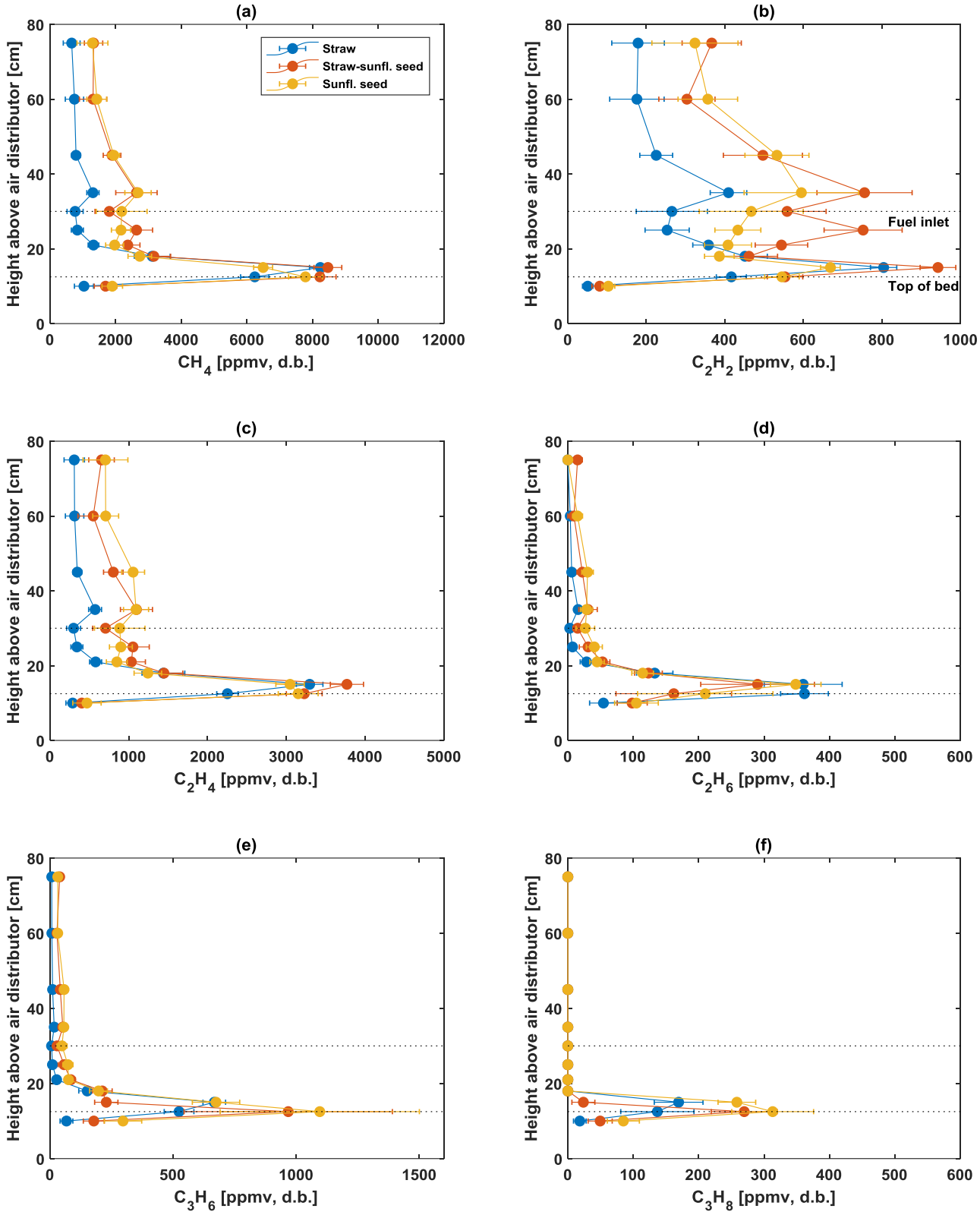

Figure A.24: Axial CH_4 (a), C_2H_6 (b), C_2H_4 (c), C_2H_2 (d), C_3H_8 (e), and C_3H_6 (f) profiles during fluidized bed combustion of straw, sunflower seed, and straw-sunflower seed. Conditions: T_{bed} = 850ºC; λ = 1.4; λ_1/λ = 1.

A.11 Local gas concentration measurements during air-staged combustion

Figure A.25 demonstrates the local gas measurements from air staged combustion of straw, sewage sludge, and straw-sewage sludge, while Figure A.26 shows the air staged and un-staged results from sewage sludge combustion.

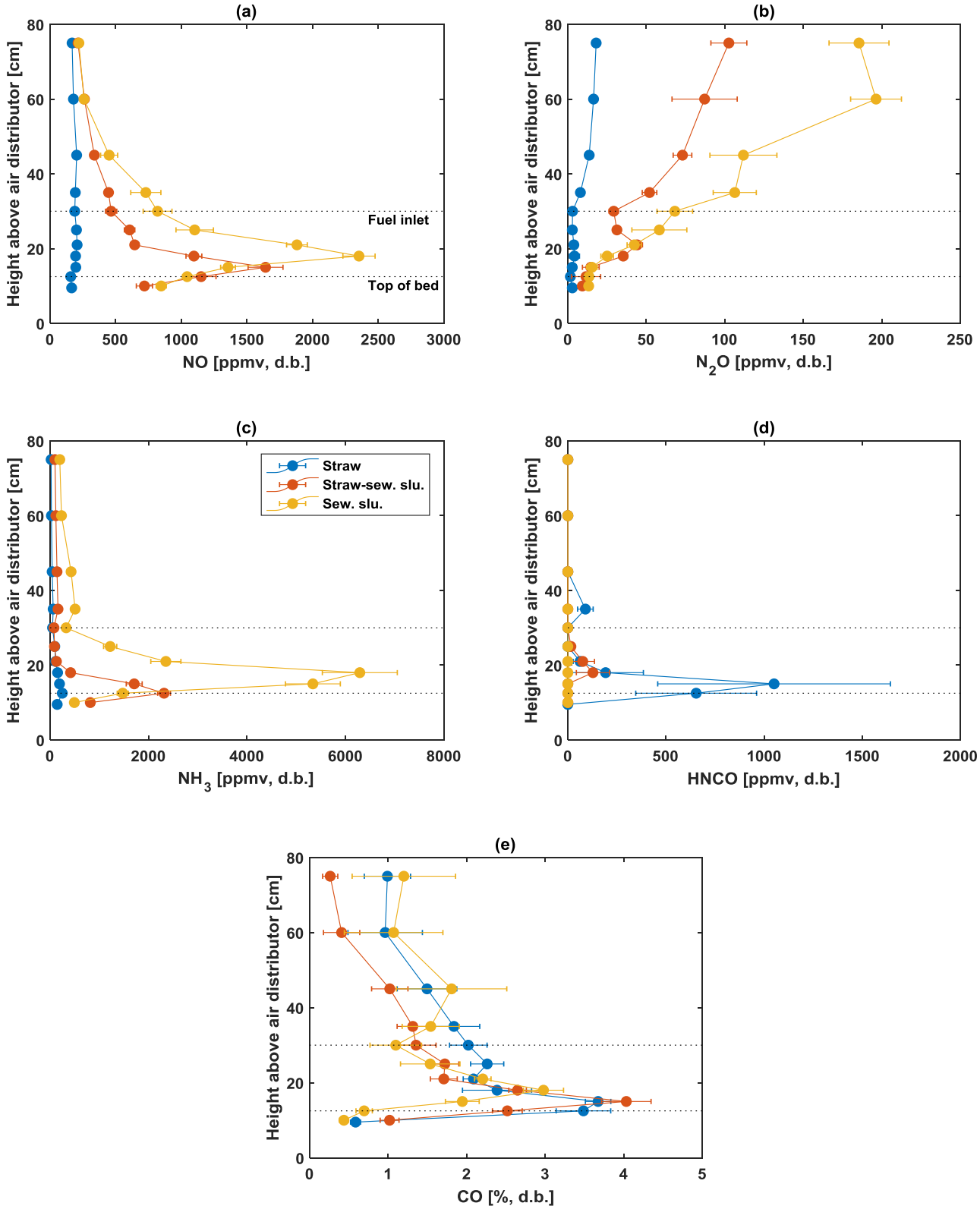

Figure A.25: Axial NO (a), N_2O (b), NH_3 (c), HNCO (d), and CO (e) profiles during air staged fluidized bed combustion of straw, sewage sludge, and straw-sewage sludge. Conditions: T_{bed} = 850ºC; λ = 1.4; λ_1/λ = 0.5.

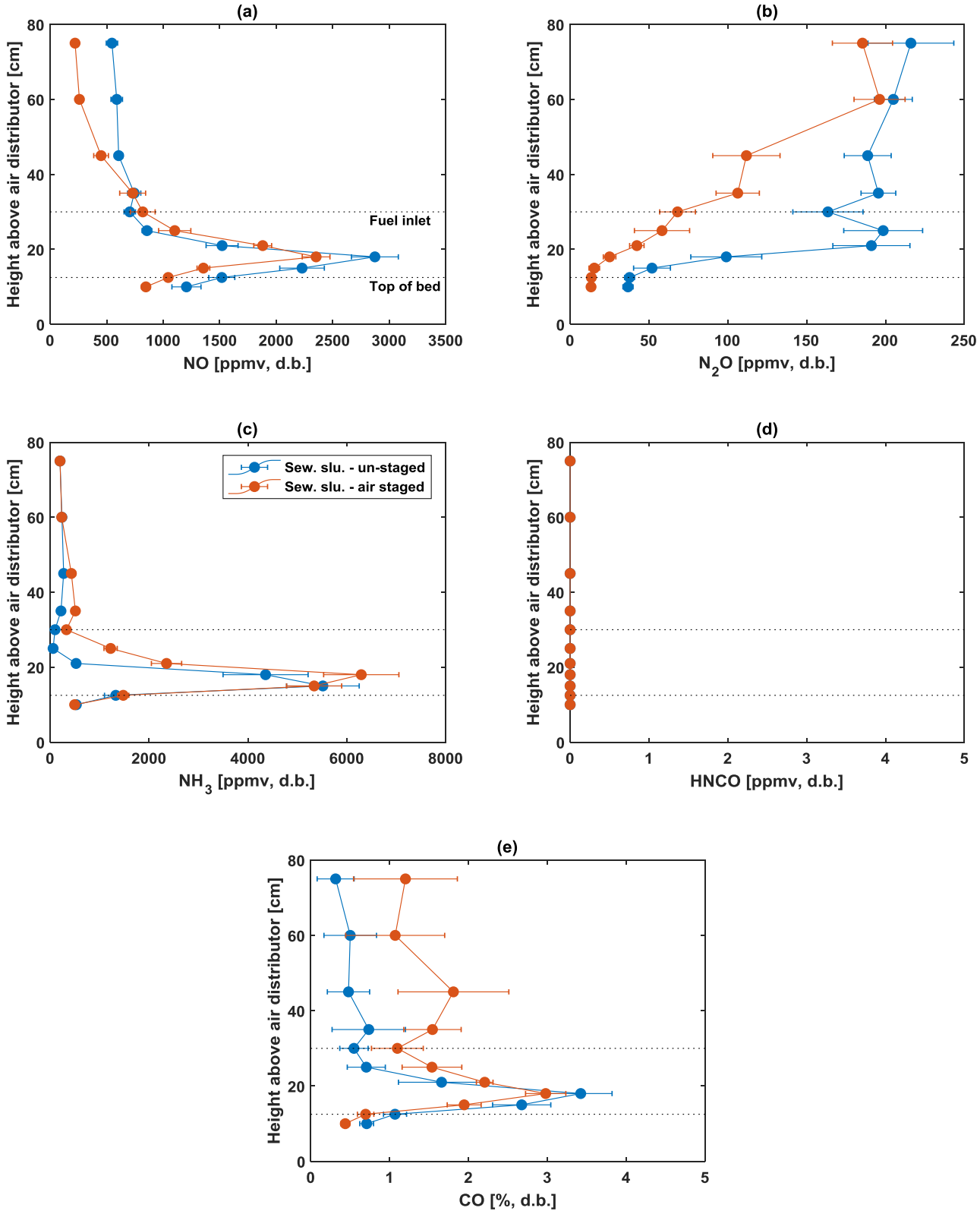

Figure A.26: Axial NO (a), N_2O (b), NH_3 (c), HNCO (d), and CO (e) profiles during air staged and un-staged fluidized bed combustion of sewage sludge. Conditions: T_{bed} = 850ºC; λ = 1.4; λ_1/λ = 1 and 0.5.

A.12 CO, C_XH_Y, CH_2O, H_2SO_4, and SO_X – air staged combustion of straw and sewage sludge

CO and CH_2O

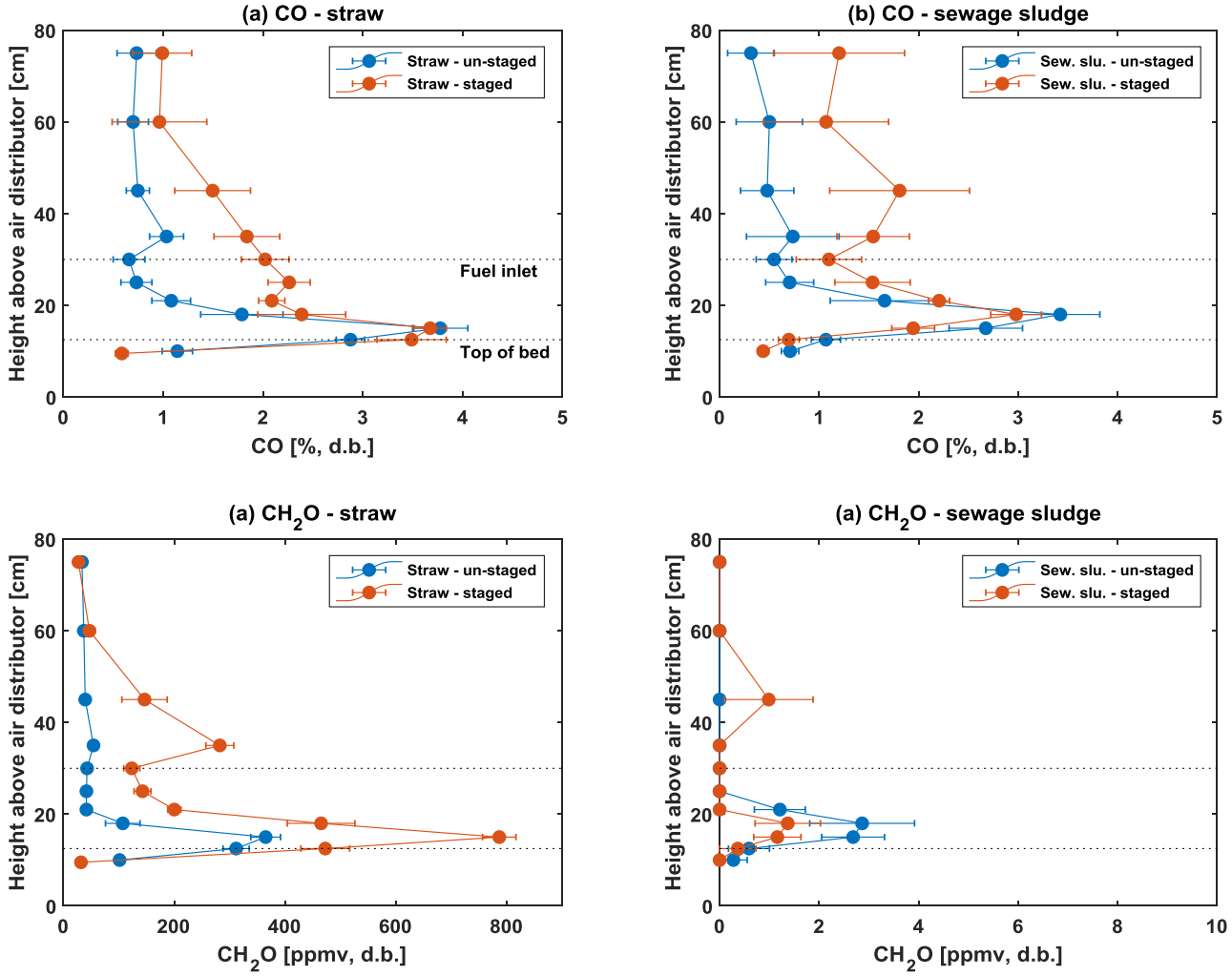

Figure A.27: Axial CO (a,b) and CH_2O (c,d) profiles during fluidized bed mono-combustion of straw and sewage sludge. Conditions: T_{bed} = 850ºC; λ = 1.4; λ_1/ λ = 1 and 0.5.

C_XH_Y – straw air staged and un-staged combustion

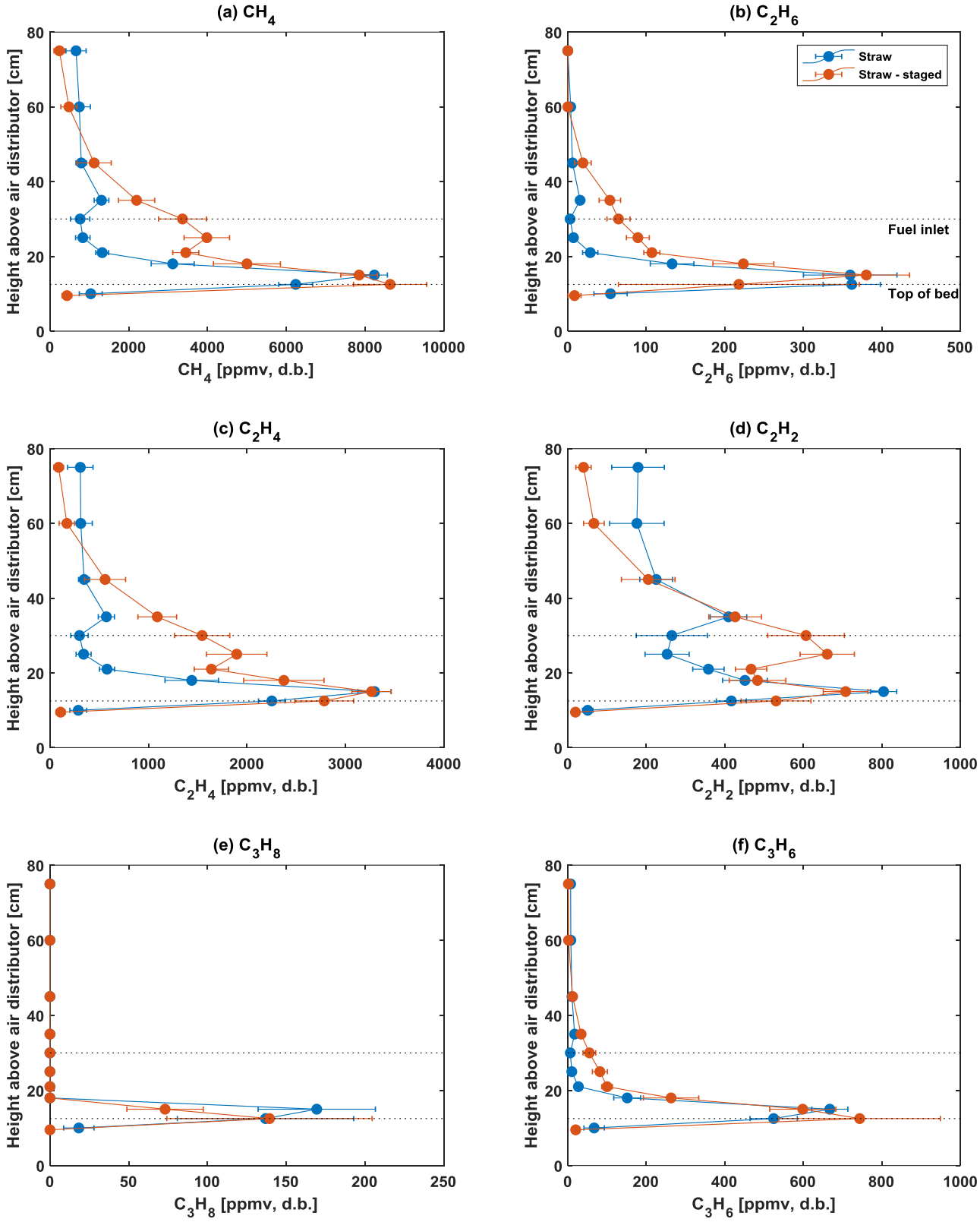

Figure A.28: Axial CH_4 (a), C_2H_6 (b), C_2H_4 (c), C_2H_2 (d), C_3H_8 (e), and C_3H_6 (f) profiles during fluidized bed mono-combustion of straw. Conditions: T_{bed} = 850ºC; λ = 1.4; λ_1/λ = 1 and 0.5.

CxHy – sewage sludge air staged and un-staged combustion

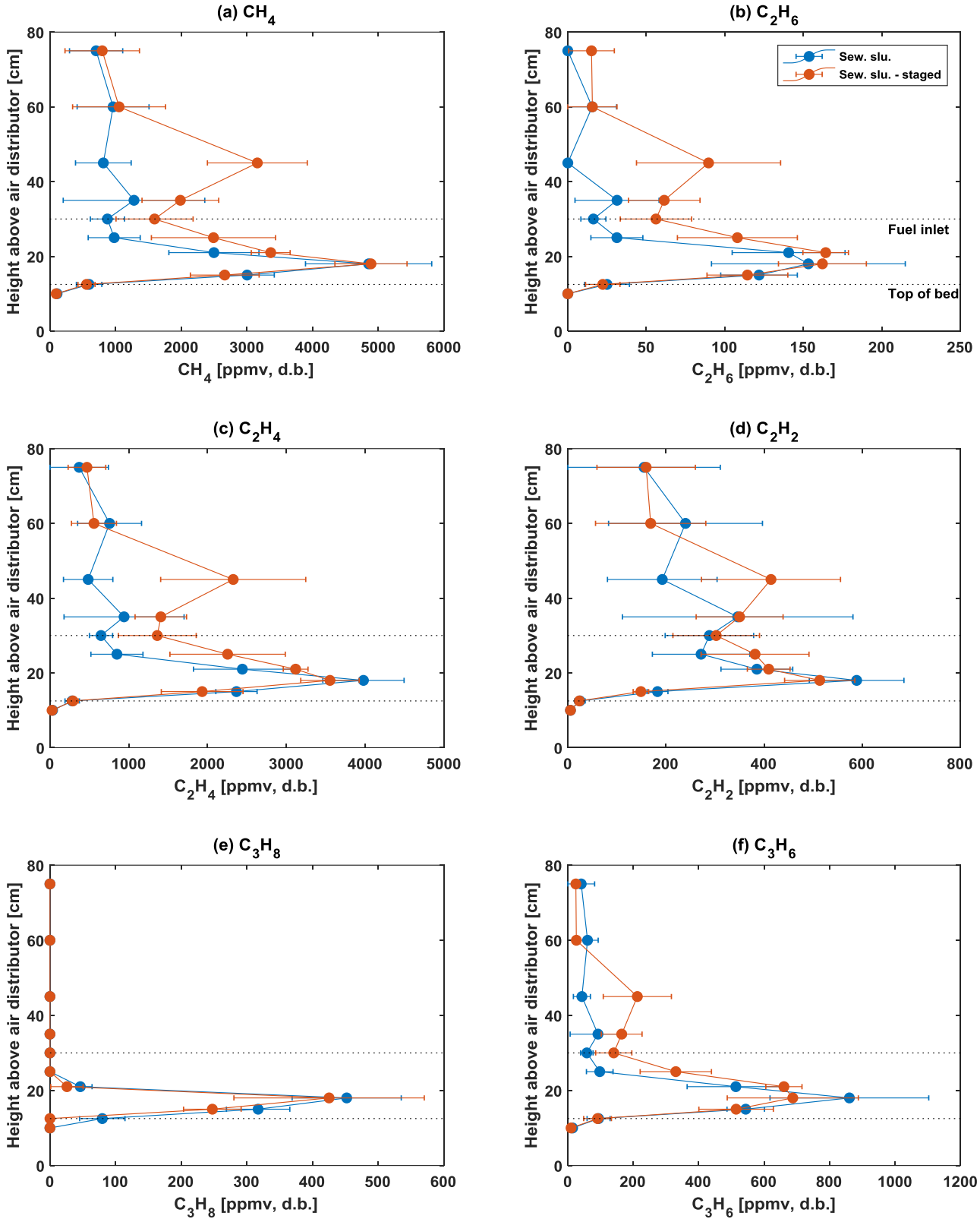

Figure A.29: Axial CH_4 (a), C_2H_6 (b), C_2H_4 (c), C_2H_2 (d), C_3H_8 (e), and C_3H_6 (f) profiles during fluidized bed mono-combustion of sewage sludge. Conditions: T_{bed} = 850ºC; λ = 1.4; λ_1/λ = 1 and 0.5.

Appendix B

B.1 Temperature profiles

Temperature profiles during straw combustion using different bed material at un-staged conditions (Figure B.1) and using different primary gas at $\lambda_1/\lambda = 0$ (Figure B.2).

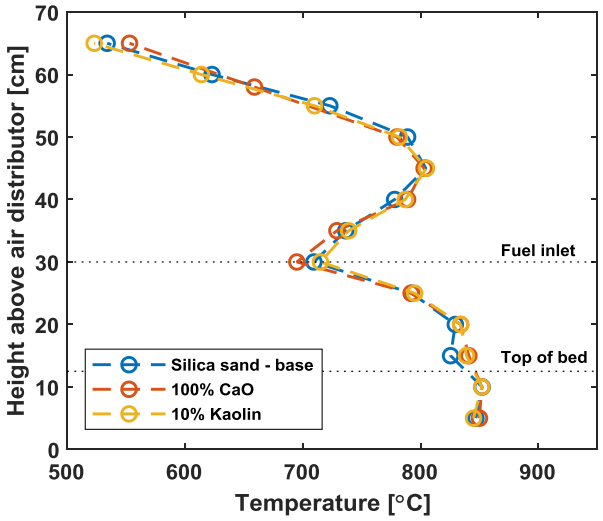

Figure B.1: Axial temperature profile during combustion of straw with different bed material. Conditions: T_{bed} = 850ºC; λ = 1.4; λ_1/λ = 1.

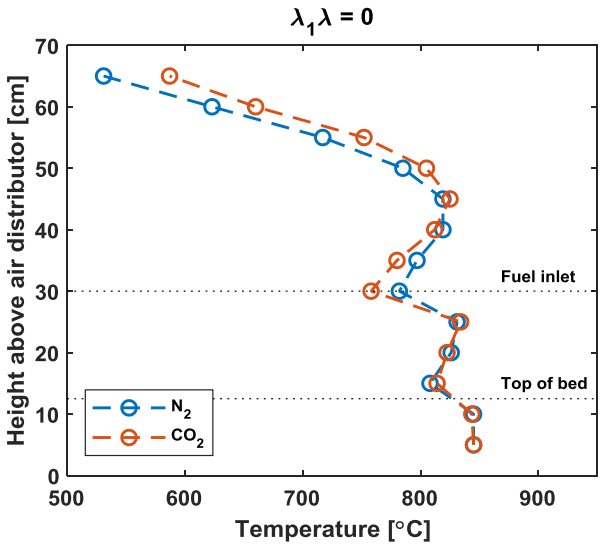

Figure B.2: Axial temperature profile during combustion of straw using N_2 or CO_2 as primary gas. Conditions: T_{bed} = 850ºC; λ = 1.4; λ_1/λ = 0.

Appendix C

C.1 Repeatability of local gas concentration measurements of straw-$(NH_4)_2SO_4$ combustion

The repeatability of the local gas concentration measurements during combustion of straw mixed with $(NH_4)_2SO_4$ at air un-staged conditions are illustrated in Figure C.1. The qualitative trends and to a large extent quantitative values of the repetitions were similar. Notably, the extrapolation of HNCO above the maximum range (300 ppmv) of the FTIR spectrometer generally leads to an overestimation of the concentration. While the qualitative trend of this compound is credible, the quantitative data must be viewed with care.

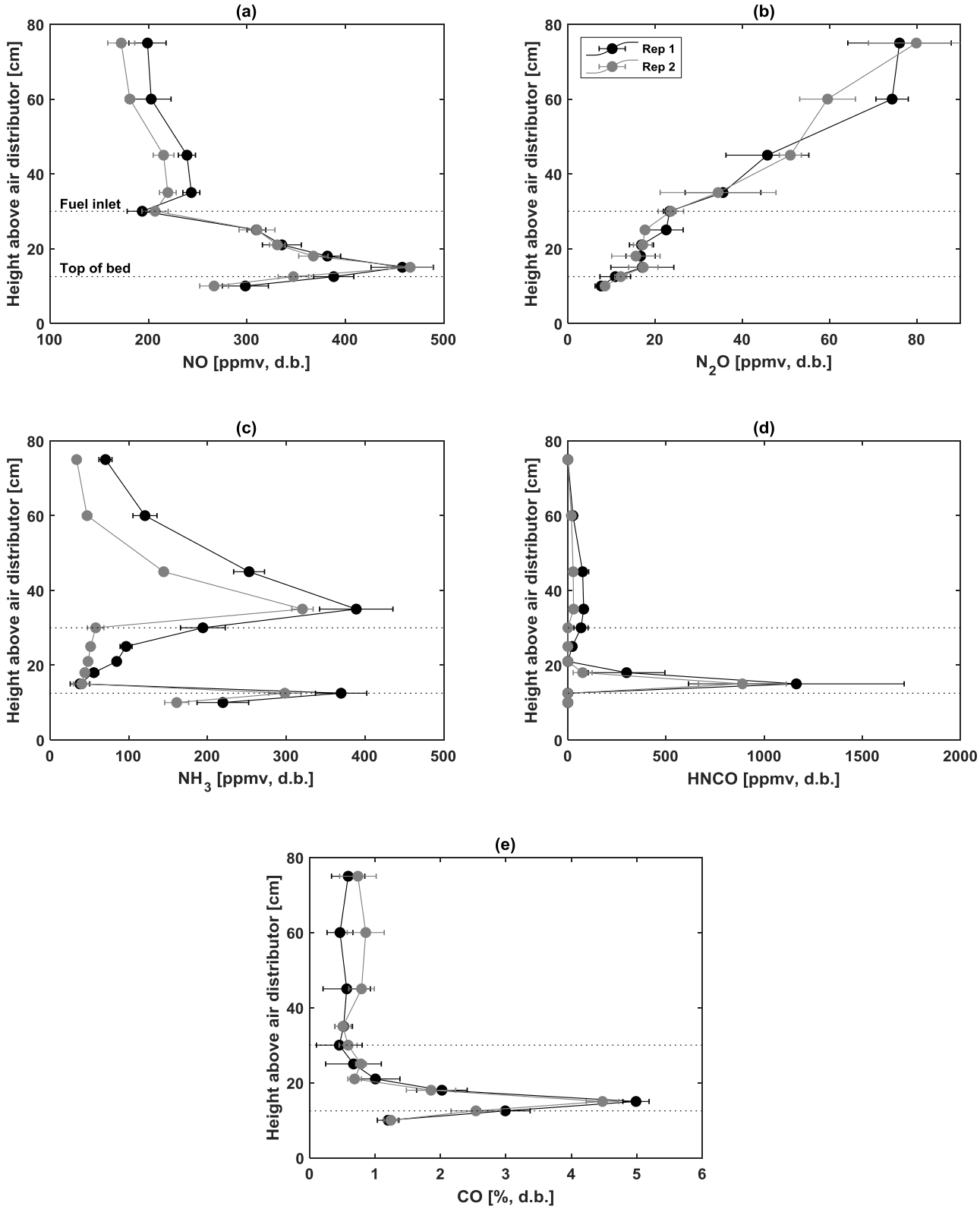

Figure C.1: Axial NO (a), N_2O (b), NH_3 (c), HNCO (d), and CO (e) profiles during fluidized bed combustion of straw mixed with $(NH_4)_2SO_4$. Two repetitions are shown. Conditions: T_{bed} = 850ºC; λ = 1.4; λ_1/λ = 1.

C.2 Decomposition products of NH_4MgPO_4 and $AlNH_4(SO_4)_2$

The decomposition products of NH_4MgPO_4 and $AlNH_4(SO_4)_2$ are demonstrated in Figure C.2. The signals have been shifted to fluctuate around zero and the fluctuations in HCN and N_2 have been dampened. Consequently, the absolute values of the signals are not descriptive and these should be viewed qualitatively to show the presence or absence of the investigated species. Generally, H_2O and NH_3 were the main species, while NO and N_2O were additionally formed from $AlNH_4(SO_4)_2$ under oxidizing conditions.

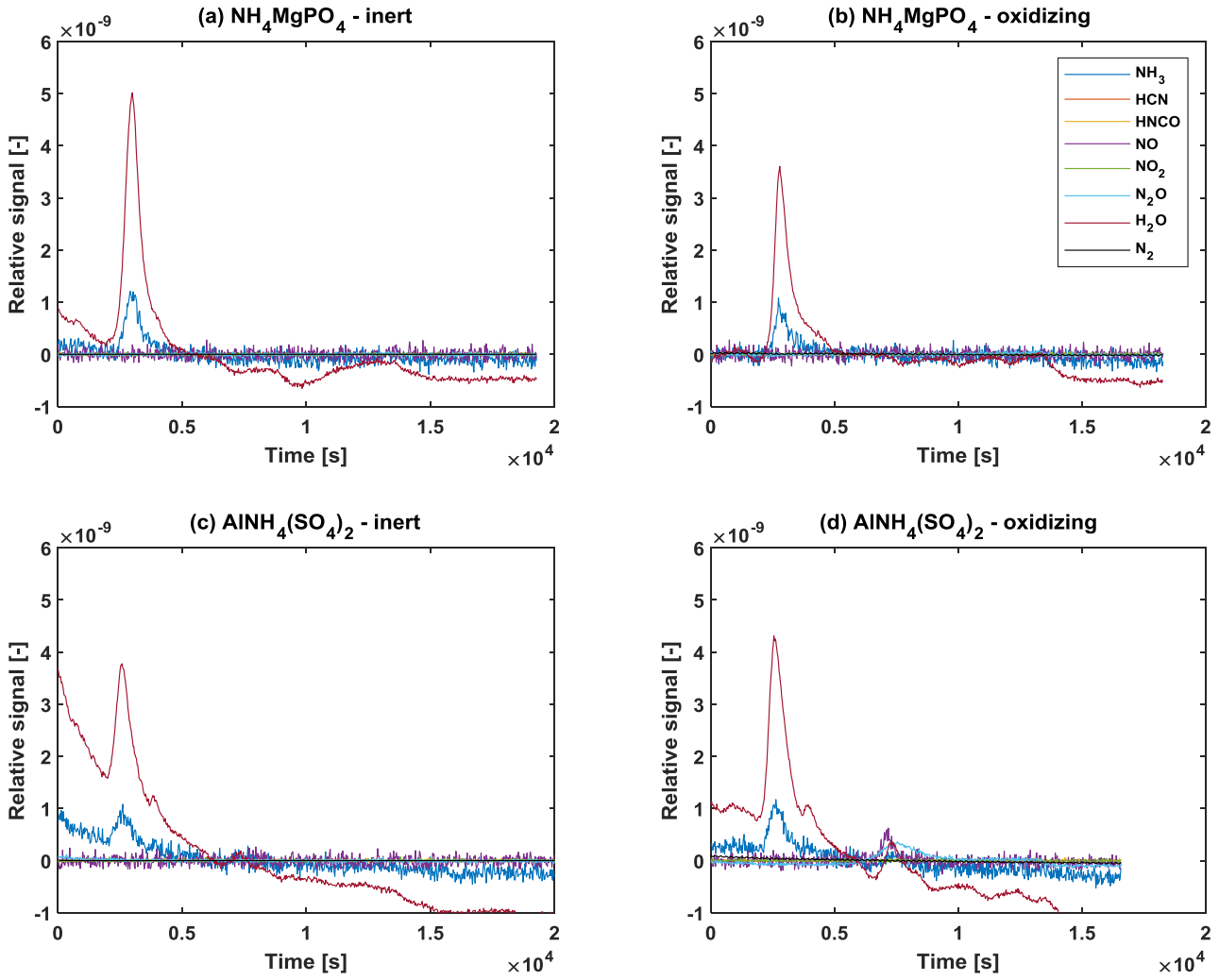

Figure C.2: Decomposition products from TGA of NH_4MgPO_4 (a,b) and $AlNH_4(SO_4)_2$ (c,d) under inert and oxidizing conditions. The experimental conditions are described in Chapter 5, Section 5.2.3.

C.3 CO, C_XH_Y and CH_2O from un-staged straw-additive combustion

Axial profiles of combustibles from straw-additive combustion are presented below. The plots on the left in each figure include the additives that led to a decrease in the overall fuel-N to NO conversion, while the figures on the right include the additives that did not alter the fuel-N to NO conversion significantly (cf. Figure 5.3a).

CO

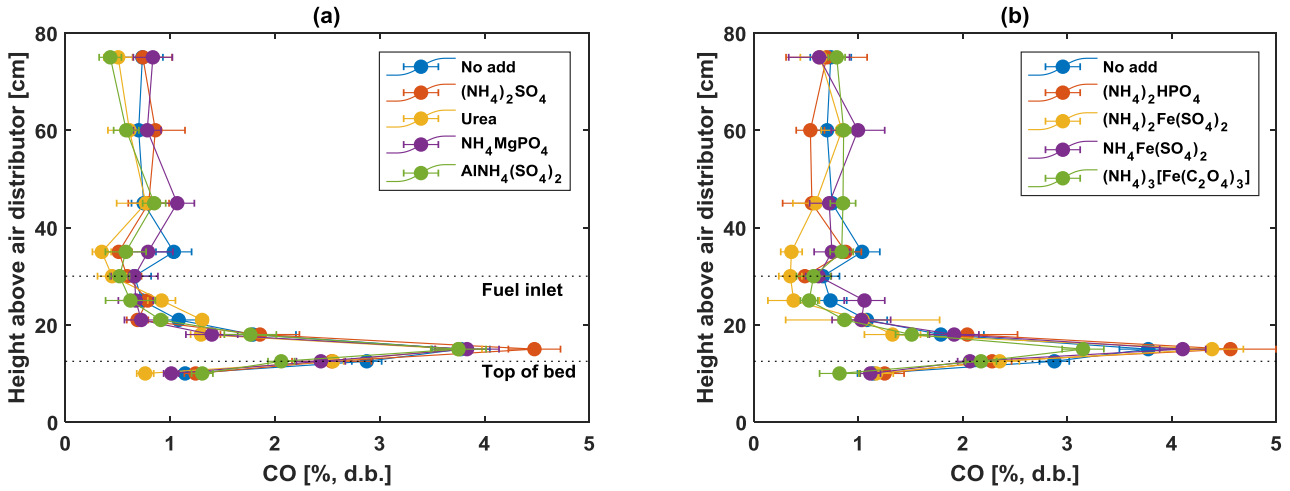

Figure C.3: Axial CO profiles during un-staged fluidized bed combustion of straw-additive. Conditions: T_{bed} = 850ºC; λ = 1.4; λ_1/λ = 1.

CH_2O

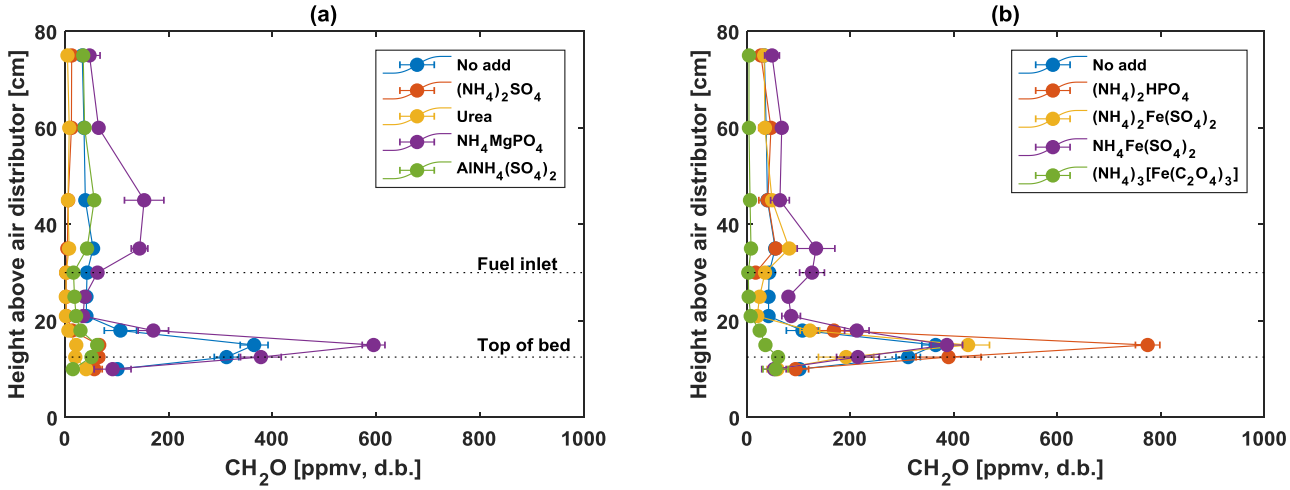

Figure C.4: Axial CH_2O profiles during un-staged fluidized bed combustion of straw-additive. Conditions: T_{bed} = 850ºC; λ = 1.4; λ_1/λ = 1.

CH_4, C_3H_6, and C_3H_8

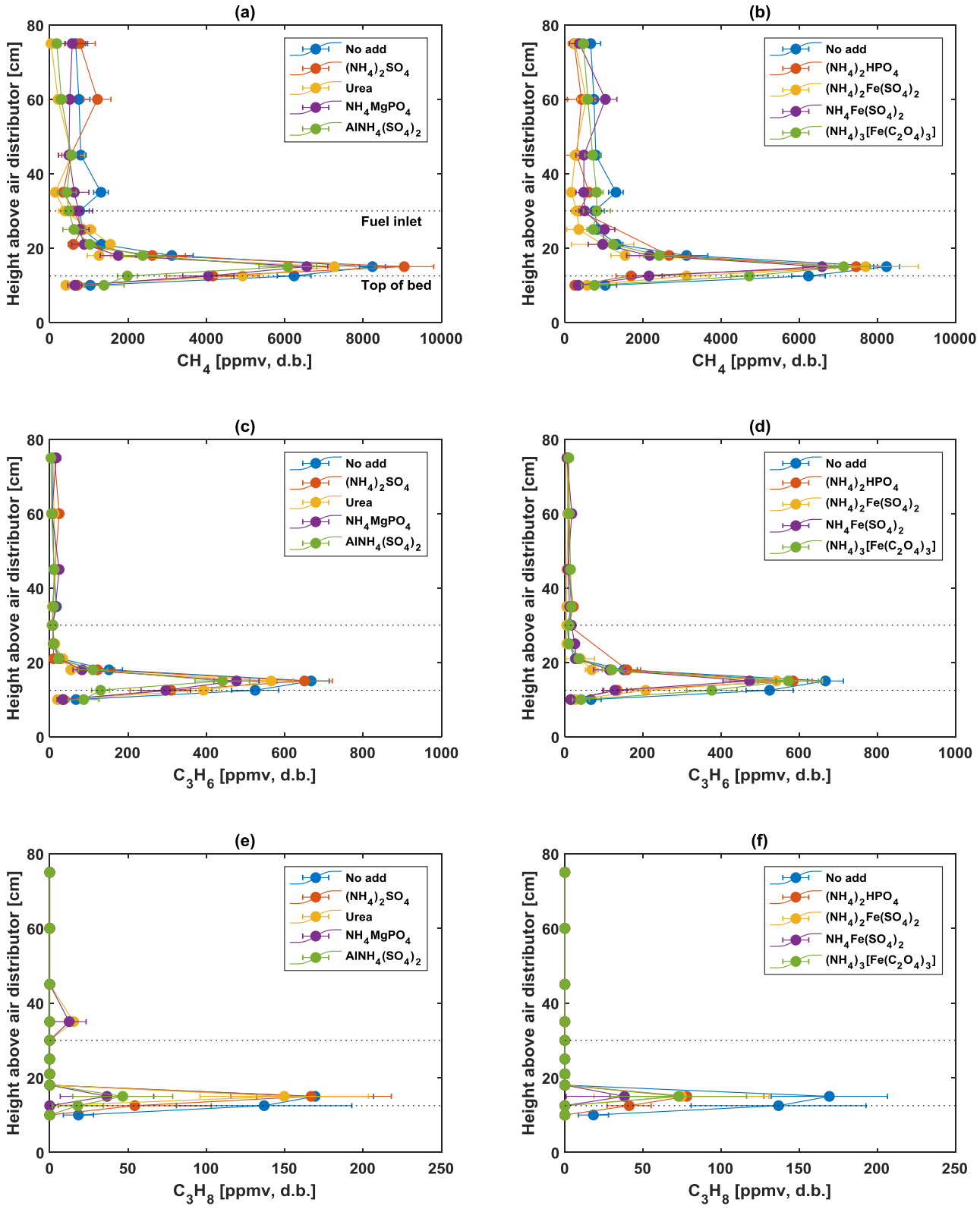

Figure C.5: Axial CH_4 (a,b), C_3H_6 (c,d), and C_3H_8 (e,f) profiles during un-staged fluidized bed combustion of straw-additive. Conditions: T_{bed} = 850ºC; λ = 1.4; λ_1/λ = 1.

C_2H_2, C_2H_4, and C_2H_6

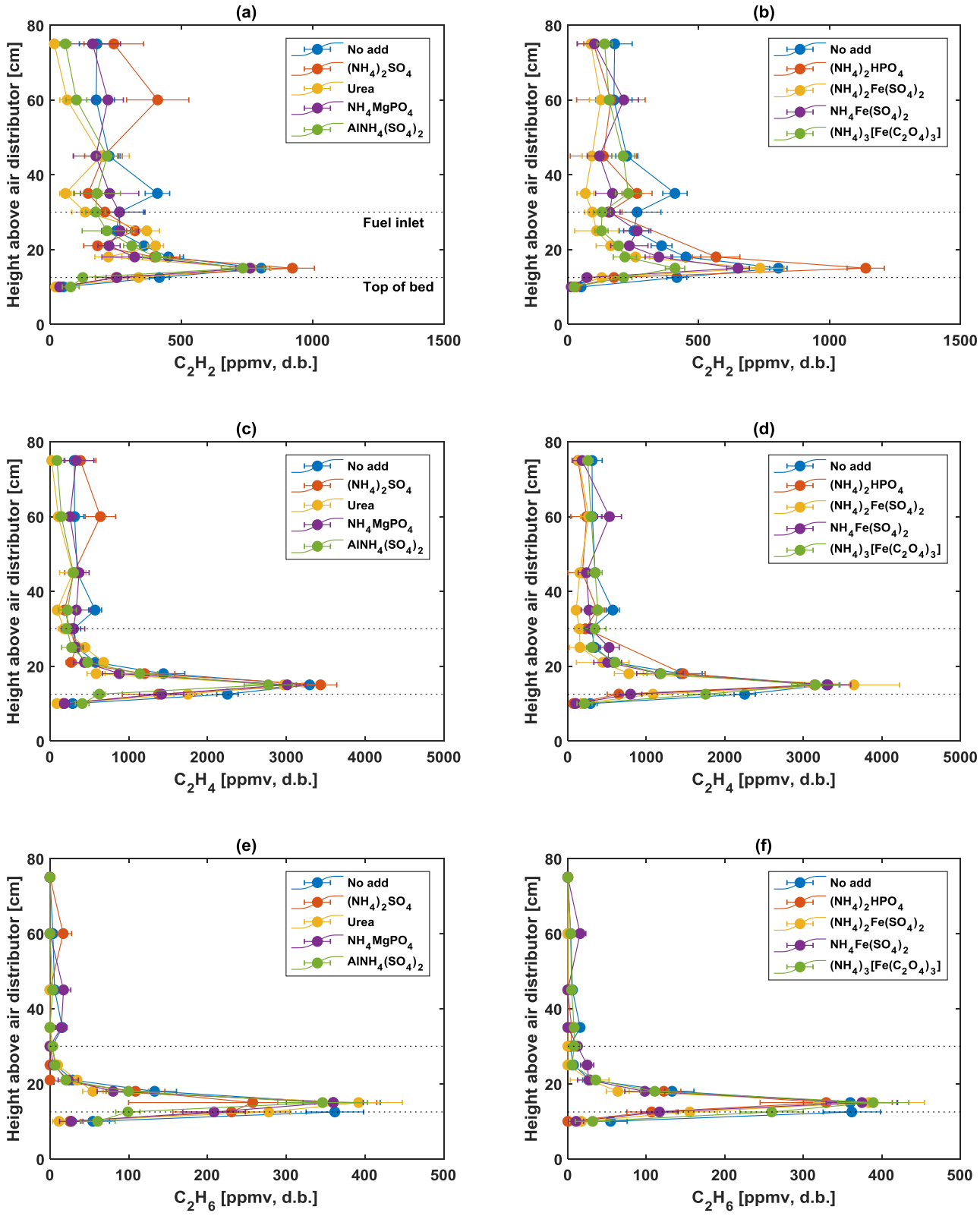

Figure C.6: Axial C_2H_2 (a,b), C_2H_4 (c,d), and C_2H_6 (e,f) profiles during un-staged fluidized bed combustion of straw-additive. Conditions: T_{bed} = 850ºC; λ = 1.4; λ_1/λ = 1.

C.4 S-compounds during straw-$(NH_4)_2SO_4$ combustion

The local SO_2, SO_3, and H_2SO_4 concentrations during combustion of straw with and without $(NH_4)_2SO_4$ are depicted Figure C.7. The SO_2 and H_2SO_4 profiles were comparable between experiments, while a slightly higher SO_3 concentration near the bed may be prominent for the larger $(NH_4)_2SO_4$ particle size range.

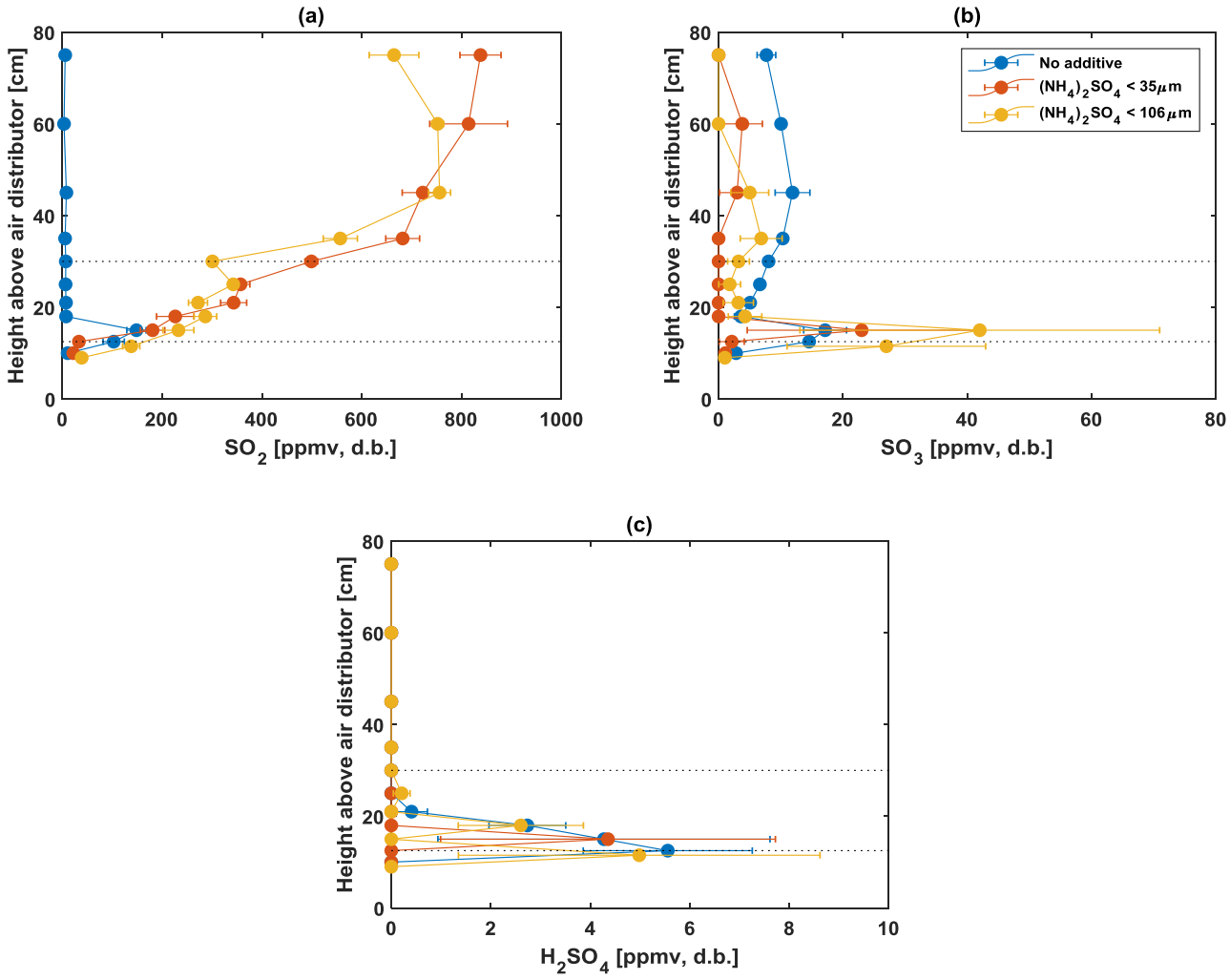

Figure C.7: Axial SO_2 (a), SO_3 (b), and H_2SO_4 (c) profiles during fluidized bed combustion of straw mixed with $(NH_4)_2SO_4$ of two different particle sizes. Conditions: T_{bed} = 850ºC; λ = 1.4; λ_1/λ = 1.

C.5 Axial temperature profiles

The axial temperature profiles from straw combustion with and without additives under air staged and un-staged conditions are depicted in Figure C.8.

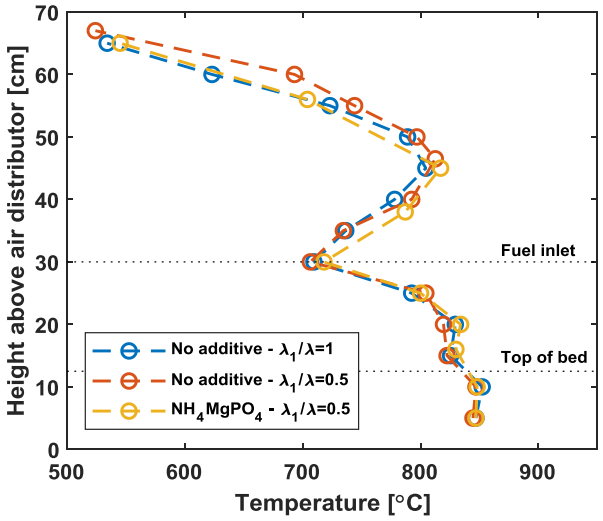

Figure C.8: Temperature profile in air staged and un-staged fluidized bed combustion of straw with and without NH_4MgPO_4. Conditions: T_{bed} = 850ºC; λ = 1.4; λ_1/ λ = 0.5 and 1.

The axial temperature profiles from sunflower husk combustion with and without NH_4MgPO_4 under are depicted in Figure C.9.

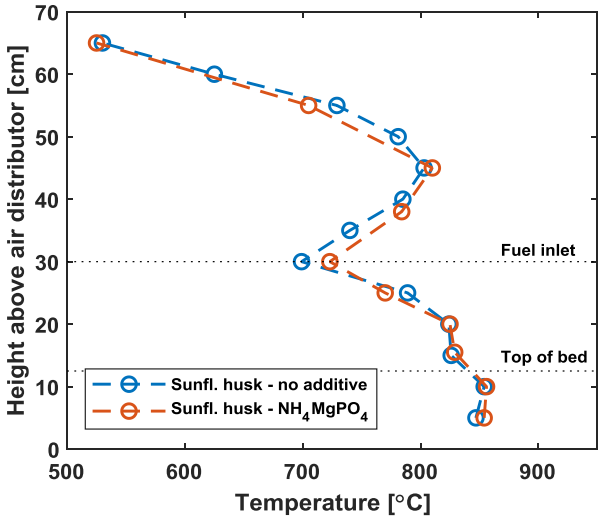

Figure C.9: Temperature profile in air un-staged fluidized bed combustion of sunflower husk with and without NH_4MgPO_4. Conditions: T_{bed} = 850ºC; λ = 1.4; λ_1/ λ = 0.5 and 1.

C.6 Air staged combustion of straw-$AlNH_4(SO_4)_2$

Figure C.10 depicts the results of the local concentration measurements during combustion of straw-$AlNH_4(SO_4)_2$ at air staged ($\lambda_1/\lambda = 0.5$) and un-staged ($\lambda_1/\lambda = 1$) conditions.

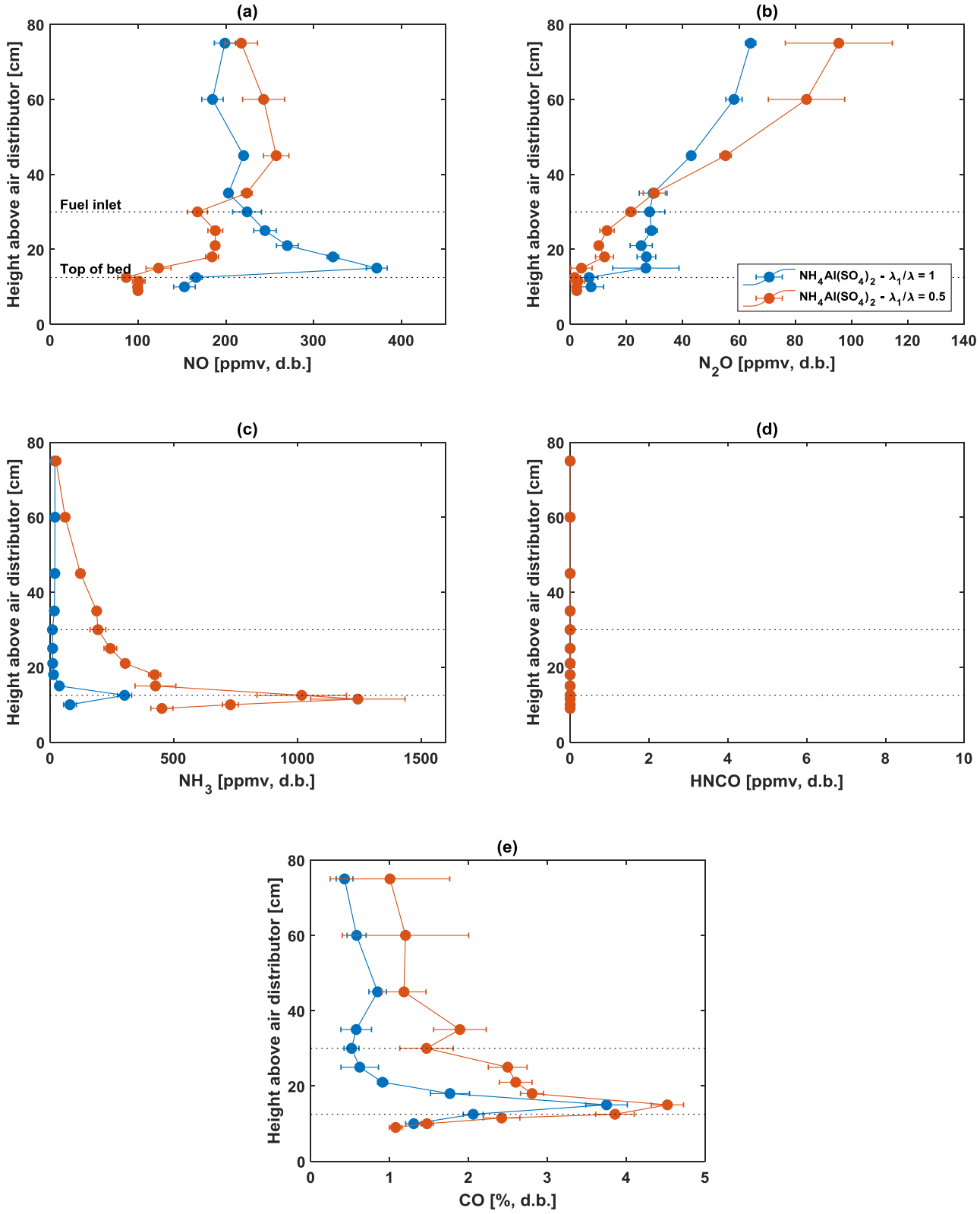

Figure C.10: Axial NO (a), N_2O (b), NH_3 (c), HNCO (d), and CO (e) profiles during fluidized bed combustion of straw-$AlNH_4(SO_4)_2$ under air staged and un-staged conditions. Conditions: T_{bed} = 850ºC; λ = 1.4; λ_1/λ = 0.5 and 1.

C.7 CO, C_XH_Y and CH_2O from un-staged sunflower husk combustion – influence of ash accumulation

Axial profiles of combustibles from sunflower husk combustion are presented below for the initial and late stages of combustion, thereby elucidating the influence of ash accumulation and incipient bed defluidization. The initial stage (init) measurements were conducted during the feeding of 0.04-0.15 kg d.b. sunflower husk (1.3-4.8 g ash), while the late stage (late) measurements were performed between 0.23-0.30 kg d.b. sunflower husk (7.4-9.6 g ash).

CO and CH_2O

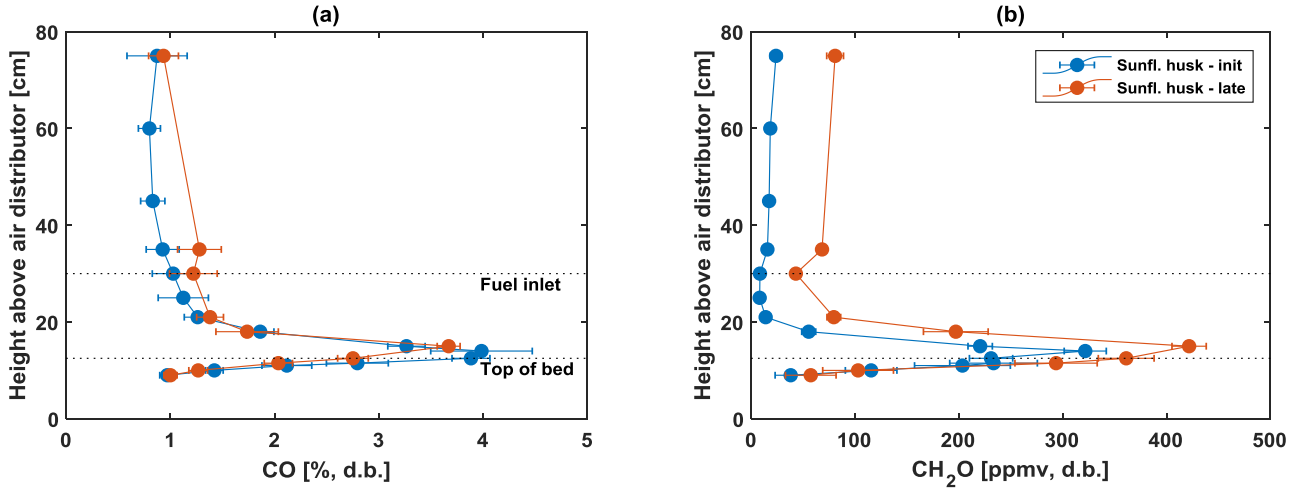

Figure C.11: Axial CO (a) and CH_2O profiles during fluidized bed combustion of sunflower husk. Measurements were performed initial (init: 0.04-0.15 kg d.b. sunfl. husk) and late (init: 0.23-0.30 kg d.b. sunfl. husk) stages of combustion. Conditions: T_{bed} = 850ºC; λ = 1.4; λ_1/λ = 1.

CxHy

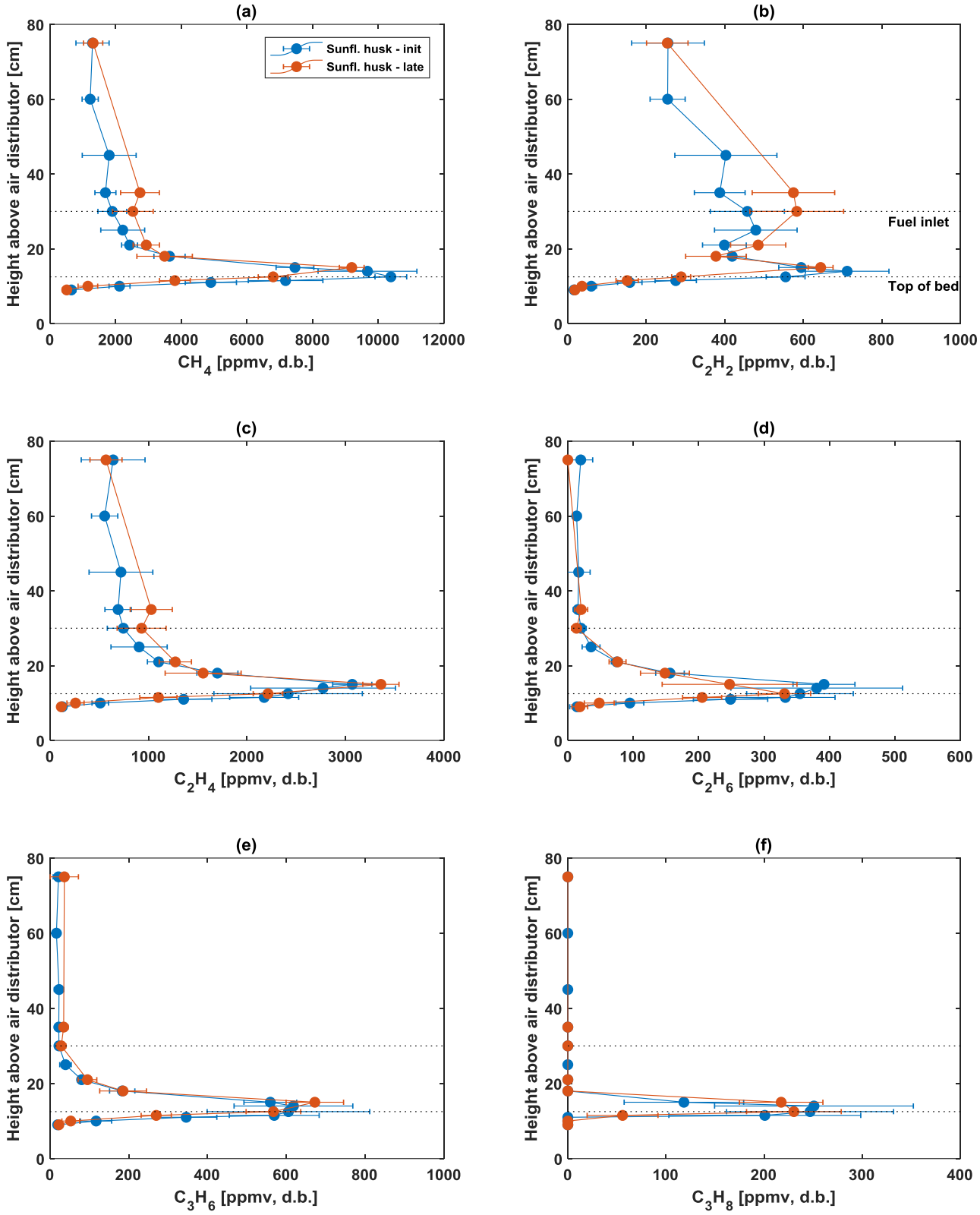

Figure C.12: Axial CH_4 (a), C_2H_2 (b), C_2H_4 (c), C_2H_6 (d), C_3H_6 (d), and C_3H_8 (f) profiles during fluidized bed combustion of sunflower husk. Conditions: T_{bed} = 850ºC; λ = 1.4; λ_1/λ = 1.

Appendix D

D.1 Fuel properties and influence of mass transfer limitations on the NO-char reaction

Table D.1: Complete chemical composition of the biomass fuels.

Property	Unit	Pine wood	Wheat straw	Waste wood	Bran	Sunflower seed	DDGS
Moisture	% (wb.)	4.0	7.4	13.2	8.2	8.7	9.2
Ash	% (db.)	0.2	4.2	1.70	5.3	14	6.4
Volatile	% (db.)	82.4	75.9	-	-	-	-
C	% (db.)	51.5	46.9	49.0	45.0	40.5	43.7
H	% (db.)	6.20	6.0	6.13	6.3	5.73	6.55
N	% (db.)	<0.20	0.56	1.33	2.65	6.14	5.13
S	% (db.)	0.007	0.12	0.037	0.19	0.23	0.23
Cl	% (db.)	0.016	0.67	0.31	0.071	-	-
Al	mg/kg (db.)	32	44	443	80	3,095	75
Ca	mg/kg (db.)	950	2,300	3,200	920	7,328	1,105
Fe	mg/kg (db.)	26	41	363	210	1730	91
K	mg/kg (db.)	480	14,000	703	13,000	18,416	11,723
Mg	mg/kg (db.)	140	960	443	3,800	6,724	3,442
Na	mg/kg (db.)	95	230	326	50	410	3,255
P	mg/kg (db.)	52	910	93	11,000	12,810	10,204
Si	mg/kg (db.)	<200	3,900	1,710	1,300	-	-
Ti	mg/kg (db.)	<5	4	-	-	49	<2

Due to the lack of physical data of the chars, the density was presumed to be 500 kg/m^3, while the effective diffusivity $1.26 \cdot 10^{-4}$ m^2/s, adopted from the work of Garijo et al. [308]. Moreover, the mass transfer constant in the gas film, k_g, was calculated to be 2.1 m/s using the correlation of Dwidewi and Upadhyay [340]. The mass of char was calculated from the CO and CO_2 profiles at the point where the reactivity reached maximum. At the highest investigated temperature and for the largest particle size, the influence of internal and external mass transport limitations were deemed negligible in the case of the most reactive biomass char, straw char. Hence, reaction kinetics dominated the calculated rates, i.e., zone 1 conditions were assumed.

Table D.2: Investigation of the influence of external and internal mass transfer limitations regarding the NO reduction reactions. $-r_{obs} = \frac{1}{W} F_{NO,in} X_{NO}$, Maer's criterion $\varphi_{Maer} = \frac{-r_{obs} \rho_C R_C}{k_g C_{NO,0}} < 0.15$, relative mass transfer resistance $Rel_{ext} = \frac{d_C/(6k_g)}{1/(k_{obs}\rho_C)}$, Weisz Prater modulus and criterion $\varphi_{WP} = \frac{-r_{obs} \rho_C R_C^2}{D_{eff} C_{NO,0}} \ll 1$, Thiele modulus: $\varphi = \frac{d_c}{6} \cdot \left(\frac{k \cdot \rho_c}{D_{eff}}\right)^{\frac{1}{2}}$, and effectiveness factor: $\eta = \frac{3 \cdot \varphi \cdot \coth(3 \cdot \varphi) - 1}{3 \cdot \varphi^2}$. Symbols: W is the instantaneous mass of char, , $F_{NO,in}$ inlet molar flow of NO, X_{NO} conversion of NO at given W, $\boldsymbol{\rho_C}$ is the char density, d_C and R_C are char diameter and radius, respectively, k_g is the gas film mass transfer constant, $\mathbf{k}$ is the first order reaction rate constant, and $\mathbf{D_{eff}}$ is the effective diffusivity.

Char	**Conditions**	$\mathbf{X_{NO}}$	**Maximum observed first order k [m^3/kg char/s]**	$\mathbf{r_{obs}}$ **[mol/kg char/s]**	$\boldsymbol{\varphi_{Maer}}$	$\mathbf{Rel_{ext,max}}$ **[%]**	$\boldsymbol{\varphi_{WP}}$	$\boldsymbol{\varphi}$	$\boldsymbol{\eta}$
Straw	900ºC, 400 ppm NO	0.9	12.3	0.020	0.027	9.0	0.040	0.210	0.975

D.2 Experiment repeatability, and influence of temperature and NO concentration

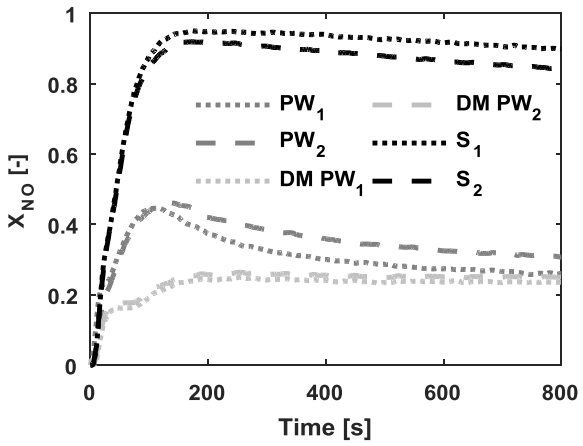

Figure D.1: Repeatability investigation of the NO reduction over char at 800°C using an NO inlet concentration of 400 ppmv NO. The subscripts denote the repetition number. DM: Demineralized, PW: pine wood, and S: straw.

Arrhenius plots of the steady state rate constant of the chars using 400 ppmv NO are illustrated in Figure D.2. The reactivity of all chars increased with temperature. A significant effect of temperature was observed for the pine wood char, which was not prominent for the demineralized char. Consequently, this effect was attributed to the activation of the catalytic elements present in pine wood char. At higher temperatures, a change in the reactivity of presumably calcium could have activated the char. A change in mechanism/activation energy from adsorption to reaction control has previously been reported at temperatures around 700°C [16]. At the investigated temperatures, the increased reactivity of the pine wood char is suspected to be due to the content of ash forming elements. Although, the pine wood contained the least amount of ash forming elements of the raw chars, it exhibited the second highest reactivity towards NO at higher temperatures. In addition, the demineralized bran char increased in reactivity, which due to the depletion of catalytically active elements could be ascribed physical changes, such as surface area or pore size distribution.

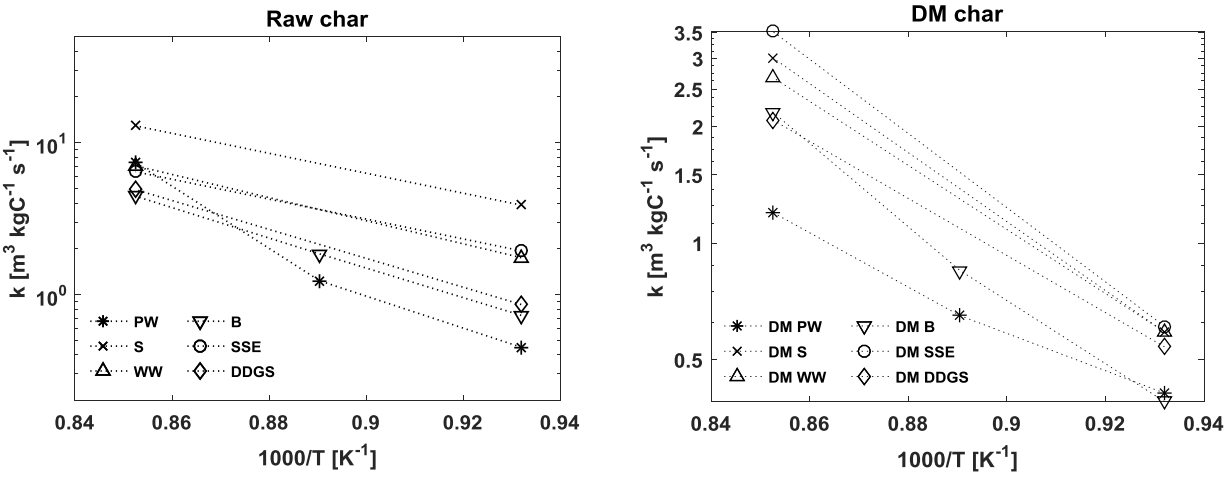

Figure D.2: Arrhenius plots of raw and demineralized chars using 400 ppmv NO. PW: pine wood, S: straw, WW: waste wood, B: bran, SSE: sunflower seed, DDGS: dried distillers grains with solubles and DM: demineralized.

Figure D.3 demonstrates the influence of NO inlet concentration on the first order carbon mass based NO reduction rate constant for selected chars. Given the expression for the first order rate constant in Eq. 1 in the original paper, this should be independent on the initial NO concentration. The results indicate that the reactivity depends on the NO inlet concentration. This in turn suggests that the first order rate expression used for comparison between the chars is inadequate in describing the reactivity at varying NO inlet concentrations. Therefore, other rate expressions such as fractional order, concentration averaged, or mechanistic models must be used to capture this effect in large scale modelling studies. However, the first order rate constant can be used as a qualitative comparison of the char reactivity under similar NO concentration.

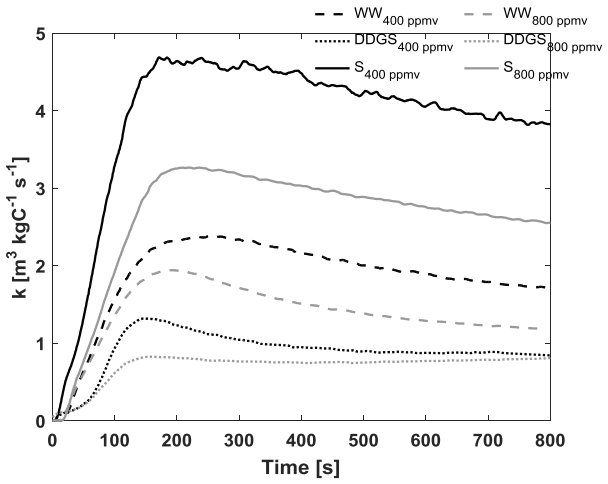

Figure D.3: First order carbon mass based NO reduction rate constant at different inlet concentrations of NO at 800°C. WW: waste wood, DDGS: dried distillers grains with solubles and S: straw.

D.3 Correlation study – surface area and char-N content

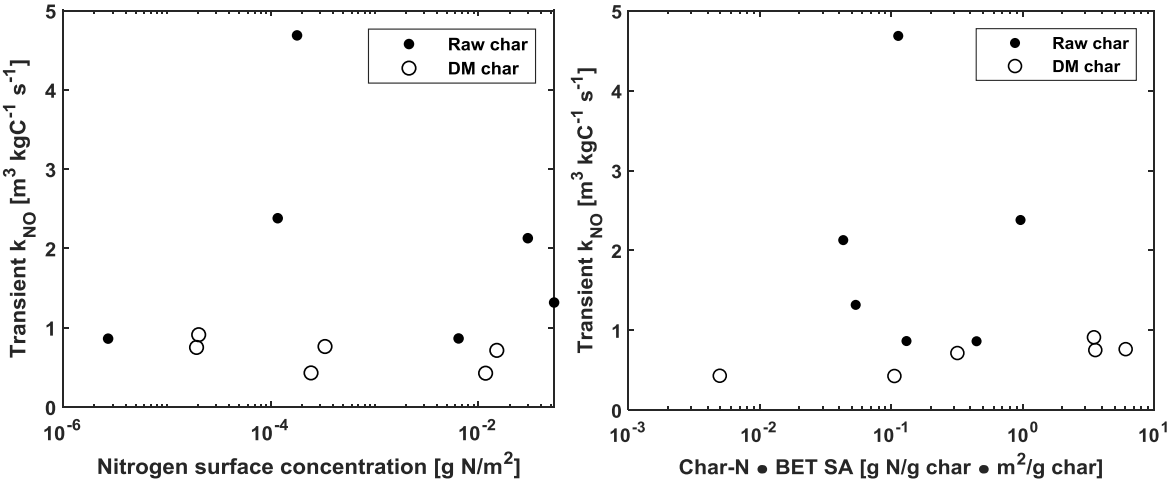

Figure D.4: Transient first order reactivity versus the ratio (left) and product (right) of char-N and surface area. No improved correlation was observed in either case.

D.4 XPS curve fitting

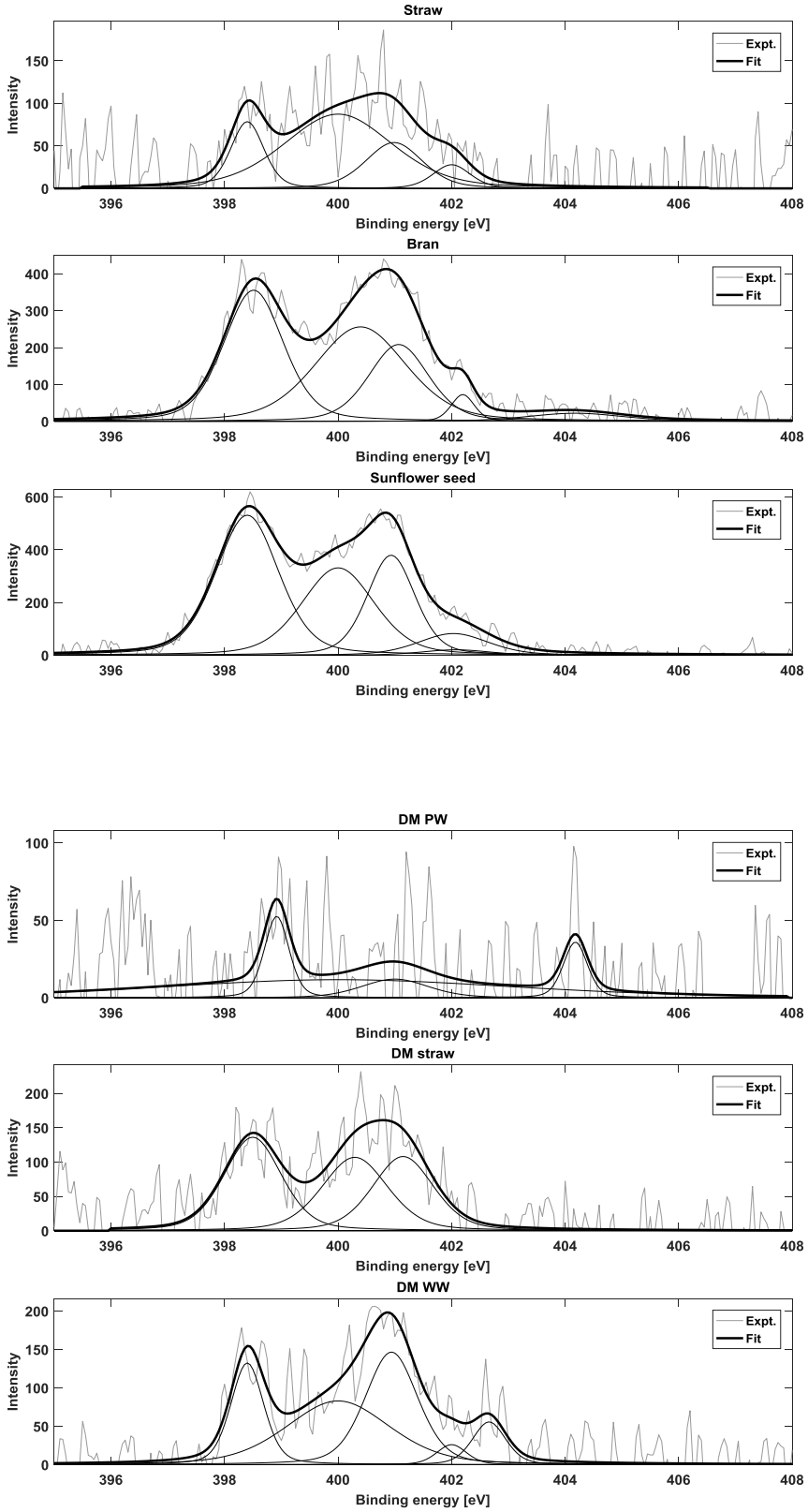

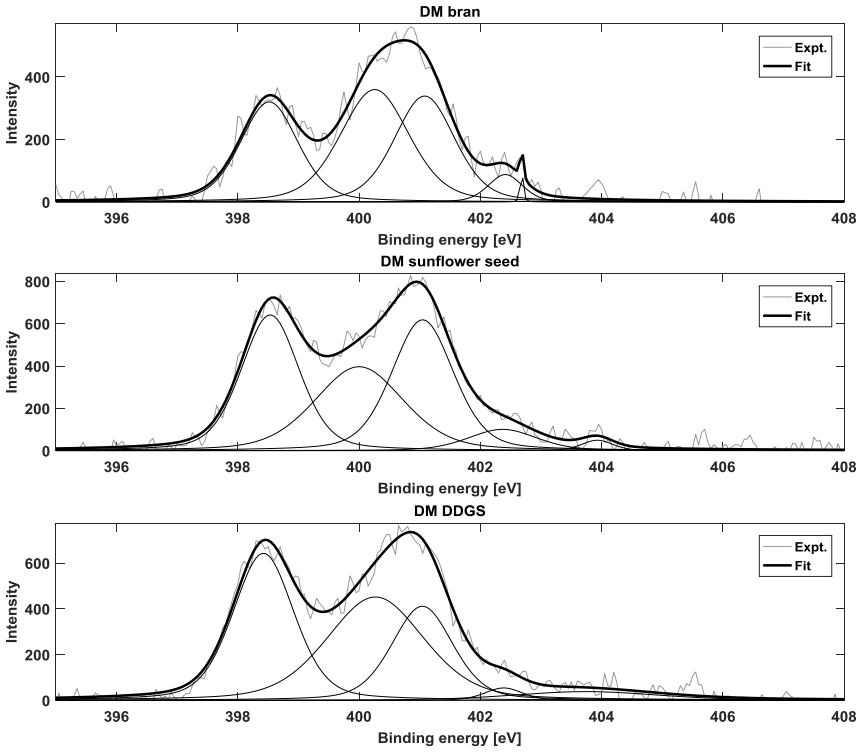

Figure D.5: Deconvolved XPS results for the relevant chars.

D.5 Correlation study – N and O functionality versus measured properties

Table D.3: Oxygen functionality in the chars from the C1s peak based on the work of Figueiredo and Pereira [341]. The large content of N in the chars was taken into account when determining the functionality.

	Oxygen functionality [mol%]			
	C-(C,H)	**C-(O,N)**	**$R_2C=O$**	**O=C-O**
Binding energy [eV]	284.6 ± 0.3	286.1 ± 0.3	287.6 ± 0.3	289.1 ± 0.3
Char				
Straw	76.8	15.1	5.50	2.60
Bran	73.0	19.3	5.62	2.08
Sun. seed	72.0	21.3	5.00	1.70
DM pine wood	81.9	12.6	1.00	4.50
DM straw	77.6	15.9	4.09	2.41
DM waste wood	77.8	14.5	4.54	3.16
DM bran	63.8	27.0	5.27	3.93
DM sunfl. seed	71.8	22.6	3.66	1.94
DM DDGS	71.2	22.1	5.08	1.62

Table D.4: Combustion and NO reduction properties used in the correlation analysis below. $\boldsymbol{\eta}$: fractional conversion of char N, X_{NO}: conversion of NO from reduction experiments, k: first order carbon mass based rate constant ($m^3\ kgC^{-1}\ s^{-1}$) from NO reduction experiments, subscript s: steady state (post 750 s rate constant) and t: transient value (maximum rate constant).

Chars	**Combustion properties**		**NO reduction properties**				
	$\boldsymbol{\eta_{NO}}$	$\boldsymbol{\eta_{N_2O,FTIR}}$	$\boldsymbol{X_{NO,s,800°C}}$	$\boldsymbol{k_{t,800°C}}$	$\boldsymbol{k_{s,800°C}}$	$\boldsymbol{k_{t,900°C}}$	$\boldsymbol{k_{s,900°C}}$
Straw	0.58	0.0183	0.90	4.69	3.88	17.3	12.9
Bran	0.32	0.0341	0.27	0.86	0.73	4.66	4.44
Sun. seed	0.33	0.0573	0.65	2.12	1.94	6.83	6.43
DM pine wood	0.99	0.0249	0.24	0.43	0.42	1.23	1.20
DM straw	0.6	0.0351	0.32	0.75	0.58	3.36	3.01
DM waste wood	0.58	0.0472	0.32	0.91	0.59	3.91	2.68
DM bran	0.38	0.0755	0.23	0.43	0.39	2.26	2.18
DM sunfl. seed	0.32	0.0976	0.31	0.76	0.61	4.34	3.52
DM DDGS	0.29	0.1045	0.28	0.71	0.54	2.65	2.08

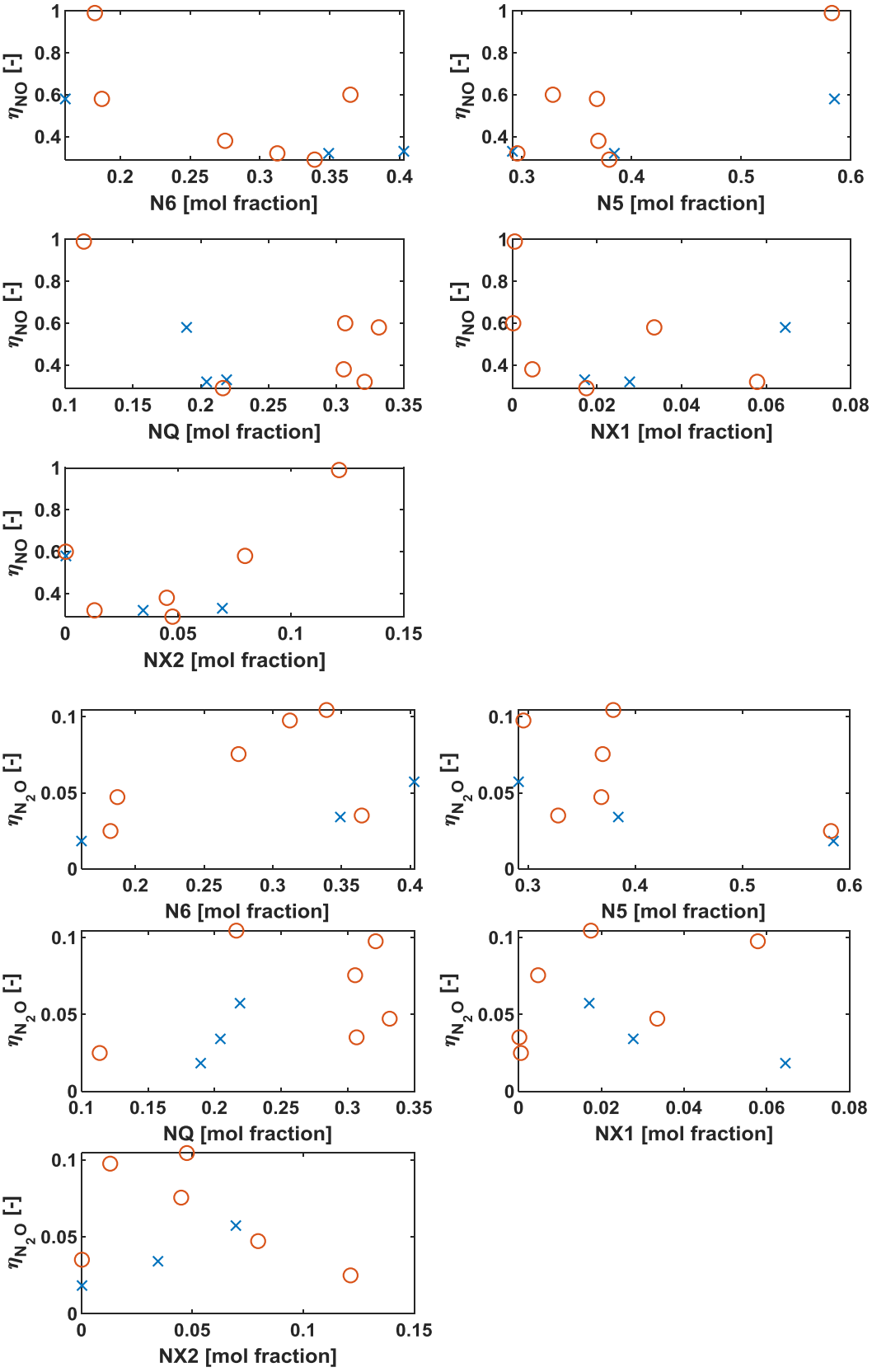
η_{NO} [-]
N6 [mol fraction]
N5 [mol fraction]
NQ [mol fraction]
NX1 [mol fraction]
NX2 [mol fraction]
η_{N_2O} [-]
N6 [mol fraction]
N5 [mol fraction]
NQ [mol fraction]
NX1 [mol fraction]
NX2 [mol fraction]

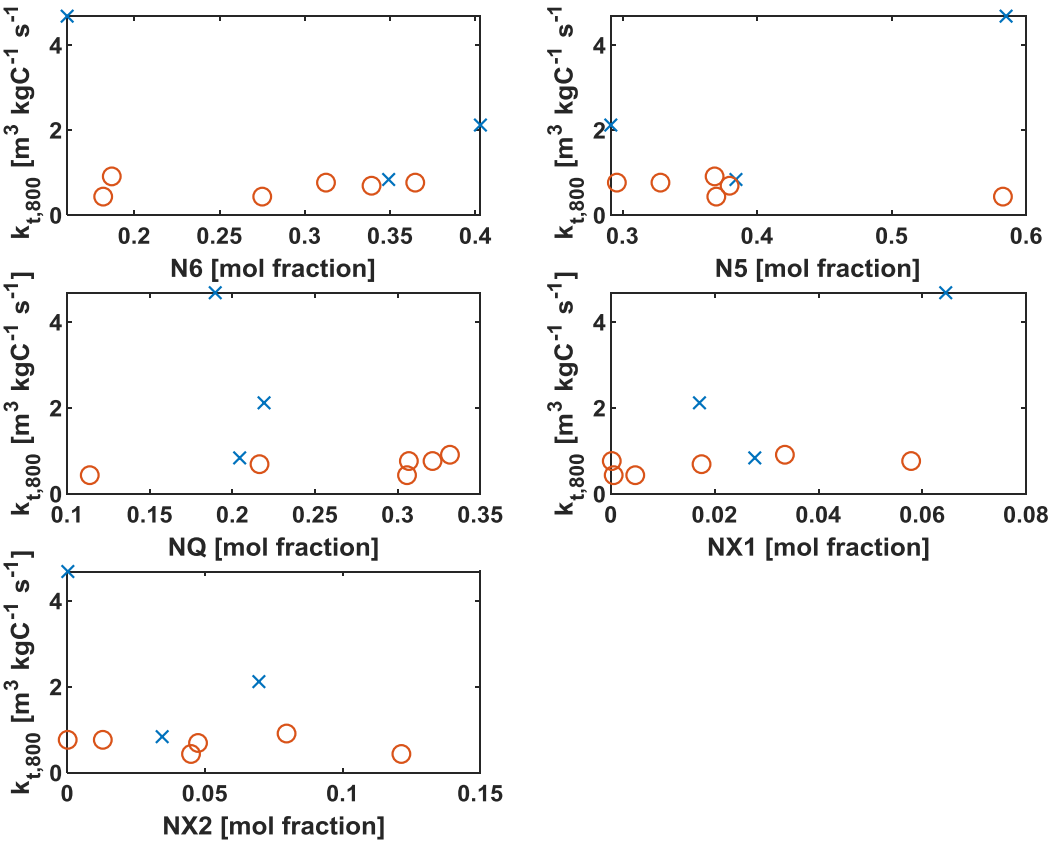

Figure D.6: Correlation study of selected parameters and the nitrogen functionality in all chars. Blue crosses denote raw chars while red circles are demineralized chars.

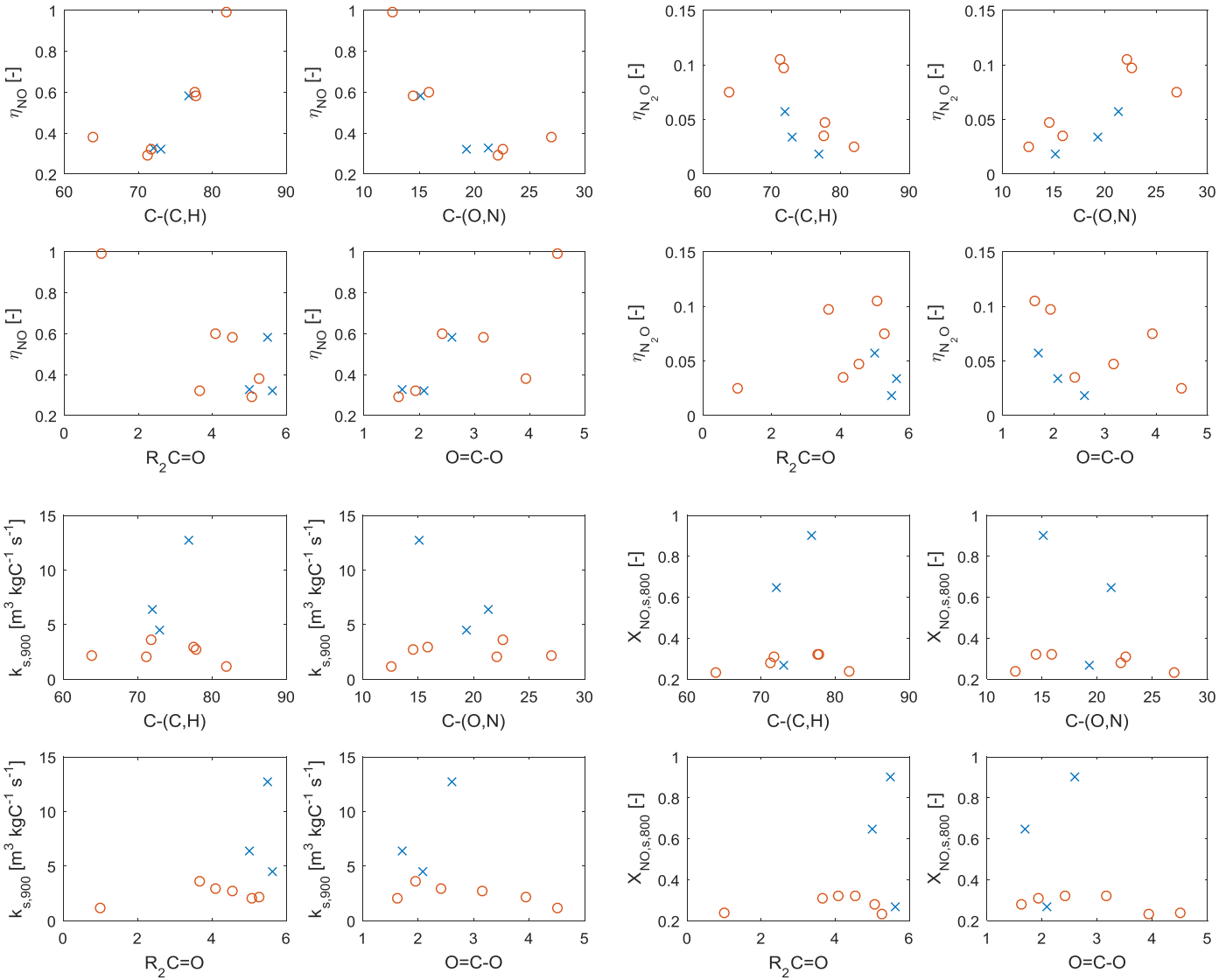

Figure D.7: Correlation study of selected parameters and the oxygen functionality in all chars. Blue crosses denote raw chars while red circles are demineralized chars.

D.6 Elemental surface population

Table D.5: Surface and bulk elemental composition on a molar basis of the relevant chars.

	Surface content [mol%]			Surface ratio [mol/mol]			Bulk ratio [mol/mol]		
Char	**C**	**N**	**O**	**N/C**	**O/C**	**N/O**	**N/C**	**O/C**	**N/O**
Straw	83.17	0.9	15.93	0.011	0.192	0.056	0.006	0.089	0.067
Bran	84.77	3.69	11.54	0.044	0.136	0.320	0.041	0.124	0.333
Sun. seed	77.04	4.86	18.1	0.063	0.235	0.269	0.054	0.148	0.366
DM pine wood	91.09	0.65	8.26	0.007	0.091	0.079	0.0011	0.092	0.013
DM straw	91.03	0.96	8.01	0.011	0.088	0.120	0.086	0.065	0.134
DM waste wood	92.09	1.15	6.76	0.012	0.073	0.170	0.094	0.166	0.058
DM bran	88.32	2.71	8.97	0.031	0.102	0.302	0.039	0.075	0.523
DM sunfl. seed	87.04	4.39	8.58	0.050	0.099	0.512	0.054	0.086	0.624
DM DDGS	86.89	5.58	7.53	0.064	0.087	0.741	0.081	0.098	0.824

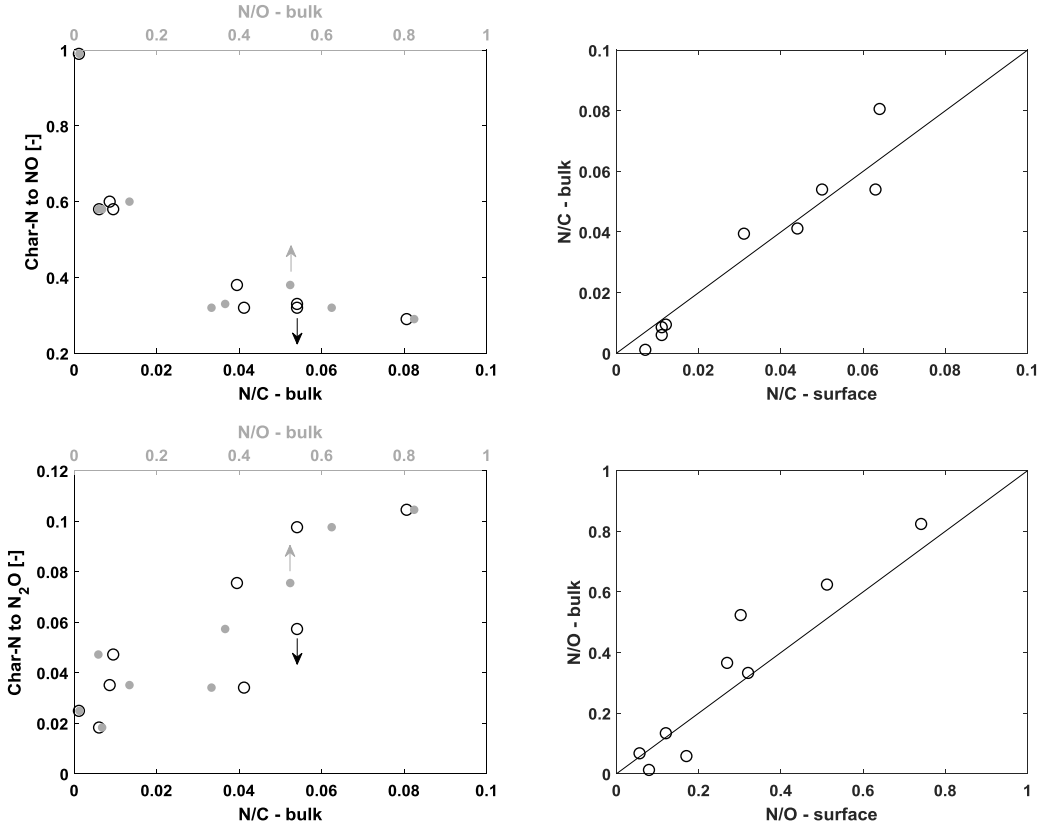

Figure D.8: Char-N to NO (top left) and N_2O (bottom left) against bulk N/C and N/O molar ratios. Molar bulk N/C (top right) and N/O (bottom right) against surface ratios. The combustion properties were determined from 20 mg char combustion at 800°C in 10vol% O_2.

D.7 SEM EDX of leached biomass chars

Straw

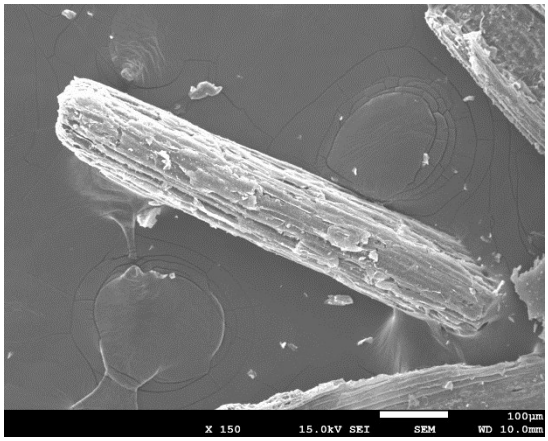

Straw

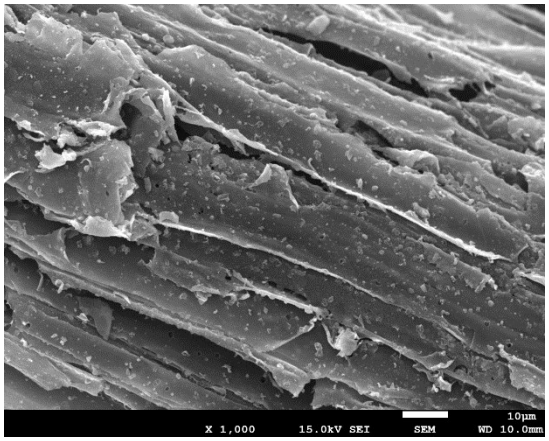

WW straw

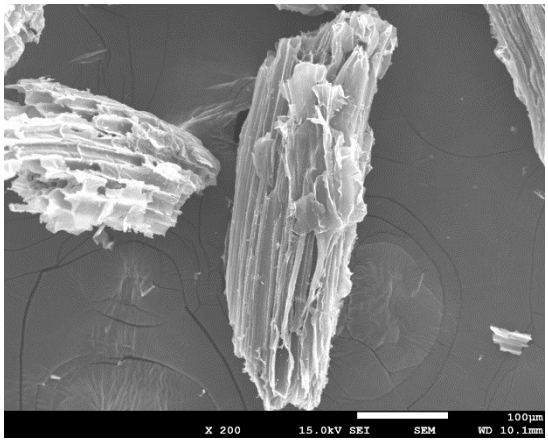

WW straw

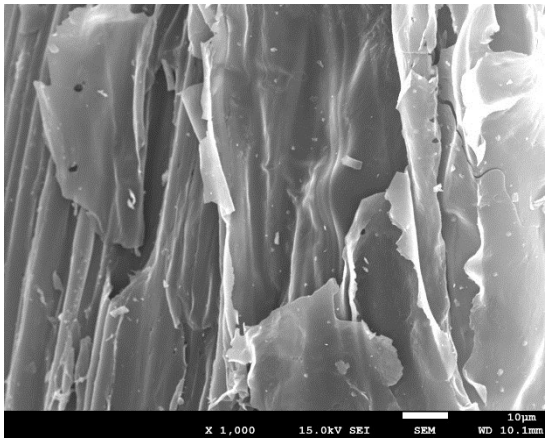

OW straw

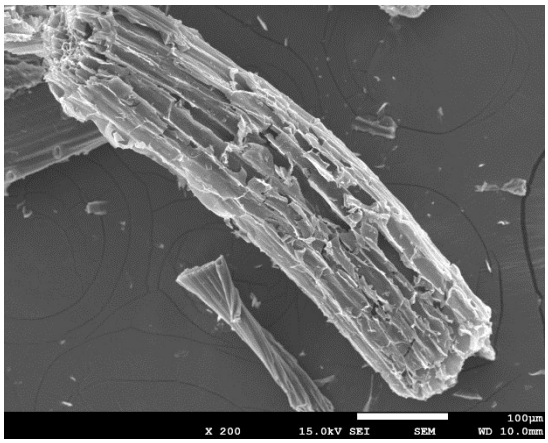

OW straw

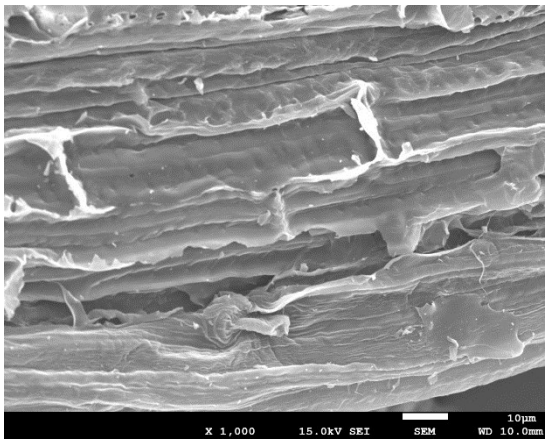

DM straw

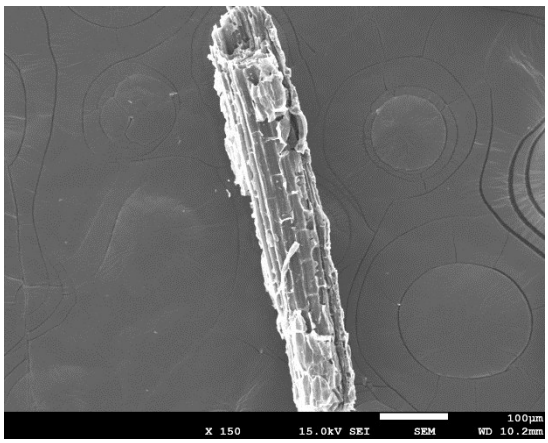

DM straw

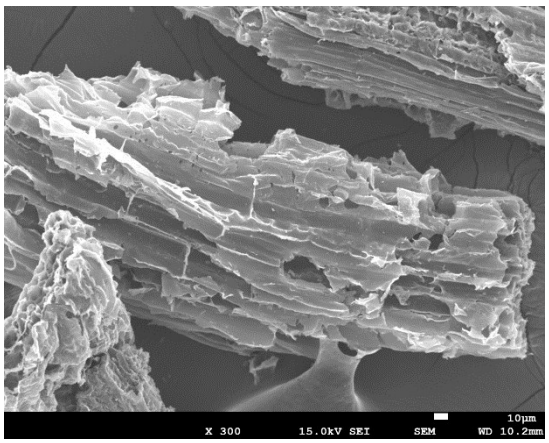

Figure D.9: SEM images of chars of treated straw, showing similar morphology. WW straw: water washed straw, OW straw: organic washed straw, DM straw: demineralized straw.

Straw

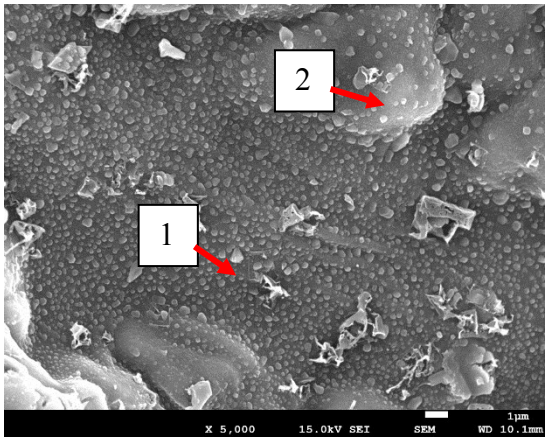

WW straw

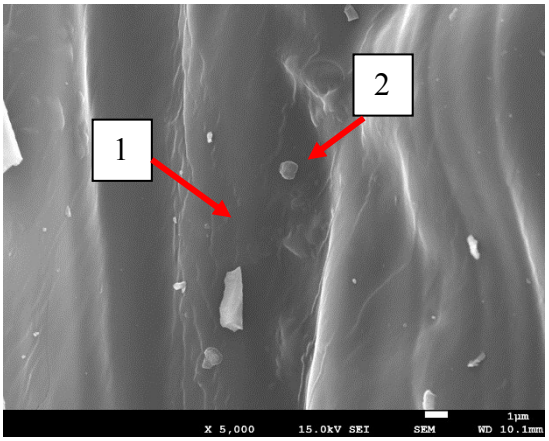

OW straw

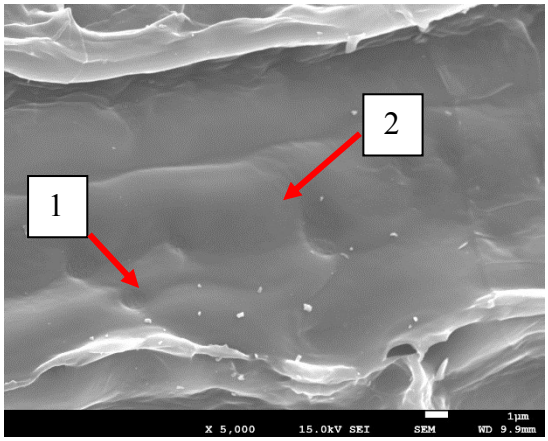

DM straw

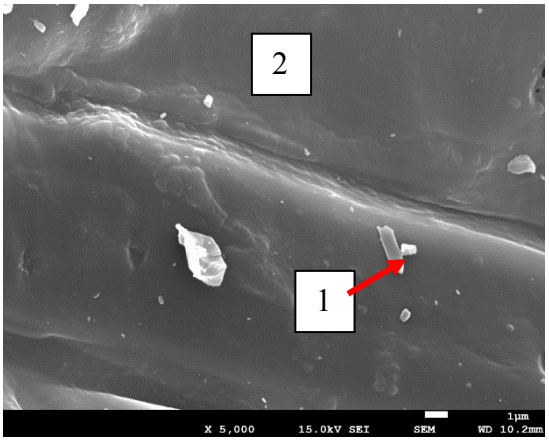

	[at%]							
Char	**K**	**P**	**Mg**	**Ca**	**Fe**	**Na**	**Cl**	**S**
Straw 1	9.27	0.12	1.44	1.51	0.08	0.10	2.23	0.56
2	3.14	1.24	0.78	0.51	0.00	0.12	0.85	0.30
WW straw 1	0.25	0.14	0.10	0.09	0.00	0.00	0.01	0.11
2	0.23	0.00	0.12	0.96	0.00	0.01	0.03	0.25
OW straw 1	0.01	0.25	0.00	0.17	0.04	0.00	0.04	0.24
2	0.02	0.17	0.01	0.05	0.01	0.01	0.01	0.12
DM straw 1	0.00	0.13	0.00	0.01	0.00	0.00	0.02	0.12
2	0.00	0.12	0.00	0.00	0.02	0.00	0.01	0.11

Figure D.10: SEM-EDX of chars of pretreated straw qualitatively showing the depletion of minerals on the surface, in agreement with ICP-OES measurements.

Appendix E

E.1 Fuel and char properties, and mass transfer limitations for the char-NO reaction

Table E.1: Complete ICP-OES of fuels and chars

	ICP-OES, all concentrations are in mg/kg											
	K	**P**	**Si**	**Mg**	**Ca**	**Al**	**Fe**	**Na**	**Mn**	**Pb**	**Zn**	**Cu**
Straw	14000	910	3900	960	2300	44	41	230	-	-	-	-
Sewage sludge	6300	34000	75000	4300	37000	18000	85000	2400	-	-	-	-
RDF	1600	760	1800	4440	37300	879	454	2000	160	<60	1373	105
Straw char	43642	2789	751	2329	4459	23	<3	740	<1	<60	<4	<4
Sew. slu. char	5803	16708	957	6745	61579	19746	39697	1485	1038	<60	1802	520
RDF char	4314	1673	842	9778	95688	23199	9675	5880	34.1	509	1873	340
DM straw char	530	727	1791	<0.2	283	799	<3	<120	<1	<60	<4	<4
DM sew. slu. char	3090	10614	2475	4175	5698	20732	33059	603	629	107	296	406

The calculations procedure and assumptions used in the calculations were similar to those described in Appendix D, Section D.1 for straw char. At the highest temperature and for the largest particle size, the effect of internal mass transport limitations is negligible for RDF and sewage sludge char, while up to 21% external transport limitations is possible. Since smaller particles would induce issues in feeding, this resistance was deemed acceptable. In addition the Thiele modulus and corresponding first order, irreversible, isothermal effectiveness factor confirm that internal limitations can be neglected, consequently zone 1 conditions were assumed.

Table E.2: Investigation of the influence of external and internal mass transfer limitations on the char-NO reaction. $-r_{obs}=\frac{1}{W} F_{NO,in} X_{NO}$, Maer's criterion $\varphi_{Maer}=\frac{-r_{obs}\,\rho_C\,R_C}{k_g\,C_{NO,0}}<0.15$, relative mass transfer resistance $Rel_{ext}=\frac{d_C/(6k_g)}{1/(k_{obs}\rho_C)}$, Weisz Prater modulus and criterion $\varphi_{WP}=\frac{-r_{obs}\,\rho_C\,R_C^2}{D_{eff}\,C_{NO,0}}\ll 1$, Thiele modulus: $\varphi=\frac{d_c}{6}\cdot\left(\frac{k\cdot\rho_c}{D_{eff}}\right)^{\frac{1}{2}}$, and effectiveness factor: $\eta=\frac{3\cdot\varphi\cdot\coth(3\cdot\varphi)-1}{3\cdot\varphi^2}$. Symbols: W is the instantaneous mass of char, , $F_{NO,in}$ inlet molar flow of NO, X_{NO} conversion of NO at given W, $\boldsymbol{\rho_C}$ is the char density, d_C and R_C are char diameter and radius, respectively, k_g is the gas film mass transfer constant, $\mathbf{k}$ is the first order reaction rate constant, and $\mathbf{D_{eff}}$ is the effective diffusivity.

Char	Conditions	X_{NO}	Maximum observed first order k [m^3/kg char/s]	r_{obs} [mol/kg char/s]	φ_{Maer}	$Rel_{ext,max}$ [%]	φ_{WP}	φ	η
Sewage sludge	900ºC, 400 ppm NO	0.95	29	0.0332	0.044	20.8	0.065	0.322	0.943
RDF	900ºC, 400 ppm NO	0.95	26	0.0288	0.038	18.6	0.057	0.305	0.948

E.2 Residence time distribution measurements

The dispersion downstream of the packed bed reactor was examined using both short pulse and step response experiment. The discrepancy between the methods was small, and therefore the pulse method is shown here, as this did not involve error propagation by differentiation. Based on the residence time distribution curves, the mean residence time and variation were calculated, from which the number of ideal CSTRs was determined.

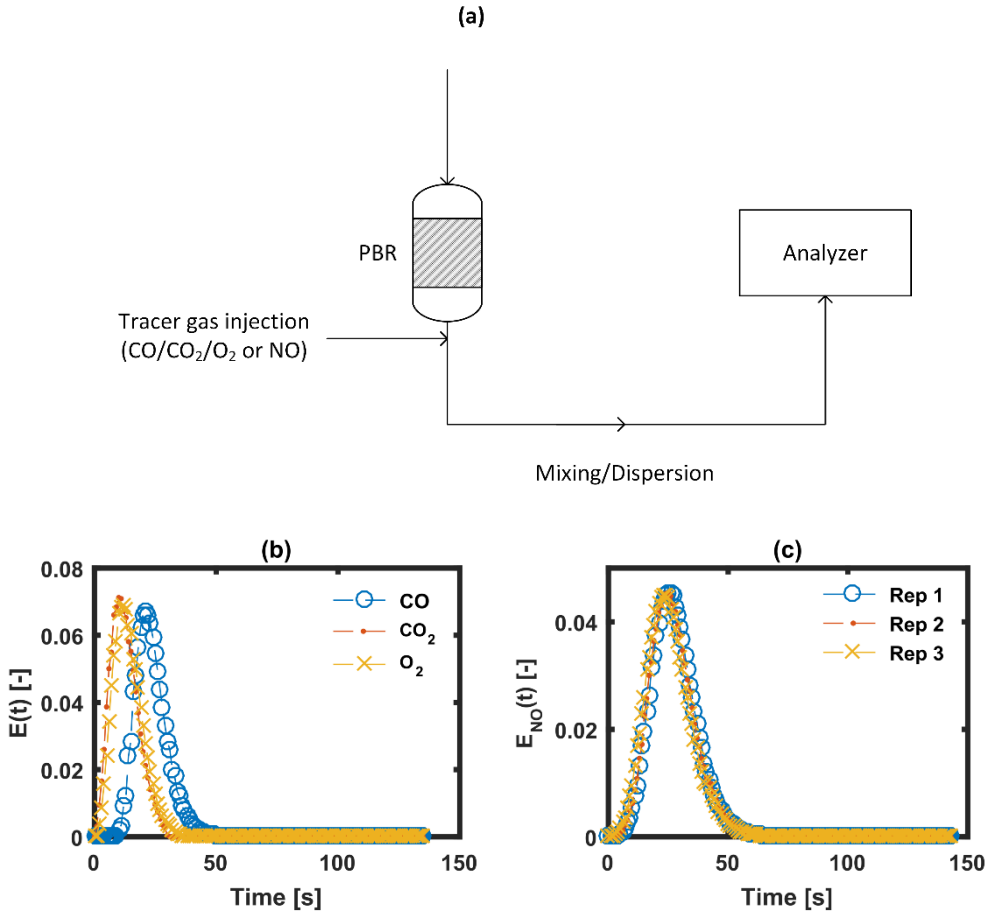

Figure E.1: Schematic showing the input of tracer to determine the dispersion subsequent to the packed bed reactor (a). Residence time distribution plots (pulse method) for CO, CO_2, O_2 (b), and NO (c). Repetitions are shown in the distribution plot of NO.

Table E.3: Mean residence time (t_m) and number of ideal reactors n_{CSTR} for each compound.

Compound	O_2	CO_2	CO	NO
t_m (s)	13	13	24	24
n_{CSTR}	6	5	7	7

E.3 Experimental and modelled O_2, CO_2, CO, and NO combustion profiles for RDF char

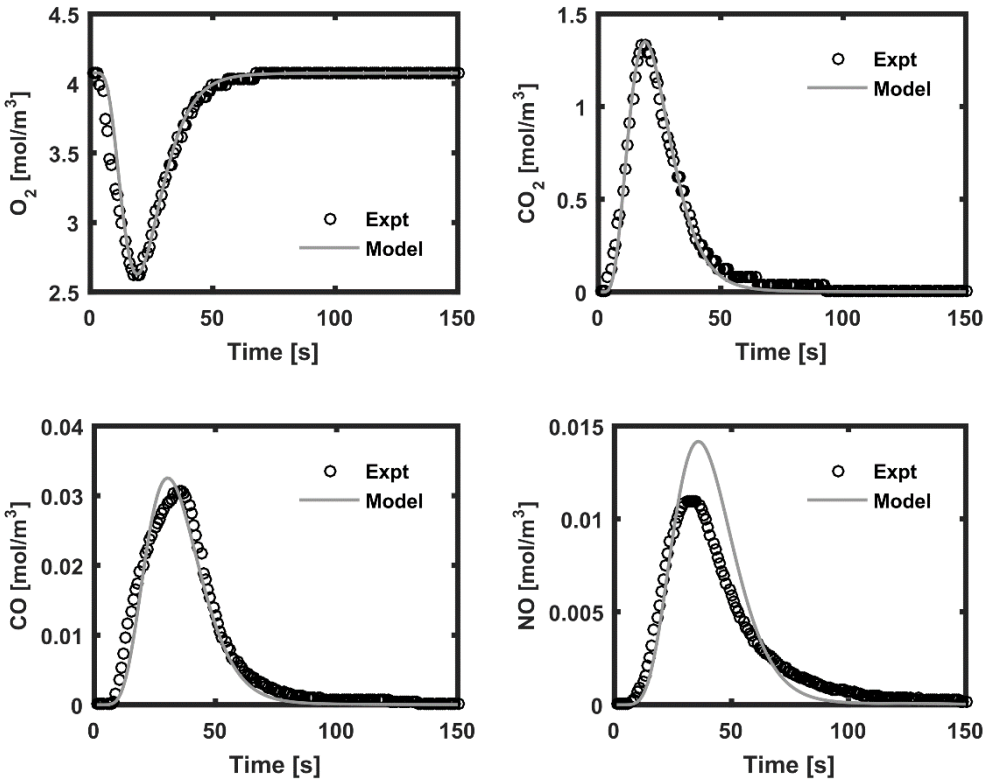

Figure E.2: O_2, CO_2, CO, and NO concentration profiles from combustion of 20 mg RDF char at 800°C in 10 vol% O_2. The combustion kinetic parameters were fit to the CO_2 and O_2 profiles, while the CO was calculated based on a CO_2 fraction of 0.97 based on experimental data. The NO concentration plot was calculated from the combustion kinetic parameters and the experimentally obtained reduction rate constant.

E.4 Experiment repeatability

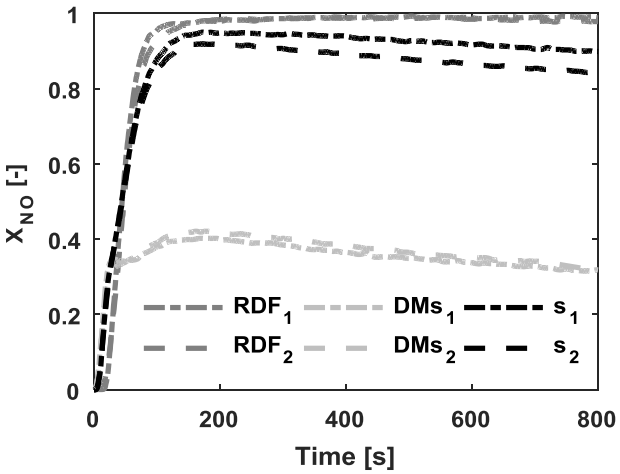

Figure E.3: Repeatability investigation of the NO reduction over char at 800°C using an NO inlet concentration of 400 ppmv NO. The subscripts denote the repetition number.

E.5 Model comparison

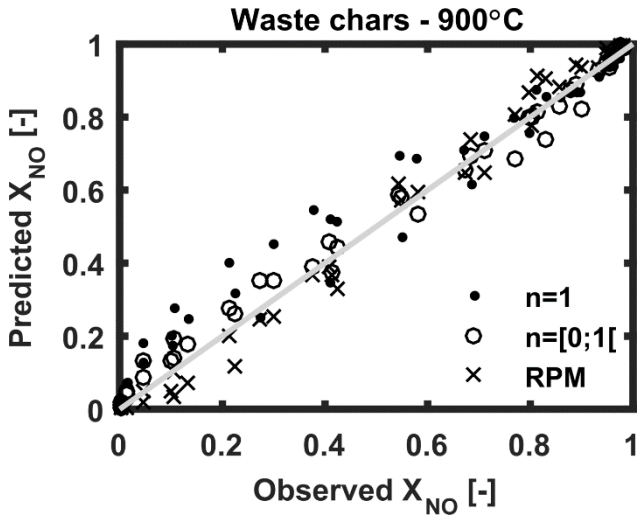

Figure E.4: Comparison of the predicted NO versus observed NO conversion for sewage sludge and RDF chars at 900°C at varying NO inlet concentrations using first order (n=1), fractional order (n=[0;1[), and random pore model (RPM) rate expressions. For the first order expression the concentration average of the maximum first order rate constant (k_{max}) was used. For the fractional order and RPM expressions, a Maximum Likelihood function was used to minimize the squared sum error between model and experiment at three different concentrations simultaneously.